The Pennsylvania State University

The Graduate School

Department of Chemistry

CHEMISTRY OF SUSTAINABILITY –

PART I: CARBON DIOXIDE AS AN ORGANIC SYNTHON AND

PART II: STUDY OF THERMODYNAMICS OF CATION EXCHANGE REACTIONS IN SEMICONDUCTOR NANOCRYSTALS

A Dissertation in

Chemistry

by

Ajay A. Sathe

Submitted in Partial Fulfillment
of the Requirements
for the Degree of

Doctor of Philosophy

December 2016

The dissertation of Ajay A. Sathe was reviewed and approved* by the following:

Robert M Rioux
Friedrich G. Helfferich Associate Professor of
Chemical Engineering & Chemistry
Dissertation Advisor

Ayusman Sen
Distinguished Professor of Chemistry

Raymond Schaak
Dupont Professor of Materials Chemistry

Chunshan Song
Distinguished Professor of Fuel Science and Professor of Chemical Engineering
John J. and Jean M. Brennan Clean Energy Chair

Thomas E. Mallouk
Evan Pugh Professor of Chemistry, Physics, Biochemistry and Molecular Biology
Head of the Department of Chemistry

*Signatures are on file in the Graduate School

ABSTRACT

Sustainability is an important part of the design and development of new chemical and energy conversion processes. Simply put sustainability is the ability to meet our needs without sacrificing the ability of the next generations to meet theirs. This thesis describes our efforts in developing two orthogonal strategies for the fixation of CO_2 by utilizing high energy intermediates which are generated via oxidative or reductive processes on common organic substrates and of thermochemical measurements of cation exchange reactions which will aid the development of new materials relevant for energy conversion and storage.

The first chapter lays a background for the challenges and opportunities for the use of CO_2 in organic synthesis. The rapidly growing field of continuous flow processing in organic synthesis is introduced, and its importance in the development of sustainable chemical conversions is highlighted. The second chapter describes the development of a novel route to α-amino acids via reductive carboxylation of imines. A mechanistic proposal is presented and the reaction is shown to proceed through the intermediacy of α-amino alkyl metal species. Possible strategies for designing catalytic and enantioselective variants of the reaction are presented. The third chapter describes the development of a catalytic oxidative carboxylation of olefins to yield cyclic carbonates. The importance of flow chemistry and membrane separation is demonstrated by allowing the combination of mutually incompatible reagents in a single reaction sequence.

While the use of carbon dioxide for synthesis of organic fine chemicals is not expected to help reduce the atmospheric carbon dioxide levels, or tackle climate change, it certainly has the potential to reduce our dependence on non-sustainable carbon feedstocks, and help achieve a carbon neutral chemical life cycle.

Having described the use of carbon dioxide and flow chemistry for sustainable *chemical conversion*, the fourth chapter introduces the role of nanomaterials in sustainable solar *energy*

conversion and storage. The use of cation exchange reactions in nanocrystals to access novel materials is highlighted. Despite having shown tremendous promise in the synthetic applications, the fundamental measurements of the thermodynamic and kinetic parameters of a cation exchange reaction are largely non-existent. This impedes the future growth of this powerful methodology. The technique of isothermal titration calorimetry is introduced, and its importance to studying the thermochemical changes occurring during cation exchange is outlined. The final chapter presents results obtained from the isothermal titration calorimetry on the prototypical cation exchange reaction between cadmium selenide and silver ions. The role of nanoparticle size, identity of the silver salt, solvent, surface ligands and temperature is studied. Recommendations for future investigations using ITC as well as other characterization techniques for discerning the kinetics of cation exchange are presented.

I believe that a more unified mechanistic understanding of the cation exchange process in nanomaterials will aid the development of more efficient and robust materials for applications in a wide variety of fields.

TABLE OF CONTENTS

LIST OF FIGURES

LIST OF TABLES

ACKNOWLEDGEMENTS

The last six years of my life have been the most challenging, rewarding and above all exciting (well… for the most part!). I have learned a lot about chemical research as well as my own strengths and weaknesses. This journey would not have been possible without the help and support of a lot of people.

Firstly I would like to thank my advisors Dr. Robert Rioux and Dr. Alexander Radosevich who gave me a platform for pursuing engaging research problems, upon which this dissertation is built. Their desire for excellence and attention to detail is inspiring. I am especially grateful for their encouragement and support during the time I decided to change the focus of my research. Thank you for believing in me when I came to you with ideas that were completely new to either one of us, and providing me with all the possible guidance and resources to help me succeed in the endeavor. All that I have learnt about designing, executing and presenting science I owe it to them.

I sincerely thank my doctoral committee members past and present, Dr. Schaak, Dr. Sen, Dr. Song and Dr. Weinreb, for helpful suggestions and guidance during the various exams and presentations, and for all the insightful comments on this dissertation.

Having spent a good part of six years in lab, I feel really lucky to have met an incredible group of colleagues both in chemistry as well as chemical engineering departments. A special shout out to Kyle Reichl, Nicole Dunn and Wei Zhao the first students of the Radosevich group who were a constant source of encouragement and a good sounding board for discussing new research ideas. I would also like to thank Dr. Nick Sturgis for teaching me all about designing and fabricating flow reactors, Dr. Ji Woong Chang for introduction to ITC and Dr. Choumini Balasanthiran and Dr. Sem Tamang for introduction to nanomaterial synthesis. I would be remiss

if I did not acknowledge the tremendous help of Anirudh Nambiar and Suprita Jharimune in designing and executing experiments that are an integral part of this dissertation.

I would like to thank all the wonderful friends I've made over the course of my time in State College who provided an outlet for all the frustrations research can present one with. Pradeep, Vaibhav, Saurabh, Anirudh, Ozgur and Fatma thanks for all the memories! I would also like to thank Drs. Anil and Shama Kulkarni, who welcomed me into their home during my first few weeks in State College.

Most importantly I would like to thank my parents Arun and Hemalata Sathe, my sister Anita and my grandparents for their unconditional love and support and for helping me become the person I am today. They taught me at a young age to give my best to whatever enterprise I undertake. My sister has been a constant source of inspiration and has always pushed me to explore new things. She and my brother-in-law Narendra Kulkarni were largely instrumental in my training for a half marathon; a feat I never dreamed would be possible!

Lastly I would like to thank my wife Dr. Gautami Newalkar who has been there for me through the ups and downs, during the course of this PhD, and has tolerated all the temper tantrums during the writing of this dissertation. Thank you for all the love, support and encouragement! I cannot wait to start the next phase of my life with you. There is no one else I would rather grow old with, I love you!

Ajay Sathe

August 28, 2016

Chapter 1

Use of CO_2 and Continuous Flow Methods in Organic Chemistry

In a world of finite resources, the design of chemical processes that promote the use of renewable resources, minimize material and energy waste and eliminate the use of hazardous substances is the fundamental requirement of sustainable chemical conversion. To this end use of catalysts, non-fossil fuel based chemical feedstocks, and reaction sequences that are efficient in atom and step economy are of great importance. Carbon dioxide is a good candidate for a cheap and sustainable source of carbon feedstock. This chapter reviews the use of carbon dioxide as a C-1 synthon in the synthetic organic chemistry laboratory. Additionally, flow chemistry has emerged as a powerful tool in the synthetic chemist's repertoire as it improves safety, speed and efficiency in the design and development of new chemical processes. Reviewed here are some of the recent advances in the field of flow chemistry and how they help to push the boundaries of traditional synthetic organic chemistry.

1.1 Carbon Dioxide- A cheap and sustainable synthon

Fossil fuels are the major source of energy for all of mankind. An inevitable outcome of this is the production of large amount of carbon dioxide, which has been implicated as the major contributor to climate change. Carbon dioxide is a cheap, renewable, non-toxic, and widely available carbon source, and offers a possibility of establishing a renewable carbon economy.[1-2] The incentive to use CO_2 to make useful commodity chemicals has never been higher, as it allows for a sustainable strategy to help mitigate its growing atmospheric levels. The current industrial utilization of CO_2 as a carbon synthon is around 200 Mt/y, which represents less than 1% of the

global anthropogenic emissions.[3] Urea production represents the single largest use of CO_2 as an industrial carbon source, with the process consuming about 120 Mt/y. Other important products made using CO_2 are inorganic carbonates and pigments, methanol, salicylic acid, and organic carbonates. Additionally, around 28Mt/y is used as a technological fluid.[4]

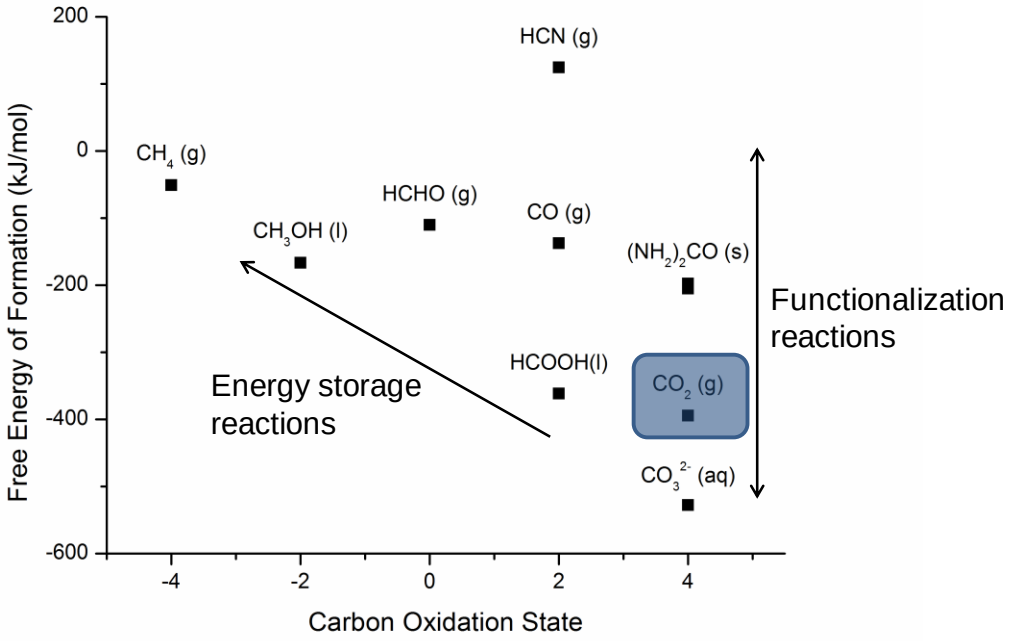

Figure 1.1. Energy of formation of various C-1 compounds vs carbon oxidation state.[4]

The major challenge in utilizing CO_2 as a carbon source, via reduction, is its high thermodynamic and kinetic stability (ΔH_f = -393.51 kJ/mol, $E^o_{CO_2/CO_2^-}$ = -1.90V),[3] which require a huge energy input for transforming CO_2 into other molecules.[5] Because of this inherent barrier, an approach that does not involve the formal reduction of the carbon oxidation state is better suited for rapid large scale adoption. Such reactions can be thought of as functionalization reactions and those that involve a reduction in oxidation state as energy storage reactions (Figure 1.1). Most of the reactions relevant to synthetic organic chemistry are of the functionalization type; however a few

recent studies exploring the possibility of reduction of CO_2 and simultaneous functionalization have been reported.[6-8]

1.2 Strategies for use of CO_2 in synthetic organic chemistry

Two distinct strategies can be envisioned for tackling the inherent inertness of the CO_2. The first is to use high energy reaction partners which compensate for the low energy of CO_2, and the second is to activate the CO_2 molecule by reaction with metal catalysts (Figure 1.2).

The four major binding modes of CO_2 to metals are described in Figure 1.2 a. The η^1-C binding mode is preferred by electron rich metal centers, and arises from the charge transfer between the d_z^2 metal orbitals to the π^* orbital of CO_2. The η^2-C,O bonding arises due to the donation from the filled π orbital of CO_2 into the empty d orbital on the metal, and subsequent back bonding between the filled metal orbitals and empty π^* orbital on CO_2. The η^1-O binding is less stable and is preferred by electron poor metals. The η^2-O, O binding can be thought of as a metal carboxylate and is usually encountered with electron poor and highly electropositive metals.

Once coordinated to the metal the synthetic utility of CO_2 is only apparent when a new bond is formed between the central carbon and a suitable nucleophile. Such reactions have been demonstrated using either catalytic or stoichiometric amounts of organometallic complexes. The most common reactions are those involving carbon, nitrogen or oxygen nucleophiles.

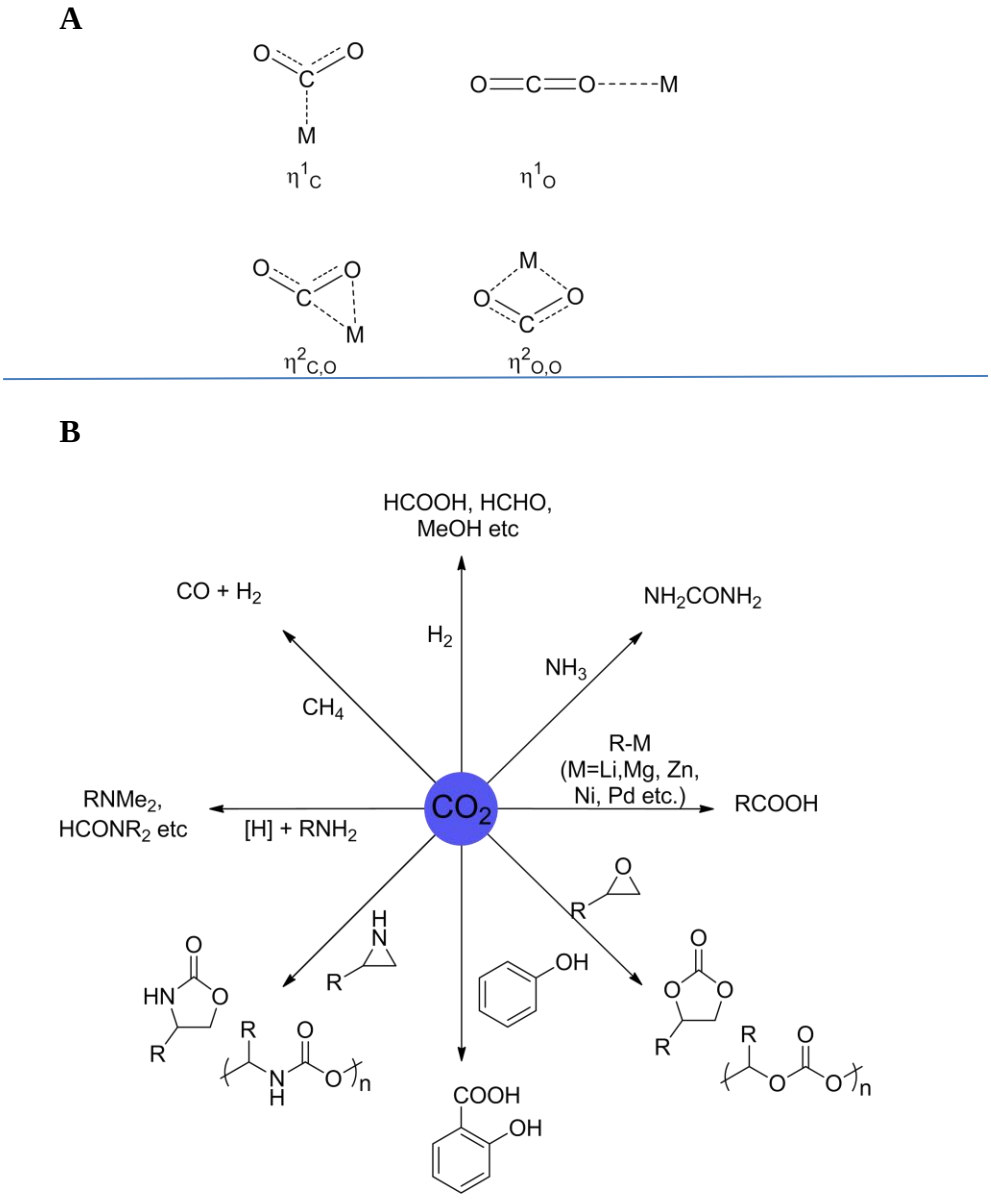

Figure 1.2. Strategies for the use of CO_2 in organic synthesis A: Activation via co-ordination of CO_2 to metals,[9] B: Reaction with high energy reaction partners

1.2.1 Transformations forming new C-C bonds.[10]

The reaction of CO_2 with carbon nucleophiles such as organomagnesium (Grignard reagents) or organolithium reagents is one of the most classical reactions of synthetic organic chemistry for the synthesis of carboxylic acids. The current industrial synthesis of salicylic acid derivatives exemplifies this reaction paradigm. These compounds are highly reactive owing to the polarity of the carbon-metal (Li, Mg, Na etc.) bond. While this allows a very facile reaction with CO_2, it also limits the functional groups that can be tolerated in the backbone resulting to limited applicability. On the other hand boronic esters can be prepared from readily available starting materials, and many are commercially available due to the advances in cross coupling chemistry. They are weaker nucleophiles compared to organolithium or organomagnesium reagents, and as such can tolerate the presence of other functional groups (like carbonyl, halogens, esters etc.) during their synthesis. These compounds have been shown to undergo efficient carboxylation in the presence of Rhodium[11] and Copper[12-13] catalysts. These reactions require the use of a butoxide base to activate the boronic ester for reaction with CO_2. Similarly, the coupling of organozinc reagents with CO_2 was demonstrated by the use of low valent nickel and palladium catalysts.[14-15]

While these examples show an expanded tolerance to various functional groups, they still require the preformation of organoboron or organozinc reagents. A significant advance in the synthesis of carboxylic acids using CO_2 is the ability to carboxylate unfunctionalized acidic C-H bonds. The carboxylation of alkynes or electron poor heteroaromatic has been successfully demonstrated using copper,[16-17] silver,[18] gold[19] or palladium[20] catalysts.

The carboxylation reactions discussed above are the result of insertion of CO_2 in a high valent transition metal-carbon bond, another class of reactions is the metal catalyzed couplings of CO_2 with unsaturated compounds, catalyzed by low valent transition metals (Figure 1.3). These reactions were developed following the isolation and characterization of the first metal CO_2 complex

by Aresta.[21] While the first reports relied on stoichiometric amount of Ni(0) complexes,[22-23] significant progress has been made in development of catalytic reactions.[24-27] These oxidative coupling reactions are usually only feasible with molecules containing highly delocalized π systems such as those found in dienes and diynes.

Figure 1.3. Common reaction manifolds for the C-C bond forming reactions using CO_2

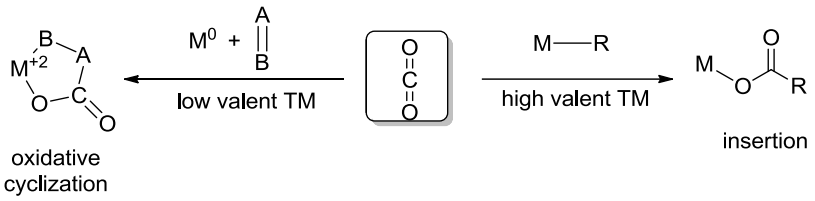

1.2.2 Transformations forming new C-N bonds

Like carbon nucleophiles carbon dioxide can also react with nitrogen containing nucleophiles generating highly functionalized and widely used chemical feedstocks (Figure 1.4).[28] The most prominent example is the industrial synthesis of urea using CO_2 and ammonia, which represents the single largest industrial process consuming CO_2.[4] The process consists of formation of ammonium carbamate which is subsequently dehydrated to yield the urea. Substituted ureas can be prepared in a similar fashion using alkyl amines.[29-31]

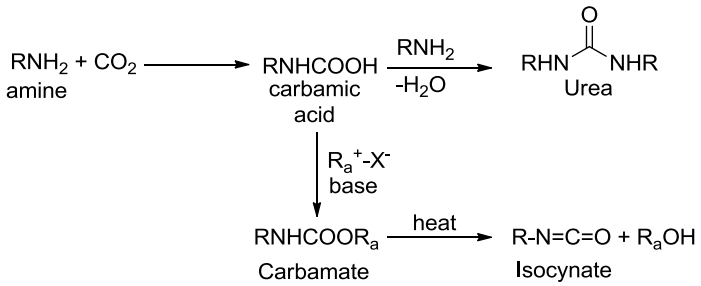

Figure 1.4. Various products from the reaction of CO_2 with amines.

Instead of dehydration, the ammonium carbamates (or carbamic acids) can be alkylated using various electrophiles to produce carbamates (or urethanes).[32,33-36] These urethanes can be further subjected to thermolysis to yield isocyanates.[37] Lastly CO_2 can react with aziridines[38] or amino alcohols[39] to yield oxazolidinones which are important fine chemical intermediates.

1.2.3 Transformations forming new C-O bonds

The reaction of CO_2 with oxygen nucleophiles is also widely studied.[40] Particularly the highly atom economic reaction between epoxides and carbon dioxide has been the subject of a lot of catalyst development, and has found commercial applications for the production of ethylene, propylene and dimethyl carbonates. The reaction between epoxides and CO_2 is usually catalyzed by a combination of Lewis acid and base catalysts, where in the Lewis acid activates the epoxide and the Lewis base aids to activate the carbon dioxide molecule. Amongst the most studied catalysts are the salen complexes of aluminum,[41-42] nickel,[43] copper,[44], cobalt,[45-48] chromium,[49-51] or manganese.[52-53]

Recently the Kleij group has reported on an aluminum complex based on an amiotrisphenolate ligand that is highly active not only for carboxylation of epoxides but also oxetanes.[54] The developed catalysts also showed remarkable activity for sterically hindered epoxides which are traditionally hard to carboxylate.

Acyclic or linear carbonates are another important class of molecules. They are currently utilized in the production of polycarbonates, and as electrolytes in Li-ion batteries. The linear carbonates can be produced by the reaction of CO_2 with alcohols such as methanol and ethanol, followed by dehydration. This route is highly energy intensive and the use of stoichiometric dehydration agents makes its commercialization difficult. Alternatively the liner carbonates are made

by alcoholysis of ethylene or propylene carbonate, and the by-product ethylene or propylene glycol is also an industrially important compound.

Apart from the inherent thermodynamic and kinetic barriers to the use of CO_2 in routine organic synthesis, another limiting factor is the mass transfer of CO_2 from the gas phase into the liquid phase, which is most commonly employed for carrying out organic transformations. This necessitates the need for use of high pressures to increase the solubility of the gas and consequently specialized and oft times expensive equipment is needed. Continuous flow technology can provide significant advantages for gas liquid systems as they can provide a high interfacial area for the contact between the two phases. The next section describes the rapidly growing field of continuous flow organic synthesis.

1.3 Flow chemistry as a new enabling technology for organic chemistry

Organic synthesis has been conventionally carried out in batch reactors such as flasks, test-tubes and pressure vessels, while on the other hand the manufacture of commodity chemicals has been almost exclusively carried out in continuous flow mode. Recently scaled down versions of these flow systems have become widely available to the synthetic chemist, partly due to advances in precision machining and fabrication. These systems offer superior control over mass and energy (heat and light) transfer, allow the controlled use of highly reactive or toxic substances and make the scale up trivial by running multiple reactors in parallel or increasing the rector dimensions while keeping the system variables similar. Most of these advantages come from the improved surface to volume ratio of the reactants made possible by the small dimensions of the reactor. Depending on the internal dimensions of the reactor they are classified as micro (10-500 μm) or milli or mesofluidic (500 μm to several mm) reactors. The micro reactors provide a superior surface to volume, but are more prone to clogging and require involved machining for fabrication. On the other hand meso or millifludic reactors are easier to construct using commercially available components.

A typical flow reactor can be assumed to be a combination of several batch reactors connected in series, such that the instantaneous concentration of the reactant (or product) remains constant at a given point (spatially) in the reactor (Figure 1.5). For comparison, in a reaction with typical first order kinetics, the concentration in a batch reactor reduces exponentially with time, in a flow reactor however this decay is exponentially related to the distance along the reactor from the inlet.

This distinction becomes particularly useful when studying kinetics of a reaction, as you can use the same reaction stream and analyze along various points spatially in the reactor (using in situ spectroscopy) to get snapshots of the reaction at various time points. This allows for significant reduction in the quantity of materials required for reaction optimization.

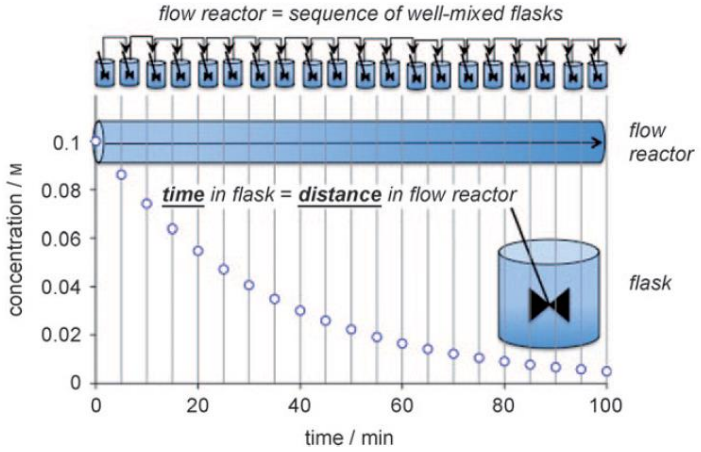

Figure 1.5. Flow reactor as a summation of differential batch reactors.[55]

Figure 1.6 shows a schematic of a generalized flow reactor set-up. The reagents are typically introduced into the system via the use of pumps (HPLC, syringe, peristaltic etc.). These are mixed together using a T-mixer or in-line static mixers and then introduced into a thermostated reactor, which is usually a piece of tubing or pre-etched channels on a support plate. The reactor tubing can be made out of a variety of materials such as glass, metal, or polymers depending on the kind of chemistry being explored. The output of the reactor can be fed to an online spectroscopy device which feeds real time monitoring data into a computer which can in turn adjust the reagent and recycle flow rates.

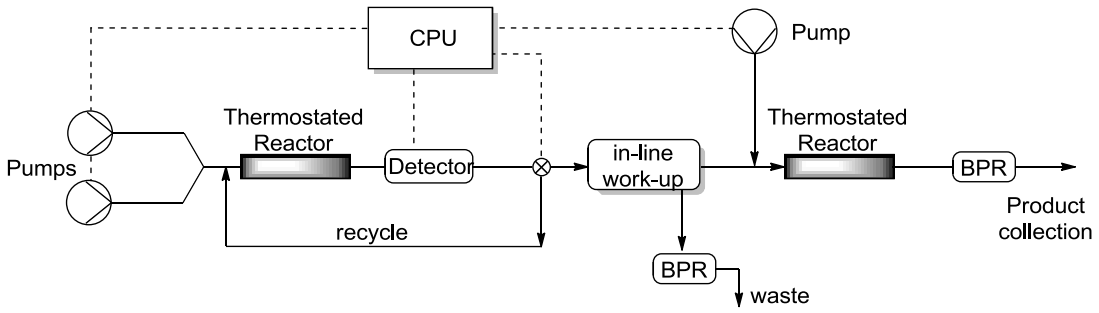

Figure 1.6. Generalized flow reactor configuration

The outlet stream from the detector device could be connected to an in-line work-up device for product separation and purification. This set-up can then be connected to another pump (input

device) for multistep synthesis, or a product collection vessel. Lastly, one can employ back pressure regulators at the exit streams to manipulate the pressure (and boiling points of the solvents for superheating) for more aggressive reaction chemistries. Since each component of the flow setup performs a specific function, they can be used as very modular "Lego blocks" to construct more complex reaction networks.

1.3.2 Unit operations in flow

One of the major considerations while designing multistep sequences in flow is the work-up or processing of the effluent coming out of one reactor before being passed on to the next. While traditional batch chemistries rely on robust and standard equipment like separatory funnels, rotary evaporators, filtration funnels for work-up and product purification, new technology has to be developed in order to carry out these processes in flow. Reviewed here is the current state of the art of in-flow downstream processing techniques.

1.3.2.1 Distillation

Separation of liquid mixtures or solvent switching is routinely carried out in organic synthesis. This is usually achieved by distilling off one of the components of the mixture and adjusting the final composition of the reaction mixture as required. The technologies developed for continuous flow distillation (or solvent evaporation) all employ a gas stream which helps to vaporize one of the components of the liquid mixture.

The device developed by Jensen and co-workers utilizes a microfluidic platform which incorporates a thermostat allowing for temperature control during the separation. The liquid stream was contacted with the gas stream before passing through a serpentine capillary pattern in which was

vapor-liquid equilibrium is established using segmented flow. This segmented flow then reaches a PTFE membrane which separates the gas and liquid streams thus realizing distillation (Figure 1.7).[56]

This device was later utilized in the multi-step Heck coupling. The process consisted of conversion of phenol to aryl triflate, and coupling of the triflate with n-butyl vinyl ether. The distillation device was used to switch out the chlorinated solvent used in the first step with DMF for the heck coupling. [57]

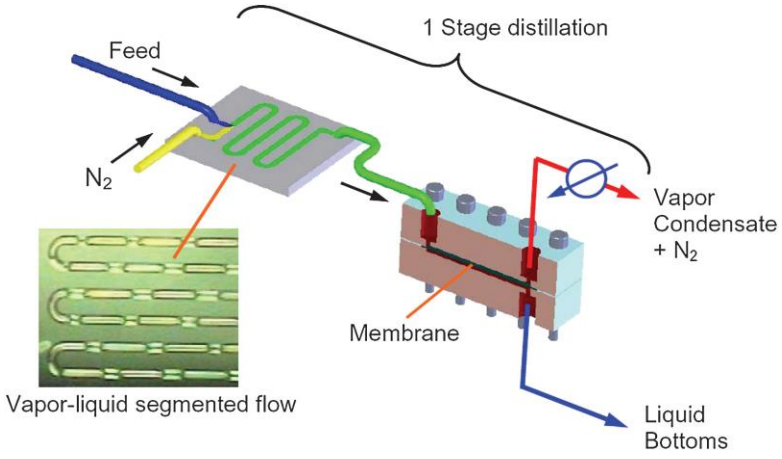

Figure 1.7: In-flow microfluidic continuous solvent evaporator using gas liquid segmented flow.[56]

On the other hand Ley and co-workers have developed a meso scale in-line evaporation device using commonly available fittings and materials. Their device acts as a spray drier for an incoming liquid stream. It consists of a nebulizing gas inlet connected with a T-junction to the incoming liquid stream, which leads to the evaporation of the solvent. The gas stream exits the device and can be connected to a condenser to recovery the evaporated solvent for recycle or reuse. The concentrated liquid stream can be modified by addition of suitable solvent leading to either concentration of the product or complete solvent switch. This device was used to switch solvents from methanol to toluene during the flow synthesis of Melinertant (SR48692).[58]

1.3.2.2 Extraction

One of the most common work-up techniques involve quenching or washing of the reaction mixture using various aqueous reagents. This necessitates the use of liquid-liquid extraction and separation techniques, such as the use of separatory funnels. In flow systems two approaches have been utilized to accomplish this.

The first one uses machine vision, pumps and a computer program to achieve separation of the aqueous and organic phases (Figure 1.8). The biphasic reaction mixture from the outlet of the reactor is fed into a chamber which contains a colored float which rests at the interface of the two phases and helps identify the relative position of the interface which can be read by a webcam. The position data from the webcam is processed by a computer which then adjusts the flow rate of the aqueous and organic effluent streams thus enabling efficient separation.[59]

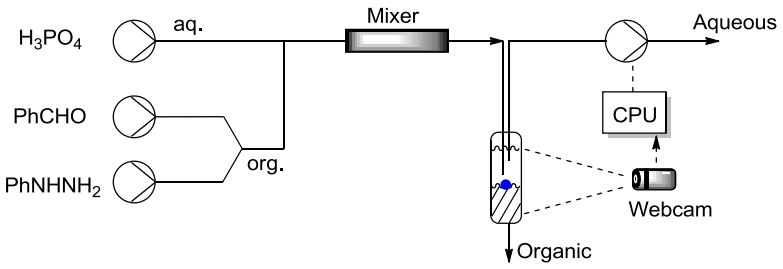

Figure 1.8: Using machine vision for continuous liquid-liquid extraction and separation.[59]

The second approach involves the use of a hydrophobic PTFE membrane which is selectively wet by the organic phase and does not let the aqueous phase pass through. The device also incorporates a pressure control mechanism which maintains the pressure difference across the membrane such that there is minimal breakthrough of the aqueous phase.[60-61] The fluidic connections to the device are made using standard flat bottom fittings. This device is now commercially available from Zaiput flow technologies.

1.3.2.3 Filtration

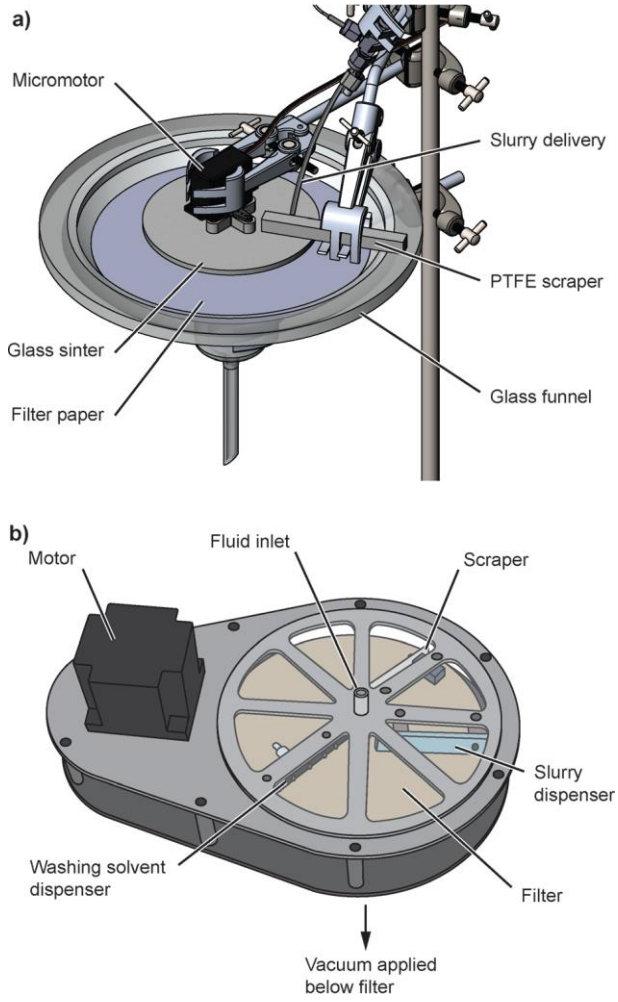

Figure 1.9: Devices for in-line continuous flow filtration.[62-63]

The formation or use of solids is inevitable while carrying out organic synthesis and hence the separation of the solids from the rest of the reaction mixture becomes important. Depending on the identity of the solids the filtration process can be carried out for the collection of liquid (filtrate) or the collection of the solids (residue) for further processing.

Two techniques have been described for continuous in-flow filtration. The first one (Figure 1.9 a) uses a rotating sintered glass disk which serves as the filter media. The slurry is passed over

this disk, and a PTFE scraper attachment removes the solids while the liquid is able to drip through for collection. This was utilized in a system which required the separation of waste salts from the reaction mixture for the next step of the multistep reaction sequence.[62]

The second device (Figure 1.9 b) uses a rotating filter with a vacuum on the other side for fast separation. This device was utilized in the continuous manufacturing of pharmaceuticals including API synthesis, purification and tableting.[63]

1.3.2.4 Chromatography

Chromatographic separation of reaction mixtures represents one of the most time and labor intensive operation in the synthetic organic chemistry laboratory. While a variety of automated systems have been developed to aid the researchers (Biotage, Teledyne Isco, Buchi), these systems cannot be modified for continuous flow applications.

Simulated Moving Bed Chromatography (SMBC) is a form of continuous counter-current chromatography used industrially can be applied for flow chemistry in lab. SMBC employs four zones of columns connected in series with fluid connections at each vertex (Figure 1.10). A relative flow between the stationary and mobile phase is simulated by periodically shifting the two inlet and outlet ports in the direction of the mobile phase flow after a certain time, known as the shift time. The crude reaction mixture and eluent are fed at the opposite end of the system, and the strongly adsorbed and weakly adsorbed fractions are collected at the remaining two positions.

The switch time is adjusted such that the “simulated” rate of stationary phase flow is faster than the rate of elution of the strongly adsorbed component, but slower than the rate of elution of weakly adsorbed component.

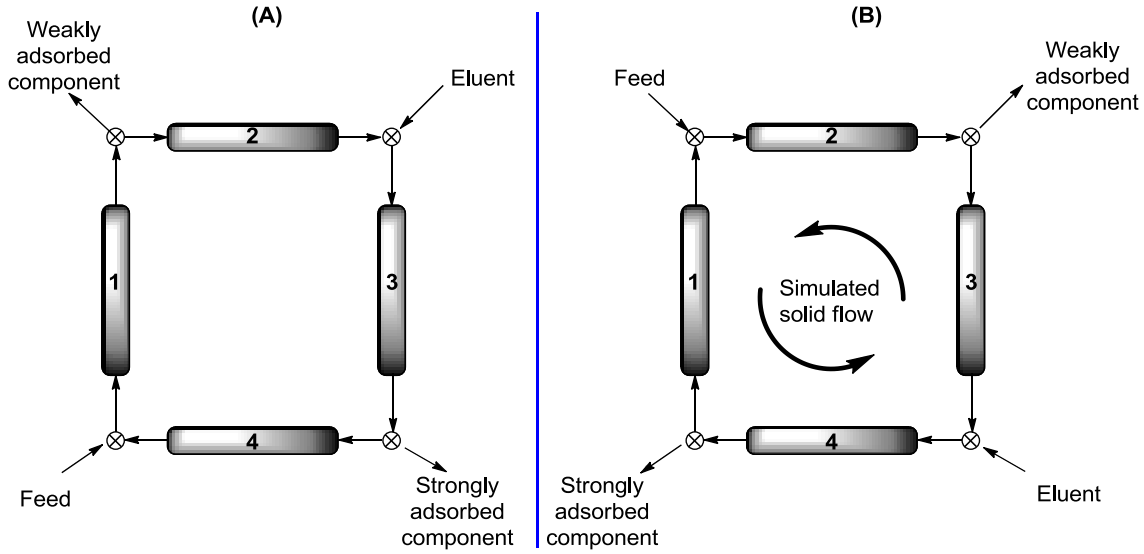

Figure 1.10. General operating principle of simulated moving bed chromatography.

1.3.3 Advantages of Flow Chemistry over Batch

Flow systems help close the gap between bench top chemistry and process chemistry, by mimicking large scale production on the laboratory scale.[64] The basic variables that make scale up such a challenging task are heat, mass transfer and kinetic profiles. Due to the inherent design of flow reactors, these remain largely unchanged with scale allowing for scale-up with minimal or no process development work. Additionally, the throughput of a process developed in flow can be increased by just "numbering up" which is running multiple reactor setups in parallel. This obviates the need for any additional optimization.

In addition to the benefits due to physical properties like increased surface to volume ratios, flow systems also enable new chemistries to be explored by expanding the process windows available for carrying out organic transformations. The term "New Process Windows" was coined in 2007 by the German Environmental Agency, and was defined as "the use of process conditions far from conventional practices".[65]

One of the most common ways to access the conditions is by the use of a back pressure regulator at the end of the flow reactor sequence. The increase in pressure allows for reactions to be carried out at temperatures far beyond the boiling point of the solvent involved in the reaction. This was shown in the methylation reaction of phenolic compounds using dimethyl carbonate where the use of higher temperature in a flow reactor allowed for catalytic use of base and significantly lower reaction times for comparable yields (Figure 1.11).[66-67] The increasing pressure and temperature also allow the use of supercritical fluids as solvents for organic transformations, and the use of micro reactors reduces the hazards of handling these supercritical fluids in high volumes.[68-69]

Figure 1.11. Process intensification allows for catalytic use of base and shorter reaction times.[67]

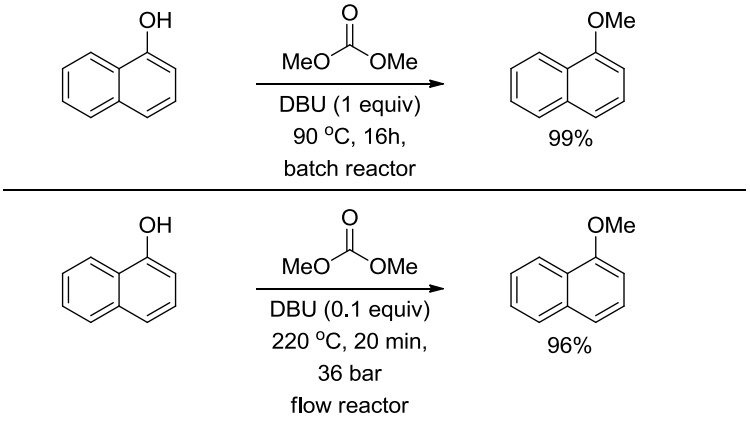

Since the dimensions of the flow reactors are usually smaller than the corresponding batch reactors only μL quantities of reagents are exposed to one another at a given time. This makes the operation of such reactors much safer as the hazards of reactor failure are low. This significantly reduces the risk in the use of hazardous or toxic chemicals, allowing for the use of fluorine gas,[70] azides[71-72] or diazo compounds[73-74] with ease. Another example is the "on-demand" generation and use of diazomethane, a highly useful but toxic and explosive compound.[75]

Flow systems also provide better control over the reaction temperatures due to a high surface to volume ratio. This is especially crucial while conducting highly exothermic reactions which can

lead to runaway if not properly thermostated. Nitration reactions are one such example. The high heat of the reaction combined with the fact that nitration reactions are typically carried out using a two phase aqueous-organic system, both heat and mass transfer issues become significant when carrying out this reaction. The use of flow reactors have been shown to be particularly useful in this regard especially in large scales.[76-78]

In addition to the exquisite temperature control, flow reactors also allow for precise control over the reaction time. This is usually achieved by manipulating the length of the reactor tubing (or channels) or varying the flow rate of the reagents. This opens up the field of flash chemistry, where extremely fast reactions are carried out in a controlled manner, to produce the desired compounds with high selectivity.[79-81]

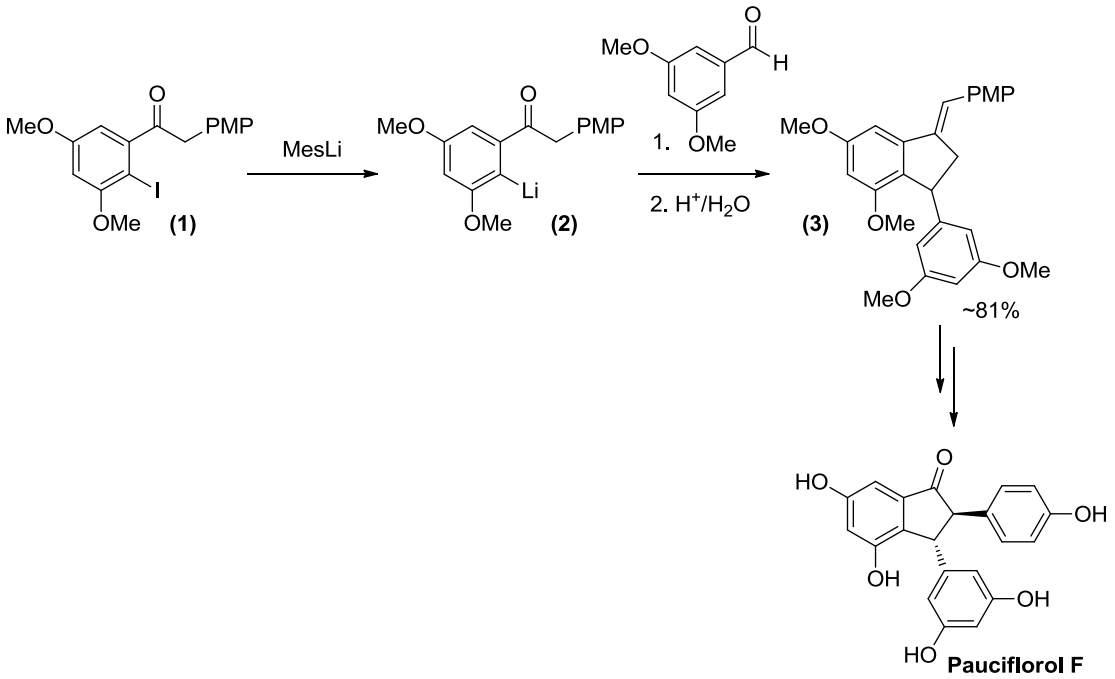

Figure 1.12. Protecting group free synthesis of Pauciflorol F enabled by flow microreactors.[82]

An elegant use of this principle was demonstrated in the protecting group free synthesis of Pauciflorol-F by the Yoshida group (Figure 1.12).[82] Organolithium reagents are highly reactive, and their addition to carbonyl compounds is one of the most basic reactiolns taught in introductory organic chemistry courses. Subsequently, halogen metal exchange reactions using organolithium reagents require all carbonyl groups to be protected prior to the reaction. The Yoshida group carried out the Iodine-Lithium exchange reaction of the ketone (1) to generate the aryl lithium without protection of the carbonyl group. They further reacted this aryl lithium with 3,5-dimethoxybenzaldehyde to yield product (3) after aqueous work up in 81% yield. This was made possible by a residence time of only 0.003s for the halogen metal exchange reaction. The construction of complex organic frameworks without the use of protecting groups is especially important from the point of view of green and sustainable synthesis,[83] as it enables improved atom economy,[84] step economy,[85] and redox economy.[86]

In line with the role of flow chemistry in aiding sustainable synthesis, is its ability to enable safe and practical options for handling of gases. Gases such as CO, NH_3, CH_4, CO_2, H_2, and O_2 are amongst the most widely available and atom economic sources of most of the elements that make up organic molecules. Indeed one can trace the industrial origin of most of the chemical used in a synthetic organic chemistry laboratory to these gases.[87] The use of flow reactors allows the synthetic chemist to replicate the conditions applied in the industry on scales that are manageable at the bench top level. Additionally, the use of mass flow controllers and other metering devices, enable the precise control over the stoichiometry of the gases being injected in the reaction mixture, something that is not easily achievable in a batch process. The two most common ways of contacting gases and liquids in a flow mode are either introducing them in a single tube or channel in a “plug flow” mode or in a specially designed membrane reactor.[88]

Finally, flow processes are highly amenable towards automation and self-optimization and discovery. By using an inline detector with a flow reactor, it is possible to measure the extent of a

reaction in situ. This information can be fed to a computer program which, based on statistical tools, can alter the input to the reactor (either stoichiometry or physical variables like time, temperature and pressure) there-by self-optimizing the reaction parameters.[89-90]

1.5 Conclusions

While the co-ordination of the CO_2 molecule to a metal center represents an "activation" of CO_2, as evidenced by the increasing bond length and distortion in the OCO bond angle,[9] such activation does not always yield intermediates potent for further conversion. This is usually due to the high energy of the bonds formed with the metal center. As a consequence, in most of the coupling reactions (forming C-C, C-N or C-O bonds), the metal catalyst (or promoter) serves to activate the coupling partner, forming a transient organometallic species, and making the CO_2 molecule accessible by co-ordination, facilitating its reaction. Such transformations are not explicitly dependent on the activation by pre co-ordination of the CO_2 to the metal center. However, the activation by pre-coordination becomes important when conversion to CO or other energy storing reactions are considered, where the C=O bond is broken.

While flow processes have been a mainstay of high volume chemical manufacturing, they are slowly starting to make way in the laboratory of the synthetic chemist. Further development in the devices for discreet unit operations coupled with the rapid development in prototyping and fabrication will enable widespread use of this technology.

The following two chapters describe orthogonal strategies for the utilization of CO_2 in organic synthesis by employing reductive and oxidative processes on common organic substrates like imines and olefins (Figure 1.13). The use of flow reactors to couple two reactions containing mutually incompatible reagents is also described. We believe that the work described here can serve to inspire future development in the use of CO_2 and flow chemistry for environmentally benign and sustainable chemical synthesis.

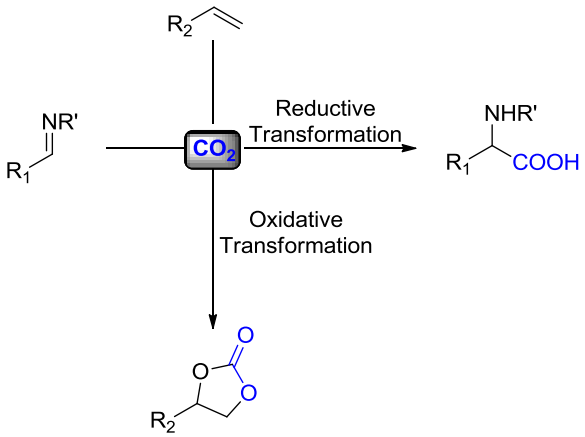

Figure 1.13. Orthogonal strategies for the utilization of CO_2 in organic synthesis.

1.4 References

1. Olah, G. A.; Goeppert, A.; Prakash, G. K. S., *J. Org. Chem* **2009,** *74* (2), 487-498.
2. Olah, G. A., *Angew. Chem. Int. Ed.* **2005,** *44* (18), 2636-2639.
3. Aresta, M.; Dibenedetto, A., *Dalton Trans.* **2007,** (28), 2975-2992.
4. Aresta, M.; Dibenedetto, A.; Angelini, A., *Chem. Rev.* **2014,** *114* (3), 1709-1742.
5. Benson, E. E.; Kubiak, C. P.; Sathrum, A. J.; Smieja, J. M., Chem. Soc. Rev. 2009, 38 (1), 89-99.
6. Jacquet, O.; Frogneux, X.; Das Neves Gomes, C.; Cantat, T., *Chem. Sci.* **2013,** *4* (5), 2127-2131.
7. Das Neves Gomes, C.; Jacquet, O.; Villiers, C.; Thuéry, P.; Ephritikhine, M.; Cantat, T., *Angew. Chem. Int. Ed.* **2012,** *51* (1), 187-190.
8. Li, Y.; Fang, X.; Junge, K.; Beller, M., *Angew. Chem. Int. Ed.* **2013,** *52* (36), 9568-9571.
9. Gibson, D. H., *Chem. Rev.* **1996,** *96* (6), 2063-2096.
10. Huang, K.; Sun, C.-L.; Shi, Z.-J., *Chem. Soc. Rev.* **2011,** *40* (5), 2435-2452.
11. Ukai, K.; Aoki, M.; Takaya, J.; Iwasawa, N., *J. Am. Chem. Soc.* **2006,** *128* (27), 8706-8707.
12. Takaya, J.; Tadami, S.; Ukai, K.; Iwasawa, N., *Org. Lett.* **2008,** *10* (13), 2697-2700.
13. Ohishi, T.; Nishiura, M.; Hou, Z., *Angew. Chem. Int. Ed.* **2008,** *47* (31), 5792-5795.
14. Ochiai, H.; Jang, M.; Hirano, K.; Yorimitsu, H.; Oshima, K., *Org. Lett.* **2008,** *10* (13), 2681-2683.
15. Yeung, C. S.; Dong, V. M., *J. Am. Chem. Soc.* **2008,** *130* (25), 7826-7827.
16. Boogaerts, I. I. F.; Fortman, G. C.; Furst, M. R. L.; Cazin, C. S. J.; Nolan, S. P., *Angew. Chem. Int. Ed.* **2010,** *49* (46), 8674-8677.
17. Zhang, L.; Cheng, J.; Ohishi, T.; Hou, Z., *Angew. Chem. Int. Ed.* **2010,** *49* (46), 8670-8673.

18. Zhang, X.; Zhang, W.-Z.; Ren, X.; Zhang, L.-L.; Lu, X.-B., *Org. Lett.* **2011,** *13* (9), 2402-2405.

19. Boogaerts, I. I. F.; Nolan, S. P., *J. Am. Chem. Soc.* **2010,** *132* (26), 8858-+.

20. Sasano, K.; Takaya, J.; Iwasawa, N., *J. Am. Chem. Soc.* **2013,** *135* (30), 10954-10957.

21. Aresta, M.; Nobile, C. F.; Albano, V. G.; Forni, E.; Manassero, M., *J. Chem. Soc., Chem. Commun.* **1975,** (15), 636-637.

22. Steiniger, M.; Schäfer, H. J., *Angew. Chem.* **1982,** *94* (1), 75-76.

23. Hoberg, H.; Peres, Y.; Krüger, C.; Tsay, Y.-H., *Angew. Chem.* **1987,** *99* (8), 799-800.

24. Takimoto, M.; Mori, M., *J. Am. Chem. Soc.* **2002,** *124* (34), 10008-10009.

25. Takimoto, M.; Nakamura, Y.; Kimura, K.; Mori, M., *J. Am. Chem. Soc.* **2004,** *126* (19), 5956-5957.

26. Ogoshi, S.; Ikeda, H.; Kurosawa, H., *Pure Appl. Chem.* **2008,** *80* (5), 1115-1125.

27. Behr, A.; Juszak, K.-D., *J. Organomet. Chem.* **1983,** *255* (2), 263-268.

28. Yang, Z.-Z.; He, L.-N.; Gao, J.; Liu, A.-H.; Yu, B., *Energy & Environmental Science* **2012,** *5* (5), 6602-6639.

29. Nomura, R.; Hasegawa, Y.; Ishimoto, M.; Toyosaki, T.; Matsuda, H., *J. Org. Chem* **1992,** *57* (26), 7339-7342.

30. Tai, C.-C.; Huck, M. J.; McKoon, E. P.; Woo, T.; Jessop, P. G., *J. Org. Chem* **2002,** *67* (25), 9070-9072.

31. Shi, F.; Deng, Y.; SiMa, T.; Peng, J.; Gu, Y.; Qiao, B., *Angew. Chem. Int. Ed.* **2003,** *42* (28), 3257-3260.

32. McGhee, W. D.; Riley, D. P., *Organometallics* **1992,** *11* (2), 900-907.

33. Abla, M.; Choi, J.-C.; Sakakura, T., *Green Chem.* **2004,** *6* (10), 524-525.

34. Srivastava, R.; Manju, M. D.; Srinivas, D.; Ratnasamy, P., *Catal. Lett.* **2004,** *97* (1), 41-47.

35. Yoshida, M.; Hara, N.; Okuyama, S., *Chem. Commun.* **2000,** (2), 151-152.

36. Salvatore, R. N.; Shin, S. I.; Nagle, A. S.; Jung, K. W., *J. Org. Chem* **2001,** *66* (3), 1035-1037.

37. Valli, V. L. K.; Alper, H., *J. Org. Chem* **1995,** *60* (1), 257-258.

38. Sudo, A.; Morioka, Y.; Sanda, F.; Endo, T., *Tetrahedron Lett.* **2004,** *45* (7), 1363-1365.

39. Bhanage, B. M.; Fujita, S.-i.; Ikushima, Y.; Arai, M., *Green Chem.* **2003,** *5* (3), 340-342.

40. North, M.; Pasquale, R.; Young, C., *Green Chem.* **2010,** *12* (9), 1514-1539.

41. Alvaro, M.; Baleizao, C.; Carbonell, E.; El Ghoul, M.; García, H.; Gigante, B., *Tetrahedron* **2005,** *61* (51), 12131-12139.

42. Clegg, W.; Harrington, R. W.; North, M.; Pasquale, R., *Chem. Eur. J.* **2010,** *16* (23), 6828-6843.

43. Lu, X.-B.; Feng, X.-J.; He, R., *Appl. Catl. A* **2002,** *234* (1–2), 25-33.

44. Shen, Y.-M.; Duan, W.-L.; Shi, M., *J. Org. Chem* **2003,** *68* (4), 1559-1562.

45. Lu, X.-B.; Xiu, J.-H.; He, R.; Jin, K.; Luo, L.-M.; Feng, X.-J., *Appl. Catl. A* **2004,** *275* (1–2), 73-78.

46. Paddock, R. L.; Nguyen, S. T., *Chem. Commun.* **2004,** (14), 1622-1623.

47. Lu, X.-B.; Liang, B.; Zhang, Y.-J.; Tian, Y.-Z.; Wang, Y.-M.; Bai, C.-X.; Wang, H.; Zhang, R., *J. Am. Chem. Soc.* **2004,** *126* (12), 3732-3733.

48. Miao, C.-X.; Wang, J.-Q.; Wu, Y.; Du, Y.; He, L.-N., *ChemSusChem* **2008,** *1* (3), 236-241.

49. Paddock, R. L.; Nguyen, S. T., *J. Am. Chem. Soc.* **2001,** *123* (46), 11498-11499.

50. Alvaro, M.; Baleizao, C.; Das, D.; Carbonell, E.; García, H., *J. Catal.* **2004,** *228* (1), 254-258.

51. Ramin, M.; Jutz, F.; Grunwaldt, J.-D.; Baiker, A., *J. Mol. Catal. A: Chem.* **2005,** *242* (1–2), 32-39.

52. Jutz, F.; Grunwaldt, J.-D.; Baiker, A., *J. Mol. Catal. A: Chem.* **2008,** *279* (1), 94-103.

53. Jutz, F.; Grunwaldt, J.-D.; Baiker, A., *J. Mol. Catal. A: Chem.* **2009,** *297* (2), 63-72.

54. Whiteoak, C. J.; Kielland, N.; Laserna, V.; Escudero-Adán, E. C.; Martin, E.; Kleij, A. W., *J. Am. Chem. Soc.* **2013,** *135* (4), 1228-1231.

55. Valera, F. E.; Quaranta, M.; Moran, A.; Blacker, J.; Armstrong, A.; Cabral, J. T.; Blackmond, D. G., *Angew. Chem. Int. Ed.* **2010,** *49* (14), 2478-2485.

56. Hartman, R. L.; Sahoo, H. R.; Yen, B. C.; Jensen, K. F., *Lab on a Chip* **2009,** *9* (13), 1843-1849.

57. Hartman, R. L.; Naber, J. R.; Buchwald, S. L.; Jensen, K. F., *Angew. Chem. Int. Ed.* **2010,** *49* (5), 899-903.

58. Deadman, B. J.; Battilocchio, C.; Sliwinski, E.; Ley, S. V., *Green Chem.* **2013,** *15* (8), 2050-2055.

59. O'Brien, M.; Koos, P.; Browne, D. L.; Ley, S. V., *Org. Biomol. Chem.* **2012,** *10* (35), 7031-7036.

60. Kralj, J. G.; Sahoo, H. R.; Jensen, K. F., *Lab on a Chip* **2007,** *7* (2), 256-263.

61. Adamo, A.; Heider, P. L.; Weeranoppanant, N.; Jensen, K. F., *Industrial & Engineering Chemistry Research* **2013,** *52* (31), 10802-10808.

62. Ingham, R. J.; Battilocchio, C.; Fitzpatrick, D. E.; Sliwinski, E.; Hawkins, J. M.; Ley, S. V., *Angew. Chem. Int. Ed.* **2015,** *54* (1), 144-148.

63. Mascia, S.; Heider, P. L.; Zhang, H.; Lakerveld, R.; Benyahia, B.; Barton, P. I.; Braatz, R. D.; Cooney, C. L.; Evans, J. M. B.; Jamison, T. F.; Jensen, K. F.; Myerson, A. S.; Trout, B. L., *Angew. Chem.* **2013,** *125* (47), 12585-12589.

64. Wegner, J.; Ceylan, S.; Kirschning, A., *Adv. Synth. Catal.* **2012,** *354* (1), 17-57.

65. Hessel, V.; Kralisch, D.; Kockmann, N.; Noël, T.; Wang, Q., *ChemSusChem* **2013,** *6* (5), 746-789.

66. Glasnov, T. N.; Holbrey, J. D.; Kappe, C. O.; Seddon, K. R.; Yan, T., *Green Chem.* **2012,** *14* (11), 3071-3076.

67. Tilstam, U., *Org. Process Res. Dev.* **2012,** *16* (12), 1974-1978.

68. Perez, E.; Fraga-Dubreuil, J.; Garcia-Verdugo, E.; Hamley, P. A.; Thomas, M. L.; Yan, C.; Thomas, W. B.; Housley, D.; Partenheimer, W.; Poliakoff, M., *Green Chem.* **2011,** *13* (9), 2397-2407.

69. Benito-Lopez, F.; Tiggelaar, R. M.; Salbut, K.; Huskens, J.; Egberink, R. J. M.; Reinhoudt, D. N.; Gardeniers, H. J. G. E.; Verboom, W., *Lab on a Chip* **2007,** *7* (10), 1345-1351.

70. McPake, C. B.; Sandford, G., *Org. Process Res. Dev.* **2012,** *16* (5), 844-851.

71. Palde, P. B.; Jamison, T. F., *Angew. Chem. Int. Ed.* **2011,** *50* (15), 3525-3528.

72. Gutmann, B.; Roduit, J.-P.; Roberge, D.; Kappe, C. O., *Angew. Chem. Int. Ed.* **2010,** *49* (39), 7101-7105.

73. Zaborenko, N.; Murphy, E. R.; Kralj, J. G.; Jensen, K. F., *Industrial & Engineering Chemistry Research* **2010,** *49* (9), 4132-4139.

74. Fortt, R.; Wootton, R. C. R.; de Mello, A. J., *Org. Process Res. Dev.* **2003,** *7* (5), 762-768.

75. Struempel, M.; Ondruschka, B.; Daute, R.; Stark, A., *Green Chem.* **2008,** *10* (1), 41-43.

76. Pelleter, J.; Renaud, F., *Org. Process Res. Dev.* **2009,** *13* (4), 698-705.

77. Kulkarni, A. A.; Kalyani, V. S.; Joshi, R. A.; Joshi, R. R., *Org. Process Res. Dev.* **2009,** *13* (5), 999-1002.

78. Gage, J. R.; Guo, X.; Tao, J.; Zheng, C., *Org. Process Res. Dev.* **2012,** *16* (5), 930-933.

79. Yoshida, J.-i.; Nagaki, A.; Yamada, T., *Chem. Eur. J.* **2008,** *14* (25), 7450-7459.

80. Yoshida, J.-i., *Chem. Commun.* **2005,** (36), 4509-4516.

81. Yoshida, J.-i.; Takahashi, Y.; Nagaki, A., *Chem. Commun.* **2013,** *49* (85), 9896-9904.

82. Kim, H.; Nagaki, A.; Yoshida, J.-i., *Nat Commun* **2011,** *2*, 264.

83. Poliakoff, M.; Fitzpatrick, J. M.; Farren, T. R.; Anastas, P. T., *Science* **2002,** *297* (5582), 807-810.

84. Trost, B. M., *Acc. Chem. Res.* **2002,** *35* (9), 695-705.

85. Wender, P. A.; Verma, V. A.; Paxton, T. J.; Pillow, T. H., *Acc. Chem. Res.* **2008,** *41* (1), 40-49.

86. Burns, N. Z.; Baran, P. S.; Hoffmann, R. W., *Angew. Chem. Int. Ed.* **2009,** *48* (16), 2854-2867.

87. Jessop, P. G., *Green Chem.* **2011,** *13* (6), 1391-1398.

88. Noël, T.; Hessel, V., *ChemSusChem* **2013,** *6* (3), 405-407.

89. McMullen, J. P.; Stone, M. T.; Buchwald, S. L.; Jensen, K. F., *Angew. Chem. Int. Ed.* **2010,** *49* (39), 7076-7080.

90. Fabry, D. C.; Sugiono, E.; Rueping, M., *Reaction Chemistry & Engineering* **2016,** *1* (2), 129-133.

Chapter 2

Direct Reductive Carboxylation of Imines for the Synthesis of α-Amino Acids using Carbon Dioxide

The most widely used strategy for the synthesis of non-natural amino acids is the condensation of aldehydes, ammonia equivalent and cyanide, in the prototypical Strecker synthesis. Its utility however, is mitigated by the fact that it is an indirect method to install the carboxylic acid group through the use of highly toxic cyanide. This chapter describes the design and development of a direct one step alternative to the Strecker synthesis of aromatic amino acids using carbon dioxide and other readily available reagents. The developed method is easily scaled to multi gram quantities and possible mechanistic pathway is described.

2.1 Introduction and Reaction Design

Non-natural α-amino acids find use in a broad spectrum of applications, including synthesis,[1-3] catalysis,[4-8] and enzymology.[9-11] As a consequence, the chemical synthesis of these valuable compounds has long been an important area of research.[12-14] Among the diverse approaches to the synthesis of non-natural α-amino acids,[15-18] the strategic bond disconnection exemplified by the classic Strecker synthesis is appealing in its convergency.[19-20] Despite the demonstrated scope and selectivity of this reliable protocol,[21] the Strecker sequence is at root an indirect method for the installation of the carboxyl unit that necessitates both the use of hazardous cyanide derivatives and a subsequent hydrolysis of the resultant nitrile in order to reveal the target α-amino acid. Alternate approaches that capture the convergency of the Strecker synthesis,[22-23] but result in the direct installation of the carboxyl group from a readily available C1 synthon might offer an expedient complementary route to α-amino acids.

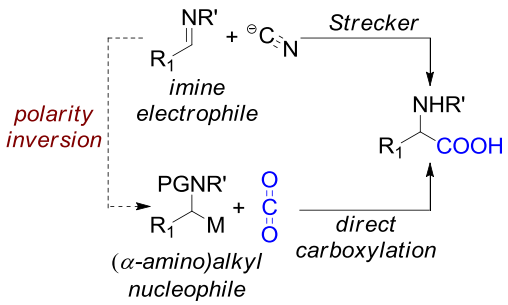

Figure 2.1. Strategy for direct carboxylation of imines by reversal of polarity at the α-carbon.

Carbon dioxide is an ideal C1 synthon due to its low cost, low toxicity, and wide availability.[24-29] The direct use of carbon dioxide in the synthesis of α-amino acids from imines would require an inversion of polarity at the imine carbon, involving the intermediacy of nucleophilic (α-amino)alkyl anion equivalents. (Figure 2.1).[30] Synthetically, these reactive intermediates have traditionally been accessed via directed α-metalation of alkylamine derivatives.[31-33] For instance, *N*-acyl amine derivatives may be selectively α-lithiated with *sec*-butyl lithium at low temperature; subsequent quenching with carbon dioxide then leads to α-amino acids. An alternative entry into (α-amino)alkyl metal reagents that avoids the use of highly basic alkyllithium reagents was recently reported by Mita and Sato.[34-36] This method employs bis(metal) reagents (*i.e.* silylstannanes and silylboranes) to adjust the oxidation state of the imine substrate in situ and gain access to reactive (α-amino)alkyl carbanion equivalents (Figure 2.2). The utility of this promising methodology is mitigated only by the relatively high expense and low atom economy of the demonstrated bis(metal) reagents.

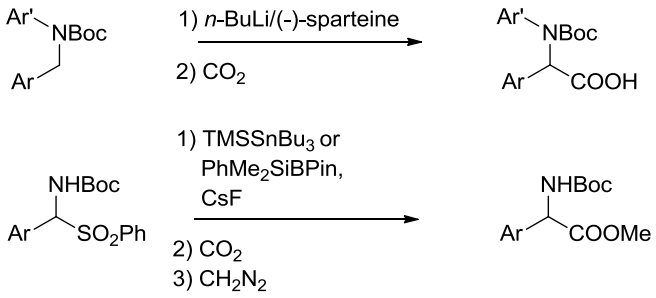

Figure 2.2. Precedents for α-amino acid synthesis by carboxylation of α-amino alkyl carbanions[31, 34-36]

We have developed a simple and effective method for the direct reductive carboxylation of imines with carbon dioxide that employs readily available and inexpensive commercial reagents. In a reactivity principle drawn from the vast body of research regarding reductive transformations mediated by low-valent metals,[37-41] we posited that reductive metallation of an imine would furnish a reactive (α-amino)alkyl metal intermediate or functional equivalent that could be trapped with carbon dioxide to yield α-amino acids.[42-46]

2.2 Reaction Development and Optimization

As an initial entry point, we investigated the simple reductive carboxylation of imines using common base metal reagents (Table 2.1). Our optimization efforts converged on the following conditions: for each equivalent of imine substrate, five equivalents each of magnesium turnings, chlorotrimethylsilane, and triethylamine in dimethylformamide were stirred under 45 atm of carbon dioxide for 24 h (entry 1).[41, 47-49] Following an aqueous extraction and product precipitation, *p*-methoxyphenyl benzaldimine was converted under these conditions into *N*-(*p*-methoxy)phenyl phenylglycine in 75% isolated yield. The decrease or omission (entries 2-11) of any of these components was found to negatively impact the desired reaction. For instance, a reduction in the applied pressure of carbon dioxide from 45 atm to 1 atm (compare entries 6 through 8) was attended

by a decrease in isolated yield of α-amino acid and an increase in the formation of *C*-silylated compound **(3)** and imine homocoupling product **(4)**. While bases other than triethylamine also lead to an increase in the overall yield of the desired amino acid (entries 2 & 3), triethylamine was selected for the next part of the study owing to its ease of availability and low cost. We believe the primary function of the requisite amine base is to buffer against adventitious HCl, although the formation of reactive ammonium carbamates through chemisorption of CO_2 cannot be excluded.[50]

Table 2.1. Optimization of reductive carboxylation reaction.

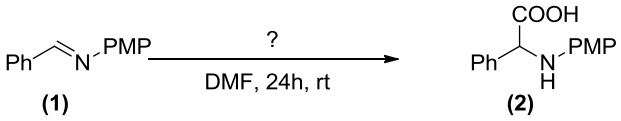

(1) **(2)**

Entry[a]	Reductant	CO_2 (psi)	Additive	Yield (%)[b,c]
1	5 equiv. Mg^0	675	3 equiv. TMSCl; 3 equiv. Et_3N	75
2	3 equiv. Mg^0	675	3 equiv. TMSCl; 3 equiv. DABCO	72
3	3 equiv. Mg^0	675	3 equiv. TMSCl; 3 equiv. Piperidine	58
4	3 equiv. Mg^0	675	3 equiv. TMSCl; 5 equiv. Et_3N	60
5	3 equiv. Mg^0	675	3 equiv. TMSCl; 3 equiv. DABCO	72
6	3 equiv. Mg^0	450	3 equiv. TMSCl; 3 equiv. Et_3N	68
7	3 equiv. Mg^0	150	3 equiv. TMSCl	56
8	3 equiv. Mg^0	15	3 equiv. TMSCl	35
9	3 equiv. Mg^0	300	1.5 equiv. TMSCl	12
10	3 equiv. Mg^0	300	None	N.R.
11	3 equiv. Zn^0	1	3 equiv. TMSCl	N.R.

[a] Reactions performed on 1 mmol scale. [b] Isolated yield of amino acid. [c] Compounds (3) and (4) were also observed by TLC in the reaction mixture.

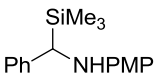

(3)

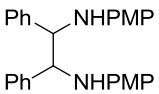

(4)

2.3 Exploring the Scope of the Reaction

With the reaction conditions optimized as detailed above, a survey of substrate scope was conducted (Figure 2.3). A diverse panel of substituted phenylglycine derivatives could be prepared from the corresponding benzaldimines by reductive carboxylation. Both electron-deficient and electron-rich benzaldimines underwent reaction to give the product α-amino acids in moderate to good yields. The suite of regioisomeric trifluoromethylated compounds were all isolated in good to moderate yield. It is interesting to note that the reaction tolerates cyano, ester and amide functionalities. The reaction appears to be impacted by steric congestion about the imine centre; mesityl derivative could only be obtained in low yield (20 %). Attempts to extend this reactivity to both alkyl aldimines and ketimines have not been successful to date. However, substitution on the *N*-aryl moiety was successfully tolerated, permitting the synthesis of *N*-aryl phenylglycines.[51]

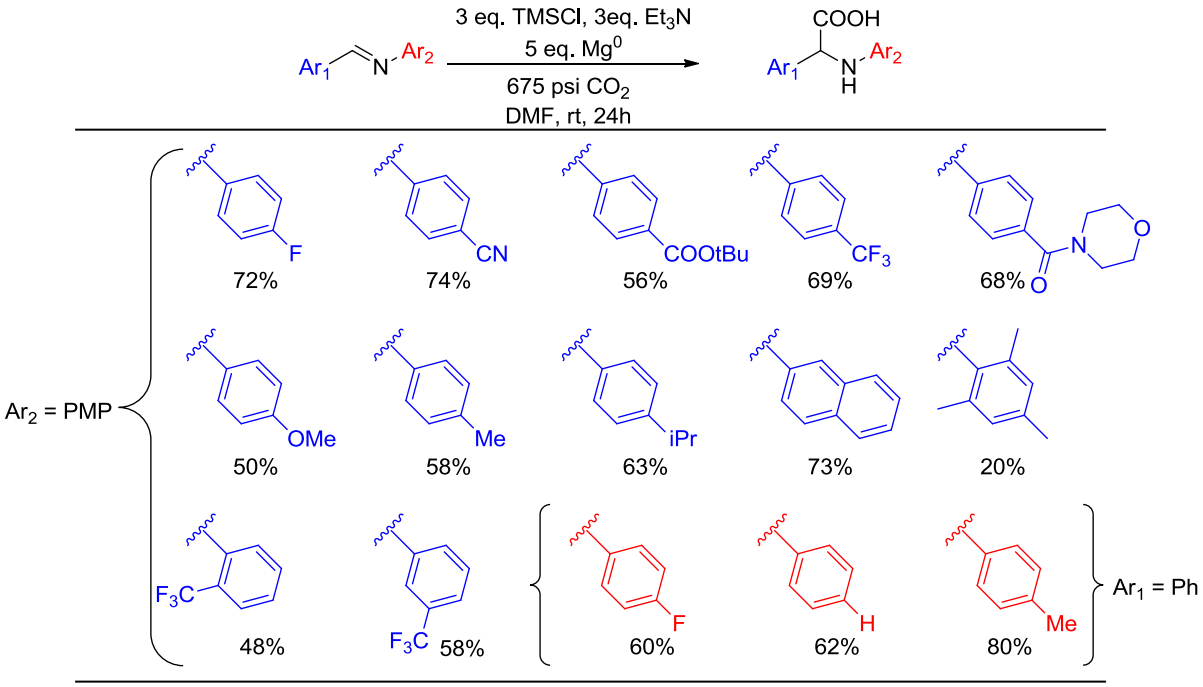

Figure 2.3. Substrate scope of the reductive carboxylation of imines.

The reductive carboxylation method is scalable to a multigram batch without complication (Figure 2.4). Specifically, reductive carboxylation of *p*-methoxyphenyl benzaldimine on a 25 mmol scale yields *N*-(*p*-methoxyphenyl) phenylglycine in 80% yield. This can be readily converted to methyl phenylglycinate in 53% yield via a two-step protecting group exchange sequence.

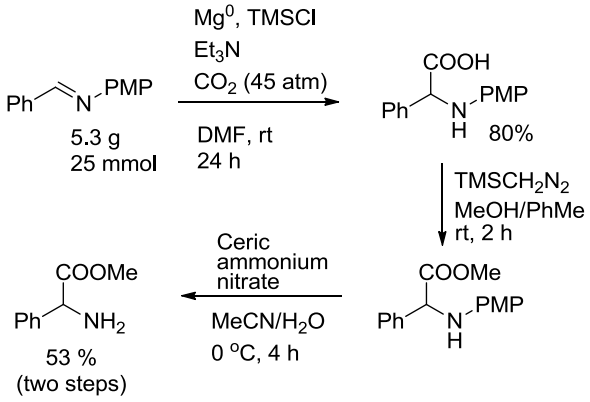

Figure 2.4. Multigram scale reductive carboxylation of *N*-(*p*-methoxyphenyl) protected benzaldimine.

2.4 Mechanistic Insights into the Reductive Carboxylation of Imines

Given the strong reducing power of magnesium (E = –3.01 V vs Fc/Fc^+)[52] and the known reduction potentials of *N*-aryl benzaldimines (E ~ –2.20 V vs Fc/Fc^+),[44-45] we believe this reductive carboxylation method is gated by one-electron reduction steps (Figure 2.5). Mechanistically, the first electron transfer event would likely occur subsequent to an *N*-silylation of imine with chlorotrimethylsilane, which would lower the thermodynamic potential for electron transfer by conversion to *N*-silyliminium.[53] The α-aminobenzyl radical intermediate resulting from reduction would be anticipated to be long-lived and largely unreactive given the extensive delocalization and captodative stabilization of the unpaired electron.[54-56] Consistent with this supposition, *o*-allyl benzaldimine substrate was found to resist intramolecular radical cyclization, instead undergoing

clean reductive carboxylation to give the α-amino acid in 64% yield (Figure 2.6). We therefore believe that the key reactive intermediate in this chemistry is α-aminobenzyl magnesium chloride, formed by a second electron transfer. A competition between electrophiles in solution consumes α-aminobenzyl magnesium chloride; high concentrations of CO_2 result in productive carboxylation,[57-60] whereas at lower applied pressures undesired reaction with either chlorotrimethylsilane to give *C*-silylated product,[61] or another equivalent of imine resulting in homocoupling, become significant.

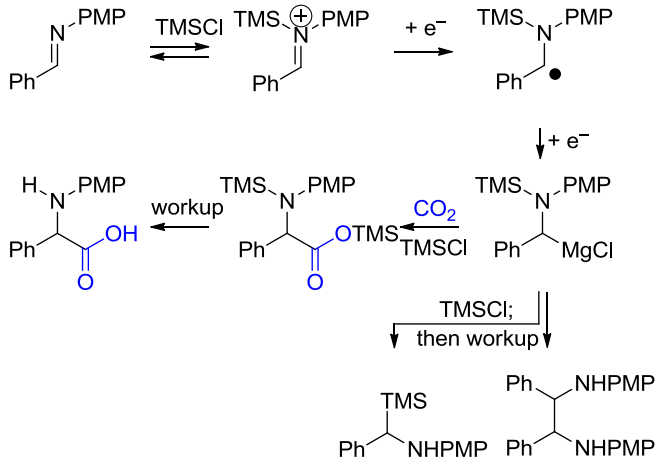

Figure 2.5. Proposed mechanism for the reductive carboxylation of imines.

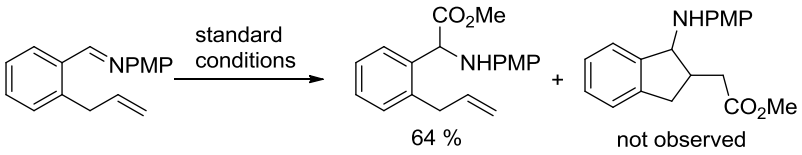

Figure 2.6. *o*-allyl benzaldimine resists cyclization. Standard conditions: (a) 5 eq. Mg^0, 3 eq. TMSCl, 3 eq. Et_3N, 675 psi CO_2, DMF, rt, 24h. (b) $TMSCHN_2$, MeOH-Et_2O, rt, 30 min.

To test whether the *C*-silylated product was an intermediate along the reaction pathway, in analogy to the imino stannane methodology,[34] it was synthesized separately and subjected to the carboxylation conditions (Scheme 5). No amino acid product was detected, leading to the conclusion

that this silylation was a competing side reaction. This prompted us to investigate the use of other Lewis acids for the transformation. Unfortunately, triethylsilyl chloride, alumina, boron trifluoride, or exogenous magnesium cations could not aid the conversion of the imine to the desired amino acid.

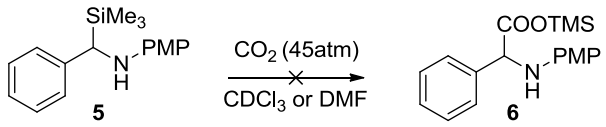

Figure 2.7. Attempted carboxylation of *C*-silylamine.

2.5 Summary and Outlook

In summary, we have described a reductive carboxylation method for the synthesis of substituted phenylglycine derivatives from imines and CO_2. The developed methodology utilizes inexpensive and readily available starting materials and does not rely on chromatography for the isolation of products.

A shortcoming of the current protocol is the use of magnesium metal. The fairly negative reduction potential (-3.01V vs Fc/Fc^+) compromises functional group tolerance, and hence limits substrate scope. We believe this methodology can be expanded to alkyl imines and provide an ability to exert control over the stereochemistry of the newly formed C-C bond. Three distinct pathways are considered here which present opportunities for further development of this chemistry.

2.5.1 Early transition metal mediated reductive carboxylation of imines

Reactions of low valent titanium species with imines to generate titanaziridines are well known.[62-64] These titanaziridines are dianionic species capable of reaction with a variety of electrophiles (Figure 2.8). Their synthesis usually involves treatment of an imine and titanium isopropoxide with an organometallic reagent such as *i*-PrMgCl or *n*-BuLi. Two strategies for

stereocontrol are possible, the first one involves the use of a chiral alcohol such as TADDOL derivative or binol,[65] which can complex with the titanium and influence the stereochemical outcome of the carboxylation. The second is to use a chiral protecting group on the imine nitrogen for a diasteroselective carboxylation.[66]

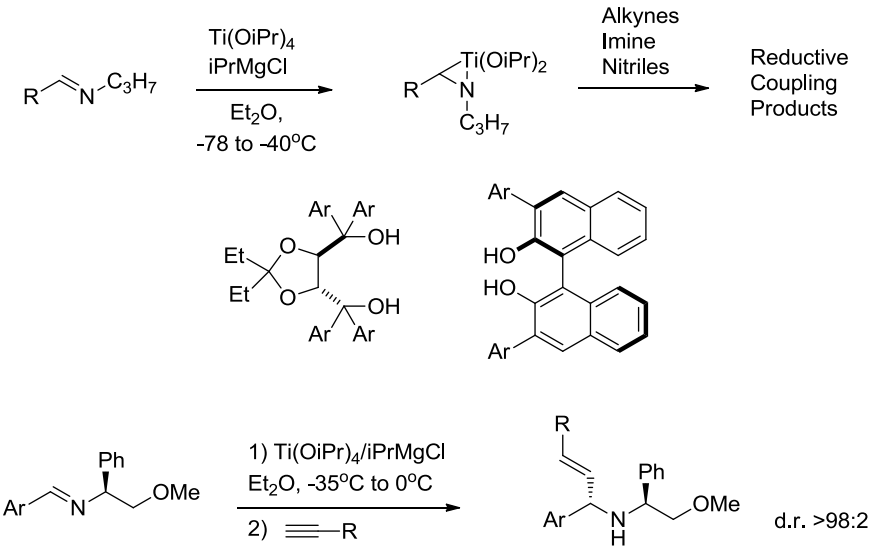

Figure 2.8. Titanaziridines formed by reaction of imines with low valent titanium generated *in-situ* from Ti(O*i*Pr)$_4$ can be trapped with CO_2 to yield amino acids.

Preliminary studies on the titanium mediated carboxylation led to moderate yield (~60%) of the amino acid, while using excess of the titanium isopropoxide (Figure 2.9). It was found that the titanzaridiation proceeded to completion but the reaction yield was limited by carboxylation. Sparging CO_2 gas led to nominal improvement in the yields. We believe this system could benefit from the use of flow technology, however initial studies were impeded due to sever clogging, likely due to precipitation of titanium and magnesium salts. A careful optimization of concentration or use of ultrasonication might prove helpful for the further development of this chemistry in flow reactors.

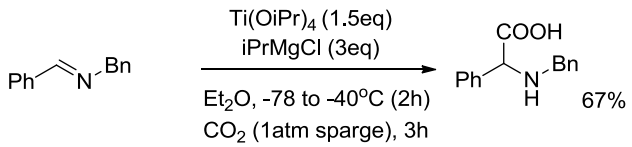

Figure 2.9. Attempted carboxylation of titanaziridine.

2.5.2 Late transition metal mediated reductive carboxylation of imines

Copper-NHC complexes have been shown to be viable catalysts for borylation of sulfinimines. The methodology developed by the Ellman group leads to a highly diasteroselective synthesis of α-amino boronate esters starting with the chiral sulfinimine.[67] The Cu-NHC complex has also been shown to catalyze the carboxylation of alkyl boronic esters (Figure 2.10).[68] These results taken together should in theory allow for the conversion of sulfinimines to a-amino acids, by carrying out the borylation reaction under a CO_2 atmosphere.

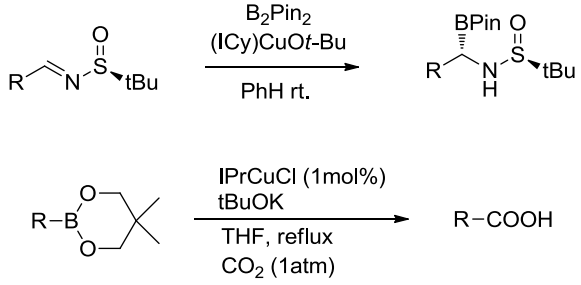

Figure 2.10. NHC-Cu complex catalyzed boronation of sulfinimines and carboxylation of alkyl boranes.[67-68]

While the auxiliary assisted diasterocontrol has been shown to be highly effective for the borylation, it is not clear whether the carboxylation reaction would proceed with stereoretention. A more economical and sustainable approach would be a catalyst controlled enantioselective borylation and carboxylation. The use of chiral NHC ligands on the copper center should allow for such enantiocontrol and can be explored as an extension of this chemistry.

2.5.3 Photocatalytic reductive carboxylation of imines

In recent years the groups of MacMillan,[69] and Stephenson[70] have successfully demonstrated the use of visible light photocatalysts as efficient reagents for the generation of single electron intermediates. These catalysts allow the conversion of energy from visible light radiation into chemical energy there-by allowing for the use of milder reductants to derive high energy intermediates.

Initial investigations using $Ru(bpy)_3(BF_4)_2$ were not successful with PMP protected imines. Preliminary cyclic voltammetric studies of the imines indicate that the reduction potentials of the imines are more negative (-2.30 V vs Fc/Fc^+ for benzaldehyde PMP imine) as compared to the reduction potential of the excited state Ru^+ (-1.65 V vs Fc/Fc^+).[70] Thus there is a need to use a stronger reductant to affect the electron transfer. $Ir(ppy)_3$ (ppy = 2-phenylpyridyne) is another widely used photocatalyst which has an excited state reduction potential comparable to the aromatic imines of interest (-2.6 V vs Fc/Fc^+).[71] This may be a viable catalyst for future study.

Building upon the work described here, expansion of the reactivity to more diverse substrates and enantiocontrol during the carboxylation step will make the reaction a powerful alternative to the classical Strecker synthesis.

2.8 Experimental Section

2.8.1 General Experimental Remarks

All solvents were degassed by sparging with argon, dried by passage over an activated alumina column, and stored under argon prior to use. All glassware used was dried in a 120 °C oven and cooled in a desiccator before use. All reagents were obtained from commercial vendors (TCI, Sigma-Aldrich, Alfa-Aesar) and used without purification unless noted. Magnesium metal was activated by crushing in a mortar immediately before use. NMR data was collected on Bruker Avance CDPX 300 or DRX 400 MHz instruments. Spectra were referenced internally to residual protiated solvent ($CDCl_3$: 7.26 ppm (^1H), 77.16 ppm (^{13}C); DMSO-d_6: 2.50 ppm (^1H) and 39.5 ppm (^{13}C). Mass spectrometric measurements were performed at University of Illinois at Urbana Champaign with Q-Tof Ultima mass spectrometer. PMP stands for *p*-methoxyphenyl.

2.8.2 Synthetic Procedures

2.8.2.1 General Procedure for the synthesis of imines.

All the imines were synthesized by reacting the appropriate aldehyde and amine in ethanol or DCM in the presence of $MgSO_4$. The reaction was stirred overnight, and the imine was obtained by filtration and evaporation of the solvent *in vacuo*. The crude solid was purified by recrystallization from either ethanol or hexanes. The following prepared imines are known compounds

4-methoxy-*N*-[[4-(trifluoromethyl)phenyl]methylene]-Benzenamine[72]

4-methoxy-*N*-[(4-fluorophenyl)methylene]-Benzenamine[73]

4-methoxy-*N*-[[3-(trifluoromethyl)phenyl]methylene]-Benzenamine[74]

4-methoxy-*N*-(phenylmethylene)-Benzenamine[75]

4-methoxy-*N*-[[4-(1-methylethyl)phenyl]methylene]-Benzenamine[76]

4-fluoro-*N*-(phenylmethylene)- Benzenamine[77]

4-methoxy-*N*-[(4-methoxyphenyl)methylene]-Benzenamine[77]

4-methoxy-*N*-[(4-methylphenyl)methylene]-Benzenamine[78]

4-methoxy-*N*-[(2,4,6-trimethylphenyl)methylene]-Benzenamine[79]

4-methoxy-*N*-(2-naphthalenylmethylene)-Benzenamine[79]

4-methoxy-*N*-[[2-(trifluoromethyl)phenyl]methylene]-Benzenamine[79]

N-(phenylmethylene)-Benzenamine[80]

4-methyl-*N*-(phenylmethylene)-Benzenamine[81]

4-(((4-methoxyphenyl)imino)methyl)benzonitrile[82]

Characterization Data for Imines

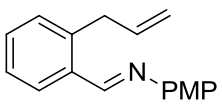

N-(2-allylbenzylidene)-4-methoxyaniline (): Synthesized according to the general procedure with 2-allyl benzaldehyde (1.05 equiv) and *p*-anisidine (1 equiv). The title imine was isolated as yellow oil after evaporation of solvent, which was further purified by vacuum distillation to remove off the excess of aldehyde. ^{1}H NMR ($CDCl_3$, 400 MHz): 8.78 (s, 1H), 8.18 (d, 1H, *J* = 7.6 Hz), 7.44-7.36 (m, 2H), 7.28-7.24 (m, 3H), 6.98-6.96 (m, 2H), 6.13-6.04 (m, 1H), 5.15 (dd, 1H, *J* = 10.1, 1.5 Hz), 5.05 (dd, *J* = 17.1, 1.7 Hz), 3.86 (s, 3H), 3.73 (d, 2H, *J* = 5.8 Hz) ; ^{13}C ($CDCl_3$, 75 MHz) δ= 158.3, 156.9, 145.5, 139.9, 137.3, 134.4, 131.0, 130.5, 127.7, 127.0, 122.3, 116.3, 114.4, 55.5, 37.1; MS (ESI) calcd. for $C_{14}H_{14}NO_2$ (M+H) = 252.1399, found 252.1388.

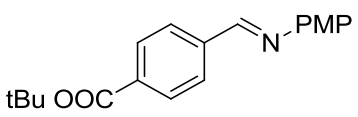

***t*-butyl 4-[[(4-methoxyphenyl)imino]methyl] benzoate ()**:^{1}H ($CDCl_3$ 400 MHz) δ = 8.51 (s, 1H), 8.08 (d, 2H, *J* = 8.3 Hz), 7.94 (d, 2H, *J* = 8.3 Hz), 7.28 (d, 2H, *J* = 8.9 Hz), 6.95 (d, 2H, *J* = 8.9 Hz), 3.82 (s, 3H), 1.62 (s, 9H); ^{13}C ($CDCl_3$, 75 MHz) δ=165.3, 158.7, 157.0, 157.0, 144.3, 139.9, 133.9, 129.8, 128.3, 122.5, 122.5, 114.5, 81.4, 55.5, 28.2; MS (ESI) calcd. for $C_{19}H_{22}NO_3$ (M+H) = 312.1600, found 312.1607.

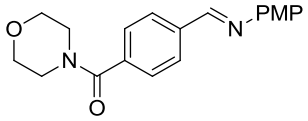

4-[[[(4-methoxyphenyl)imino]methyl]phenyl] (morpholino) methanone:^{1}H ($CDCl_3$ 400 MHz) δ = 8.50 (s, 1H), 7.94 (d, 2H, *J* = 8.1 Hz), 7.51 (d, 2H, *J* = 8.1 Hz), 7.28 (d, 2H, *J* = 8.8 Hz), 6.95 (d, 2H, *J* = 8.9 Hz), 3.82-3.45 (m, 11H); ^{13}C ($CDCl_3$, 75 MHz) δ=169.8, 158.7, 156.9, 156.8, 144.4, 137.8, 137.5, 128.7, 127.7, 127.6, 122.4, 122.3, 114.5, 66.9; MS (ESI) calcd. for $C_{19}H_{21}N_2O_3$ (M+H) = 324.1500, found 324.1478.

2.8.2.2 General procedure for the reductive carboxylation of imines.

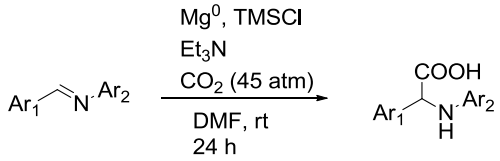

In a dry test tube was added imine (1 mmol), magnesium (120 mg, 5 mmol), triethylamine (0.42 mL, 3 mmol) and DMF (5 mL). Chlorotrimethylsilane (0.38 mL, 3 mmol) was then added to the mixture. The test tube was then quickly transferred to an autoclave that was charged with molecular sieves and dry ice. The autoclave was sealed tightly and then heated to sublime the dry ice. The final pressure was adjusted to 45 atm after the vessel warmed up to room temperature. After 24 h the vessel was depressurized and the reaction mixture was diluted with 35 mL of 10% (wt/vol) NaOH solution. The solution was then extracted with ether (3 x 50 mL). The aqueous phase was collected and cooled to 0 ^{o}C and the pH was adjusted to 4 with conc. HCl. The amino acid precipitate was isolated by filtration. The dry solid was then purified by trituration with 10% Et_2O in hexanes unless otherwise noted.

Multigram scale carboxylation of 4-methoxy-*N*-(phenylmethylene)-Benzenamine

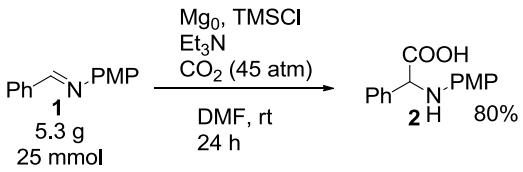

The imine (5.28 g 25 mmol) was dissolved in DMF (125 mL) in an autoclave. To this solution was added triethylamine (10.5 mL, 75 mmol) and chlorotrimethylsilane (9.6 mL 75 mmol). The autoclave was charged with dry ice and sealed tightly. It was then heated to sublime the dry ice. The final pressure was adjusted to 45 atm after the vessel warmed up to room temperature. After 24h the vessel was depressurized and the reaction mixture was diluted with 800 mL of 10% (wt/vol) NaOH solution. This solution was then filtered through a pad of celite. The filtrate was then

extracted with ether (3 x 900 mL). The aqueous phase was cooled to 0 ^{o}C in an ice bath and its pH was adjusted to 4 with conc. HCl. The amino acid precipitate was isolated by filtration. The dry solid was then purified by trituration with 10% Et_2O in hexanes to yield **2** (5.10 g, 80%) as a white powder.

Methyl esterification of N-(*p*-methoxyphenyl) phenyl glycine.

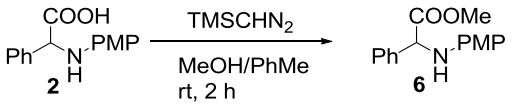

N-(*p*-methoxyphenyl) phenyl glycine **2** (5.10 g, 19.8 mmol) was suspended in a mixture of toluene (120 mL) and methanol (60 mL) under N_2. To this suspension was added $TMSCHN_2$ (25 mL of 2.0 M soln. in Et_2O) dropwise over 15 mins. This solution was stirred at room temperature for 2 h. The excess $TMSCHN_2$ was then quenched with acetic acid and the resulting solution was concentrated *in vacuo*. The product was then dissolved in 100 mL of ethyl acetate and washed with sat. $NaHCO_3$ solution (3 x 20 mL). The organic phase was dried over Na_2SO_4 and concentrated *in vacuo* to yield the methyl ester **6** as a yellow solid. (5.13 g, 96%). ^{1}H ($CDCl_3$, 300 MHz) δ = 7.53 (d, 2H, *J* = 7.8 Hz), 7.40-7.30 (m, 3H), 6.74 (d, 2H, *J* = 8.9 Hz), 6.58 (d, 2H, *J* = 8.9 Hz), 5.06 (s, 1H), 3.73 (s, 3H), 3.72 (s, 3H).

Procedure for the removal of *p*-methoxyphenyl group[83]

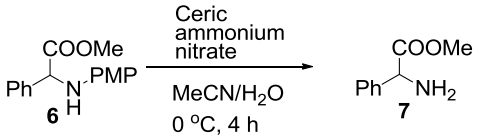

Ceric ammonium nitrate (26 g, 47.5 mmol) was dissolved in water (60 mL) and the solution was cooled to 0 ^{o}C. To this solution was added a solution of **6** (5.11 g, 19 mmol) in MeCN (200 mL) dropwise over 45 min. The resulting dark solution was stirred at 0 °C for 4 h before treating with 2N HCl to pH = 1. The aqueous phase was washed with EtOAc (3 x 500 mL) and brought to pH 8 by

saturated $NaHCO_3$. The resulting suspension was then filtered and the filtrate was extracted with CH_2Cl_2 (3 x 500 mL). The combined organic phase was dried over anhydrous Na_2SO_4 and the solvent evaporated *in vacuo* to yield **7** (1.71 g, 55% yield) as yellow oil. ^1H ($CDCl_3$, 300 MHz) δ = 7.34-7.27 (m, 5H), 4.58 (s, 1H), 3.65 (s, 3H), 2.09 (brs, 2H).

Procedure for the carboxylation of N-(2-allylbenzylidene)-4-methoxyaniline

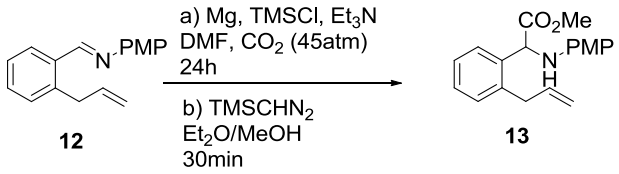

In a dry test tube was added imine **12** (1 mmol), magnesium (120 mg, 5 mmol), triethylamine (0.42 mL, 3 mmol) and DMF (5 mL). Chlorotrimethylsilane (0.38 mL, 3 mmol) was then added to the mixture. This test tube was then quickly transferred to an autoclave that was charged with molecular sieves and dry ice. The autoclave was sealed tightly and then heated to sublime the dry ice. The final pressure was adjusted to 45 atm after the vessel had warmed up to room temperature. After 24 h the vessel was depressurized and the reaction mixture filtered to separate the excess magnesium. The filtrate was diluted with 40 mL of 2N HCl solution. This solution was then extracted with ether (3 x 50 mL), dried over anhydrous Na_2SO_4 and concentrated *in vacuo*. The residue was diluted with 20 ml of Et_2O-MeOH (v/v, 1/1) and treated with 2 mL of 2.0 M $TMSCHN_2$ solution in Et_2O. This mixture was stirred for 30 mins and then quenched with AcOH. The solvent was evaporated and the crude mixture purified by chromatography (5% EtOAc in Hexanes) to yield 0.199 g of compound **13** (64% yield) as colorless oil.

^1H ($CDCl_3$, 300 MHz) δ = 7.50 (d, 2H, *J* = 7.2 Hz), 7.35-7.27 (m, 3H), 6.83 (d, 2H *J* = 8.8 Hz), 6.64 (d, 2H, *J* = 8.8 Hz), 6.16-6.07 (m, 1H), 5.39 (d, 1H, *J* = 5.8Hz), 5.22-5.14 (m, 2H), 4.53 (d, 1H, *J* = 5.4Hz), 3.77-3.69 (m, 8H); ^{13}C ($CDCl_3$, 100 MHz) δ = 173.1, 152.7, 140.5, 138.4, 136.7, 135.8, 130.4, 128.5, 127.1, 126.8, 116.5, 114.8, 58.1, 55.6, 52.5, 36.9. MS (ESI) calcd. for $C_{19}H_{22}NO_3$ (M+H) = 312.1600, found 312.1596.

Characterization Data for amino acids

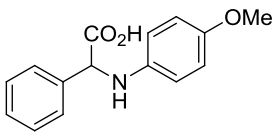

2-((4-methoxyphenyl)amino)-2-phenylacetic acid (2.8): The general procedure was followed to give 0.201g of compound 2 (78% yield). ^{1}H (DMSO-d_6, 400 MHz) δ = 7.51 (d, 2H, *J* = 6.6 Hz), 7.35-7.28 (m, 3H), 6.68 (d, 2H, *J* = 7.8 Hz), 6.63 (d, 2H, *J* = 7.8 Hz), 5.02 (s, 1H), 3.60 (s, 3H); ^{13}C (DMSO-d_6, 100 MHz), δ = 173.2, 151.2, 141.1, 138.8, 128.4, 127.7, 127.5, 114.4, 114.3, 60.5, 55.2; MS (ESI) calcd for $C_{15}H_{16}NO_3$ (M+H) = 258.1127, found 258.1130.

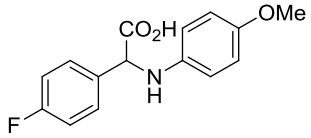

2-(4-fluorophenyl)-2-((4-methoxyphenyl)amino)acetic acid (2.9): The general procedure was used followed by recrystallization from ethanol/water to give 0.183g of compound 5a (72% yield). ^{1}H (DMSO-d_6, 400 MHz) δ = 7.54 (s, 2H), 7.19 (t, 2H, *J* = 8.2 Hz), 6.68 (d, 2H, *J* = 7.9 Hz), 6.63 (d, 2H, *J* = 7.9 Hz), 5.05 (s, 1H), 3.6 (s, 3H); ^{13}C (DMSO-d_6, 100 MHz), δ = 173.1, 162.9, 160.4, 151.3, 140.9, 135.1, 129.4, 115.4, 115.1, 115.0, 114.4, 59.7, 55.2; MS (ESI) calcd for $C_{15}H_{15}NO_3F$ (M+H) = 276.1036, found 258.1026.

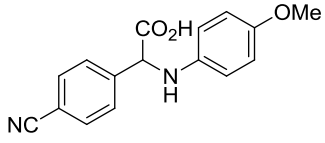

2-(4-cyanophenyl)-2-((4-methoxyphenyl)amino)acetic acid The general procedure was followed to give 0.208g of compound 5b (74% yield). ^{1}H (DMSO-d_6, 300 MHz) δ = 7.84 (d, 2H, *J* = 8.2 Hz), 7.72 (d, 2H, *J* = 8.2 Hz), 6.59-6.65 (m, 4H), 5.22 (s, 1H), 3.59 (s, 3H); ^{13}C (DMSO-d_6, 75 MHz), δ = 172.1, 151.4, 144.8, 140.5, 132.3, 128.5, 118.7, 114.4, 110.5, 60.1, 55.2; MS (ESI) calcd. for $C_{16}H_{15}N_2O_3$ (M+H) = 283.1083, found 283.1082.

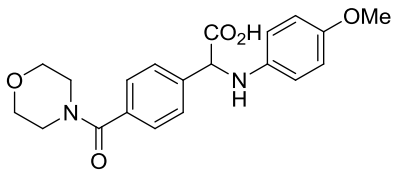

2-((4-methoxyphenyl)amino)-2-(4-(morpholine-4-carbonyl)phenyl) acetic acid: The general procedure was used followed by recrystallization from ethanol to give 0.250g of compound 5c (68% yield). ^{1}H (DMSO-d_6, 400 MHz) δ = 7.58-7.56 (m, 2H), 7.40-7.38 (m, 2H), 6.68-6.62 (m, 4H), 5.09 (s, 1H), 3.70-3.34 (m, 12H); ^{13}C (DMSO-

d_6, 100 MHz) δ = 172.8, 168.8, 151.3, 140.9, 140.3, 134.9, 127.5, 127.2, 114.4, 114.3, 110.4, 66.1, 60.2, 55.2; MS (ESI) calcd for $C_{15}H_{15}NO_3F$ (M+H) = 276.1036, found 371.1610.

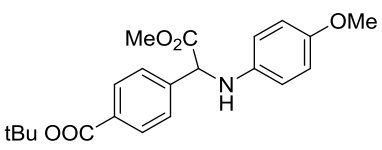

***tert*-butyl4-(2-methoxy-1-((4-methoxyphenyl)amino)-2-oxoethyl) benzoate**: The general procedure was followed to give a pale yellow solid which was suspended in 50ml (1:1) Et_2O:MeOH. To this suspension was added 2ml of TMS-Diazomethane solution (2.0M in Et_2O). The reaction was let stir for half an hour and quenched by acetic acid. Flash chromatography (10% Ethyl Acetate in Hexanes) yielded 0.206g of **5d** (56% yield.)

^{1}H ($CDCl_3$ 300 MHz) δ = 7.96 (d, 2H, *J* = 8.3 Hz), 7.56 (d, 2H, *J* = 8.2 Hz), 6.72 (d, 2H, *J* = 6.8 Hz), 6.51 (d, 2H, *J* = 6.8 Hz), 5.07 (d, 1H, *J* = 5.7Hz), 4.77 (d, 2H, *J* = 5.7 Hz) 3.72 (s, 3H), 3.69 (s, 3H), 1.58 (s, 9H) ; ^{13}C ($CDCl_3$, 75 MHz), δ =172.0, 165.4, 152.7, 142.5, 139.9, 132.1, 130.1, 127.3, 115.0, 114.9, 81.2, 61.5, 55.8, 53.0, 28.3; MS (ESI) calcd for $C_{21}H_{26}NO_5$ (M+H) = 372.17 found 372.1806.

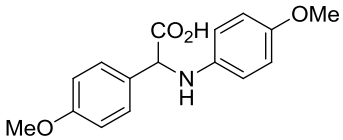

2-(4-methoxyphenyl)-2-((4-methoxyphenyl)amino)acetic acid: The general procedure was followed to give 0.144g of compound 5e (50% yield). ^{1}H (DMSO-d_6, 400 MHz) δ = 7.42 (d, 2H, *J* = 8.5 Hz), 6.92 (d, 2H, *J* = 8.5 Hz), 6.68 (d, 2H, *J* = 8.9 Hz), 6.62 (d, 2H, *J* = 8.9 Hz), 4.95 (s, 1H), 3.73 (s, 3H), 3.60 (s, 3H) ; ^{13}C (DMSO-d_6, 100 MHz), δ = 173.4, 158.8, 151.2, 141.1, 130.6, 128.6, 114.4, 114.2, 113.8, 59.8, 55.2, 55.0; MS (ESI) calcd for $C_{16}H_{18}NO4$ (M+H) = 288.1236, found 288.1232.

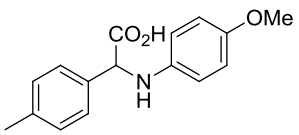

2-((4-methoxyphenyl)amino)-2-(p-tolyl)acetic acid:

The general procedure was followed to give 0.157g of compound 5f (58% yield). ^{1}H (DMSO-d_6, 400 MHz) δ = 7.39 (d, 2H, *J* = 4Hz), 7.15 (d, 2H, *J* = 4 Hz), 6.68 (d, 2H, *J* = 8.5 Hz), 6.62 (d, 2H, *J* = 8.5 Hz), 4.97 (s, 1H), 3.60 (s, 3H), 2.27 (s, 3H); ^{13}C (DMSO-d_6, 100 MHz), δ = 173.3, 151.2, 141.1, 136.9, 135.7, 128.9, 127.4, 114.4, 114.3, 60.2, 55.2, 20.7; MS (ESI) calcd for $C_{16}H_{18}NO_3$ (M+H) = 272.1287, found 272.1281.

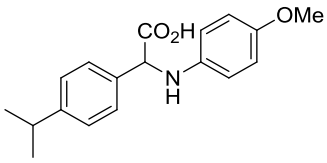

2-(4-isopropylphenyl)-2-((4-methoxyphenyl)amino)acetic acid: The general procedure was followed to give 0.188g of compound 5g (63% yield). ^{1}H (DMSO-d_6, 400 MHz) δ = 7.42 (d, 2H, *J* = 6.6 Hz), 7.22 (d, 2H, *J* = 6.6 Hz), 6.66 (m, 4H), 4.97 (s, 1H), 3.60 (s, 3H), 2.86 (s, 1H), 1.19 (d, 6H, *J* = 5.9 Hz); ^{13}C (DMSO-d_6, 100 MHz), δ = 173.3, 151.2, 147.8, 141.2, 136.1, 127.4, 126.3, 114.4, 114.3, 60.3, 55.2, 33.1, 23.9, 23.8; MS (ESI) calcd for $C_{18}H_{22}NO_3$ (M+H) = 300.1600, found 300.1606.

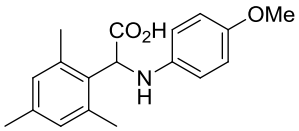

2-mesityl-2-((4-methoxyphenyl)amino)acetic acid: The general procedure was followed to give 0.060g of compound 5h (20% yield). ^{1}H (DMSO-d_6, 400 MHz) δ = 6.80 (s, 2H), 6.66 (d, 2H, *J* = 7.2 Hz), 6.50 (d, 2H, *J* = 7.2 Hz), 5.22 (s, 1H), 3.60 (s, 3H), 2.36 (s, 6H), 2.18 (s, 3H); ^{13}C (DMSO-d_6, 100 MHz), δ = 173.4, 150.9, 141.5, 136.6, 135.9, 132.7, 129.7, 114.5, 113.4, 56.3, 55.24, 20.4, 20.2; MS (ESI) calcd for $C_{18}H_{22}NO_3$ (M+H) = 300.1600, found 300.1592

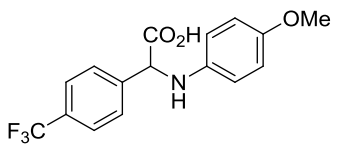

2-((4-methoxyphenyl)amino)-2-(4-(trifluoromethyl)phenyl)acetic acid: The general procedure was followed to give 0.224g of compound 5i (69% yield). ^{1}H (DMSO-d_6, 400 MHz) δ = 7.76-7.71 (m, 4H), 6.68-6.62 (m, 4H), 5.24 (s, 1H), 3.60 (s, 3H); ^{13}C (DMSO-d_6, 100 MHz), δ = 172.4, 151.4, 143.8, 140.7, 128.4, 128.3, 125.3, 125.2, 114.4, 60.1, 55.2; MS (ESI) calcd for $C_{16}H_{15}NO_3F_3$ (M+H) = 326.1004, found 326.1002.

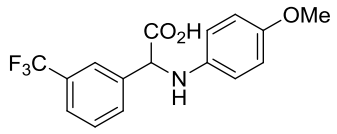

2-((4-methoxyphenyl)amino)-2-(3-(trifluoromethyl)phenyl)acetic acid: The general procedure was followed to give 0.188g of compound 5j (58% yield). ^{1}H (DMSO-d_6, 400 MHz) δ = 7.89 (s, 1H), 7.81 (s, 1H), 7.64-7.59 (m, 2H), 6.66 (s, 4H), 5.23 (s, 1H), 3.60 (s, 3H); ^{13}C (DMSO-d_6, 100 MHz), δ = 172.6, 151.4, 140.8, 140.6, 131.7, 129.6, 129.3, 129.0, 125.6, 124.4, 124.0, 122.9, 114.4, 60.0, 54.7; MS (ESI) calcd for $C_{15}H_{16}NO_3$ (M+H) = 326.1004, found 326.1012.

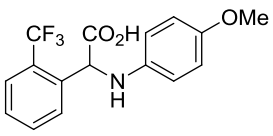

2-((4-methoxyphenyl)amino)-2-(2-(trifluoromethyl)phenyl)acetic acid: The general procedure was followed to give 0.156g of compound 5k (48% yield). ^{1}H (DMSO-d_6, 400 MHz) δ = 7.80-7.66 (m, 3H), 7.53 (t, 1H, J = 8.0Hz), 6.71 (d, 2H, J = 8.4 Hz), 6.58 (d, 2H, J = 8.4 Hz) 5.21 (s,1H), 3.61 (s, 3H) ; ^{13}C (DMSO-d_6, 100 MHz), δ = 172.3, 151.5, 141.1, 137.6, 132.8, 129.1, 128.3, 127.4, 126.0, 125.9, 125.8, 114.5, 114.0, 57.2, 55.2; MS (ESI) calcd for $C_{15}H_{16}NO_3$ (M+H) = 326.1004, found 326.1006.

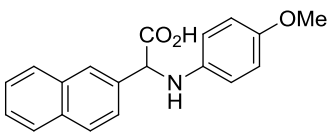

2-((4-methoxyphenyl)amino)-2-(naphthalen-2-yl)acetic acid: The general procedure was followed to give 0.224g of compound 5l (73% yield). ^{1}H (DMSO-d_6, 400 MHz) δ = 8.04 (s, 1H), 7.88 (s, 3H), 7.66 (d, 1H, J = 8.0 Hz), 7.50-7.49 (m, 2H), 6.67 (s, 4H), 5.22 (s, 1H), 3.59 (s,3H); ^{13}C (DMSO-d_6, 100 MHz), δ = 173.1, 151.2, 141.1, 136.6, 132.8, 132.5, 128.0, 127.8, 126.3, 126.2, 125.6, 114.4, 60.7, 55.2; MS (ESI) calcd for $C_{19}H_{18}NO_3$ (M+H) = 308.1287, found 308.1291.

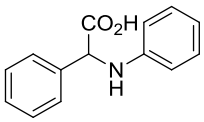

2-phenyl-2-(phenylamino)acetic acid: The general procedure was followed to give 0.141g of compound 5m (62% yield) after recrystallization from toluene. ^{1}H (DMSO-d_6, 400 MHz) δ = 7.53 (d, 2H, *J* = 7.6Hz), 7.38-7.29 (m, 3H), 7.06-7.02 (t, 2H, *J* = 7.4 Hz), 6.68-6.66 (d, 2H, *J* = 8.0 Hz), 6.57-6.53 (t, 1H *J* = 7.1 Hz), 5.09 (s, 1H); ^{13}C (DMSO-d_6, 100 MHz) δ= 172.9, 146.9, 138.6, 128.8, 128.5, 127.8, 127.5, 116.6, 113.1, 59.7; MS (ESI) calcd. for $C_{14}H_{14}NO_2$ (M+H) = 228.1025, found 228.1015.

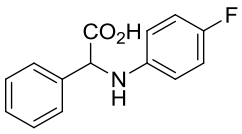

2-((4-fluorophenyl)amino)-2-phenylacetic acid: The general procedure was followed to give 0.171g of compound 5n (70% yield) after recrystallization from toluene. ^{1}H **(**DMSO-d_6, 400 MHz**)** δ = 7.52 (d, 2H, 7.4Hz), 7.37-7.28 (m, 3H), 6.90-6.86 (m, 2H), 6.68-6.65 (m, 2H), 5.07 (s, 1H); ^{13}C (DMSO-d_6, 100 MHz) δ= 172.9, 143.7, 138.5, 128.5, 127.8, 127.5, 115.2, 115.0, 114.0, 113.9, 60.2; MS (ESI) calcd. for $C_{14}H_{13}FNO_2$ (M+H) = 246.0930, found 246.0932.

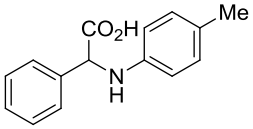

2-phenyl-2-(p-tolylamino)acetic acid: The general procedure was followed to give 0.144 g of compound 5o (60% yield). ^{1}H (DMSO-d_6, 400 MHz) δ = 7.51 (d, 2H, *J* = 6.0 Hz), 7.35-7.29 (m, 3H), 6.85 (d, 2H *J*= 6.8 Hz), 6.57 (d, 2H, *J* = 6.96Hz), 5.04 (s, 1H), 2.13 (s, 3H); ^{13}C (DMSO-d_6, 100 MHz) δ = 173.1, 144.7, 138.6, 129.2, 128.4, 127.7, 125.0, 113.2, 59.9, 20.0. MS (ESI) calcd. for $C_{15}H_{16}NO_2$ (M+H) = 242.1181, found 242.1178

2.9 Reference

1. Reetz, M. T., *Angew. Chem. Int. Ed.* **1991,** *30* (12), 1531-1546.
2. Martens, J., *Top. Curr. Chem.* **1984,** *125* (Stereochemistry), 165-246.
3. Drauz, K.; Kleeman, A.; Martens, J., *Angew. Chem. Int. Ed.* **1982,** *21* (8), 584-608.
4. Jarvo, E. R.; Miller, S. J., *Tetrahedron* **2002,** *58* (13), 2481-2495.
5. Lu, Y.; Johnstone, T. C.; Arndtsen, B. A., *J. Am. Chem. Soc.* **2009,** *131* (32), 11284-11285.
6. Paradowska, J.; Stodulski, M.; Mlynarski, J., *Angew. Chem., Int. Ed.* **2009,** *48* (24), 4288-4297.
7. List, B.; Lerner, R. A.; Barbas, C. F., III, *J. Am. Chem. Soc.* **2000,** *122* (10), 2395-2396.
8. Micskei, K.; Patonay, T.; Caglioti, L.; Palyi, G., *Chem. Biodiversity* **2010,** *7* (6), 1660-1669.
9. Liao, J., *Biotechnol. Prog.* **2007,** *23* (1), 28-31.
10. Noren, C. J.; Anthony-Cahill, S. J.; Griffith, M. C.; Schultz, P. G., *Science (Washington, D. C., 1883-)* **1989,** *244* (4901), 182-8.
11. Wang, L.; Brock, A.; Herberich, B.; Schultz, P. G., *Science (Washington, DC, U. S.)* **2001,** *292* (5516), 498-500.
12. Duthaler, R. O., *Tetrahedron* **1994,** *50* (6), 1539-650.
13. Williams, R. M.; Hendrix, J. A., *Chem. Rev.* **1992,** *92* (5), 889-917.
14. Najera, C.; Sansano, J. M., *Chem. Rev. (Washington, DC, U. S.)* **2007,** *107* (11), 4584-4671.
15. Petasis, N. A.; Zavialov, I. A., *J. Am. Chem. Soc.* **1997,** *119* (2), 445-446.
16. O'Donnell, M. J.; Bennett, W. D.; Wu, S., *J. Am. Chem. Soc.* **1989,** *111* (6), 2353-5.
17. Corey, E. J.; Xu, F.; Noe, M. C., *J. Am. Chem. Soc.* **1997,** *119* (50), 12414-12415.
18. Ooi, T.; Kameda, M.; Maruoka, K., *J. Am. Chem. Soc.* **1999,** *121* (27), 6519-6520.
19. Strecker, A., In *Ann. Chem. Pharm*, 1850; Vol. 75, p 27.
20. Gröger, H., *Chem. Rev.* **2003,** *103* (8), 2795-2828.

21. Shibasaki, M.; Kanai, M.; Mita, T., *Org. React. (Hoboken, NJ, U. S.)* **2008,** *70*, 1-119.

22. Domling, A.; Ugi, I., *Angew. Chem., Int. Ed.* **2000,** *39* (18), 3168-3210.

23. Dyker, G., *Angew. Chem. Int. Ed.* **1997,** *36* (16), 1700-1702.

24. Leitner, W., *Angew. Chem., Int. Ed. Engl.* **1995,** *34* (20), 2207-21.

25. Jessop, P. G.; Ikariya, T.; Noyori, R., *Chem. Rev. (Washington, D. C.)* **1995,** *95* (2), 259-72.

26. Leitner, W., *Coord. Chem. Rev.* **1996,** *153*, 257-284.

27. Steeneveldt, R.; Berger, B.; Torp, T. A., *Chem. Eng. Res. Des.* **2006,** *84* (9), 739-763.

28. Aresta, M.; Dibenedetto, A., *Dalton Trans.* **2007,** (28), 2975-2992.

29. Sakakura, T.; Choi, J.-C.; Yasuda, H., *Chem. Rev. (Washington, DC, U. S.)* **2007,** *107* (6), 2365-2387.

30. Cannella, R.; Clerici, A.; Panzeri, W.; Pastori, N.; Punta, C.; Porta, O., *J. Am. Chem. Soc.* **2006,** *128* (16), 5358-5359.

31. Park, Y. S.; Beak, P., *J. Org. Chem.* **1997,** *62* (6), 1574-1575.

32. Stead, D.; Carbone, G.; O'Brien, P.; Campos, K. R.; Coldham, I.; Sanderson, A., *J. Am. Chem. Soc.* **2010,** *132* (21), 7260-7261.

33. Coeffard, V.; Beaudet, I.; Evain, M.; Le Grognec, E.; Quintard, J.-P., *Eur. J. Org. Chem.* **2008,** (19), 3344-3351.

34. Mita, T.; Chen, J.; Sugawara, M.; Sato, Y., *Angew. Chem., Int. Ed.* **2011,** *50* (6), 1393-1396, S1393/1-S1393/26.

35. Mita, T.; Chen, J.; Sugawara, M.; Sato, Y., *Org. Lett.* **2012,** *14* (24), 6202-6205.

36. Mita, T.; Higuchi, Y.; Sato, Y., *Chem. - Eur. J.* **2013,** *19* (3), 1123-1128.

37. Fürstner, A., *Pure Appl. Chem.* **1998,** *70* (5).

38. Roskamp, E. J.; Pedersen, S. F., *J. Am. Chem. Soc.* **1987,** *109* (21), 6551-3.

39. McMurry, J. E.; Fleming, M. P., *J. Amer. Chem. Soc.* **1974,** *96* (14), 4708-9.

40. Fürstner, A.; Bogdanović, B., *Angew. Chem. Int. Ed.* **1996,** *35* (21), 2442-2469.

41. Nomura, R.; Matsuno, T.; Endo, T., *J. Am. Chem. Soc.* **1996,** *118* (46), 11666-11667.

42. Silvestri, G.; Scialdone, O., Recent Scientific and Technological Developments in Electrochemical Carboxylation Based on Carbon Dioxide. In *Carbon Dioxide as Chemical Feedstock*, Wiley-VCH Verlag GmbH & Co. KGaA: 2010; pp 317-334.

43. Weinberg, N. L.; Kentaro Hoffmann, A.; Reddy, T. B., *Tetrahedron Lett.* **1971,** *12* (25), 2271-2274.

44. Root, D. K.; Smith, W. H., *J. Electrochem. Soc.* **1982,** *129* (6), 1231-6.

45. Koshechko, V. G.; Titov, V. E.; Bondarenko, V. N.; Pokhodenko, V. D., *J. Fluorine Chem.* **2008,** *129* (8), 701-706.

46. Prikhod'ko, A.; Walter, O.; Zevaco, T. A.; Garcia-Rodriguez, J.; Mouhtady, O.; Py, S., *Eur. J. Org. Chem.* **2012,** *2012* (20), 3742-3746, S3742/1-S3742/33.

47. Maekawa, H.; Murakami, T.; Miyazaki, T.; Nishiguchi, I., *Chem. Lett.* **2011,** *40* (4), 368-369.

48. Zheng, X.; Dai, X.-J.; Yuan, H.-Q.; Ye, C.-X.; Ma, J.; Huang, P.-Q., *Angew. Chem., Int. Ed.* **2013,** *52* (12), 3494-3498.

49. Shohji, N.; Kawaji, T.; Okamoto, S., *Org. Lett.* **2011,** *13* (10), 2626-2629.

50. North, M.; Pasquale, R., *Angew. Chem., Int. Ed.* **2009,** *48* (16), 2946-2948.

51. Molteni, V.; Penzotti, J.; Wilson, D. M.; Termin, A. P.; Mao, L.; Crane, C. M.; Hassman, F.; Wang, T.; Wong, H.; Miller, K. J.; Grossman, S.; Grootenhuis, P. D. J., *J. Med. Chem.* **2004,** *47* (10), 2426-2429.

52. "Electrochemical Series" in CRC Handbook of Chemistry and Physics, 93rd Edition, W. M. Haynes, ed., CRC Press/Taylor and Francis, Boca Raton, FL., 2013.

53. In addition to this role, TMS-Cl may function to activate the magnesium in suspension. See: T. Ohno, M. Sakai, Y. Ishino, T. Shibata, H. Maekawa, and I. Nishiguchi, Org. Lett., 2001, 3, 3439.

54. Padwa, A.; Nimmesgern, H.; Wong, G. S. K., *J. Org. Chem.* **1985,** *50* (26), 5620-7.

55. Martin, S. F.; Yang, C.-P.; Laswell, W. L.; Rüeger, H., *Tetrahedron Lett.* **1988,** *29* (51), 6685-6687.

56. Aurrecoechea, J. M.; Fernandez, A.; Gorgojo, J. M.; Saornil, C., *Tetrahedron* **1999,** *55* (23), 7345-7362.

57. Correa, A.; Martin, R., *Angew. Chem., Int. Ed.* **2009,** *48* (34), 6201-6204.

58. Ohmiya, H.; Tanabe, M.; Sawamura, M., *Org. Lett.* **2011,** *13* (5), 1086-1088.

59. Shi, M.; Nicholas, K. M., *J. Am. Chem. Soc.* **1997,** *119* (21), 5057-5058.

60. Corbet, M.; Zard, S. Z., *Org. Lett.* **2008,** *10* (13), 2861-2864.

61. We confirm that C-silylated product 3 is not involved in the pathway for carboxylation; independent synthesis of 3 and subjection to our standard reductive carboxyaltion reaction conditions results in no reaction.

62. Gao, Y.; Yoshida, Y.; Sato, F., *Synlett* **1997,** *12* (12), 1353-1354.

63. Tarselli, M. A.; Micalizio, G. C., *Org. Lett.* **2009,** *11* (20), 4596-4599.

64. Wolan, A.; Six, Y., *Tetrahedron* **2010,** *66* (1), 15-61.

65. Corey, E. J.; Rao, S. A.; Noe, M. C., *J. Am. Chem. Soc.* **1994,** *116* (20), 9345-9346.

66. Fukuhara, K.; Okamoto, S.; Sato, F., *Org. Lett.* **2003,** *5* (12), 2145-2148.

67. Beenen, M. A.; An, C.; Ellman, J. A., *J. Am. Chem. Soc.* **2008,** *130* (22), 6910-6911.

68. Ohishi, T.; Nishiura, M.; Hou, Z., *Angew. Chem. Int. Ed.* **2008,** *47* (31), 5792-5795.

69. Nicewicz, D. A.; MacMillan, D. W. C., *Science* **2008,** *322* (5898), 77-80.

70. Dai, C.; Narayanam, J. M. R.; Stephenson, C. R. J., *Nat Chem* **2011,** *3* (2), 140-145.

71. Flamigni, L.; Barbieri, A.; Sabatini, C.; Ventura, B.; Barigelletti, F., Photochemistry and Photophysics of Coordination Compounds: Iridium. In *Photochemistry and Photophysics of Coordination Compounds II*, Balzani, V.; Campagna, S., Eds. Springer Berlin Heidelberg: Berlin, Heidelberg, 2007; pp 143-203.

72. Seayad, A. M.; Ramalingam, B.; Yoshinaga, K.; Nagata, T.; Chai, C. L. L., *Org. Lett.* **2010,** *12* (2), 264-267.

73. Ojima, I.; Habus, I.; Zhao, M.; Zucco, M.; Park, Y. H.; Sun, C. M.; Brigaud, T., *Tetrahedron* **1992,** *48* (34), 6985-7012.

74. Maginnity, P. M.; Eisenmann, J. L., *J. Am. Chem. Soc.* **1952,** *74* (23), 6119-6121.

75. He, L.-P.; Chen, T.; Gong, D.; Lai, Z.; Huang, K.-W., *Organometallics* **2012,** *31* (14), 5208-5211.

76. Al-Rawi, J. M. A.; Saleem, L. M. N., *Magn. Reson. Chem.* **1989,** *27* (6), 540-543.

77. Zucca, C.; Bravo, P.; Corradi, E.; Meille, S.; Volonterio, A.; Zanda, M., *Molecules* **2001,** *6* (5), 424.

78. Zanardi, A.; Mata, J. A.; Peris, E., *Chem. Eur. J.* **2010,** *16* (34), 10502-10506.

79. Anderson, J. C.; Blake, A. J.; Koovits, P. J.; Stepney, G. J., *J. Org. Chem* **2012,** *77* (10), 4711-4724.

80. Esteruelas, M. A.; Honczek, N.; Oliván, M.; Oñate, E.; Valencia, M., *Organometallics* **2011,** *30* (9), 2468-2471.

81. García Ruano, J. L.; Alemán, J.; Alonso, I.; Parra, A.; Marcos, V.; Aguirre, J., *Chem. Eur. J.* **2007,** *13* (21), 6179-6195.

82. Anderson, J. C.; Howell, G. P.; Lawrence, R. M.; Wilson, C. S., *J. Org. Chem* **2005,** *70* (14), 5665-5670.

83. Shang, G.; Yang, Q.; Zhang, X., *Angew. Chem. Int. Ed.* **2006,** *45* (38), 6360-6362.

Chapter 3

Catalytic Oxidative Carboxylation of Olefins in Flow Reactors

While there are numerous reports on the catalytic carboxylation of epoxides the literature on direct catalytic oxidative carboxylation of olefins is lacking. This chapter describes the design and development of a catalytic manifold to convert olefins directly into cyclic carbonates. We take advantage of the superior mass transfer properties of flow reactors to carry out the transformation under relatively mild conditions of temperature and pressure. Further we show that the use of an in-line membrane separator is a powerful strategy to couple reactions containing orthogonally reactive reagents, and can enable the design of new flow processes involving incompatible reagents.

3.1 Introduction and Reaction Design

Organic carbonates are versatile molecules serving as raw materials for polycarbonate and polyurethane synthesis,[1] green solvents,[2] gasoline additives,[3-4] electrolytes in energy storage devices,[5-7] and fine chemical intermediates.[8-12] While acyclic carbonates are produced by oxidative carbonylation of alcohols or phenols, the five membered cyclic carbonates can be produced from diols, or epoxides and a one carbon synthon (Figure 3.1).[13] Traditionally the most commonly used one carbon synthon for carbonate production has been phosgene,[14] but its toxicity and low atom economy make this route unattractive. Alternatively, carbon dioxide is an ideal C1 synthon due to its low cost, low toxicity, and wide availability.[15-19] The reaction of carbon dioxide and epoxide represents a 100% atom efficient approach for the production of cyclic carbonates and is one of the few industrially relevant reactions utilizing carbon dioxide.[20-21]

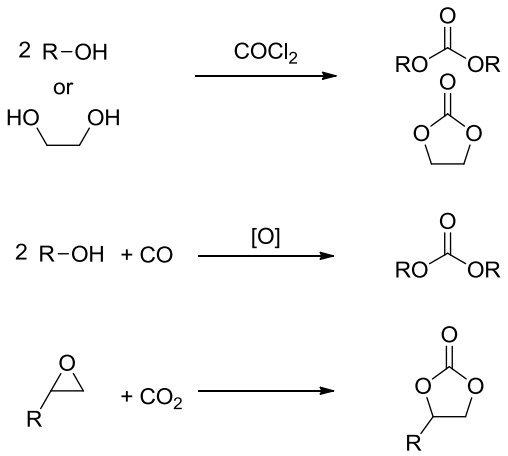

Figure 3.1. Strategies for synthesis of organic carbonates

A more straightforward approach to the synthesis of these important molecules would be the direct oxidative carboxylation of olefins (Figure 3.2). Such a process would obviate the need for isolation and purification of, often unstable and highly reactive epoxides. The strategies for oxidative carboxylation can be broadly classified into: i) sequential one-pot oxidation followed by carboxylation,[22] ii) simultaneous one-pot oxidation and carboxylation,[23-25] and iii) carboxylation via oxy-halogenation.[26-30] Only a handful of examples of catalytic approaches to organic carbonates from olefins are known. Although these present an excellent proof-of-concept, they suffer from low yields, low selectivity, long reaction times, and are applicable to very specific substrates.[23-24, 27-28] The utility of the elegant work by the Jamison group describing the flow synthesis of these molecules is mitigated only by the use of super-stoichiometric bromide reagents and the subsequent waste generation.[29-30]

Of the described strategies for oxidative carboxylation, sequential epoxidation and carboxylation are most suited for the design of a catalytic approach as both the individual reactions, olefin epoxidation and epoxide carboxylation, are well studied. The challenge associated with conducting these reactions in a single pot comes from the fact that an oxidant is essential to carry out the epoxidation reaction, but it is incompatible with the carboxylation

catalyst system which usually employs a Lewis base. Hydrogen peroxide is the oxidant of choice for the epoxidation reaction as it produces water as the only by-product. This however, leads to a biphasic epoxidation reaction (as most olefins are hydrophobic) and hence requires long reaction times as mass transfer across the aqueous-organic interface control the rate of the reaction.[31] Reaction rates are proportional to the extent of this interface, which can be increased by mixing or by a reduction in volume of the individual phases. The latter can be achieved through reactor configurations leading to an increased surface area to volume ratio.

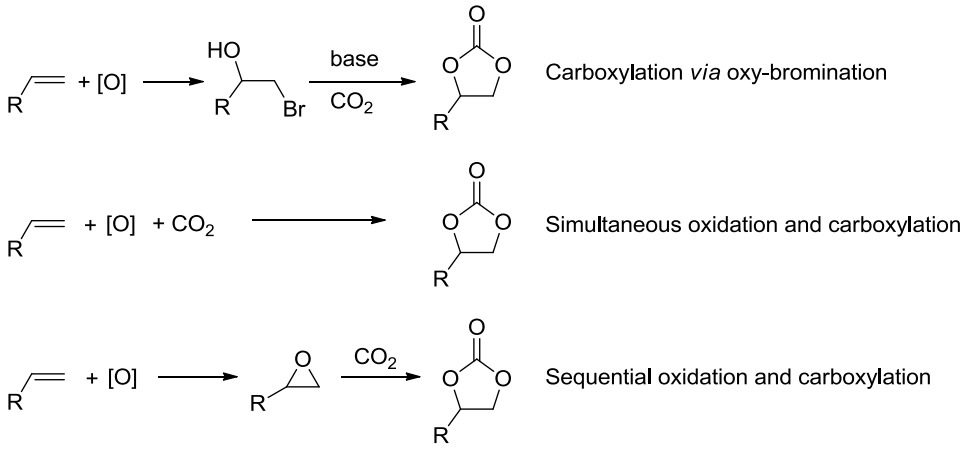

Figure 3.2 Precedents for direct oxidative carboxylation of olefins for the synthesis of cyclic organic carbonates

Flow chemistry has emerged as an enabling technology which can be utilized to overcome both of these problems.[32-39] The superior surface area to volume ratio afforded by flow reactors make them especially advantageous for carrying out multiphase reactions due to increased interfacial area between phases.[40-42] For reactions involving gases, flow reactors provide an added advantage of increased process safety by enabling superior control over the amount of gas required for the reaction, while also eliminating the need for highly capital intensive pressure vessels required to maintain a constant pressure in the headspace above the reaction mixture.[43-44] Finally, flow processes enable multicomponent reactions which employ

mutually incompatible reagents by allowing sequential introduction of reagents at different points, both spatially and temporally.[29, 45-46] We describe here the utility of flow reactors by presenting a direct catalytic synthesis of cyclic organic carbonates starting from olefins and utilizing carbon dioxide. Our strategy involves a rhenium catalyzed epoxidation of the olefin followed by trapping the epoxide by CO_2 in the presence of an aluminum catalyst and iodide salt. The key to the success of this methodology is the use of a membrane separator to compartmentalize the mutually incompatible oxidizer and the Lewis basic carboxylation catalyst system.

3.2 Selection and optimization of epoxidation catalyst system and flow reactor

The methyltrioxorhenium (MTO) catalyzed epoxidation of olefins is an efficient and general methodology employing H_2O_2 as a benign and green terminal oxidant.[47-48] The system is also highly selective towards the epoxide. We started our investigation by employing styrene as a model substrate. During preliminary batch investigations we noted that the conversion of styrene to styrene oxide was influenced by the rate of mixing, with negligible conversion at 100 rpm which increased to around 95% at 600 rpm (Figure 3.3). Increasing the stirring rate further had no effect on the conversion. This confirmed our hypothesis that the rate of epoxidation is influenced by the rate of mass transfer across the aqueous-organic interface.

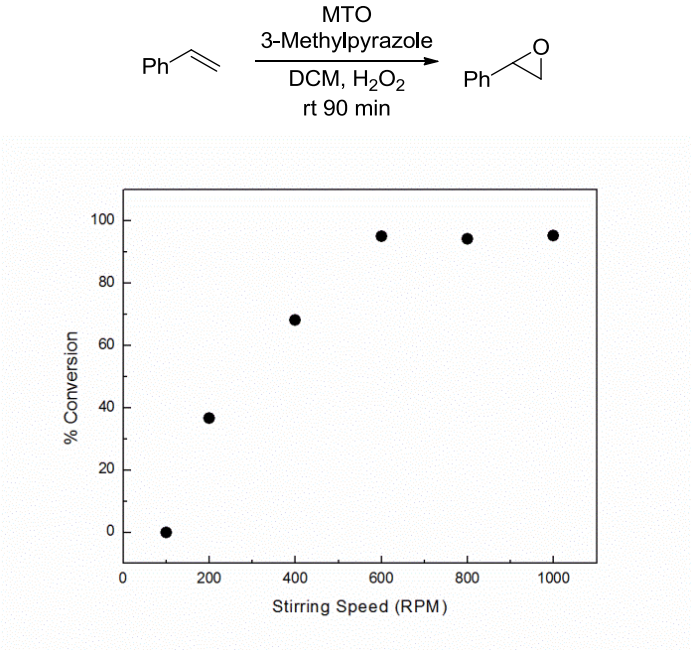

Figure 3.3. Effect of stirring speed on conversion of styrene to styrene oxide. Conditions: styrene: 3 mmol, MTO: 0.03 mmol, 3-methylpyrazole: 0.72 mmol, H_2O_2: 6 mmol. Conversions based on GC-FID analysis of crude reaction mixture

A packed bed reactor, made from polytetrafluoroethylene (PTFE) tubing and packed with sand, was utilized to maximize the contact between the two phases. PTFE was chosen as the material of construction because stainless steel is known to decompose H_2O_2.[49] Only 1 mol% catalyst was found to be sufficient to effect almost complete conversion of styrene to styrene oxide at 40°C in 30 minutes (Figure 3.6).

The MTO catalyzed epoxidations have been shown to be markedly improved, both in terms of activity and selectivity, by the use of N-donor ligands.[48, 50-52] We decided to utilize 3-methylpyrazole at an optimum of 24 mol% loading (Table 3.1 entries 2-4, Figure 3.7) owing to its demonstrated activity in the epoxidation of a wide variety of olefin substrates.[53] Deviation from the optimized temperature led to lower conversion (Table 3.1 entries 7-9, Figure 3.8), which at higher temperatures was attributed to catalyst decomposition.[54] An excess of the oxidant was required to achieve good conversion of the olefin within 30 minutes (Table 3.1, entries 6, 10, 11,

Figure 3.9). Although 30 minutes was found to be sufficient time for almost complete conversion of styrene (Figure 3.10) we employed 45 minutes in the subsequent substrate scope studies to negate any effect of the change in steric or electronic properties of the olefin employed. Finally, we optimized the styrene concentration to 4M which provided a high concentration of the epoxide for the next step of the reaction sequence, while ensuring solubility of all reactants, including the epoxides. (Figure 3.11).

Table 3.1. Optimization of epoxidation reaction in flow reactor

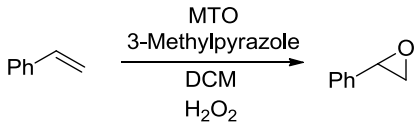

Entry	Catalyst loading (mol %)	Co-catalyst loading (mol %)	Residence time (min)	Temp (°C)	Eq. H_2O_2	Conversion (%)[a]
1	0.5	12	30	40	5	78
2[c]	1	24	30	40	5	97
3[c]	1	12	30	40	5	82
4	1	6	30	40	5	68
5	1	24	10	40	5	80
6	1	24	60	40	5	97
7	1	24	30	30	5	84
8	1	24	30	60	5	81
9	1	24	30	80	5	50
10	1	24	30	40	3	88
11	1	24	30	40	1	51

[a] Conversion based on GC-FID analysis of reaction mixture using dodecane as internal standard.

3.3 Selection and optimization of carboxylation catalyst system and flow reactor

We next turned our attention towards optimizing epoxide carboxylation utilizing styrene oxide as a model substrate. The carboxylation of epoxides is a well-studied reaction and a variety of systems utilizing a combination of Lewis acids and Lewis bases have been shown to catalyze the transformation.[55-57] Amongst them, the aluminum based systems have shown to be most active and were hence chosen in this study.[58-60]

Specifically, an amino trisphenolate complexed aluminum catalyst with a tetrabutylammonium iodide (TBAI) co-catalyst was employed. Stainless steel tubing packed with sand was used as the reactor. We found that a modest 2 mol% catalyst loading in the presence of 10 mol% TBAI was sufficient to obtain complete conversion of styrene oxide to styrene carbonate at 100°C in 40 minutes (Figure 3.12-Figure 3.14). This represents an improvement over the typical conditions found in the literature for these reactions which require longer reactions times or higher temperatures and pressures under neat conditions.[58, 60] Deviation from these conditions led to a decrease in the yield of the carbonate (Table 3.2, entries 2-8). We also note that the product is stable under the reaction conditions for extended time (Table 3.2, entry 9)

Table 3.2. Optimization of carboxylation flow reactor using styrene oxide as model substrate

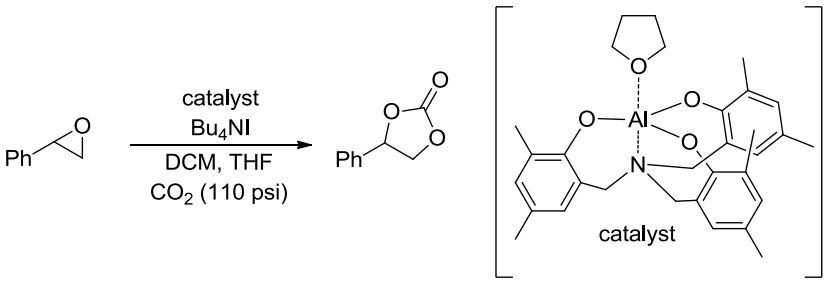

Entry	Catalyst loading (mol %)	Co-catalyst loading (mol %)	Residence time (min)	Temp (°C)	Conversion (%)[a]
1	2	10	40	100	100
2	2	6	40	100	97
3	2	2	40	100	49
4	2	10	40	80	79
5	2	10	40	60	67
6	2	10	40	40	62
7	2	10	20	100	86
8	2	10	30	100	94
9	2	40	75	100	100

[a] Conversion based on ^{1}H-NMR analysis of crude reaction mixtures.

3.4 Combining epoxidation and carboxylation in one pass: Role of in-line membrane separator

With the individual reactions optimized, we coupled the two reactions to realize our aim of direct oxidative carboxylation. The reactor system was assembled as shown in (Figure 3.4). The epoxidation and carboxylation reactors were identical to those described above. The organic solution, containing the olefin, catalyst and co-catalyst, and the aqueous peroxide solution were loaded into gas-tight syringes and introduced into the system using syringe pumps. The streams were mixed using a T-mixer, forming a segmented flow pattern, before entering the epoxidation reactor. As the excess peroxide employed in the epoxidation reaction is detrimental to the

carboxylation reaction we utilized a PTFE membrane based separator to partition the aqueous and organic phases coming out of the epoxidation reactor. Phase separation is achieved by preferential wetting of the fluoropolymer membrane by the permeating organic phase and retention of the aqueous solution.[61] The aqueous phase was sent to a bulk collection vessel and the separator outlet containing the organic stream was mixed with the carboxylation catalyst solution in another T-mixer. This solution was then mixed with CO_2 gas introduced from a mass flow controller. The gas-liquid segmented flow then entered the carboxylation reactor. The back pressure of the system was set by pressurizing the bulk collection vessels with Argon. A slow bleed was maintained in order to ensure steady state conditions. The reaction mixture was withdrawn from the system using a 6-way sampling valve and analyzed using ^{1}H-NMR spectroscopy

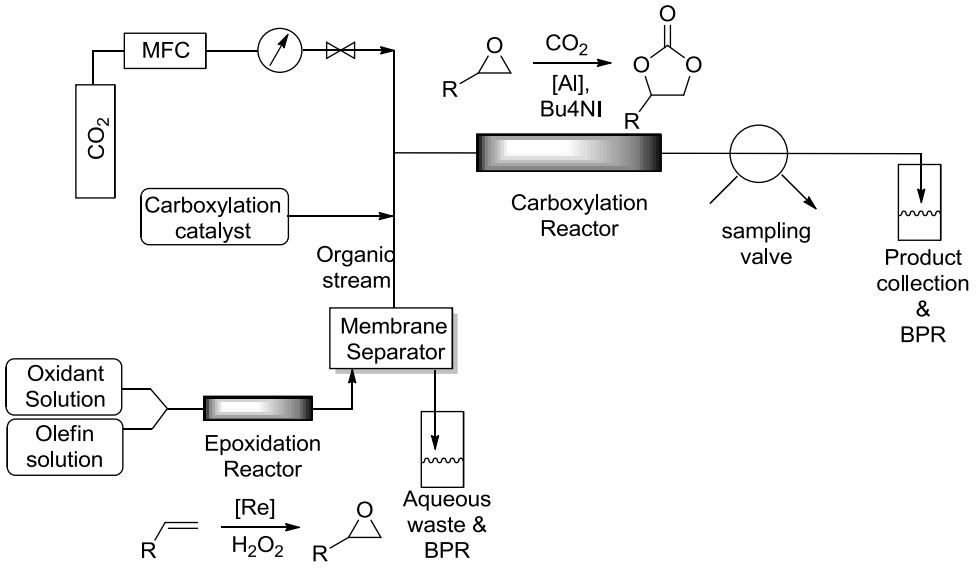

Figure 3.4. Reactor schematic for oxidative carboxylation of olefins.

3.5 Substrate scope of direct catalytic oxidative carboxylation of olefins

Gratifyingly when styrene was subjected to the reaction conditions quantitative yield of the corresponding carbonate was obtained. The transformation is influenced by steric bulk around the olefin as evidenced by the reduced yield of ortho and meta substituted styrenes (Table 3.3, entries e&f). Both electron-rich and electron-poor styrenes undergo the reaction; however, internal olefins do not undergo the transformation.[62] We found the epoxidation reaction proceeds without complications, but the carboxylation of internal epoxides was not successful under the developed conditions, presumably due to the increased steric bulk around the epoxide ring.

Table 3.3. Substrate scope of catalytic oxidative carboxylation.

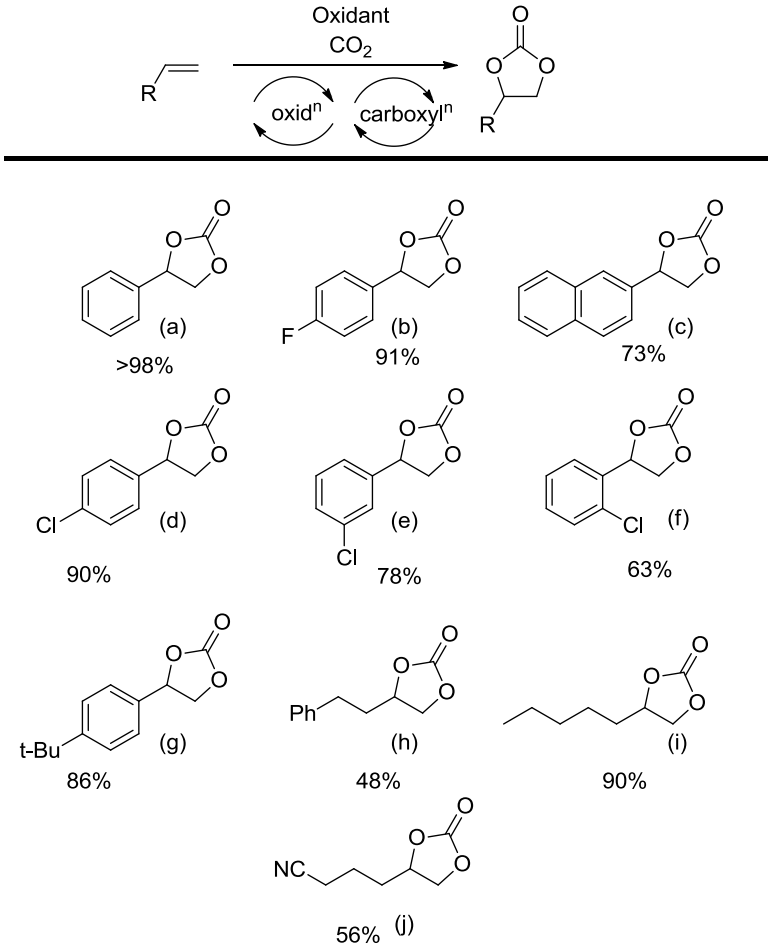

The developed protocol can also be extended to aliphatic olefins and functional groups such as halogens and nitrile were well tolerated. Additionally, we note that there is no erosion in the yield of the carbonate when the system was maintained online for a period of 7 hours in the case of oxidative carboxylation of styrene. The present protocol is limited by the partitioning capability of the epoxides, generated in the first step, between water and the organic phase. As a consequence olefins having low molecular weight or highly polar substituents are not viable substrates for the developed protocol as they are freely miscible with water and hence cannot be separated using the membrane separator. It is important to note that this reaction sequence cannot be carried out in a typical batch set up as the tetrabutylammonium iodide and hydrogen peroxide are incompatible with each other and react violently when mixed. When we ran the reaction in sequential mode using styrene (by separating the peroxide and adding the carboxylation catalyst mixture to the resulting organic layer) we found that the yield of the styrene carbonate was 88%, as compared to a quantitative yield in the flow reactor.

To test whether the separation of the aqueous and organic phase can help with the recycling of the rhenium catalyst, we decided to analyze the partitioning of the Re between the two phases. Unfortunately we found that the Re concentration in the two phases was almost identical, making straightforward recycling difficult.[63] However, we believe that this work can also be applied towards heterogeneous supported catalysts which will facilitate the catalyst recovery and reuse.[64]

3.6 Summary and Outlook

In conclusion we have developed a novel strategy for the synthesis of cyclic organic carbonates starting from olefins and utilizing carbon dioxide. Our methodology employs a cheap and green oxidant, is scalable and enables carrying out the reaction under relatively mild conditions of temperature and pressure. To the best of our knowledge, this is the first example of catalytic oxidative carboxylation in flow reactors. We believe the in-line liquid-liquid separation can be utilized as a general strategy to segregate incompatible reagents (Lewis acids and bases, oxidizer and reductants, etc.) and couple syntheses requiring orthogonally reactive intermediates.

As more active catalysts are developed for carboxylation of internal and sterically hindered epoxides, this method can be extended to a wider variety of substrates. The future direction of research could be directed towards using air or oxygen as the terminal oxidant for the epoxidation reaction. Since the aerobic oxidation of ethylene is widely studied and practiced industrially, it could provide a good entry point into the study of such systems. Direct gas phase oxidative carboxylation of ethylene or propylene to the respective carbonates also has the potential to be scaled up as ethylene and propylene carbonates are industrially relevant compounds.

3.8 Experimental Section

General Experimental Remarks

All reagents were obtained from commercial vendors (TCI, Sigma-Aldrich, Alfa-Aesar) and used without purification unless noted. NMR data was collected on Bruker Avance CDPX 300 or DRX 400 MHz instruments. Spectra were referenced internally to tetramethylsilane (TMS) ($CDCl_3$: 0.00 ppm (^1H), 0.0 (^{13}C). Gas chromatography was performed on Agilent 7890A equipped with a HP-5 column and flame ionization detector (GC-FID). The following method was used for analysis. Inlet temperature: 230 °C, carrier gas (Argon) flow rate: 5 mL/min (column), split ratio 38:1, oven program: 50 °C for 1 minute, 10 °C/min to 100 °C, hold at 100 °C for 2.5 minutes, FID temperature: 250 °C, H_2 flow rate: 30 mL/min, air flow rate: 300 mL/min, make-up flow rate: 30 mL/min. Mass spectrometric measurements were performed at University of Illinois (Champaign, IL) and the Pennsylvania State University Proteomics and Mass Spectrometry Core Facility (University Park, PA). Standard tube fittings were purchased from Swagelok and IDEX health and science.

II. Effect of stirring speed on yield in batch reactor

In a 25 ml round bottom flask equipped with a 1/4 inch stir bar were added methyltrioxorhenium (7.5 mg, 0.03 mmol), dodecane (68 μL, 0.3 mmol), styrene (0.345 mL, 3 mmol), 3-methylpyrazole (58 μL, 0.72 mmol), and dichloromethane (to adjust final volume to 1.5 mL). 30% H_2O_2 (aq) solution (0.64 mL, 6 mmol) was then added to the mixture and the flask was sealed with a rubber septum. The flask was placed on a stir plate and the reaction mixture was stirred at the desired RPM for 1.5 hours at room temperature.

After 1.5 hours the stirring was stopped and approximately 0.5 mL of the organic layer was pipetted into a 2 mL vial. The crude organic layer was analyzed using GC. The styrene

conversion was determined by gas chromatography. Figure S1 shows the plot for conversion as a function of stirring rate.

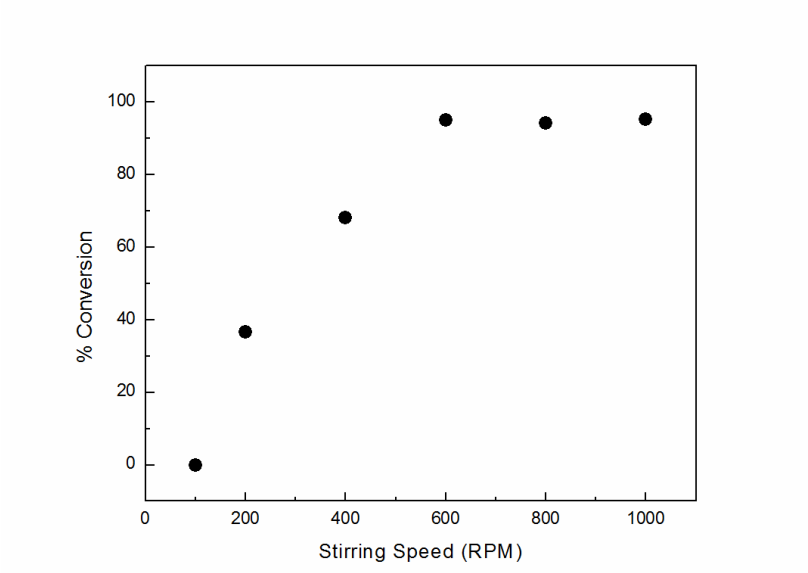

Figure 3.5. Effect of stirring speed on the conversion of styrene to styrene oxide.

III. Optimization of epoxidation flow reactor

a. Preparation of reactant solutions

In a 20 mL scintillation vial, methyltrioxorhenium, dodecane (internal standard) (10 mol%), styrene, 3-methylpyrazole and dichloromethane were added together. The quantity of reactants added depended on the variable being optimized. The mixture was stirred until the catalyst dissolved and subsequently loaded into a 5 mL gas-tight glass syringe after passing through a 0.2 μm PTFE syringe filter. A small aliquot of the solution was analyzed using GC before the reaction. Another 5 mL glass gas tight syringe was filled with 30% H_2O_2 (aq) solution.

b. Reaction procedure and product quantification

The temperature controller was turned on and the epoxidation reactor was set to the desired temperature. After the temperature stabilized the gas tight syringes containing the styrene and H_2O_2 (aq) solutions were loaded onto syringe pumps (New Era NE-510). A 40 psi back pressure regulator from IDEX was attached to the reactor outlet. The pumps were started with their respective flow rates. After constant segmented flow was seen, the system was run for 1.5 residence times. This ensured that the system reached steady state when the reaction mixture was analyzed. For analysis, the reaction mixture was collected in a vial containing MnO_2 to quench the excess peroxide and terminate the reaction. After effervescence ceased, approximately 0.5 mL of DCM was added to the reaction mixture. The organic layer was separated from the aqueous layer using a Pasteur pipette. The crude organic layer was analyzed using GC-FID. The conversion of styrene was determined by comparing the initial and final area ratios of styrene to the internal standard (dodecane).

The conversion of styrene as a function of catalyst loading, co-catalyst loading, oxidant equivalents, residence time, concentration and temperature was studied and the data collected is presented below.

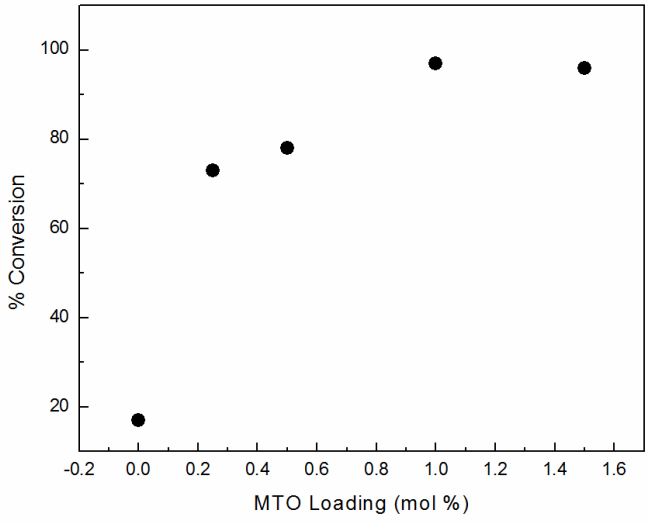

Figure 3.6. Effect of catalyst loading on styrene epoxidation. Temperature = 40 °C, oxidant = 5 equiv, co-catalyst = 24 mol%, residence time = 30 mins, concentration = 4M, organic flow rate = 0.32 mL/h, aqueous flow rate = 0.68 mL/h.

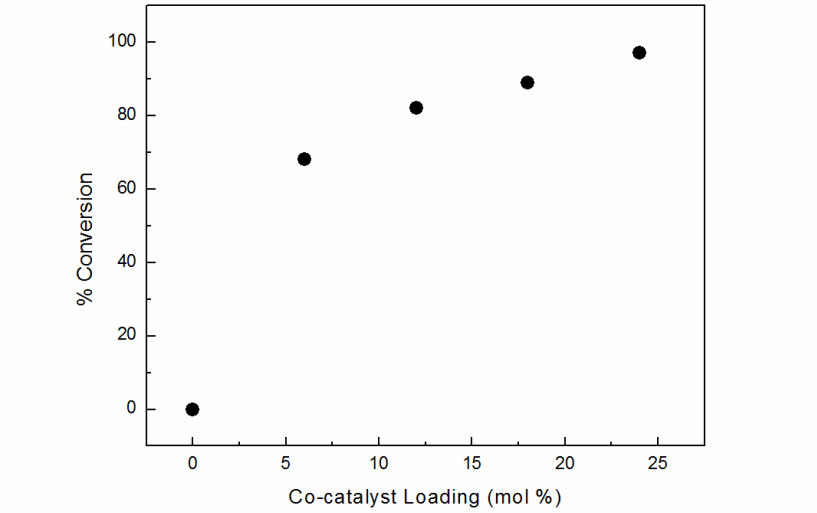

Figure 3.7 Effect of co-catalyst loading on styrene epoxidation. Temperature = 40 °C, oxidant = 5 equiv, catalyst = 1 mol%, residence time = 30 mins, concentration = 4M, organic flow rate = 0.32 mL/h, aqueous flow rate = 0.68 mL/h.

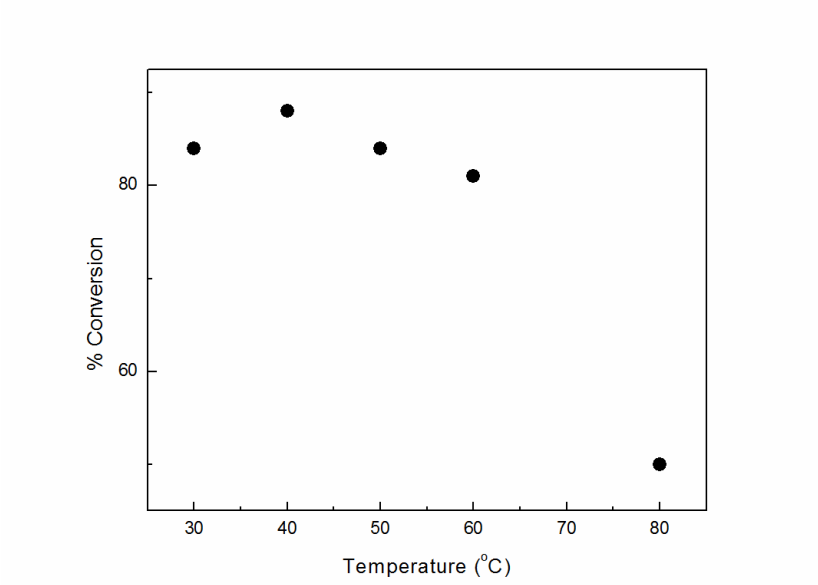

Figure 3.8. Effect of temperature on styrene epoxidation. Oxidant = 4.7 equiv, co-catalyst = 24 mol%, catalyst = 1 mol%, residence time = 30 mins, concentration = 2M, organic flow rate = 0.5 mL/h, aqueous flow rate = 0.5 mL/h.

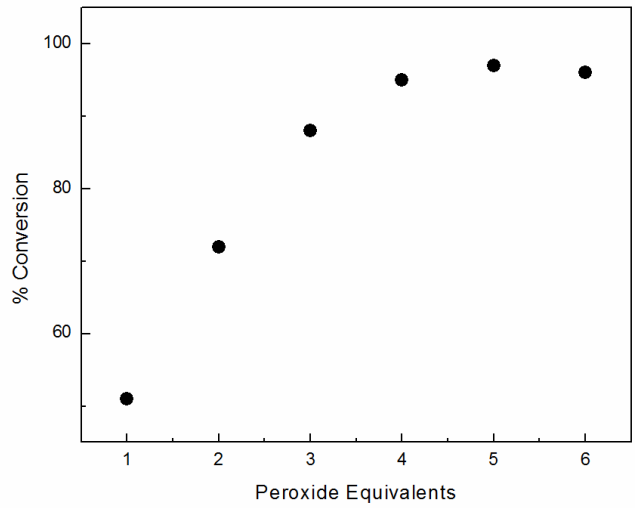

Figure 3.9. Effect of H_2O_2 equivalents on styrene epoxidation. Temperature = 40 °C, co-catalyst = 24 mol%, catalyst = 1 mol%, residence time = 30 mins, concentration = 4M, total flow rate = 1 mL/h. Note: Oxidant equivalents were varied by changing the ratio of organic to aqueous flow rate.

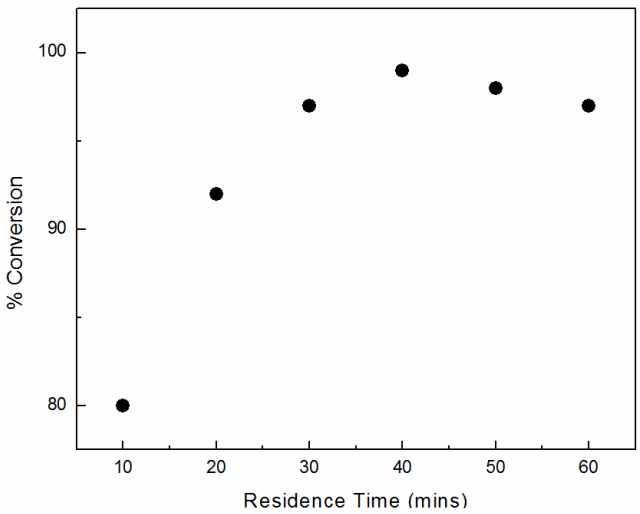

Figure 3.10. Effect of residence time on styrene epoxidation. Temperature = 40 °C, oxidant = 5 equiv., co-catalyst = 24 mol%, catalyst = 1 mol%, concentration = 4M.

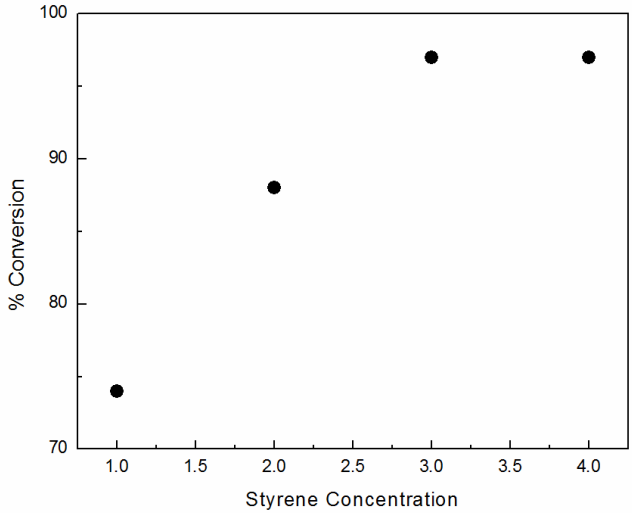

Figure 3.11. Effect of concentration on styrene epoxidation. Temperature = 40 °C, oxidant = 5 equiv, co-catalyst = 24 mol%, catalyst = 1 mol%, residence time = 30 mins, total flow rate = 1 mL/h. Note: Oxidant equivalents were kept constant by changing the ratio of organic to aqueous flow rate.

IV. Optimization of carboxylation flow reactor

a. Preparation of reactant solutions

In a 20 mL scintillation vial, aluminum catalyst, styrene oxide, tetrabutylammonium iodide, DCM and THF were combined. The mixture was stirred until all the solids dissolved and subsequently transferred into a 5 mL gas-tight glass syringe after passing through a 0.2 μm PTFE syringe filter.

b. Initialization of flow reactor

A syringe containing dichloromethane was loaded onto the syringe pump and the CO_2 cylinder was pressurized to 140 psi, and the Argon cylinder for the back pressure regulator (BPR) was pressurized to 100 psi. The pressure was allowed to equilibrate and the CO_2 mass flow controller was adjusted to the desired setting. The micro metering valve on the BPR was opened to maintain a slow bleed. After the pressure at the CO_2 inlet to the reactor stabilized, the temperature controllers were turned on and adjusted to the desired set point.

c. Reaction procedure and product quantification

After the temperature stabilized the syringes were replaced with those containing the reagent solution. The liquid flow rates were set to 10 mL/h until the liquid pressure just exceeded the system pressure, i.e. when flow starts. The liquid and gas flow rates were adjusted to obtain the desired residence times. After steady state was reached (2 residence times), the reaction mixture was withdrawn using the 6-way valve. Approximately 200 μL of the sample was withdrawn and the solvent removed *in-vacuo*. The crude mixture was analyzed using ^{1}H NMR (in $CDCl_3$) and the conversion was determined by comparing the ratio of the protons of the styrene oxide to the protons of the cyclic carbonate.

The styrene oxide conversion was studied as a function of residence time, temperature and co-catalyst loading.

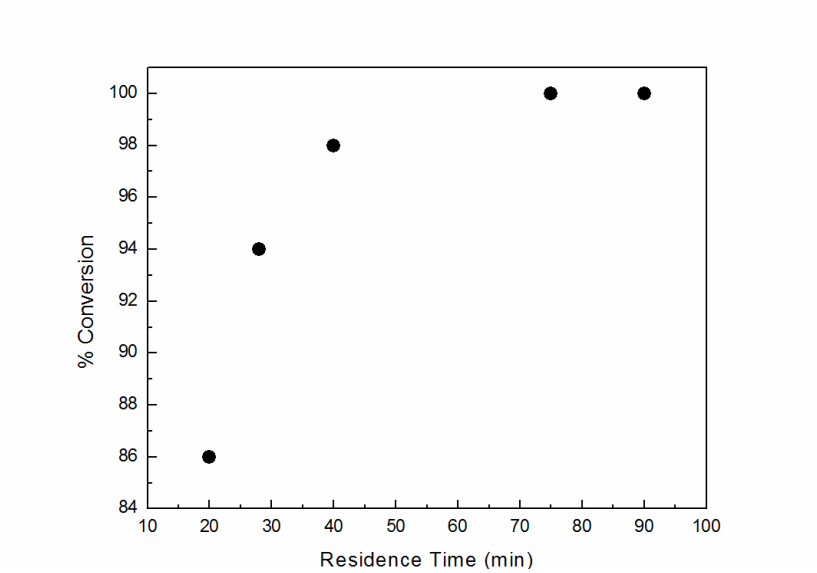

Figure 3.12. Effect of residence time on conversion of styrene oxide to styrene carbonate. Temperature = 100 °C, Al catalyst loading = 2 mol%, co-catalyst (Bu_4NI) = 10 mol%, concentration = 2M, CO_2 pressure = 110 psi.

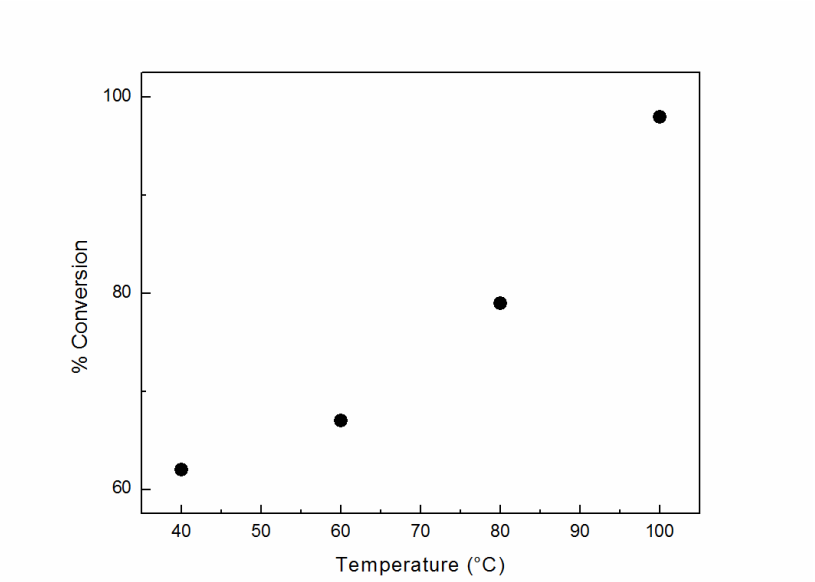

Figure 3.13. Effect of temperature on conversion of styrene oxide to styrene carbonate. Al catalyst loading = 2 mol%, co-catalyst (Bu_4NI) = 10 mol%, concentration = 2M, CO_2 pressure = 110 psi, residence time = 40 mins.

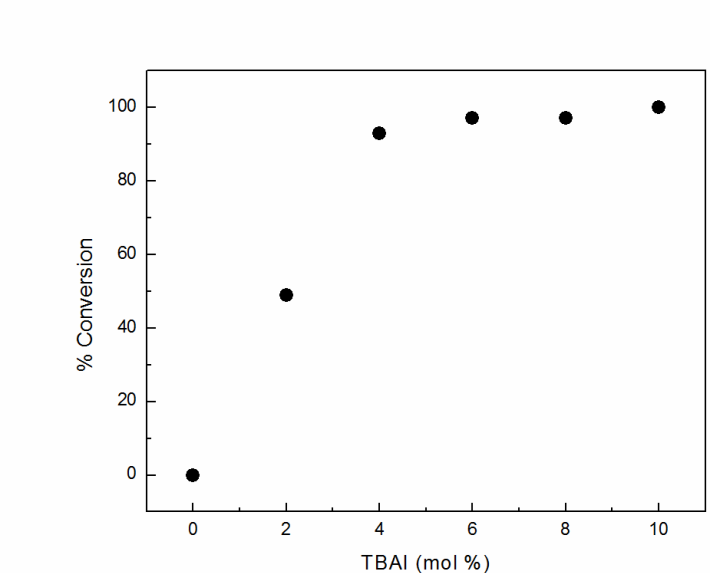

Figure 3.14. Effect of co-catalyst loading on conversion of styrene oxide to styrene carbonate. Al catalyst loading = 2 mol%, concentration = 2M, CO_2 pressure = 110 psi, residence time = 40 mins.

V. Procedure for sequential batch epoxidation and carboxylation of styrene

To a 20 mL three necked flask equipped with a reflux condenser, methyltrioxorhenium (30 mg), 1,4-dinitrobenzene (internal standard) (50.4 mg), olefin (12 mmol), 3-methylpyrazole (0.232 mL), and dichloromethane (to adjust final volume to 3 mL) were added together. This flask was placed in an ice bath and 6.4 mL of 30% H_2O_2 solution was added dropwise to the vial. Once the addition was complete the flask was removed from the ice bath and transferred to an oil bath set at 40 °C. The reaction was carried out for 30 minutes, after which the contents of the flask were transferred to a separating funnel. The aqueous and organic layers were separated and the organic layer was collected in a 20 mL vial.

To the vial was added the aluminum catalyst (0.124 g, 0.24 mmol), Bu_4NI (0.443g, 1.2mmol), DCM (2.4mL) and THF (0.6 mL). This was then transferred to an autoclave which was subsequently pressurized to 110 psi. The autoclave was placed in an oil bath maintained at 110 °C. After 45 minutes the autoclave was placed in an ice bath and once it cooled down to room temperature was vented.

An aliquot of the reaction mixture was withdrawn for NMR analysis in $CDCl_3$, which indicated a yield of 88% styrene carbonate.

VI. General procedure for the direct oxidative carboxylation of olefins

a. Preparation of reactant solutions

In a 20 mL scintillation vial, methyltrioxorhenium (30 mg), 1,4-dinitrobenzene (internal standard) (50.4 mg), olefin (12 mmol), 3-methylpyrazole (0.232 mL), and dichloromethane (to adjust final volume to 3 mL) were added together. The mixture was stirred until all the solids dissolved and subsequently transferred into a 5 mL gas tight glass syringe. Another 5 mL gas-tight glass syringe was filled with 30% H_2O_2 (aq) solution. In another 20 mL scintillation vial, the aluminum catalyst (0.124 g, 0.24 mmol), Bu_4NI (0.443g, 1.2mmol), DCM (2.4mL) and THF (0.6 mL) were combined. The mixture was stirred until all the solids were dissolved, and the solution loaded into a 5 mL gas-tight glass syringe after passing through a 0.2 μm PTFE syringe filter.

b. Initialization of flow reactor

The syringe pumps were initially loaded with syringes containing pure solvents, dichloromethane for the organic reaction streams and distilled water for the aqueous stream. All three pumps were started with an initial flow rate of 6 mL/h. The CO_2 cylinder was pressurized to 140 psi, and the Argon cylinder for the back pressure regulator (BPR) was pressurized to 100 psi. The pressure was allowed to equilibrate and the CO_2 mass flow controller was adjusted to the desired setting (1 sccm). The micro metering valve on the BPR was opened to maintain a slow bleed. After the pressure at the CO_2 inlet to the reactor stabilized, the temperature controllers were turned on and the epoxidation reactor was set to 40 °C and the carboxylation reactor was set to 100 °C.

c. Reaction procedure and product quantification

After the temperature stabilized the syringes were swapped with those containing the reagent solutions. The liquid flow rates were set to 10 mL/h until the liquid pressure reached the system pressure i.e. when flow starts. The liquid flow rates were then adjusted as follows: olefin – 0.32 mL/h; peroxide – 0.68 mL/h; and the carboxylation catalyst – 0.32 mL/h. The CO_2 flow rate was set at 1 sccm.

After steady segmented flow was seen, the system was run for 7 h. This ensures that the system is at steady-state when analyzing the reaction mixture. The reaction mixture was then withdrawn using a 6 way valve. Approximately 200 μL of the sample was withdrawn and the solvent removed *in-vacuo*. The crude mixture was analyzed using ^1H NMR (in $CDCl_3$) and the yield of the reaction is determined by comparing the ratio of the protons of the internal standard (1,4-dinitrobenzene) to the protons of the cyclic carbonate.

Once the reaction was completed, the flow reactor was depressurized by turning off the gas inlets and opening the micro metering valve to vent the BPR. The product collected in the BPR was chromatographed on silica gel using ethyl acetate/hexanes on a Combiflash Rf+.

VII. Procedure for ICP analysis of Re in reactor effluent.

50 μL of reactor effluent (aqueous or organic) was taken in a 20 mL scintillation vial. It was evaporated to dryness under vacuum. To the residue was added 2 mL of conc. HNO_3 which was subsequently boiled off to digest all the Re. To this solution was added 10 mL of 2% HNO_3 solution and the resulting solution was filtered through a 0.2 μm PTFE syringe filter. The solution was analyzed by ICP-OES to determine the concentration of the rhenium in each phase.

It was found that the Re partitioned to 56% in the aqueous and 44% in the organic phase.

VIII. Reactor Setup

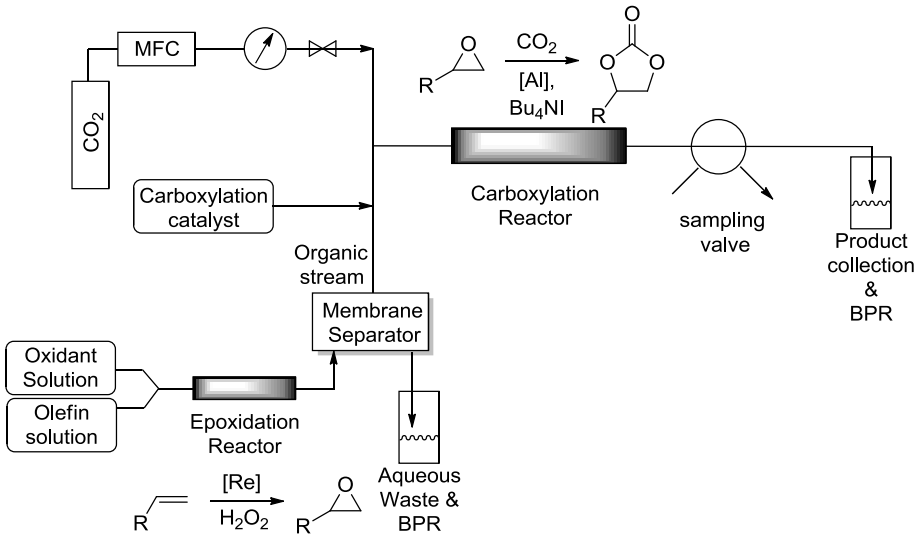

Figure 3.15: Reactor setup for oxidative carboxylation of olefins.

The oxidative carboxylation reactor was setup as shown in Figure S11. The organic solution, containing the olefin, catalyst and co-catalyst, and the aqueous peroxide solution were loaded into gas-tight syringes and introduced into the system using syringe pumps. The fluidic connections were made using either flat bottom or compression fittings. The streams were mixed using a T-mixer before entering the epoxidation reactor, which was made from 1/8" PTFE tubing and packed with sand. A PTFE membrane based separator was utilized to partition the aqueous and organic phases coming out of the epoxidation reactor. The aqueous phase was sent to a bulk collection vessel and the separator outlet containing the organic stream was mixed with the carboxylation catalyst solution in another T-mixer. This solution was then mixed with CO_2 gas which was introduced from a mass flow controller. The gas-liquid segmented flow then entered the carboxylation reactor, made from 1/8" stainless steel tubing and packed with sand. The back pressure of the system was set by pressurizing the bulk collection vessels with Argon. The temperature of both reactors was maintained using heat tape and a PID temperature controller. Effluent sampling from the carboxylation reactor was done using a 6-way valve.

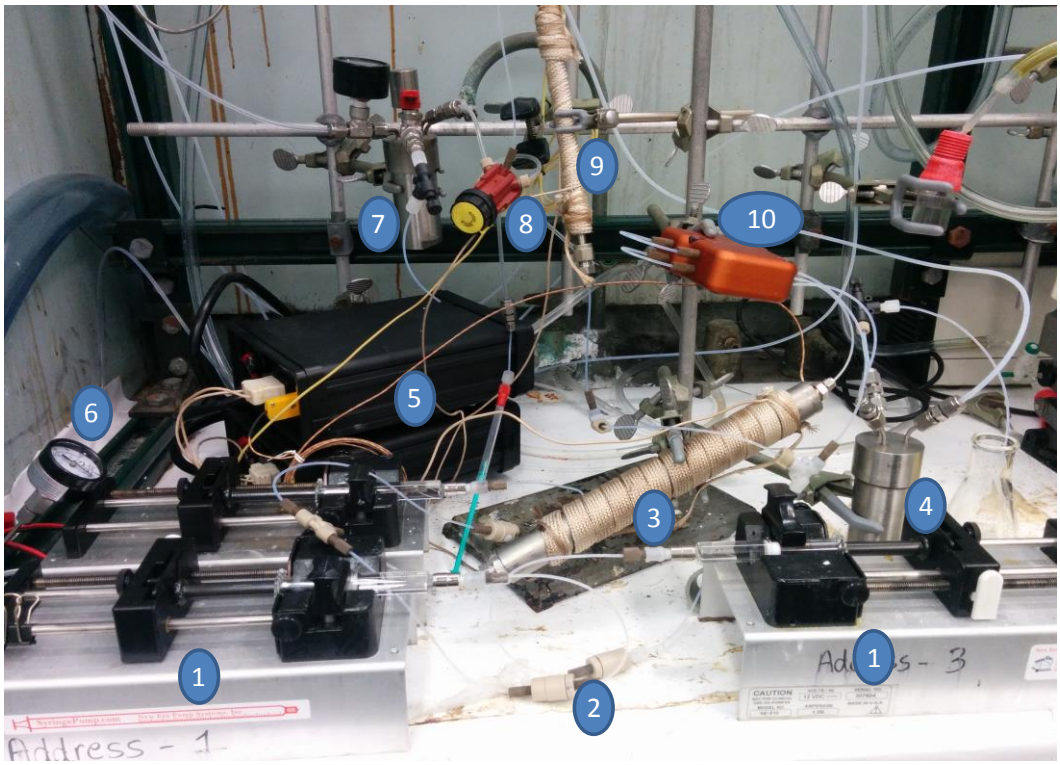

Figure 3.16. Reactor set-up: (1) syringe pumps, (2) check valves, (3) epoxidation reactor, (4) BPR and aqueous waste, (5) temperature controller, (6) pressure gauge, (7) BPR and product collection, (8) sampling valve, (9) carboxylation reactor, (10) membrane separator.

Figure 3.17. The membrane separator splitting an inlet stream of food dye (aqueous) and dichloromethane (organic) into respective components.

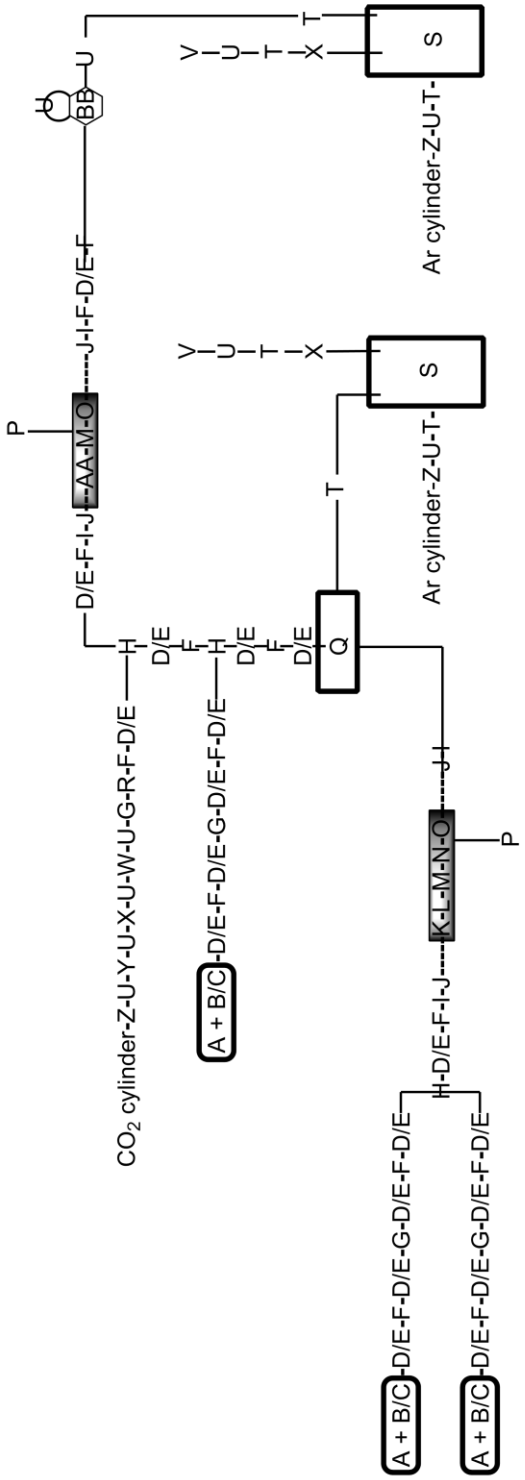

Figure 3.18. Components used for construction of the reactor set-up in Figure S12.

Table 3.4. Oxidative carboxylation reactor parts list

Item	Vendor	Part #	Part description
A	New Era Pump Systems Inc.	NE-510	Syringe pump
B	Hamilton	81520	5 mL glass syringe
C	IDEX H&S	P-628/P-678	Luer adapter
D	IDEX H&S	P-287	Super flangeless nut for 1/16” tubing
E	IDEX H&S	P-250	Super flangeless ferrule for 1/16” tubing
F	Zeus tubing	IWTT-063-C	1/16” PTFE tubing (1/32” ID)
G	IDEX H&S	CV-3330	Check valve
H	IDEX H&S	P-632	Mixing tee
I	Swagelok	SS-400-6-1	Steel reducing union, 1/4" x 1/16”
J	Sigma Aldrich	18421	Glass wool
K	Saint Gobain	TSPF35-0250-062-25	1/4” PTFE tubing (1/8” ID) (epoxidation reactor)
L	Fischer Scientific	S23-3	Sand for packed bed reactor
M	Fischer Scientific	S25-500	Sand for heating reactor
N	McMaster Carr		Aluminum tube for heating reactor
O	N/A	N/A	Heat tape
P	Auber Instruments	WS-1510DPM	PID temperature controller & thermocouple
Q	Zaiput Flow Technologies	SEP10	Membrane Separator with 0.2 μm membrane from sterlitech
R	Swagelok	SS-200-6-1	Steel reducing union, 1/8” x 1/16”
S	PSU ChE Machine Shop	N/A	Autoclave
T	Swagelok	SS-200-6	Steel union, 1/8”
U	McMaster Carr	5239K24	1/8” PTFE tubing (1/16” ID)
V	IDEX H&S	P-445	Micro metering valve
W	Hoke	7155G2Y	Shut off valve
X	McMaster Carr	2227T44	Pressure gauge
Y	Tylan	FC-260V/ AA9304091	MFC (0-10 sccm CO_2)
Z	Air Gas		Gas regulators
AA	Swagelok	89785K824	1/4" steel tubing (0.18” ID) (carboxylation reactor)
BB	IDEX H&S	V-540	6-way valve

IX. Characterization Data

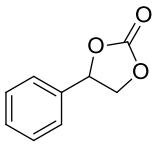

(a) 4-phenyl-1,3-dioxolan-2-one

^{1}H ($CDCl_3$, 300 MHz) δ = 7.47-7.26 (m, 5H), 5.70 (t, 1H, *J* = 8 Hz), 4.82 (t, 1H, *J* = 8.4 Hz), 4.35 (t, 1H, *J* = 8 Hz); ^{13}C ($CDCl_3$, 75 MHz) δ = 154.9, 135.8, 129.7, 129.2, 125.9, 78.0, 71.2. HRMS calculated for $C_9H_{12}NO_3$ $[M+NH_4]^+$: 182.0817. Found: 182.0831. R_f (silica gel with 30% EtOAc in Hexanes as eluent): 0.35

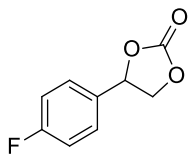

(b) 4-(4-fluorophenyl)-1,3-dioxolan-2-one

^{1}H ($CDCl_3$, 300 MHz) δ = 7.40-7.35 (m, 2H), 7.15-7.09 (m, 2H), 5.72 (t, 1H, *J* = 8 Hz), 4.84 (t, 1H, *J* = 8.5 Hz), 4.36 (t, 1H, *J* = 8.3 Hz); ^{13}C ($CDCl_3$, 75 MHz) δ = 165.0, 161.7, 154.8, 131.7, 131.7, 128.2, 128.1, 116.4, 116.1, 77.6, 71.2. HRMS: calculated for $C_9H_7O_3F$: 182.0379. Found: 182.0370. Rf (silica gel with 30% EtOAc in Hexanes as eluent): 0.28

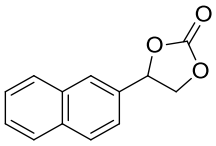

(c) 4-(naphthalen-2-yl)-1,3-dioxolan-2-one

^{1}H ($CDCl_3$, 300 MHz) δ = 7.87-7.77 (m, 4H), 7.52-7.49 (m, 2H), 7.37 (dd, 1H, *J* = 8.5, 1.6 Hz), 5.78 (t, 1H, *J* = 8 Hz), 4.81 (t, 1H, *J* = 9 Hz), 4.38 (t, 1H, *J* = 9 Hz); ^{13}C ($CDCl_3$, 75 MHz) δ = 155.0, 133.6, 132.9, 132.8, 129.4, 128.1, 127.8, 127.1, 126.9, 125.9, 122.5, 78.2, 71.0. HRMS calculated for $C_{13}H_{14}NO_3$ $[M+NH_4]^+$: 232.0974. Found: 232.0955. R_f (silica gel with 30% EtOAc in Hexanes as eluent): 0.28

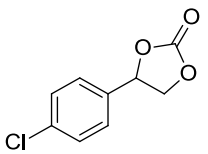

(d) 4-(4-chlorophenyl)-1,3-dioxolan-2-one

^{1}H ($CDCl_3$, 300 MHz) δ = 7.40 (d, 2H, *J* = 9 Hz), 7.32 (d, 2H, *J* = 9 Hz), 5.71 (t, 1H, *J* = 9 Hz), 4.85 (t, 1H, *J* = 9 Hz), 4.33 (t, 1H, *J* = 9 Hz); ^{13}C ($CDCl_3$, 75 MHz) δ = 154.8, 135.5, 134.4, 129.4, 127.5, 77.3, 71.0. HRMS: calculated for $C_9H_7O_3Cl$: 198.0084. Found: 198.0074.. R_f (silica gel with 30% EtOAc in Hexanes as eluent): 0.36

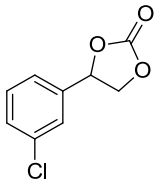

(e) 4-(3-chlorophenyl)-1,3-dioxolan-2-one

^{1}H ($CDCl_3$, 300 MHz) δ = 7.39-7.37 (m, 3H), 7.27-7.24 (m, 1H), 5.70 (t, 1H, *J* = 7.9 Hz), 4.86 (t, 1H, *J* = 8.5 Hz), 4.34 (t, 1H, *J* = 8.2 Hz); ^{13}C ($CDCl_3$, 75 MHz) δ = 154.6, 137.9, 135.1, 130.6, 129.8, 126.0, 123.9, 77.0, 71.0. HRMS: calculated for $C_9H_7O_3Cl$: 198.0084. Found: 198.0074. Rf (silica gel with 30% EtOAc in Hexanes as eluent): 0.42

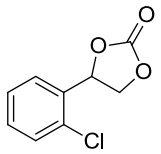

(f) 4-(2-chlorophenyl)-1,3-dioxolan-2-one

^{1}H ($CDCl_3$, 300 MHz) δ = 7.50-7.47 (m, 1H), 7.41-7.33 (m, 3H), 6.00 (t, 1H, *J* = 9 Hz), 4.99 (t, 1H, *J* = 8.5 Hz), 4.27 (t, 1H, *J* = 8 Hz); ^{13}C ($CDCl_3$, 75 MHz) δ = 154.7, 134.5, 131.1, 130.4, 129.9, 127.6, 126.2, 75.0, 70.4. HRMS calculated for $C_9H_{11}ClNO_3$ $[M+NH_4]^+$: 216.0427. Found: 216.0436. R_f (silica gel with 30% EtOAc in Hexanes as eluent): 0.38

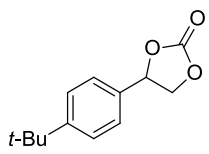

(g) 4-(4-(tert-butyl)phenyl)-1,3-dioxolan-2-one

^{1}H ($CDCl_3$, 400 MHz) δ = 7.45 (d, 2H, *J* = 8.4 Hz), 7.31 (d, 2H, *J* = 8 Hz), 5.66 (t, 1H, *J* = 8 Hz), 4.77 (t, 1H, *J* = 8.4 Hz), 4.33 (t, 1H, *J* = 8 Hz), 1.31 (s, 9H); ^{13}C ($CDCl_3$, 75 MHz) δ = 155.0, 152.9, 132.8, 126.1, 125.9, 78.0, 71.1, 34.7, 31.2. HRMS calculated for $C_{13}H_{20}NO_3$ $[M+NH_4]^+$: 238.1443. Found: 238.1438. R_f (silica gel with 30% EtOAc in Hexanes as eluent): 0.45

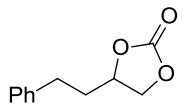

(h) 4-phenethyl-1,3-dioxolan-2-one

^{1}H ($CDCl_3$, 300 MHz) δ = 7.29-7.13 (m, 5H), 4.61-4.57 (m, 1H), 4.39 (t, 1H, *J* = 9 Hz), 3.97 (t, 1H, *J* = 9 Hz), *2*.76-2.63 (m, 2H), 2.03-1.88 (m, 2H); ^{13}C ($CDCl_3$, 75 MHz) δ = 155.1, 140.0, 128.6, 128.4, 126.4, 76.2, 69.3, 35.3, 30.7. HRMS calculated for $C_{11}H_{16}NO_3$ $[M+NH_4]^+$: 210.1130. Found: 210.1132. R_f (silica gel with 30% EtOAc in Hexanes as eluent): 0.30

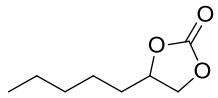

(i) 4-pentyl-1,3-dioxolan-2-one

^{1}H ($CDCl_3$, 300 MHz) δ = 4.74-4.70 (m, 1H), 4.57 (t, 1H, *J* = 9 Hz), 4.10 (t, 1H, *J* = 9 Hz), 1.82-1.65 (m, 2H), 1.48-1.30 (m, 8H), 0.89 (t, 3H); ^{13}C ($CDCl_3$, 75 MHz) δ = 155.2, 69.5, 33.9, 31.5, 28.8, 24.4, 22.5, 14.0. HRMS calculated for $C_8H_{18}NO_3$ $[M+NH_4]^+$: 176.1287. Found: 176.1269. R_f (silica gel with 30% EtOAc in Hexanes as eluent): 0.31

(j) 4-(2-oxo-1,3-dioxolan-4-yl)butanenitrile

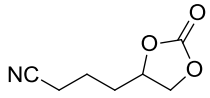

^{1}H ($CDCl_3$, 300 MHz) δ = 4.80 (t, 1H, *J* = 6 Hz), 4.61 (t, 1H, *J* = 8.2 Hz), 4.14 (t, 1H, *J* = 8 Hz), 2.49-2.45 (m, 2H), 1.91-1.75 (m, 4H); ^{13}C ($CDCl_3$, 75 MHz) δ = 155.0, 119.6, 76.4, 69.3, 32.5, 20.9, 16.6. HRMS calculated for $C_7H_{13}N_2O_3$ $[M+NH_4]^+$: 173.0926. Found: 173.0919. R_f (silica gel with 50% EtOAc in Hexanes as eluent): 0.23

3.9 References

1. Reitz, A.; Wilhelm, R.; Kuckling, D., *Macromolecular Symposia* **2013,** *334* (1), 92-97.
2. Schäffner, B.; Schäffner, F.; Verevkin, S. P.; Börner, A., *Chem. Rev.* **2010,** *110* (8), 4554-4581.
3. Kowalewicz, A.; Wojtyniak, M., Proceedings of the Institution of Mechanical Engineers, Part D: Journal of Automobile Engineering **2005,** 219 (1), 103-125.
4. Zevenhoven, R.; Eloneva, S.; Teir, S., *Catal. Today* **2006,** *115* (1–4), 73-79.
5. Eshetu, G. G.; Bertrand, J.-P.; Lecocq, A.; Grugeon, S.; Laruelle, S.; Armand, M.; Marlair, G., *J. Power Sources* **2014,** *269*, 804-811.
6. Skarmoutsos, I.; Ponnuchamy, V.; Vetere, V.; Mossa, S., *J. Phys. Chem. C* **2015,** *119* (9), 4502-4515.
7. Kühnel, R. S.; Böckenfeld, N.; Passerini, S.; Winter, M.; Balducci, A., *Electrochim. Acta* **2011,** *56* (11), 4092-4099.
8. Laserna, V.; Fiorani, G.; Whiteoak, C. J.; Martin, E.; Escudero-Adán, E.; Kleij, A. W., *Angew. Chem. Int. Ed.* **2014,** *53* (39), 10416-10419.
9. Khan, A.; Yang, L.; Xu, J.; Jin, L. Y.; Zhang, Y. J., *Angew. Chem. Int. Ed.* **2014,** *53* (42), 11257-11260.
10. Vitvitskaya, A. S.; Naidis, F. B.; Katsnel'son, E. Z.; Karpinskaya, I. A., *Pharm. Chem. J.* **1981,** *15* (7), 512-515.
11. Tundo, P.; Selva, M., *Acc. Chem. Res.* **2002,** *35* (9), 706-716.
12. Shieh, W.-C.; Dell, S.; Repič, O., *Org. Lett.* **2001,** *3* (26), 4279-4281.
13. Shaikh, A.-A. G.; Sivaram, S., *Chem. Rev.* **1996,** *96* (3), 951-976.

14. Ballivet-Tkatchenko, D.; Dibenedetto, A., Synthesis of Linear and Cyclic Carbonates. In *Carbon Dioxide as Chemical Feedstock*, Wiley-VCH Verlag GmbH & Co. KGaA: 2010; pp 169-212.

15. Aresta, M.; Dibenedetto, A., *Dalton Trans.* **2007,** (28), 2975-2992.

16. Sakakura, T.; Choi, J.-C.; Yasuda, H., *Chem. Rev. (Washington, DC, U. S.)* **2007,** *107* (6), 2365-2387.

17. Leitner, W., *Angew. Chem., Int. Ed. Engl.* **1995,** *34* (20), 2207-21.

18. Sathe, A. A.; Hartline, D. R.; Radosevich, A. T., *Chem. Commun.* **2013,** *49* (44), 5040-5042.

19. Omae, I., *Coord. Chem. Rev.* **2012,** *256* (13–14), 1384-1405.

20. Fukuoka, S.; Kawamura, M.; Komiya, K.; Tojo, M.; Hachiya, H.; Hasegawa, K.; Aminaka, M.; Okamoto, H.; Fukawa, I.; Konno, S., *Green Chem.* **2003,** *5* (5), 497-507.

21. Sakakura, T.; Kohno, K., *Chem. Commun.* **2009,** (11), 1312-1330.

22. Srivastava, R.; Srinivas, D.; Ratnasamy, P., *Catal. Lett.* **2003,** *91* (1), 133-139.

23. Aresta, M.; Dibenedetto, A., *J. Mol. Catal. A: Chem.* **2002,** *182–183*, 399-409.

24. Bai, D.; Jing, H., *Green Chem.* **2010,** *12* (1), 39-41.

25. Chen, F.; Dong, T.; Xu, T.; Li, X.; Hu, C., *Green Chem.* **2011,** *13* (9), 2518-2524.

26. Sun, J.; Fujita, S.-i.; Bhanage, B. M.; Arai, M., *Catal. Today* **2004,** *93–95*, 383-388.

27. Eghbali, N.; Li, C.-J., *Green Chem.* **2007,** *9* (3), 213-215.

28. Wang, J.-L.; Wang, J.-Q.; He, L.-N.; Dou, X.-Y.; Wu, F., *Green Chem.* **2008,** *10* (11), 1218-1223.

29. Wu, J.; Kozak, J. A.; Simeon, F.; Hatton, T. A.; Jamison, T. F., *Chem. Sci.* **2014,** *5* (3), 1227-1231.

30. Yang, X.; Wu, J.; Mao, X.; Jamison, T. F.; Hatton, T. A., *Chem. Commun.* **2014,** *50* (24), 3245-3248.

31. The epoxidation of styrene was found to be influenced by the stirring speed during the initial optimization study. See supporting information for more details

32. Webb, D.; Jamison, T. F., *Chem. Sci.* **2010,** *1* (6), 675-680.

33. Pastre, J. C.; Browne, D. L.; Ley, S. V., *Chem. Soc. Rev.* **2013,** *42* (23), 8849-8869.

34. McQuade, D. T.; Seeberger, P. H., *J. Org. Chem* **2013,** *78* (13), 6384-6389.

35. Newman, S. G.; Jensen, K. F., *Green Chem.* **2013,** *15* (6), 1456-1472.

36. Mason, B. P.; Price, K. E.; Steinbacher, J. L.; Bogdan, A. R.; McQuade, D. T., *Chem. Rev.* **2007,** *107* (6), 2300-2318.

37. Jas, G.; Kirschning, A., *Chem. Eur. J.* **2003,** *9* (23), 5708-5723.

38. Wegner, J.; Ceylan, S.; Kirschning, A., *Adv. Synth. Catal.* **2012,** *354* (1), 17-57.

39. Watts, P.; Wiles, C., *Org. Biomol. Chem.* **2007,** *5* (5), 727-732.

40. Yoshida, J.-i.; Kim, H.; Nagaki, A., *ChemSusChem* **2011,** *4* (3), 331-340.

41. Kobayashi, J.; Mori, Y.; Kobayashi, S., *Chem. Asian. J.* **2006,** *1* (1-2), 22-35.

42. Doku, G. N.; Verboom, W.; Reinhoudt, D. N.; van den Berg, A., *Tetrahedron* **2005,** *61* (11), 2733-2742.

43. Brzozowski, M.; O'Brien, M.; Ley, S. V.; Polyzos, A., *Acc. Chem. Res.* **2015,** *48* (2), 349-362.

44. Mallia, C. J.; Baxendale, I. R., *Org. Process Res. Dev.* **2016,** *20* (2), 327-360.

45. Baxendale, I. R.; Deeley, J.; Griffiths-Jones, C. M.; Ley, S. V.; Saaby, S.; Tranmer, G. K., *Chem. Commun.* **2006,** (24), 2566-2568.

46. Nagaki, A.; Matsuo, C.; Kim, S.; Saito, K.; Miyazaki, A.; Yoshida, J.-i., *Angew. Chem. Int. Ed.* **2012,** *51* (13), 3245-3248.

47. Herrmann, W. A.; Fischer, R. W.; Marz, D. W., *Angew. Chem. Int. Ed.* **1991,** *30* (12), 1638-1641.

48. Rudolph, J.; Reddy, K. L.; Chiang, J. P.; Sharpless, K. B., *J. Am. Chem. Soc.* **1997,** *119* (26), 6189-6190.

49. Lin, C. C.; Smith, F. R.; Ichikawa, N.; Baba, T.; Itow, M., *Int. J. Chem. Kinet.* **1991,** *23* (11), 971-987.

50. Wang, W.-D.; Espenson, J. H., *J. Am. Chem. Soc.* **1998,** *120* (44), 11335-11341.

51. Coperet, C.; Adolfsson, H.; Barry Sharpless, K., *Chem. Commun.* **1997,** (16), 1565-1566.

52. Adolfsson, H.; Converso, A.; Sharpless, K. B., *Tetrahedron Lett.* **1999,** *40* (21), 3991-3994.

53. Yamazaki, S., *Org. Biomol. Chem.* **2007,** *5* (13), 2109-2113.

54. No other products were observed by gas chromatography leading us to conclude that the product stability is not an issue. Also the effluent from the reactor was colorless as opposed to bright yellow which is indicative of the rhenium peroxo complex. We also note that the concentration of the peroxide in the effluent was within expected limits, ruling out peroxide decomposition.

55. North, M.; Pasquale, R.; Young, C., *Green Chem.* **2010,** *12* (9), 1514-1539.

56. Martín, C.; Fiorani, G.; Kleij, A. W., *ACS Catl.* **2015,** *5* (2), 1353-1370.

57. Dai, W.-L.; Luo, S.-L.; Yin, S.-F.; Au, C.-T., *Appl. Catl. A* **2009,** *366* (1), 2-12.

58. Clegg, W.; Harrington, R. W.; North, M.; Pasquale, R., *Chem. Eur. J.* **2010,** *16* (23), 6828-6843.

59. Ren, W.-M.; Liu, Y.; Lu, X.-B., *J. Org. Chem* **2014,** *79* (20), 9771-9777.

60. Whiteoak, C. J.; Kielland, N.; Laserna, V.; Escudero-Adán, E. C.; Martin, E.; Kleij, A. W., *J. Am. Chem. Soc.* **2013,** *135* (4), 1228-1231.

61. Adamo, A.; Heider, P. L.; Weeranoppanant, N.; Jensen, K. F., *Industrial & Engineering Chemistry Research* **2013,** *52* (31), 10802-10808.

62. Cyclohexene and 4-phenyl-2-butene were tried as model substrates for internal olefins

63. See supporting information for details on the ICP analysis.

64. Supported epoxidation catalysts: Chem. Commun. 1997, (19), 1915-1916; Angew. Chem. Int. Ed. 2011, 50 (50), 12062-12066; supported Carboxylation catalysts: Chem. Commun. 2009, (18), 2577-2579; Chem. Eur. J. 2009, 15 (43), 11454-11457.

Chapter 4

Role of Isothermal Titration Calorimetry and Cation Exchange Reactions in the Design of Nanomaterials for Energy Conversion and Storage

One of the biggest challenges of the twenty first century is the generation and storage of energy. Having looked at use of CO_2 and flow chemistry for the sustainable chemical conversion, the following chapter describes at the role of nanomaterials in sustainable energy conversion and storage. Nanomaterials are structured materials with components that have at least one dimension smaller than 0.1μm, which is partly responsible for a variety of novel properties. We also introduce the concept of cation exchange for the synthesis of nanomaterials and how isothermal titration calorimetry can be utilized to unravel some important fundamentals of this versatile technique.

4.1 Role of nanomaterials in sustainable energy conversion and storage

The process of chemical and energy conversion or storage fundamentally involves some kind of physical interaction or chemical reaction at a surface, and hence the importance of controlling surface area, surface energetics and surface chemistry cannot be overstated. Nanostructured materials allow facile manipulation of these variables which leads to high surface to volume ratios, improved mass and heat and charge transfer and unique physico-chemical properties. For example, the band gap (and consequently optical spectra) of semiconductors can be tuned by changing the size to meet the requirements of a particular application.[1-2] Similarly gold nanoparticles display size dependent optical absorption due to the surface plasmon

resonance and finds applications in surface enhanced Raman spectroscopy (SERS).[3-4] Apart from the modification of physical properties, nanostructuring can also help modify the chemical properties of materials. The case of gold nanoparticles is a classic example; while bulk elemental gold is largely considered to be chemically inert, gold nanoparticles of the order of a few nanometers have shown to exhibit remarkable catalytic activity.[5-7] The following section gives a brief overview of the application of nanomaterials in the areas of solar energy conversion, energy storage, and chemical catalysis.

4.1.1 Applications of nanomaterials in solar energy conversion and storage.

Solar energy is the single most abundant, renewable energy source on the planet, with more energy striking the earth's surface in an hour and a half, than the global annual energy demand.[8] There are three major strategies to utilize this energy resource: 1) Photo-voltaic (and photo-electrochemical) technology – which directly converts light into electricity, 2) Photo-chemical (artificial photosynthesis) – which converts light into fuels by storing the energy in the form of chemical bonds (hydrogen from water, liquid fuels from CO_2 etc.) and 3) Photo-thermal systems – which converts solar energy into heat for applications in thermal power plants, or domestic heating requirements. The use of biomass for energy can also be considered an example of solar energy conversion as plants store the solar energy via photosynthesis. Of these strategies, nanomaterials have been instrumental in the explosive growth and development of the photovoltaic and artificial photosynthesis technologies.

Photovoltaic applications depend on the ability of the material to absorb photons and produce separated high energy electron hole pairs (excitons) in devices called solar cells. The design of a solar cell aims to increase optical absorption and minimize the loss of electrons during transport.[9] Figure 4.1 shows the general construction of a solar cell, which consists of a suitable semiconductor containing light absorbing materials sandwiched between two electrically conducting thin films. Additionally a layer of transparent anti-reflective coating is utilized to maximize light absorption.

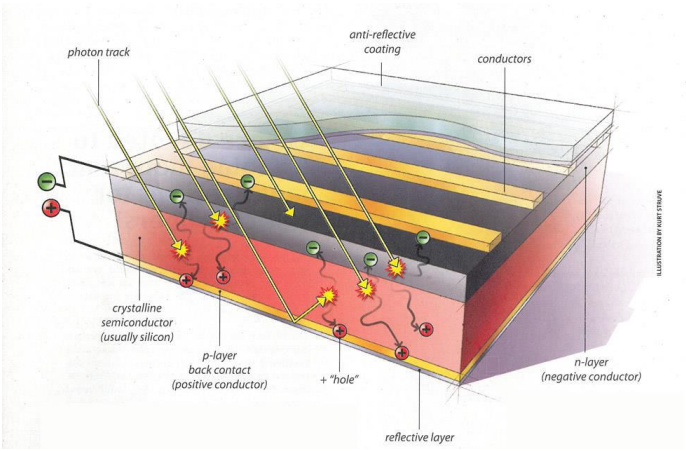

Figure 4.1. General schematic of a photovoltaic cell.[10]

Nanomaterials can provide solutions to increase the efficiency of solar cells by improving each of the components of the solar cell. For instance, light absorption over the entire solar spectrum can be increased by embedding quantum dots into the solar cell.[11] Quantum dots exhibit size dependent optical absorption, and robust synthetic techniques are available for highly size selective synthesis of some semiconductor quantum dots. Another phenomenon which is considered to be highly significant for the future of solar cells is the multiple exciton generation (MEG), or carrier multiplication effect.[12] The MEG effect describes the generation of multiple excitons per photon absorption. Quantum dots are uniquely suited to demonstrate this effect due

to reduced cooling rate of hot-electrons because of the discreet energy levels. This leads to a "reversed Auger recombination" process known as impact ionization.[13-14]

Apart from quantum dots, light harvesting can also be done using organic dyes, and the devices so fabricated are called dye-sensitized solar cells (DSSC).[15-17] Nanostructured wide band gap semiconductors are usually utilized in DSSCs, and the high surface area afforded by nanostructuring enables high density of dye molecules to adsorb on the surface thereby maximizing light absorption and electron injection into the conduction band of the semiconductor.

Additionally nanostructured materials have also shown promise in antireflective coatings on solar cells. These thin films allow for reduction in loss of incident light by reflection up to 30%.[18] The antireflective coatings can be either deposited on top of fabricated solar cells, or formed via etching off some of the semiconductor layer to form nanorods or wires enabling a gradually varying refractive index ideally allowing for almost complete transmission of the incident light onto to the light absorber.[19-20]

Once light absorption leads to the generation of excitons, it is important that they be separated before recombination. One dimensional nanostructures such as nanorods or nanowires are promising candidates for improvement in the electron transport and collection. Their one dimensional structure, along with high crystallinity provides less defect sites and a direct path for electron transport. One of the first uses of single crystalline ZnO nanowires for DSSCs was reported by Yang et. al.[21] Although the device demonstrated high electron diffusivities its overall efficiency was on the order of 1.5-2% due to lower surface area as compared to the thin film DSSCs which have shown efficiencies upwards of 12%. Nevertheless the report of easy solution based methodologies for the synthesis of such one dimensional nanostructures will help the design of better solar cells due to efficient charge transport.[22]

Unlike photovoltaic cells where the excitons are used to generate electricity, artificial photosynthesis employs the photo generated electrons and holes to carry out various chemical redox transformations. Such systems store the light energy in the form of chemical bonds, and enable the production of liquid or gaseous fuels. Amongst the most widely studied systems are water splitting for hydrogen production, and conversion of CO_2 and water vapor into hydrocarbon fuels.[23-26] Figure 4.2 shows a general schematic of water splitting photo-electrochemical cell. The light absorption by a semiconductor leads to the formation of excited electrons which are used to drive the proton reduction reaction at the anode, producing hydrogen, while the excited holes are sent to the cathode to oxidize water and produce oxygen.

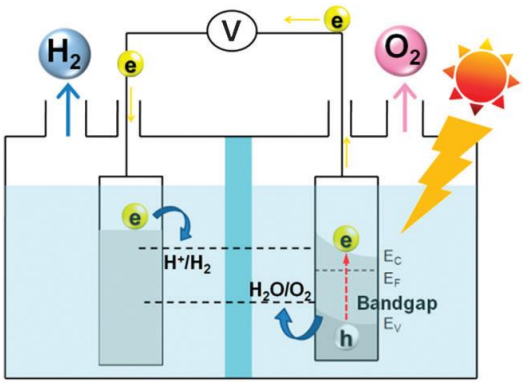

Figure 4.2. General schematic of a photo-electrochemical cell.[27]

For applications in artificial photosynthesis the semiconductor must have a band gap that is higher than the difference between the two target redox reactions, and must be compatible with the various chemical species being formed in the reaction system. Additionally, the conduction band energy level must be higher than the reduction potential of the species being reduced, and the valence band energy level must be lower than the oxidation potential of the species being oxidized. The electrodes must also be fabricated with a high surface area to achieve meaningful throughputs, and highly active catalysts based on cheap and earth abundant metals must be employed. These requirements put significant limitations on the type of materials that can be

utilized, in addition to making the solar to hydrogen process economically unfavorable. The development of new nanomaterials could help alleviate these problems,[8, 28-34] and make the carbon neutral generation of fuels a reality.

Energy storage is an important component of a sustainable energy technology. As such the development of rechargeable batteries having high energy density, low costs and safe operating conditions is an active area of research.[35-36] The lithium ion battery is the state of the art technology for portable rechargeable batteries due to its superior performance characteristics over traditional batteries such as lead-acid or Ni-Cd. A prototypical Li-ion battery (Figure 4.3) consists of an anode, a cathode and a lithium ion conducting electrolyte. When the battery is in use (discharge) the lithium metal gives up it electrons at the anode and the resulting lithium ions travel to the cathode through the electrolyte. During the charge cycle, the lithium ions travel back from the cathode to the anode where they are reduced back to lithium metal.

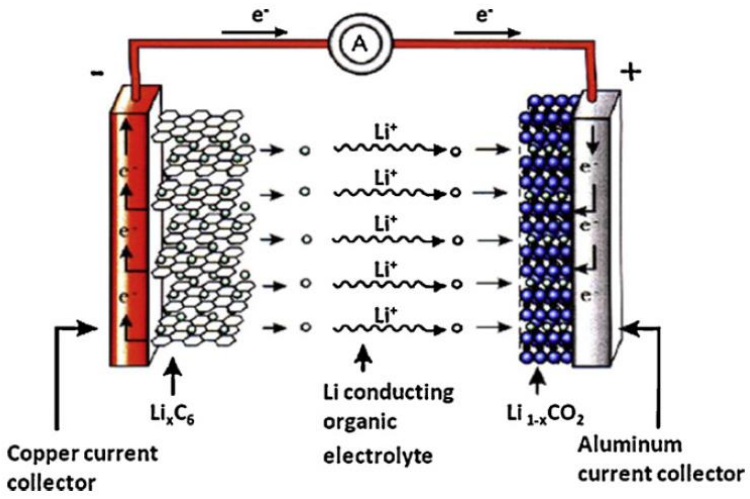

Figure 4.3. General schematic of a Li-ion battery.[37]

Despite commercialization of the Li-ion batteries, significant problems still exist with regards to volume changes and fracture of the electrode materials upon cycling, ion and electron transport, and stability of the electrode-electrolyte interface. Nanostructured materials are promising candidates to help solve these problems.[38-40] The nanostructuring of electrode materials

results in enhanced ion transport kinetics which leads to improvements in cycling rate and performance. However, the enhanced surface area also increases the potential for unwanted secondary reactions at the electrode interface. The development of new electrode materials[41-49] and battery chemistries[50-56] is expected to further the improvements in battery performance and cost.

4.1.2 Need for better materials.

There is little doubt that nanostructured materials have ushered in significant advances in the field of energy conversion and storage by improving efficiencies of light absorption, charge separation and charge utilization. However, there are still some aspects that need improvements before these materials can be applied on large scales in a sustainable manner.

The process of synthesizing nanostructured materials still relies on tedious trial and error processes for optimization, and very few reliable techniques exist which allow synthesis of nanomaterials with desired morphology, structure, surface chemistry etc. There is also a significant lack of studies highlighting structure activity (or performance) relationships due to difficulty in synthesizing materials with different chemical composition, or morphology while keeping the other properties constant. This inhibits the rapid discovery of new materials for performance testing and applications. In addition, the cost of nanomaterial fabrication is usually high, and little emphasis has been placed on the low-cost synthesis of high-performance nanostructured materials.[9, 40]

Cation exchange in nanocrystals has recently emerged as a powerful technique to synthesize new nanomaterials having compositions or morphologies that are inaccessible by using conventional synthesis techniques. We believe that advances in the development of the cation exchange protocol for nanomaterials have the potential to solve some of the problems

outlined above. The next section describes rapidly growing field of cation exchange in nanomaterials.

4.2 Cation exchange as a novel technique for the synthesis of nanomaterials

The most common way of synthesizing nanostructured materials with high degree of control over size, shape morphology and surface chemistry is the hot injection method, where in the metal or organometallic precursors are thermolyzed in the presence of surfactants or templating agents.[57-59] A typical reaction consists of organometallic precursor decomposition, nanocrystal nucleation, growth of the nuclei and quenching, before final work up or purification. While exquisite shape and size control has been demonstrated for solution phase synthesis of II-VI and IV-VI semiconductor nanocrystals,[19, 60-61] extensive optimization is required for extending the "hot injection" protocol to make other semiconductor compositions and morphologies, and some are simply not accessible via this methodology. The nature of the nucleation and growth regime causes the size, shape and composition of the nanocrystals to be interdependent. The ability to independently modify one parameter, while keeping the others constant would enable the systematic tuning of the properties of the resulting nanomaterial.[62]

A strategy to overcome the shortcomings of the solvothermal synthesis would be a post-synthetic modification of nanomaterials having required properties. Cation exchange is one such technique where in the cations in a nanocrystal are replaced with new cations from solution, while maintaining the original anion sublattice, and hence retaining the morphology of the starting nanostructure (Figure 4.4).[63] While anion exchange reactions are also shown to occur in nanocrystals, they usually require forcing conditions due to the larger radius and lower diffusivities of anions as compared to cations.[64-69] Although still in its infancy, the anion exchange reactions could prove to be of significant importance in the design and development of

new materials in the future.[70-74] We focus here on the cation exchange reactions in nanomaterials.

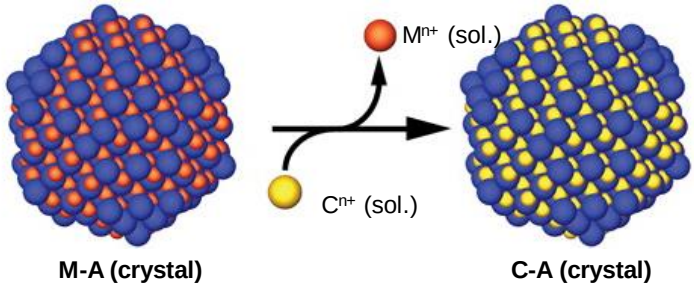

Figure 4.4. A cation exchange reaction between a hypothetical nanocrystal MA and cation C.[75]

4.2.1 Fundamentals of CE

Inorganic nanocrystals are typically held together by ionic bonds. This mode of bonding allows for exchange of constituent elements in the solid state with ions from solution. The ion exchange reactions in extended solids and thin films have been known for decades and are implicated in some of the geologic equilibration reactions in rocks.[75-77] While the rate of the ion exchange in rocks or other extended solids is too slow to be of broad synthetic importance, the discovery of facile cation exchange reactions in nanocrystals under mild reaction conditions has made this technique an important post-synthetic modification tool.[63, 78]

The thermodynamic feasibility of these cation exchange reactions can often be gauged by the difference in the solvation energy of the cations in the initial and product nanocrystals. The reaction will take place if the outgoing cation is fully solvated in the reaction mixture, and hence these reactions are typically carried out in polar solvents.

Synthetically cation exchange can be carried out in two distinct ways. The most common methodology is to subject already synthesized and purified nanocrystals to a solution of the exchanging ion in a suitable solvent, or in the presence of appropriate ligands to drive the cation exchange process. Another way to carry out the cation exchange is by exchanging the cations in

the nanocrystal during the initial cation exchange growth. Such a technique is applicable when one cation (C_1) has a much greater initial reactivity with the anion (A) leading predominantly to the formation of C_1A. As the reaction proceeds, the other cation (C_2) can slowly replace the original cation to form C_2A. This can be brought about by increasing the temperature or by addition of a ligand that can favorably bind C_1. In effect C_1 acts as a templating agent, and can be employed when it offers superior crystal growth characteristics (morphology, size distribution, ease of nucleation or low temperature synthesis etc.) compared to C_2.[79-80]

4.2.2 Advantages of CE

The traditional routes of synthesis such as hot injection or heating up methods yield nanostructures that are usually in equilibrium with the monomer in solution. This gives rise to the formation of phases and compositions that are most thermodynamically stable.[81] As opposed to this, cation exchange yields products that are kinetically controlled, allowing for the synthesis of non-equilibrium or metastable structures. This property gives it the power to be instrumental in the discovery of new materials that are currently inaccessible by solution phase synthesis. This is exemplified by the sequential transformation of CdSe to ZnSe via the formation of a metastable Cu_2Se (Figure 4.5).[82] The reaction proceeds with the retention of both shape and crystal structure of the initial CdSe template. Furthermore it was possible to observe the transition from the metastable hcp phase for the Cu_2Se to the more stable fcc phase under an electron microscope. The synthesis of metastable states by cation exchange reaction which could then be subsequently converted to the more stable phase, under an external stimulus, could enable detailed mechanistic study of the fundamentals of nanoscale solid state reactions.

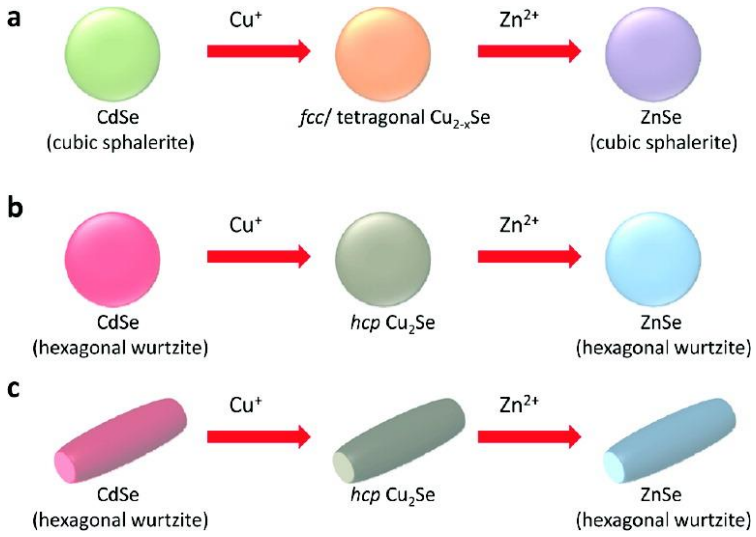

Figure 4.5. Shape, size and crystallographic templating via cation exchange allows access to metastable phases.[82]

Cation exchange has also been employed to synthesize nanomaterials having metastable compositions, as described in the synthesis of Cu_2S. The normal solvothermal synthesis of these nanocrystals usually yields a copper deficient $Cu_{1.93-1.96}S$ in contrast to the fully stoichiometric Cu_2S obtained via cation exchange of CdS with Cu^+.[83]

In addition to accessing metastable structures, cation exchange can also provide a route to traditionally challenging and hitherto unknown materials. For example, unlike for the synthesis of II-VI semiconductor nanocrystals very few direct synthetic methods exist for the production of highly crystalline and monodisperse III-V nanocrystals.[84] The developments in the synthesis of II-V nanocrystals allow them to be used as templates for cation exchange routes for the synthesis of III-V semiconductor nanocrystals.[85-86] Indeed this was shown by Alivisatos and co-workers who reported the synthesis of highly crystalline and monodisperse GaP and GaAs nanocrystals starting from Cd_3P_2 and Cd_3As_2 respectively.[87]

While complete cation exchange reactions demonstrate the ability to preserve the morphological or crystallographic template of the original nanocrystal, partial cation exchange

can be utilized to form heterostructures.[88-89] In the extreme, severely sub-stoichiometric cation exchange can be used to incorporate only a few impurities in the host crystal, in a process known as doping. Doping of semiconductor nanocrystals allows for the modification of its electromagnetic and optical properties. However, reliable doping using traditional hot injection methods is challenging.[90] A highly controlled doping of nanocrystals is possible either by modulating the stoichiometry of the dopant, as in the case of doping of InAs crystals with dilute solutions of Ag or Cu salts,[91] or by altering the kinetics of the cation exchange. The later was demonstrated in the doping of CdSe with Ag^+, wherein the cation exchange was carried out in the presence of a phosphine ligand that bound the Ag^+ ion reducing its availability for cation exchange.[92] This method allowed for doping as little as ~1 Ag^+ ion per CdSe nanocrystal. Recently this was also shown to be applicable to PbSe films.[93]

Another key advantage of the cation-exchange approach to doping is that it automatically provides a control sample for determining changes due to doping. In other syntheses, where the impurities are added during the nanocrystal growth, it is challenging to prepare an undoped sample of the same size, shape, and quality as the doped one. With cation exchange, an entire series of samples that only differ by the amount of the dopant can be easily prepared.[92]

4.2.3 Applications of CE for energy conversion and storage

The ability to access complex and novel nanostructures with relative ease and under mild reaction conditions make cation exchange a prime candidate for development of materials for energy conversion and storage.

Alloyed NCs can be useful for applications in solar cells. Their bandgaps can be tuned either by changing their size or their composition.[94] The change in composition also allows for modifying the effective carrier ratios and alignment of the bandgap with other energy levels

leading to resonant enhancement of other transitions.[95] Cu_2S-CdS nanowire devices have been made with cation exchange of CdS nanowires.[96] PbSe quantum dots were also prepared by cation exchange from either CdSe or ZnSe nanoparticles by PbX_2 salts.[97-98] It was found that solar cells fabricated from these QDs were stable over 30-50 days providing over 6% efficiency under ambient conditions, and alleviating a major problem of stability in Pb based quantum dots. Materials having absorption over the entire visible spectrum were achieved by differential cation exchange of Ag_2Se nanoparticles using varying amounts of Cd^{2+} and Zn^{2+} ions.[99] These can be utilized as light harvesters in solar cells or as photocatalysts for driving energetically uphill reactions.

Materials obtained via cation exchange have also shown to have improved catalytic properties relevant to the hydrogen evolution reaction. Partial cation exchange was used to form dumbbell shaped CdS nanorods with Pd_4S tips.[100] The Pd_4S species was shown to consist of Pd^0 and Pd^{2+} using XPS, and the formation of Pd^0 was attributed to the reduction of the Pd^{2+} by the surfactant amine used in the synthesis. The particles showed good catalytic activity and stability towards photocatalytic HER.

As described earlier nanoparticles are especially suited for development of battery electrodes as they provide a high surface area and can hence enable fast intercalation leading to faster rate of charge discharge cycles. Study of cation exchange in such systems can be crucial to the development of better materials capable of enhanced performance and can be fabricated from earth abundant materials.[101]

Cation exchange reactions allow for the synthesis of a diverse variety of semiconductor nanocrystals. Computationally predicted materials that have superior properties, but have been overlooked due to metastability can now be synthesized as advances are made in the cation exchange protocols. Ultimately cation exchange can allow fabrication of new better performing

energy conversion and storage devices using mild conditions, cheap starting materials and at a reduced environmental footprint.

While cation exchange in nanomaterials has seen tremendous growth in last decade, there is a lack of quantitative thermodynamic and kinetic data which impedes the unraveling of mechanistic nuances of this useful technique. The technique has been predominantly utilized as a synthetic tool, and systematic studies of the effect of size, surface ligand, solvent etc. have been lacking. We believe isothermal titration calorimetry can be used to gain quantitative insight on the thermodynamics of cation exchange reaction and systematically gauge the impact of changes in the variables outlined above. We present here a brief introduction of the technique before presenting results from our work studying the cation exchange between colloidal CdSe particles and Ag^+ ions using an isothermal titration calorimeter in the next chapter.

4.3 Introduction to isothermal titration calorimetry

A calorimeter is an ideal and universal detector, as any physical or chemical change is inadvertently accompanied by evolution (or absorption) of heat. Consequently, a measurement of the heat given out (or taken in) by a system is proportional to the extent of the reaction that has taken place. Also if the rate of heat evolution (or absorption) were to be measured it can shed light on the rate of the transformation being studied. Thus the calorimeter is uniquely suited to measure both the thermodynamics and kinetics of the given transformation, in a single measurement. Modern ITC instruments allow precise measurements of heat rate as low as 1 nW, allowing for determination of reaction rates in the range of picomol/sec, and equilibrium constants in the range of $10^{-3} – 10^{3}$ μM.[102]

Titration calorimetry was first described in the 1960s as a technique for the simultaneous determination of the equilibrium constant (K_{eq}) and heat of reaction (ΔH).[103-104] While originally used to study acid base equilibria and formation of metal complexes,[104-106] ITC has since been routinely utilized in the determination of thermodynamic properties of protein ligand binding.[102, 107-108] Previous work from our group has extended the use of this technique to systems relevant to catalysis research such as ligand exchange reactions in palladium complexes,[109] binding of surfactant molecules on gold nanoparticles,[110] oxidative addition of amines at phosphorous centers,[111] and the influence of precursor binding on catalyst support on the final catalyst properties.[112]

4.3.1 Construction of an ITC instrument.

The calorimeter instrument consists of two cells, a reference and a sample cell. The reference cell usually contains the solvent or the reaction medium, the sample cell contains one

component of the reaction dispersed in the reaction medium. These are kept in a constant temperature bath which is usually kept at a lower temperature than the set point of the experiment. The two cells are connected to a temperature controller and a heating element which helps to keep the cell temperature constant. A syringe is utilized to deliver the reactants for the reaction under study. A stirring mechanism is usually employed to ensure complete mixing of the reagent. As the sample from the syringe is dosed in, any temperature change between the cells is detected and the power to the heating elements controlled so as to compensate for the fluctuation. The schematic of a typical ITC instrument is given in Figure 4.6

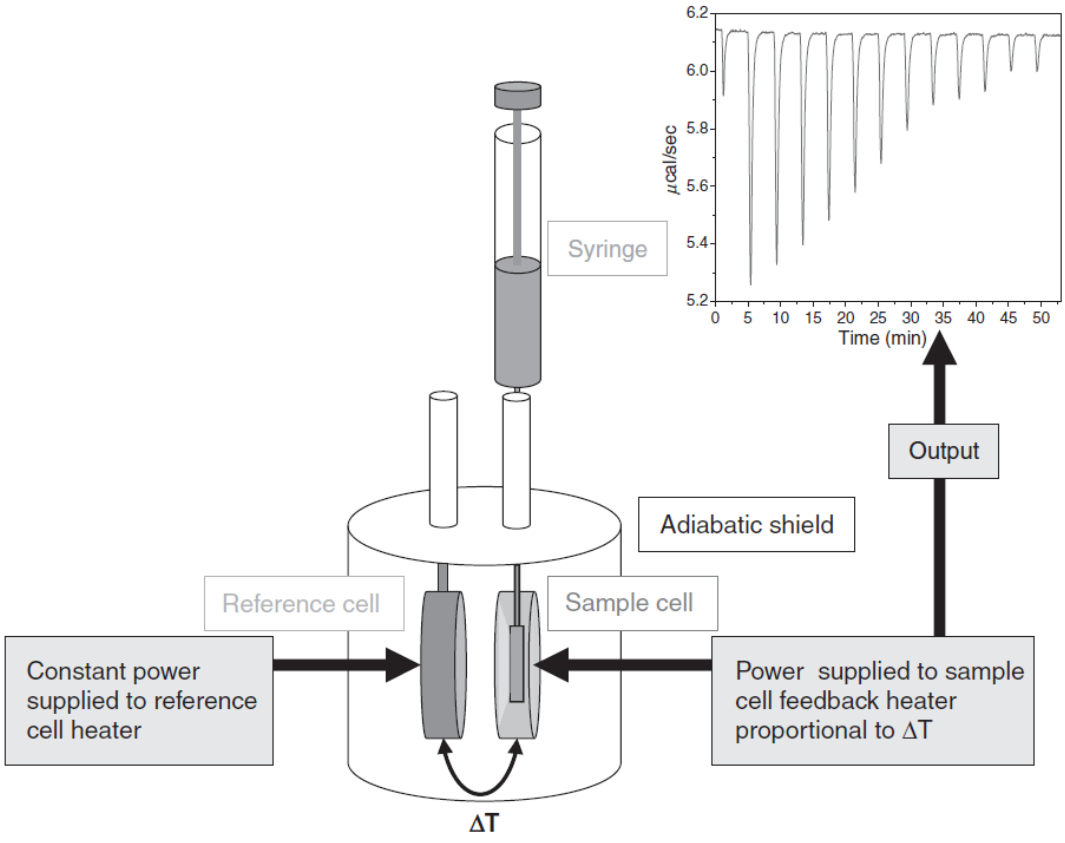

Figure 4.6. General schematic of a isothermal titration calorimeter.[113]

4.3.2 Data analysis.

The raw signal obtained from the ITC instrument is the power (in μW) applied to the control heater which keeps the cells at constant temperature plotted against time. The analysis of the obtained thermograms is done via a curve fitting process using nonlinear regression in which an appropriate model is chosen based on the expected physical, chemical or biological properties of the system and the best fit for the observed data is generated. Initial guess values are utilized for each of the fitting parameters (K, ΔH and *n*), and a theoretical curve is generated and compared to the actual data. An error function is calculated using the squared deviations between the data and the model, and successive iterations are performed until the error is minimized or remains constant.

Let us use the example of a simple ligand binding event with a metal receptor, M, and a ligand L in solution[109]:

$$M + nL \rightleftharpoons ML_n$$

n here denotes the binding stoichiometry. We will only consider two types of binding within the scope of this work, though interested readers are referred elsewhere for additional information.[113,114] The first type of binding is one-site independent binding, in which the metal may have several binding sites, but each site is thermodynamically identical and has the same thermodynamic affinity for the ligand. The equilibrium constant, *K*1, can be written as

$$K_1 = \frac{[ML]}{[M] * [L]}$$

where the terms in brackets represent concentrations of the respective species. The second type of binding is multiple-sites binding, in which the metal has two thermodynamically distinct sites. Specifically, each site has its own affinity for the same ligand, but the occupancy of

one site does not affect the affinity of the other, that is, the sites do not exhibit cooperative binding behavior. The relevant equations can be written as

$$M + L \rightleftharpoons ML$$
$$ML + L \rightleftharpoons ML_2$$

The equilibrium constant for the second binding event can be written as:

$$K_1 = \frac{[ML_2]}{[ML] * [L]}$$

With full expressions for the respective equilibrium constants, it is now possible to combine these expressions with mass balances on each component:

$$[M]_T = [M] + [ML] + [ML_2]$$

$$[L]_T = [L] + [ML] + 2 * [ML_2]$$

These mass balances can be substituted into the expressions for the equilibrium constants, such that only the total concentrations (i.e. measurable quantities) appear in the final ITC equations. This flexibility allows the experimenter to track the progress of the binding equilibria by calculating the molar ratio, of the total amount of ligand in the calorimeter cell to the total amount of metal in the cell, as the independent variable. The dependent variable in ITC experiments is the total amount of heat released per injection of ligand, *dQ*:

$$dQ = V \sum_i \Delta H_i d[ML_i]$$

where *V* is the volume of the calorimeter cell, ΔHi is the enthalpy of binding for the formation of ML_i, and $d[ML_i]$ is the incremental amount of complex, ML_i, formed during the injection. *dQ* can be written explicitly in terms of K_i, ΔH_i, [M]T, and [L]T, meaning that the heats from each injection can be fit to a statistical model as a function of the molar ratio that determines the binding parameters (K, ΔH, and n) in a single experiment. The value of ΔG is determined from the standard thermodynamic definition, $\Delta G = -RT\ln(K)$, and the entropy of adsorption, ΔS is calculated from $\Delta G = \Delta H - T\Delta S$.

4.4 Summary and Outlook

Nanomaterials hold the potential to solve challenging problems in energy conversion and storage. We believe that the design of new nanomaterials will be bolstered by development of new and robust synthetic techniques. Cation exchange is one such technology presents tremendous potential to access novel nanostructures having hitherto unattainable properties. While cation exchange has seen tremendous growth over the previous decade, very little quantitative data is available about the fundamental thermodynamic and kinetic phenomenon occurring during the transformation. Isothermal titration calorimetry can help shed light on these, helping to expand the understanding of the mechanistic nuances of cation exchange. The next chapter describes our work on quantifying the thermodynamic variables during the prototypical cation exchange reaction between CdSe and Ag.

4.5 References

1. Alivisatos, A. P., *Science* **1996,** *271* (5251), 933-937.
2. Wang, Y.; Herron, N., *The Journal of Physical Chemistry* **1991,** *95* (2), 525-532.
3. Ghosh, S. K.; Pal, T., *Chem. Rev.* **2007,** *107* (11), 4797-4862.
4. Sardar, R.; Funston, A. M.; Mulvaney, P.; Murray, R. W., *Langmuir* **2009,** *25* (24), 13840-13851.
5. Stratakis, M.; Garcia, H., *Chem. Rev.* **2012,** *112* (8), 4469-4506.
6. Haruta, M., *Catal. Today* **1997,** *36* (1), 153-166.
7. Haruta, M.; Daté, M., *Appl. Catl. A* **2001,** *222* (1–2), 427-437.
8. Kamat, P. V., *J. Phys. Chem. C* **2007,** *111* (7), 2834-2860.
9. Zhang, Q.; Uchaker, E.; Candelaria, S. L.; Cao, G., *Chem. Soc. Rev.* **2013,** *42* (7), 3127-3171.
10. from http://www.seia.org/policy/solar-technology/photovoltaic-solar-electric. Illustration by Kurt Struve (Accessed August 2016)
11. Carey, G. H.; Abdelhady, A. L.; Ning, Z.; Thon, S. M.; Bakr, O. M.; Sargent, E. H., *Chem. Rev.* **2015,** *115* (23), 12732-12763.
12. Nozik, A. J., *Chem. Phys. Lett.* **2008,** *457* (1–3), 3-11.
13. Beard, M. C.; Midgett, A. G.; Hanna, M. C.; Luther, J. M.; Hughes, B. K.; Nozik, A. J., *Nano Lett.* **2010,** *10* (8), 3019-3027.
14. Franceschetti, A.; An, J. M.; Zunger, A., *Nano Lett.* **2006,** *6* (10), 2191-2195.
15. O'Regan, B.; Gratzel, M., *Nature* **1991,** *353* (6346), 737-740.
16. Mathew, S.; Yella, A.; Gao, P.; Humphry-Baker, R.; CurchodBasile, F. E.; Ashari-Astani, N.; Tavernelli, I.; Rothlisberger, U.; NazeeruddinMd, K.; Grätzel, M., *Nat Chem* **2014,** *6* (3), 242-247.

17. Grätzel, M., Journal of Photochemistry and Photobiology A: Chemistry **2004,** 164 (1–3), 3-14.

18. Raut, H. K.; Ganesh, V. A.; Nair, A. S.; Ramakrishna, S., *Energy & Environmental Science* **2011,** *4* (10), 3779-3804.

19. Milliron, D. J.; Hughes, S. M.; Cui, Y.; Manna, L.; Li, J.; Wang, L.-W.; Paul Alivisatos, A., *Nature* **2004,** *430* (6996), 190-195.

20. Diedenhofen, S. L.; Vecchi, G.; Algra, R. E.; Hartsuiker, A.; Muskens, O. L.; Immink, G.; Bakkers, E. P. A. M.; Vos, W. L.; Rivas, J. G., *Adv. Mater.* **2009,** *21* (9), 973-978.

21. Law, M.; Greene, L. E.; Johnson, J. C.; Saykally, R.; Yang, P., *Nat Mater* **2005,** *4* (6), 455-459.

22. Hochbaum, A. I.; Yang, P., *Chem. Rev.* **2010,** *110* (1), 527-546.

23. Li, J.; Wu, N., *Catalysis Science & Technology* **2015,** *5* (3), 1360-1384.

24. Li, Z.; Luo, W.; Zhang, M.; Feng, J.; Zou, Z., *Energy & Environmental Science* **2013,** *6* (2), 347-370.

25. Smestad, G. P.; Steinfeld, A., *Industrial & Engineering Chemistry Research* **2012,** *51* (37), 11828-11840.

26. McCrory, C. C. L.; Jung, S.; Ferrer, I. M.; Chatman, S. M.; Peters, J. C.; Jaramillo, T. F., *J. Am. Chem. Soc.* **2015,** *137* (13), 4347-4357.

27. Chen, H. M.; Chen, C. K.; Liu, R.-S.; Zhang, L.; Zhang, J.; Wilkinson, D. P., *Chem. Soc. Rev.* **2012,** *41* (17), 5654-5671.

28. Kim, D.; Sakimoto, K. K.; Hong, D.; Yang, P., *Angew. Chem. Int. Ed.* **2015,** *54* (11), 3259-3266.

29. Kamat, P. V.; Tvrdy, K.; Baker, D. R.; Radich, J. G., *Chem. Rev.* **2010,** *110* (11), 6664-6688.

30. Osterloh, F. E., *Chem. Soc. Rev.* **2013,** *42* (6), 2294-2320.

31. van de Krol, R.; Liang, Y.; Schoonman, J., *J. Mater. Chem.* **2008,** *18* (20), 2311-2320.

32. Liu, C.; Dasgupta, N. P.; Yang, P., *Chem. Mater.* **2014,** *26* (1), 415-422.

33. Walter, M. G.; Warren, E. L.; McKone, J. R.; Boettcher, S. W.; Mi, Q.; Santori, E. A.; Lewis, N. S., *Chem. Rev.* **2010,** *110* (11), 6446-6473.

34. Lewis, N. S., *Science* **2016,** *351* (6271).

35. Arico, A. S.; Bruce, P.; Scrosati, B.; Tarascon, J.-M.; van Schalkwijk, W., *Nat Mater* **2005,** *4* (5), 366-377.

36. Dunn, B.; Kamath, H.; Tarascon, J.-M., *Science* **2011,** *334* (6058), 928-935.

37. Scrosati, B.; Garche, J., *J. Power Sources* **2010,** *195* (9), 2419-2430.

38. Liu, D.; Cao, G., *Energy & Environmental Science* **2010,** *3* (9), 1218-1237.

39. Guo, Y.-G.; Hu, J.-S.; Wan, L.-J., *Adv. Mater.* **2008,** *20* (15), 2878-2887.

40. Sun, Y.; Liu, N.; Cui, Y., *Nature Energy* **2016,** *1*, 16071.

41. Chan, C. K.; Peng, H.; Liu, G.; McIlwrath, K.; Zhang, X. F.; Huggins, R. A.; Cui, Y., *Nat Nano* **2008,** *3* (1), 31-35.

42. Magasinski, A.; Dixon, P.; Hertzberg, B.; Kvit, A.; Ayala, J.; Yushin, G., *Nat Mater* **2010,** *9* (4), 353-358.

43. Kim, H.; Han, B.; Choo, J.; Cho, J., *Angew. Chem. Int. Ed.* **2008,** *47* (52), 10151-10154.

44. Derrien, G.; Hassoun, J.; Panero, S.; Scrosati, B., *Adv. Mater.* **2007,** *19* (17), 2336-2340.

45. Park, C. M.; Sohn, H. J., *Adv. Mater.* **2007,** *19* (18), 2465-2468.

46. Sun, J.; Lee, H.-W.; Pasta, M.; Yuan, H.; Zheng, G.; Sun, Y.; Li, Y.; Cui, Y., *Nat Nano* **2015,** *10* (11), 980-985.

47. Poizot, P.; Laruelle, S.; Grugeon, S.; Dupont, L.; Tarascon, J. M., *Nature* **2000,** *407* (6803), 496-499.

48. Zheng, G.; Lee, S. W.; Liang, Z.; Lee, H.-W.; Yan, K.; Yao, H.; Wang, H.; Li, W.; Chu, S.; Cui, Y., *Nat Nano* **2014,** *9* (8), 618-623.

49. Taberna, P. L.; Mitra, S.; Poizot, P.; Simon, P.; Tarascon, J. M., *Nat Mater* **2006,** *5* (7), 567-573.

50. Ji, X.; Lee, K. T.; Nazar, L. F., *Nat Mater* **2009,** *8* (6), 500-506.

51. Peng, Z.; Freunberger, S. A.; Chen, Y.; Bruce, P. G., *Science* **2012,** *337* (6094), 563-566.

52. Aetukuri, N. B.; McCloskey, B. D.; García, J. M.; Krupp, L. E.; Viswanathan, V.; Luntz, A. C., *Nat Chem* **2015,** *7* (1), 50-56.

53. Li, W.; Zheng, G.; Yang, Y.; Seh, Z. W.; Liu, N.; Cui, Y., *Proceedings of the National Academy of Sciences* **2013,** *110* (18), 7148-7153.

54. Lu, Y.-C.; Xu, Z.; Gasteiger, H. A.; Chen, S.; Hamad-Schifferli, K.; Shao-Horn, Y., *J. Am. Chem. Soc.* **2010,** *132* (35), 12170-12171.

55. Yang, Y.; Yu, G.; Cha, J. J.; Wu, H.; Vosgueritchian, M.; Yao, Y.; Bao, Z.; Cui, Y., *ACS Nano* **2011,** *5* (11), 9187-9193.

56. Suo, L.; Hu, Y.-S.; Li, H.; Armand, M.; Chen, L., *Nat Commun* **2013,** *4*, 1481.

57. de Mello Donegá, C.; Liljeroth, P.; Vanmaekelbergh, D., *Small* **2005,** *1* (12), 1152-1162.

58. Kwon, S. G.; Hyeon, T., *Small* **2011,** *7* (19), 2685-2702.

59. Peng, X.; Manna, L.; Yang, W.; Wickham, J.; Scher, E.; Kadavanich, A.; Alivisatos, A. P., *Nature* **2000,** *404* (6773), 59-61.

60. Murray, C. B.; Norris, D. J.; Bawendi, M. G., *J. Am. Chem. Soc.* **1993,** *115* (19), 8706-8715.

61. Murphy, J. E.; Beard, M. C.; Norman, A. G.; Ahrenkiel, S. P.; Johnson, J. C.; Yu, P.; Mićić, O. I.; Ellingson, R. J.; Nozik, A. J., *J. Am. Chem. Soc.* **2006,** *128* (10), 3241-3247.

62. Luther, J. M.; Zheng, H.; Sadtler, B.; Alivisatos, A. P., *J. Am. Chem. Soc.* **2009,** *131* (46), 16851-16857.

63. Son, D. H.; Hughes, S. M.; Yin, Y.; Paul Alivisatos, A., *Science* **2004,** *306* (5698), 1009-1012.

64. Geng, J.; Liu, B.; Xu, L.; Hu, F.-N.; Zhu, J.-J., *Langmuir* **2007,** *23* (20), 10286-10293.

65. Saruyama, M.; So, Y.-G.; Kimoto, K.; Taguchi, S.; Kanemitsu, Y.; Teranishi, T., *J. Am. Chem. Soc.* **2011,** *133* (44), 17598-17601.

66. Park, J.; Zheng, H.; Jun, Y.-w.; Alivisatos, A. P., *J. Am. Chem. Soc.* **2009,** *131* (39), 13943-13945.

67. Dloczik, L.; Könenkamp, R., *Nano Lett.* **2003,** *3* (5), 651-653.

68. Dawood, F.; Schaak, R. E., *J. Am. Chem. Soc.* **2009,** *131* (2), 424-425.

69. Hodges, J. M.; Kletetschka, K.; Fenton, J. L.; Read, C. G.; Schaak, R. E., *Angew. Chem. Int. Ed.* **2015,** *54* (30), 8669-8672.

70. Zhang, D.; Yang, Y.; Bekenstein, Y.; Yu, Y.; Gibson, N. A.; Wong, A. B.; Eaton, S. W.; Kornienko, N.; Kong, Q.; Lai, M.; Alivisatos, A. P.; Leone, S. R.; Yang, P., *J. Am. Chem. Soc.* **2016,** *138* (23), 7236-7239.

71. Pellet, N.; Teuscher, J.; Maier, J.; Grätzel, M., *Chem. Mater.* **2015,** *27* (6), 2181-2188.

72. Akkerman, Q. A.; D'Innocenzo, V.; Accornero, S.; Scarpellini, A.; Petrozza, A.; Prato, M.; Manna, L., *J. Am. Chem. Soc.* **2015,** *137* (32), 10276-10281.

73. Nedelcu, G.; Protesescu, L.; Yakunin, S.; Bodnarchuk, M. I.; Grotevent, M. J.; Kovalenko, M. V., *Nano Lett.* **2015,** *15* (8), 5635-5640.

74. Solis-Ibarra, D.; Smith, I. C.; Karunadasa, H. I., *Chem. Sci.* **2015,** *6* (7), 4054-4059.

75. Beberwyck, B. J.; Surendranath, Y.; Alivisatos, A. P., *J. Phys. Chem. C* **2013,** *117* (39), 19759-19770.

76. Putnis, A., *Mineralogical Magazine* **2002,** *66* (5), 689-708.

77. Jenny, H., *The Journal of Physical Chemistry* **1931,** *36* (8), 2217-2258.

78. Fedorov, V. A.; Ganshin, V. A.; Korkishko, Y. N., *physica status solidi (a)* **1993,** *139* (1), 9-65.

79. Kovalenko, M. V.; Talapin, D. V.; Loi, M. A.; Cordella, F.; Hesser, G.; Bodnarchuk, M. I.; Heiss, W., *Angew. Chem. Int. Ed.* **2008,** *47* (16), 3029-3033.

80. Deka, S.; Miszta, K.; Dorfs, D.; Genovese, A.; Bertoni, G.; Manna, L., *Nano Lett.* **2010,** *10* (9), 3770-3776.

81. Peng, X.; Wickham, J.; Alivisatos, A. P., *J. Am. Chem. Soc.* **1998,** *120* (21), 5343-5344.

82. Li, H.; Zanella, M.; Genovese, A.; Povia, M.; Falqui, A.; Giannini, C.; Manna, L., *Nano Lett.* **2011,** *11* (11), 4964-4970.

83. Luther, J. M.; Jain, P. K.; Ewers, T.; Alivisatos, A. P., *Nat Mater* **2011,** *10* (5), 361-366.

84. Nozik, A. J.; Mićić, O. I., *MRS Bull.* **1998,** *23* (02), 24-30.

85. Harris, D. K.; Allen, P. M.; Han, H.-S.; Walker, B. J.; Lee, J.; Bawendi, M. G., *J. Am. Chem. Soc.* **2011,** *133* (13), 4676-4679.

86. Xie, R.; Zhang, J.; Zhao, F.; Yang, W.; Peng, X., *Chem. Mater.* **2010,** *22* (13), 3820-3822.

87. Beberwyck, B. J.; Alivisatos, A. P., *J. Am. Chem. Soc.* **2012,** *134* (49), 19977-19980.

88. De Trizio, L.; Manna, L., *Chem. Rev.* **2016**.

89. Carbone, L.; Cozzoli, P. D., *Nano Today* **2010,** *5* (5), 449-493.

90. Norris, D. J.; Efros, A. L.; Erwin, S. C., *Science* **2008,** *319* (5871), 1776-1779.

91. Mocatta, D.; Cohen, G.; Schattner, J.; Millo, O.; Rabani, E.; Banin, U., *Science* **2011,** *332* (6025), 77-81.

92. Sahu, A.; Kang, M. S.; Kompch, A.; Notthoff, C.; Wills, A. W.; Deng, D.; Winterer, M.; Frisbie, C. D.; Norris, D. J., *Nano Lett.* **2012,** *12* (5), 2587-2594.

93. Kang, M. S.; Sahu, A.; Frisbie, C. D.; Norris, D. J., *Adv. Mater.* **2013,** *25* (5), 725-731.

94. Bailey, R. E.; Nie, S., *J. Am. Chem. Soc.* **2003,** *125* (23), 7100-7106.

95. Gupta, S.; Zhovtiuk, O.; Vaneski, A.; Lin, Y.-C.; Chou, W.-C.; Kershaw, S. V.; Rogach, A. L., *Particle & Particle Systems Characterization* **2013,** *30* (4), 346-354.

96. Wong, A. B.; Brittman, S.; Yu, Y.; Dasgupta, N. P.; Yang, P., *Nano Lett.* **2015,** *15* (6), 4096-4101.

97. Zhang, J.; Gao, J.; Church, C. P.; Miller, E. M.; Luther, J. M.; Klimov, V. I.; Beard, M. C., *Nano Lett.* **2014,** *14* (10), 6010-6015.

98. Kim, S.; Marshall, A. R.; Kroupa, D. M.; Miller, E. M.; Luther, J. M.; Jeong, S.; Beard, M. C., *ACS Nano* **2015,** *9* (8), 8157-8164.

99. Nguyen, A. T.; Lin, W.-H.; Lu, Y.-H.; Chiou, Y.-D.; Hsu, Y.-J., *Appl. Catl. A* **2014,** *476*, 140-147.

100. Shemesh, Y.; Macdonald, J. E.; Menagen, G.; Banin, U., *Angew. Chem. Int. Ed.* **2011,** *50* (5), 1185-1189.

101. Rowsell, J. L. C.; Taylor, N. J.; Nazar, L. F., *J. Am. Chem. Soc.* **2002,** *124* (23), 6522-6523.

102. Freire, E.; Mayorga, O. L.; Straume, M., *Anal. Chem.* **1990,** *62* (18), 950A-959A.

103. Hansen, L. D.; Christensen, J. J.; Izatt, R. M., *Chemical Communications (London)* **1965,** (3), 36-38.

104. Christensen, J. J.; Izatt, R. M.; Hansen, L. D.; Partridge, J. A., *The Journal of Physical Chemistry* **1966,** *70* (6), 2003-2010.

105. Eatough, D., *Anal. Chem.* **1970,** *42* (6), 635-639.

106. Christensen, J. J.; Wrathall, D. P.; Oscarson, J. O.; Izatt, R. M., *Anal. Chem.* **1968,** *40* (11), 1713-1717.

107. Ababou, A.; Ladbury, J. E., *Journal of Molecular Recognition* **2006,** *19* (1), 79-89.

108. Langerman, N.; Biltonen, R. L., [13] Microcalorimeters for biological chemistry: Applications, instrumentation and experimental design. In *Methods Enzymol.*, Academic Press: 1979; Vol. Volume 61, pp 261-286.

109. Moschetta, E. G.; Gans, K. M.; Rioux, R. M., *J. Catal.* **2013,** *302*, 1-9.

110. Ravi, V.; Binz, J. M.; Rioux, R. M., *Nano Lett.* **2013,** *13* (9), 4442-4448.

111. McCarthy, S. M.; Lin, Y.-C.; Devarajan, D.; Chang, J. W.; Yennawar, H. P.; Rioux, R. M.; Ess, D. H.; Radosevich, A. T., *J. Am. Chem. Soc.* **2014,** *136* (12), 4640-4650.

112. Dr. Jason M Binz PhD Thesis

113. Freyer, M. W.; Lewis, E. A., Isothermal Titration Calorimetry: Experimental Design, Data Analysis, and Probing Macromolecule/Ligand Binding and Kinetic Interactions. In *Methods in Cell Biology*, Academic Press: 2008; Vol. Volume 84, pp 79-113.

114. Jose C. Martinez, Javier Murciano-Calles, Eva S. Cobos,

Manuel Iglesias-Bexiga, Irene Luque and Javier Ruiz-Sanz (2013). Isothermal Titration Calorimetry: Thermodynamic Analysis of the Binding Thermograms of Molecular Recognition Events by Using Equilibrium Models, Applications of Calorimetry in a Wide Context - Differential Scanning Calorimetry, Isothermal Titration Calorimetry and Microcalorimetry, Dr. Amal Ali Elkordy (Ed.), InTech, DOI: 10.5772/53311. Available from: http://www.intechopen.com/books/applications-of-calorimetry-in-a-wide-context-differential-scanning-calorimetry-isothermal-titration-calorimetry-and-microcalorimetry/isothermal-titration-calorimetry-thermodynamic-analysis-of-the-binding-thermograms-of-molecular-reco

Chapter 5

Measurement of Thermodynamics of Cation Exchange in Cadmium Selenide Nanocrystals using Isothermal Titration Calorimetry

As described in the previous chapter, cation exchange in nanocrystals is rapidly becoming a popular technique both as a complement, and in some cases a replacement to the solvothermal methods of nanoparticle synthesis. Although the technique has been extensively used as a synthetic tool, there have been no reports about quantitative thermodynamic measurements of such systems. We sought to fill this gap by utilizing isothermal titration calorimetry on the well-studied cation exchange process between CdSe nanocrystals and Ag^+ ions. This chapter describes our findings and proposes future studies that can help provide a complete thermodynamic and kinetic understanding of the cation exchange reaction in nanocrystals.

5.1 Introduction

The field of nanoparticle cation exchange has seen tremendous growth during the last decade largely due to the efforts of chemists trying to develop new methodologies for synthesis of complex nanostructures. While this development has contributed to the synthesis of novel and practical materials as shown in the previous chapter, there is still a paucity of information on the fundamentals of this important technique. Specifically there is no quantitative data available on the effect of particle size, solvent, capping agent, identity of the exchanging salt, etc. on the thermodynamics of the cation exchange reaction. Success in this endeavor could help gain insight into the mechanistic details of the process, helping to expand the scope of the cation exchange

methodology to a larger part of the periodic table enabling rational design of materials with superior physical or chemical properties.[1-2]

We decided to use isothermal titration calorimetry as the technique for this study as it allows for measurement of equilibrium constant, enthalpy of reaction, and stoichiometry in a single experiment as opposed to the traditional indirect approaches like the Van't Hoff analysis, which require multiple experiments over varying temperatures.[3]

ITC has been predominantly utilized to study the binding thermodynamics of biomolecules with various receptors. A nanoparticle cation exchange can be thought of as a ligand binding (incoming cation) with subsequent release of a different ligand (outgoing cation). Systems involving the ideologically similar ligand exchange in homogeneous organometallic complexes have been studied previously, and simple binding models have been developed.[4]

We report here on the systematic thermochemical study of the prototypical cation exchange reaction between cadmium selenide nanoparticles and silver ions. The effect of silver cation source, nanoparticle size, capping agent, solvent and reaction temperature has been studied. We also compare the values obtained by calorimetry to those based on theoretical models proposed in the literature. A discussion based on the observed results and guidelines for future experimental design in presented in the subsequent sections.

5.2 Effect of the silver salt used in the exchange reaction

Although not explicitly involved in the overall cation exchange reaction between CdSe and Ag^+ to give Ag_2Se, the anions from the silver salt are expected to significantly affect the energetics of the reaction. Since the seminal studies on cation exchange in semiconductor nanocrystals,[5] the importance of the solvation energies of the exchanging ions has been recognized as an important parameter in the success of the reaction. The solvation energy is dependent on two important factors, the solvent and the presence of ligands in solution. Based on the premise of Pearson's hard-soft acid-base (HSAB) theory,[6] the exchange between CdSe and Ag^+ was shown to be reversible. The use of a hard ion like methoxide (from MeOH) in solution could drive the transformation from CdSe to Ag_2Se while the use of a soft phosphine in solution allowed for the exchange of Ag_2Se back to CdSe.

While the phosphines in the example above are L-type neutral ligands, the anion associated with the silver salt can be thought of as X-type anionic ligands. While the HSAB is only a qualitative tool, recently Alvarez et. al. have formulated an empirical scale to quantify the coordinating ability of a large number of anions.[7] For every anion they have proposed a coordinating ability index α based on the probability of it being found in the inner vs outer sphere of complexes with transition metals or lanthanides. Their procedure consisted of searching the Cambridge Structural Database, and quantifying the number of structures with the anion in the inner vs outer co-ordination sphere of all transition metal compounds in the database. The co-ordination sphere was defined as the sum of the Van der Waals radii of the two groups in concern. The index is defined as the log of the ratio of number of structures having the anion in the inner co-ordination sphere to the number of structures having the anion in the outer co-ordination sphere. It follows from the definition that a positive value of α indicates a higher coordinating ability and a negative value highlights a poor tendency to co-ordinate. In the context

of the cation exchange reactions with silver salts, those containing stronger binding anions are expected to be more favorable enthalpically, than with those containing weakly coordinating anions.

Figure 5.1 shows a representative thermogram for cation exchange reaction between hexadecylamine (HDA) capped 2.2nm CdSe particles and $AgNO_3$ in acetonitrile at 25 °C. Under the thermogram, is shown the integrated heats and the best fit binding model to the obtained data. The integrated heat data can be divided into three distinct regions, the section prior to the point of inflection represents the active exchange of Cd^{2+} with Ag^{+}, the non-linear portion of the sigmoid near the point of inflection indicates the exchange of final few Cd^{2+} ions in the parent crystal, and the final section corresponds to the heat of mixing/dilution of the silver salt solution. A summary of the best fitting parameters obtained for $AgNO_3$, AgOTf and $AgBF_4$ are summarized in Table 5.1.

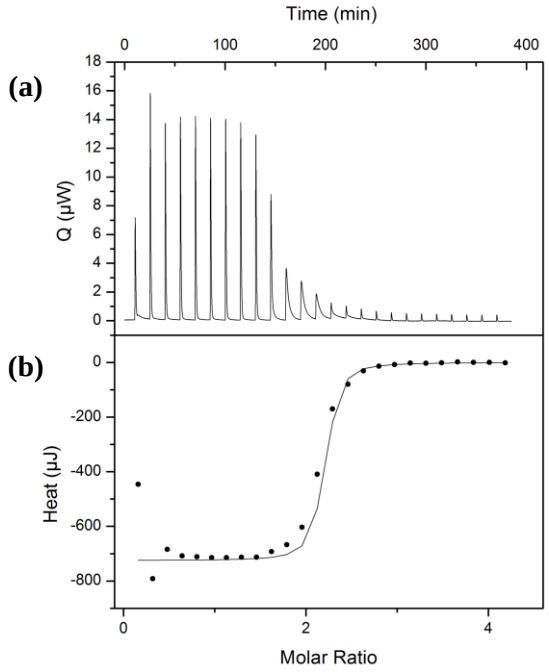

Figure 5.1. (a) Real-time ITC thermogram for exchange reaction between CdSe and $AgNO_3$ at 25 °C in acetonitrile. (b) Integrated heat data with fitted model.

Table 5.1. Effect of silver salt on the cation exchange between CdSe and Ag^+ in MeCN

Salt	Coordinating ability index[7]	K ($x10^6$ mol^{-1})	ΔG (kJ/mol)	ΔH (kJ/mol)	TΔS (kJ/mol)	n
$AgNO_3$	0.1	1.77±1.09	-35.3±2.0	-36.5±0.5	-1.2±1.9	2.1±0.0
AgOTf	-0.4	4.29±2.6	-26.2±1.8	-31.8±0.2	-5.6±1.8	2.2±0.0
$AgBF_4$	-1.1	5.29±1.6	-27.3±0.6	-32.8±0.4	-5.5±0.5	2.3±0.2

Consistent with the hypothesis, the heat of the reaction for silver nitrate, containing a more coordinating anion as compared to triflate or tetrafluoroborate, is higher than the ones observed for the other two. The insignificant difference between the heat of reaction between CdSe and silver triflate or silver tetrafluoroborate can be explained due to the higher coordinating ability of the solvent acetonitrile (α = -0.2) as compared to either anions. This would potentially cause acetonitrile to form solvent separated ion pairs drowning out any detectable influence of the anions in solution.

5.3 Effect of solvent

As described above, the identity of the solvent also plays a crucial role in dictating the solvation energy of the ions, and hence the overall energetics of the cation exchange reaction. The cation exchange reaction was carried out in acetonitrile, 2-butanone and toluene in the calorimeter to gauge the effect of the solvents on the transformation. The solvents were chosen so as to cover a wide range of dielectric constants, and also to ensure the stability of the nanoparticle suspension during the course of the titration. Silver triflate was utilized as the silver salt as it showed suitable solubility in all the solvents.

Figure 5.2 shows the integrated thermograms for the cation exchange in different solvents. The parameters obtained from the fit for the different solvents are presented in Table 5.2. While the data in acetonitrile (Figure 5.2 a) fits well with a single site model, those obtained

in 2-butanone and toluene do not. A multisite model is found to have a better fit to the observed data. While the exact cause of this behavior is presently unknown, a few possibilities exist.

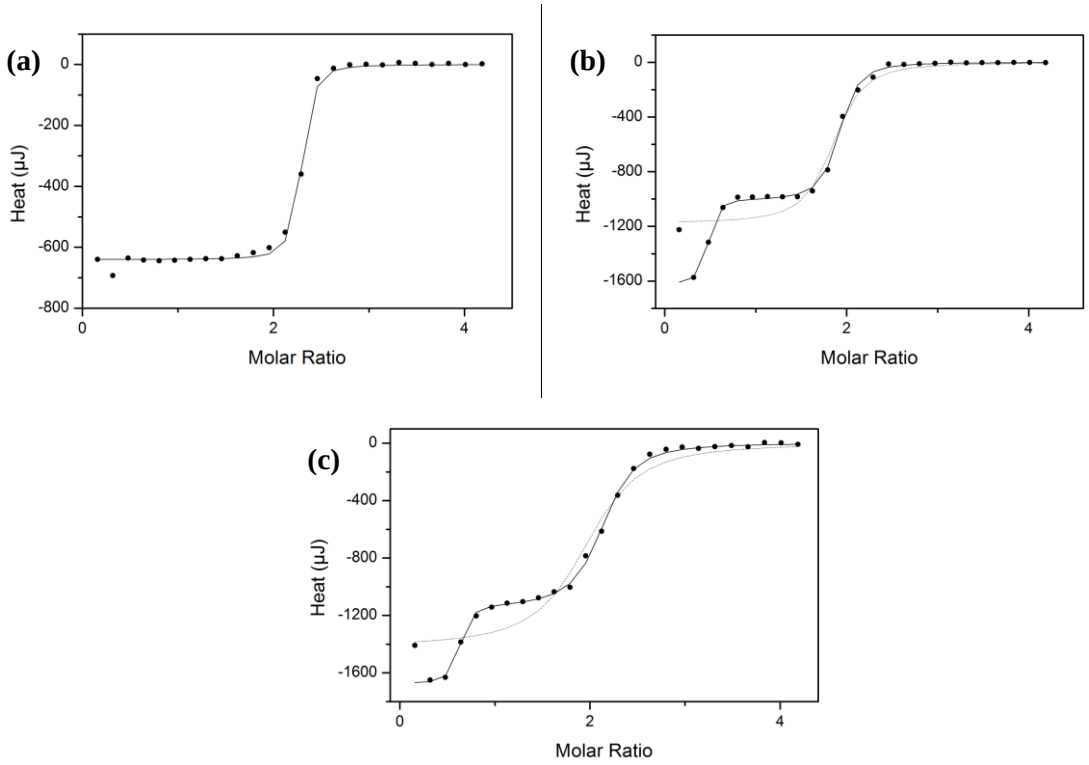

Figure 5.2. Integrated heat data for exchange reaction between CdSe and AgOTf at 25 °C in (a) Acetonitrile; fit with independent sites model, (b) PhMe: dotted lines-independent sites model; solid line-multiple sites model, (c) 2-butanone: dotted lines-independent sites model; solid line-multiple sites model.

The CdSe nanoparticles are stabilized in solution due to the presence of organic surface active ligand hexadecylamine. Analogous to the transition metal complexes, the surface ligands can be in a dynamic equilibrium between free and bound states. The identity of the solvent will dictate the extent of this equilibrium. Toluene and 2-butanone being less polar might favor the number of free ligands over acetonitrile. This phenomenon could lead to solvation of the silver ions by the free ligands, adding to the heat generated from the cation exchange reaction. The two distinct binding events could be the cause behind the improved fit using a multisite model.

Another possibility is the formation of different phases of Ag_2Se during the cation exchange reaction. Based on the bulk phase diagram of Ag_2Se and CdSe there is a possibility of existence of either a solid solution of Ag_2Se and CdSe or the coexistence of both the phases distinctly. The formation of these phases would be expected to have different equilibrium constants, and might help explain the multisite behavior seen in the integrated heat plots. The reason for a good single site fit for the data in acetonitrile could be due to the dominant role of solvation by acetonitrile which suppresses the detection of heat signals due to phase transformations. This particular observation demonstrates one of the shortcomings of the ITC, which is the inability to assign the origin of heat flow to a specific chemical or physical transformation.

Table 5.2. Effect of solvent on cation exchange between CdSe and AgOTf.

Entry	Dielectric constant	K ($x10^7$ mol^{-1})	ΔG (kJ/mol)	ΔH (kJ/mol)	TΔS (kJ/mol)	n
Acetonitrile	36.6	0.43±0.2	-26.2±1.8	-31.8±0.2	-5.6±1.8	2.2±0.0
2-Butanone	18.6	8.9±5.7	-44.8±1.9	-83.9±0.9	-39.1±1.7	0.6±0.0
		0.04±0.0	-31.5±2.8	-57.2±1.1	-25.7±2.6	1.4±0.1
Toluene	2.4	40.2±18.7	-48.9±6.7	-80.2±4.2	-31.3±5.2	0.5±0.2
		0.2±0.1	-35.3±5.6	-48.6±1.8	-13.3±3.1	1.4±0.1

However, irrespective of the model used, more heat is evolved in the less polar toluene and 2-butanone as compared to acetonitrile. This could be due to formation of tighter ion pairs between Cd^{2+} and ^-OTf in those solvents as compared to acetonitrile, where a solvent separated ion pair is more likely.

5.4 Effect of size

The cation exchange reaction in nanoparticles is distinguished from the corresponding reaction in extended solids or bulk form of the material, mainly due to the fast reaction rates. This has been attributed to the small size of the particles, which affords it a high surface to volume ratio and likely lowers the activation barriers to diffusion of ions.[1] We therefore sought to study the effect of nanoparticle size on the overall thermodynamics of cation exchange between CdSe and silver. Table 5.3 shows the best fit parameters obtained for the different sized CdSe nanoparticles.

As described above the data obtained for the 2.2 nm particles is best fit to a multisite model while those obtained for 3.5, and 6.2 nanometer particles fits to a single site model. We observe that the overall entropy change is negative for all the sizes consistent with the stoichiometry of the exchange, and the value reduces with increasing particle size. This is also to be expected as a bigger particle size means more long range order, and hence an entropically less favorable reaction.

Table 5.3. Effect of nanoparticle size on the cation exchange between CdSe and AgOTf in PhMe

Entry	K ($x10^6$ mol^{-1})	ΔG (kJ/mol)	ΔH (kJ/mol)	TΔS (kJ/mol)	n
2.2 nm	400±187	-48.9±6.7	-80.2±4.2	-31.3±5.2	0.5±0.2
	1.7±1.1	-35.3±5.6	-48.6±1.8	-13.3±3.1	1.4±0.1
3.5 nm	1.4±0.5	-33.9±6.3	-111.9±4.9	-78.0±3.9	1.7±0.0
6.2 nm	0.32±0.2	-31.2±14.1	-151.4±9.4	-120.2±10.5	1.6±0.0

This reduction in entropy is matched by a proportional increase in the enthalpy of the reaction. The plot of observed change in enthalpy vs change in entropy gives a linear relationship in a phenomenon referred to as enthalpy-entropy compensation.[8]

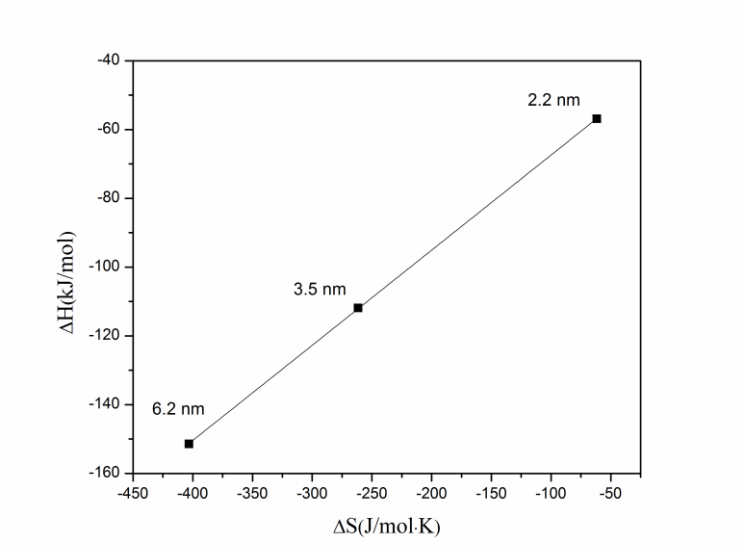

Figure 5.3. Compensation plot for the enthalpy and entropy of cation exchange between CdSe and AgOTf for 2.2, 3.5 and 6.2 nm particles.

While the origin and physical significance of the compensation effect is a topic of debate, it has been observed in many chemical systems such as coordination chemistry, solvation, molecular recognition, heterogeneous catalysis etc.[8-11] Generally speaking, a stronger intermolecular interaction or bonding (related to the enthalpy) will lead to a greater reduction of the configurational freedom and hence greater order of the system (related to the entropy).[8] The proportionality might be direct effect of the two opposing effects described above.

Another point of note is the monotonic decrease in the stoichiometry with the increase in nanoparticle size. This is expected due to increased barrier to diffusion with increasing path length the ion has to travel. In the extreme limit of this trend, cation exchange in thin films or extended solids takes days or weeks at elevated temperatures reinforcing the importance of nanostructuring on the rate of reactions.[2]

5.5 Effect of capping agent

The capping agent primarily serves to stabilize the nanoparticles in solution by preventing aggregation. Because it lies on the solid liquid interface, it has the potential to modify the physical and chemical properties of the nanoparticle. For example the variation in surface ligands can change the solubility, surface chemistry, binding affinity, and catalytic and electromagnetic performance of nanoparticles.[12-13] While the CdSe nanoparticles are synthesized using trioctylphosphine (TOP), trioctylphosphine oxide (TOPO), and oleic acid as the surface ligands, these can be easily replaced by other surfactants. Typically a concentrated nanoparticle suspension is added to a solution of the surfactant to be exchanged, and the mixture is heated to reflux for a period of 10-12 hours.[14] The nanoparticles are purified and the excess ligand is removed by successive washing with an antisolvent followed by centrifugation. The final solution is prepared by dispersing the nanoparticles in a suitable solvent.

We decided to study the effect of five commonly utilized surface ligand functional groups on the cation exchange reaction. The octyl terminated groups were chosen as they are easily available and help obtain uniform data by suppressing any variation arising due to the alkyl chain length. The best fit parameters for the observed integrated heat data are presented in Table 5.4. For the particles exchanged with trioctylphosphine oxide (TOPO), octylamine and octanethiol, the enthalpy of the cation exchange was found to be lower than for the nanoparticles obtained via synthesis (containing a mixture of oleic acid and TOPO). Octanoic acid and hexadecylamine gave much higher enthalpy of reaction as compared to the as synthesized particles. Interestingly the entropy change in these reactions scale proportionally to the enthalpy change, resulting in an overall similar value of free energy change, and the compensation effect described above is also seen in the case of different surface ligands (Figure 5.4)

Table 5.4. Effect of capping agent on cation exchange of CdSe with AgOTf in PhMe

Capping Agent	K ($x10^6$ mol^{-1})	ΔG (kJ/mol)	ΔH (kJ/mol)	TΔS (kJ/mol)	n
TOPO	6.69±2.0	-33.2±26.8	-63.1±25.4	-29.9±8.7	1.4±0.1
Octylamine	3.00±0.4	-31.3±4.5	-93.7±3.0	-62.4±3.3	1.2±0.1
Octanethiol	4.46±0.3	-32.4±3.9	-94.6±2.7	-62.2±2.8	2.1±0.1
As synthesized	6.65±4.4	-32.8±19.4	-98.9±13.2	-66.1±14.2	2.0±0.1
Octanoic Acid	7.55±3.1	-33.6±10.5	-111.1±7.5	-77.5±7.4	1.4±0.1
Hexadecylamine	0.32±0.2	-31.2±14.1	-151.4±9.4	-120±10.5	1.6±0.0

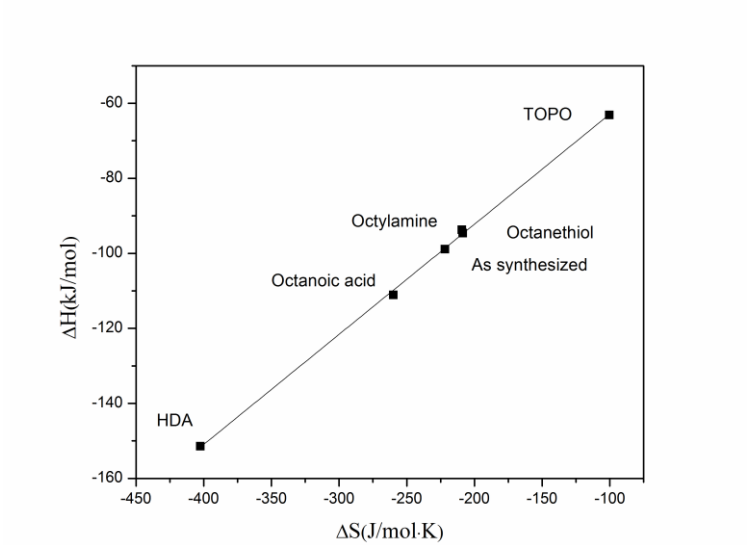

Figure 5.4. Compensation plot for the enthalpy and entropy of cation exchange between CdSe and AgOTf for 6.2 nm particles with different capping agents.

For a lot of the ligands, the observed value of *n*, the stoichiometry of the exchange, is less than the theoretically expected value of 2. There are two possible explanations for this observation. First, the surface ligand might act to hinder the diffusion of the ions across the solid/liquid interface and secondly, the ligands in solution might complex with the silver ions rendering them unavailable for cation exchange. Such an effect has previously been utilized in the literature for the partial doping of CdSe with silver ions by employing an excess of alkyl

phosphines in solution during the cation exchange reaction.[15] The second reason could be the loss of some surface cadmium atoms during the dynamic adsorption/desorption equilibrium of the surface ligands. It is also possible that the initiation of the cation exchange reaction can lead to loss of surface ligands, which could promote loss of surface cadmium ions.[16] This can be indirectly inferred from the lower stability of the suspensions of Ag_2Se as compared to the corresponding CdSe.

While an exact trend based on the chemical identity of the surface ligand is not apparent, future studies would be aimed at understanding and confirming the source of this effect. In particular, efforts are underway to quantify the amount of ligand present on the surface as well as in solution. We believe this would allow us to gauge the effect of contributions from the solution ligation and possibly also explain some of the unanswered questions regarding the multiple site behavior seen previously.

5.6 Effect of temperature

The cation exchange of CdSe with $AgNO_3$ in acetonitrile was studied at three different temperatures of 15, 25 and 35°C. The integrated heat data obtained from the study is presented in Table 5.5. We observe that the equilibrium constant reduces with an increase in temperature which is consistent with the Le Chatelier's principle for exothermic reactions.

Table 5.5. Effect of temperature on cation exchange of CdSe with $AgNO_3$ in MeCN

T (K)	K ($x10^6$ mol^{-1})	ΔG (kJ/mol)	ΔH (kJ/mol)	TΔS (kJ/mol)	n
288.15	2.95±0.93	-35.1±0.9	-37.0±0.1	-1.4±0.9	2.1±0.1
298.15	1.77±1.09	-35.3±2.0	-36.5±0.5	-1.2±1.9	2.1±0.0
308.15	1.10±0.15	-36.6±1.1	-37.2±1.0	-0.6±0.5	1.9±0.0

5.7 Comparison between the calculated and observed heat of reaction between cadmium selenide and Ag

There have been several oversimplified models for determining the free energy change, and hence the feasibility of the cation exchange process. Jain et. al. have proposed the use of bond dissociation or lattice energies in conjunction with solvation energies to gauge the spontaneity of the cation exchange.[1] While their approach accounts for the effect of solvent on the cation exchange, the precise knowledge of the solvation energies is not always available, limiting the scope of this method. Jeong et. al. have used the difference in solubility products of the reactants and products to predict if the transformation is thermodynamically favorable.[17] While solubility data for a number of compounds is easily available in water, extension to other solvent systems, which are most typically used in cation exchange, is difficult. Lastly, Alivisatos et. al. have sought to utilize the energy of formation of the starting and final nanocrystal and the difference in the redox potentials of the two cations for determining the free energy change of the reaction.[2] We believe their model is most widely applicable as formation energies are widely available for a number of compounds, and the redox potentials are known for almost all the metals in the periodic table in water. It is also easy to measure the redox potentials in other solvent systems using cyclic voltammetry.

Consider the cation exchange reaction studied above between CdSe and Ag^+. The overall reaction can be divided into two imaginary electrochemical reactions shown below.

$$CdSe + 2Ag^+ \rightleftharpoons Ag_2Se + Cd^{2+}$$

$$CdSe \rightleftharpoons Cd^{2+} + 2e^- + Se^0$$

$$2Ag^+ + 2e^- + Se^0 \rightleftharpoons Ag_2Se$$

The two half reactions can be further simplified in terms of the free energies of formation ($\Delta G°$) and standard reduction potentials ($E°$) in a given solvent for the respective species. By

$$CdSe \rightleftharpoons Cd^0 + Se^0 \qquad -(\Delta G^\circ)_{CdSe}$$

$$Cd^0 \rightleftharpoons Cd^{2+} + 2e^- \qquad -E^\circ_{Cd2+}$$

$$2Ag^0 + Se^0 \rightleftharpoons Ag_2Se \qquad (\Delta G^\circ)_{Ag2Se}$$

$$2Ag^+ + 2e^- \rightleftharpoons 2Ag^0 \qquad E^\circ_{Ag+}$$

adding the resulting terms, the overall free energy change for the process in the given solvent can be written as

$$\Delta G_{\text{reaction}} = (\Delta G^\circ)_{Ag_2Se} - (\Delta G^\circ)_{CdSe} - 2*F\,[(E^\circ)_{Ag^+} - (E^\circ)_{Cd^{2+}}]$$

Using the standard free energy of formation of cadmium selenide,[18] silver selenide,[19] and the reduction potentials of Ag^+ and Cd^{2+} in acetonitrile,[20] we calculate the value of free energy change during the reaction to be -23.3 kJ/mol. As opposed to this, the experimentally observed $\Delta G_{reaction}$ in acetonitrile with $AgNO_3$ is equal to -35.3 kJ/mol, and the ones obtained with AgOTf and $AgBF_4$ are -26.2 kJ/mol and -27.3 kJ/mol respectively. So while the theoretical calculation is close to the observed values of $\Delta G_{reaction}$ for cation exchange reaction with AgOTf and $AgBF_4$, it is far from the value observed for $AgNO_3$. This is due to the fact that the calculation does not consider the effect of nanostructuring, solvation, surface ligands and size on the heat of formation. These variables have a significant influence on the cation exchange reaction as shown in the previous sections, and hence deviations from the simplified model should be expected when extending the calculations to cation exchange in other systems.

5.8 Summary and Outlook

The effect of size, silver salt, surface ligand, solvent and temperature has been studied on the heat of reaction for the cation exchange reaction between CdSe and various silver salts. Overall the cation exchange process between CdSe and Ag^+ is enthalpically driven despite being entropically unfavorable due to the stoichiometry of the reaction requiring two silver ions to enter a solid crystal at the expense of just one cadmium ion entering the solution. This is clearly seen in all the conditions studied irrespective of the reaction variables.

The ITC data provides a description of the overall thermodynamic parameters, and the determination of the physicochemical origins of some of the effects seen in the calorimeter would require alternative characterization techniques. Some of the possibilities for future work are discussed below.

5.8.1 XRD of partial cation exchange and quantification of surface ligands to explore the origin of the multisite behavior obtained on the ITC

In addition to the ITC, the cation exchange reaction was also monitored by ex-situ UV-Vis studies. While the UV-Vis data confirms the exchange of the ions due to loss of the characteristic absorbance signal, it provides little structural or crystallographic information. To help explain the origin of the multisite behavior, detailed X-Ray Diffraction (XRD) studies would be required to assess and characterize the different phases formed during the exchange, particularly during the initial or partial exchanged state. Preliminary data suggests that there are at least two distinct Ag_2Se phases formed in addition to the residual CdSe during partial cation exchange. Benchtop experiments spanning very low conversions can be carried out to obtain samples for XRD. For partial exchange reactions, care should be taken to ensure that the reaction mixture is homogenous when the reaction starts. This can be achieved by adding the silver

solution to the CdSe suspension at low temperatures (-20 to -30 °C) under vigorous stirring and then slowly raising the temperature. This would enable complete mixing before the reaction can take place, ensuring homogeneous chemical potential of the incoming cation and hence allowing for a greater number of nanocrystals to be partially exchanged.

The other possible cause for the multisite behavior was attributed to the surface ligands, while it is unclear why this was only observed for the commercial 2.2nm particles, a quantification of the amount of surface ligands on the particle and in solution might help answer some of the questions in this regard. NMR spectroscopy, both solution and solid phase, has been utilized to study the surface ligands,[21-22] and one possible way to quantify surface coverage would be using phosphine ligands and quantifying the amount using ^{31}P-NMR. Another technique could be to utilize quantitative IR spectroscopy to determine the surface coverage of the ligands.[14] Once a reliable protocol has been established, ligand exchange reactions can be easily followed by monitoring the loss of signal to indirectly quantify the amount of NMR or IR silent ligands.

5.8.2 Utilizing the anion coordination ability index as the predictor for cation exchange

While the HSAB can help estimate the feasibility of the cation exchange reaction, a more quantitative correlation might be useful. The anion coordination ability index discussed previously can help in this regard. While the role of the anion of the silver salt on cation exchange reaction is apparent from the data presented here, a clear trend was not observed for the described experiments, likely due to the highly non-coordinating behavior of the two studied anions in acetonitrile (BF_4 and OTf). Future experimentation will focus on salts with coordination ability index higher than acetonitrile, to nullify the effect of solvent binding to the outgoing cadmium ion and form distinct ion pairs. Some examples (with their coordinating ability index in the brackets) could be silver acetate (1.4), silver iodide (0.9), silver methanesulfonate (0.5), silver sulfate (0.3)

etc. This would help achieve a better understanding of the influence of spectator anions on the overall cation exchange reaction and an established trend would enable the rational choice of salts when designing new cation exchange routes.

5.8.3 Expanding the study to other cations to gauge the effect of the mobility and size of the incoming cation on the reaction.

While the effect of the spectator anion on the cation exchange reaction has been partly ascertained, there is a paucity of information regarding the effect of the incoming cation on the thermodynamics of the reaction. It would be of broad interest to obtain the heat of reaction for different cations and correlate the data to their mobility or size. This in conjunction with the correlation between heat of reaction and anion coordination ability would guide the choice of appropriate salts when designing new cation exchange strategies.

5.8.4 Determination of kinetics using stopped flow spectroscopy in conjunction with ITC.

While the thermodynamic data obtained from the ITC helps to determine the equilibrium constants, and free energy changes, thereby informing about the feasibility of the cation exchange reaction, it gives no information about the rate of the reaction. To ascertain the details of the mechanistic landscape of the cation exchange reactions, detailed kinetic studies will be required across a broad range of variables (such as those described above).

While stopped flow optical spectroscopy technique has been previously employed to study the kinetics of this reaction,[23] a detailed study of the effect of surface ligands, spectator anions, solvents, temperature etc. is lacking. In much the same way as studied using ITC, the effect of each of these variables on the loss of fluorescence of CdSe particles can be measured on the millisecond timescale using a stopped flow fluorimeter. The data obtained from these

experiments would allow the estimation of rate constants for the forward reaction, the equilibrium constants measured from ITC experiments would give an idea of the rate constants for the reverse reaction.

Additionally, the ITC itself can be utilized to measure reaction kinetics. At root, the ITC measures a heat rate, which is proportional to the rate of the chemical or physical change occurring in the sample cell.[24-25] This makes it uniquely positioned to obtain kinetic as well as thermodynamic data from a single experiment. While new models would need to be developed for the kinetic modelling of cation exchange reactions, there has been substantial progress in the use of ITC for measuring binding kinetics.[26] The stopped flow experiments would provide a good check for the initial ITC modelling and once a robust model has been developed rapid kinetic and thermodynamic data can be accessed in a short amount of time.

While cation exchange reactions have, thus far, largely focused on ionic metal chalcogenide phases, a systematic study of the effect of solvents, exchanging salts, size and identity of the surface ligands as described here could enable the extension of the cation exchange protocol to other systems. Building off the work described here, we believe that ITC has the potential to become a truly powerful technique and in combination with other structural characterization like XRD, liquid state TEM, XPS and XAS has the potential to present a unified mechanistic theory of cation exchange in nanomaterials.

5.9 Experimental Section

Dry anhydrous solvents were obtained from Sigma-Aldrich and stored in a N_2 atmosphere glovebox. Silver salts were obtained from Strem chemicals, or Sigma-Aldrich and also stored in the glovebox. 2.2 nm CdSe particles were purchased from Sigma-Aldrich, 3.5 and 6.2nm particles were prepared following literature procedures. A typical synthesis procedure is described below.

5.9.1. Synthesis and characterization of Cadmium Selenide particles

5.9.1.1. Synthesis

In a typical synthesis,[27] cadmium oxide (CdO) is used as the cadmium precursor and a mixture of oleic acid (OA) and octadecene (ODE) as the surfactant and reaction solvent respectively. The selenium precursor is prepared from selenium powder (Se) dissolved in trioctylphosphine (TOP) and ODE. In a 100 ml three-neck round-bottom flask, CdO (≥99.99%, Sigma Aldrich, 51.36 mg, 0.4 mmol**)**, OA (90%, Sigma Aldrich, 3.15 mL, 10 mmol) and ODE (90%, Sigma Aldrich, 20mL) were degassed in primary vacuum for 30 min and then heated under argon to the reaction temperature 300ºC. At this temperature the solution becomes colorless. To this solution, the mixture of Se powder (99.99%, Sigma Aldrich, 157.94 mg, 2mmol), TOP (98%, Alfa Aesar, 5mL) and ODE (8.5 mL) was rapidly injected. The mixture was stirred for 1min (for the 3.3 nm particles) and for 10 mins (for the 6.2 nm particles) and then the heating mantle was removed to cool down the solution. When the reaction mixture was cooled to around 60°C, the solution was equally distributed into 3-4 40mL plastic centrifugation tubes. To precipitate out the nanoparticles, excess of methanol is added. Usually a formation of gel is observed. The mixture is centrifuged at 6000 rpm and the supernatant is removed. Toluene and methanol (1:4) is added to

it and centrifuged again. This process is repeated 3-4 times, until a gel-free solution is obtained. The final precipitation of CdSe was collected and dissolved in toluene and stored in refrigerator for further use. Particles with sizes of 3.5 ± 0.48 nm and 6.2 ± 0.66 nm were synthesized.

5.9.1.2. Ligand Exchange of CdSe particles

The CdSe nanocrystals initially synthesized were capped with OA and TOP/trioctylphosphine oxide (TOPO). To obtain CdSe nanocrystals with different capping ligands, the ligand exchange is first done with TOPO to obtain CdSe nanocrystals capped only with TOPO. To do this, the sample suspended in toluene was exposed to excess of TOPO (90%, Sigma Aldrich, 5g) and degassed in primary vacuum for 30 min. The mixture was then heated for 60 minutes at 130°C under inert conditions. Later, the solution was cooled and precipitated with excess methanol. To remove the excess TOPO, the particles were re-dispersed in toluene and methanol (1:4) and centrifuged at 6000 rpm.

Starting from the TOPO–capped particles, ligand exchange reactions were done to obtain particles capped with carboxylic acid, amines and thiol. Octanoic acid, octylamine, hexadecylamine and octanethiol, all purchased from Sigma Aldrich were used as capping ligands. In each case, excess of the ligand was added to the TOPO–capped nanoparticles and then stirred under argon atmosphere for 2-3 hours at 100°C. All the final solutions were obtained by washing with toluene and methanol (1:4) and centrifugation at 6000 rpm.

5.9.1.3. Characterization

Optical characterization was done using diluted CdSe nanocrystals. UV-Vis absorption spectra were acquired on Shimadzu UV-3600 UV-VIS-NIR spectrophotometer. Dilute solutions of CdSe nanocrystals in hexane were placed in 1 cm quartz cuvettes, and their absorption were measured and compared to those in literature to get an estimate for the size.[28]

The transmission electron microscope (TEM) images of the nanocrystals were acquired on a FEI Talos™ microscope operating at 200 kV. Dilute solutions of the nanocrystals in hexane were dropped onto 50 Å thick carbon coated copper grids (400 mesh) and the excess solution dried under vacuum. The average size of the particles was determined by analyzing the TEM images using ImajeJ software.

The concentration of the washed CdSe solution and the Cd:Se ratio on the particles was determined by Agilent 700 Series ICP Optical Emission Spectrometer.

Sample preparation of ICP: The standards for calibration (2ppm, 4ppm, 8ppm, 16ppm) were prepared by serial dilution of the commercial stock solution (100 µg/mL) of Cd and Se obtained from High-purity Standards in 2% HNO_3 to make 10 mL solution of each. The CdSe samples were prepared by evaporating 50 µL of the CdSe nanocrystal solution to dryness and then digesting the remaining solid in 1mL of aqua regia. The aqua regia was boiled off by heating and 10mL of 2% HNO_3 is added to prepare the final solution.

5.9.2 Isothermal titration calorimetry

Isothermal titration calorimetry (ITC) measurements were performed on a TA Instruments NanoITC with 1 mL hastelloy sample and reference cells. Analyses were carried out at 25 °C (or stated temperature) with a 100 μL syringe. A stirring rate of 250 rpm was used for all experiments to introduce minimal noise. CdSe solutions containing 0.13mM Cd were prepared by dilution of the stock solution in the given solvent. 5mM solution of the chosen silver salt was made in appropriate solvent and utilized for the titration. 4 μL injections were made every 15 minutes to allow for the baseline to stabilize after the reaction. The data presented is the average of 3 trials for each experiment. The individual ITC conditions, and experimental variables for all the experiments discussed above are summarized in Table 5.6 below.

Table 5.6. Experimental variables for ITC experiments

Entry	Size (nm)	Temperature (K)	Solvent	Capping Agent	Silver Salt
Size (nm)	2.2 3.5 6.2	298.15	Acetonitrile	HDA	$AgNO_3$
Temperature (K)	2.2	288.15 298.15 308.15	Acetonitrile	HDA	$AgNO_3$
Solvent	2.2	298.15	Acetonitrile 2-Butanone Toluene	HDA	AgOTf
Capping Agents	6.2	298.15	Toluene	As synthesized TOPO HDA Octylamine Octanoic Acid Octanethiol	AgOTf
Silver Salts	2.2	298.15	Acetonitrile	HDA	$AgNO_3$ AgOTf $AgBF_4$

HDA – Hexadecyl amine, TOPO- Trioctylphosphine oxide

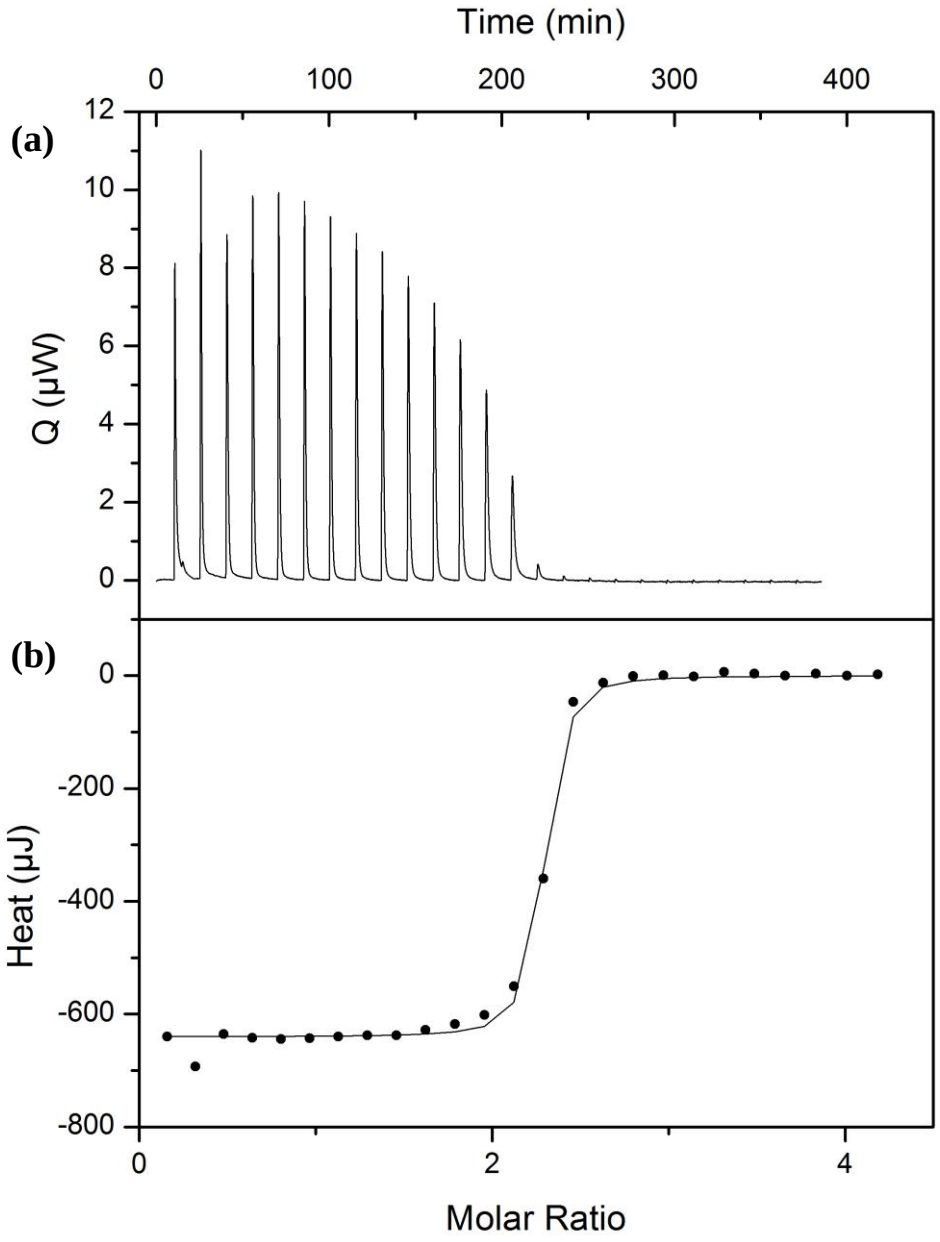

Figure 5.5. (a) Real-time ITC thermogram for exchange reaction between CdSe and AgOTf at 25 °C in acetonitrile. (b) Integrated heat data with fitted model.

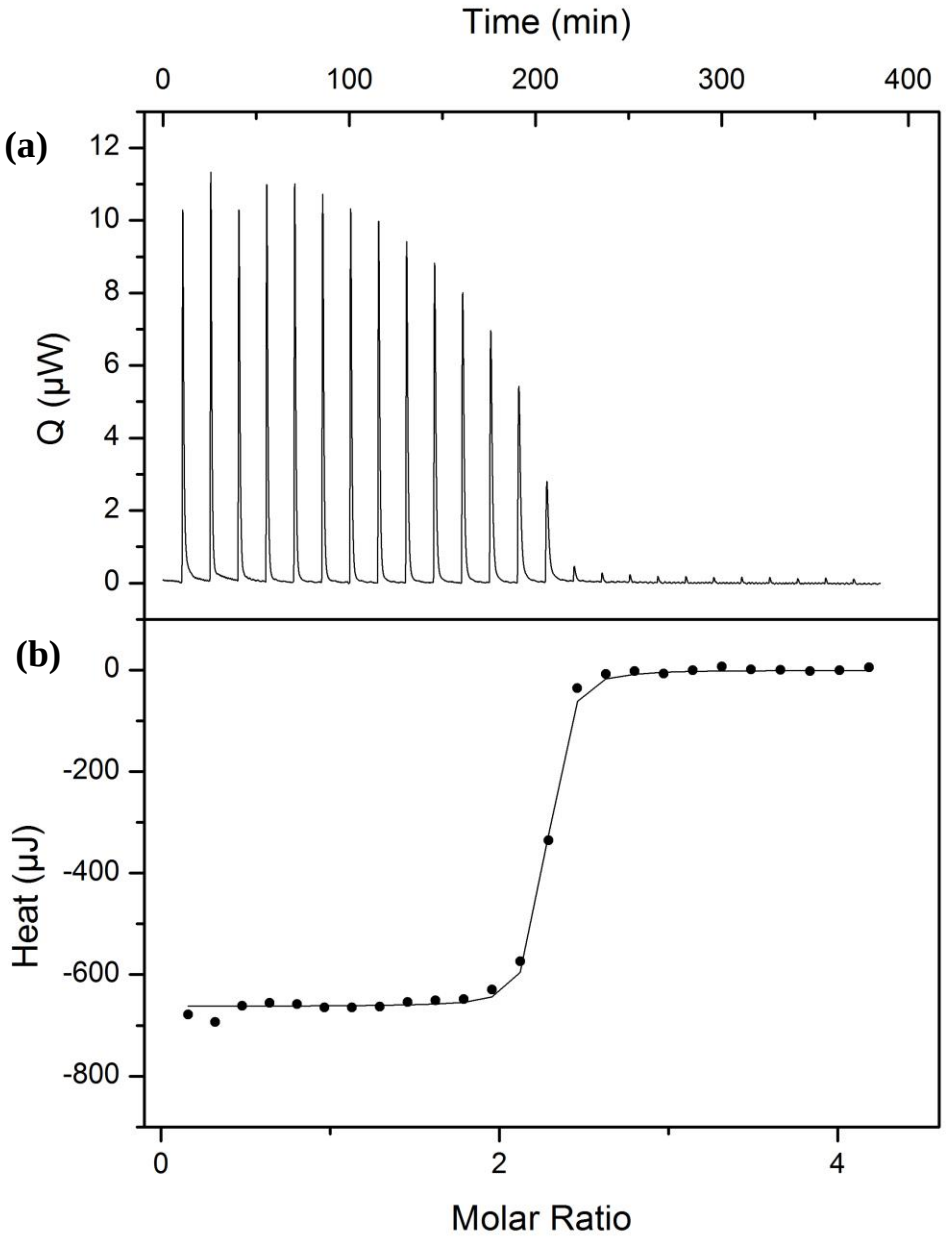

Figure 5.6. (a) Real-time ITC thermogram for exchange reaction between CdSe and $AgBF_4$ at 25 °C in acetonitrile. (b) Integrated heat data with fitted model.

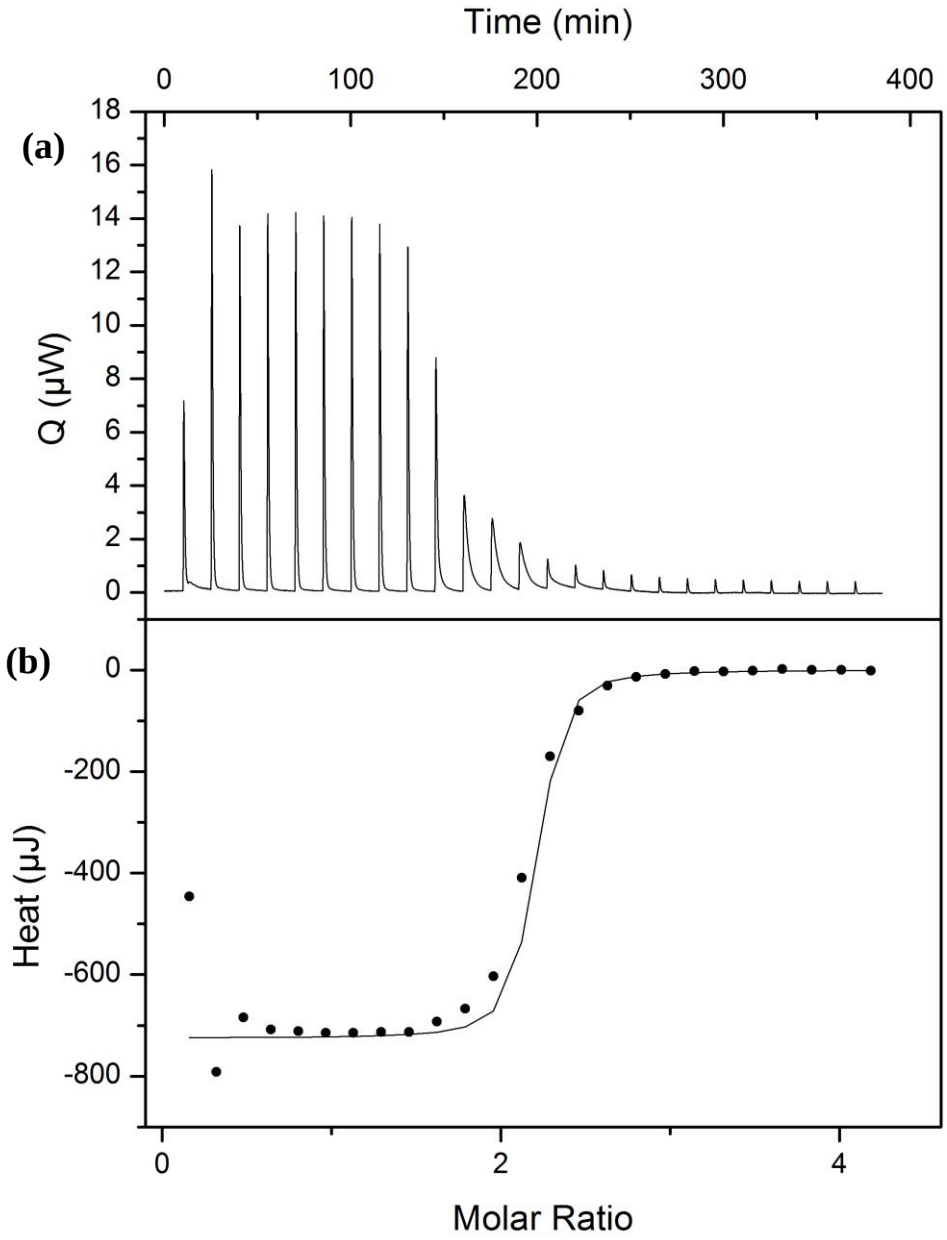

Figure 5.7. (a) Real-time ITC thermogram for exchange reaction between CdSe and $AgNO_3$ at 25 °C in acetonitrile. (b) Integrated heat data with fitted model.

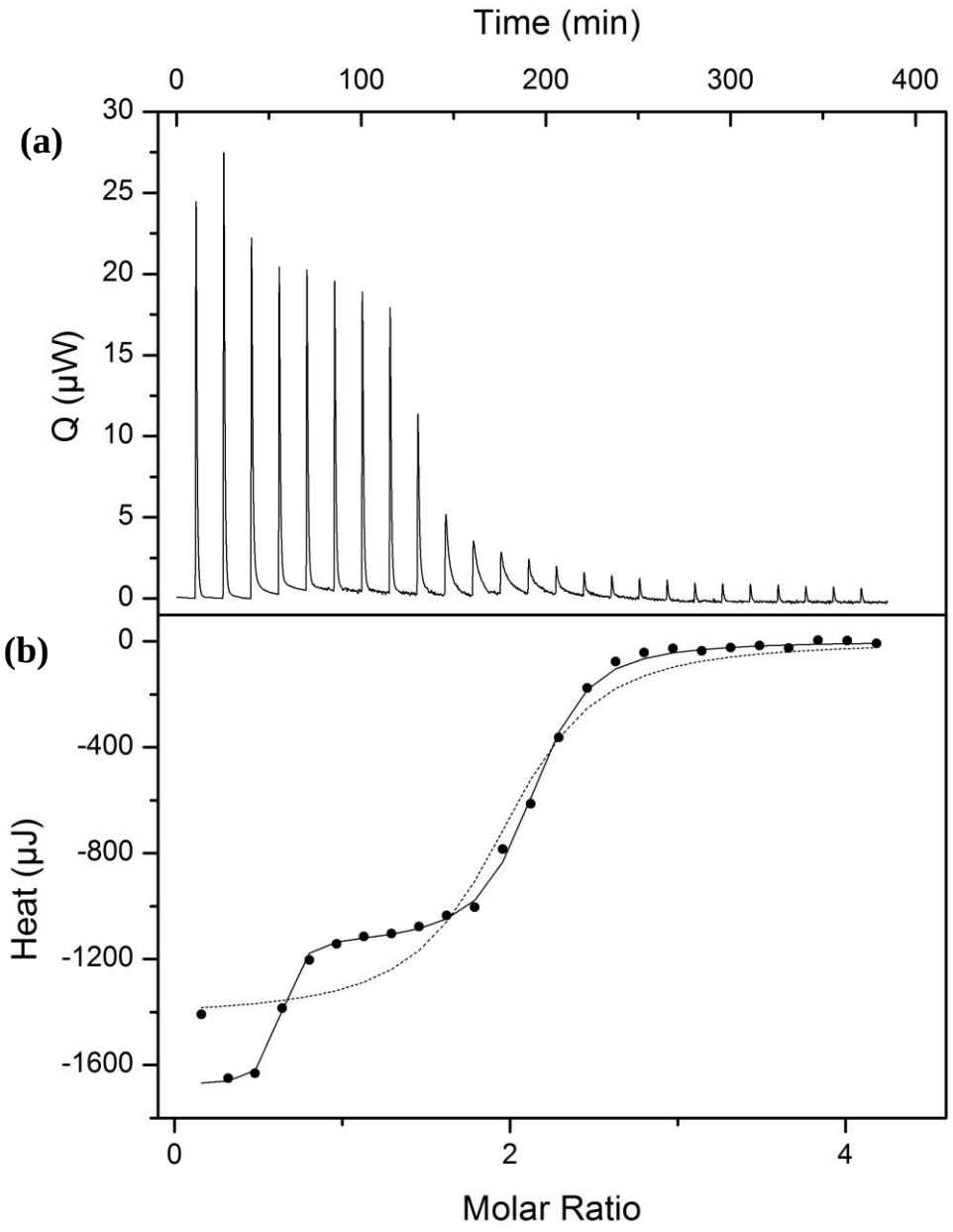

Figure 5.8. (a) Real-time ITC thermogram for exchange reaction between CdSe and AgOTf at 25 °C in 2-butanone. (b) Integrated heat data with fitted model. Dotted line - single sites; solid line - multiple sites model.

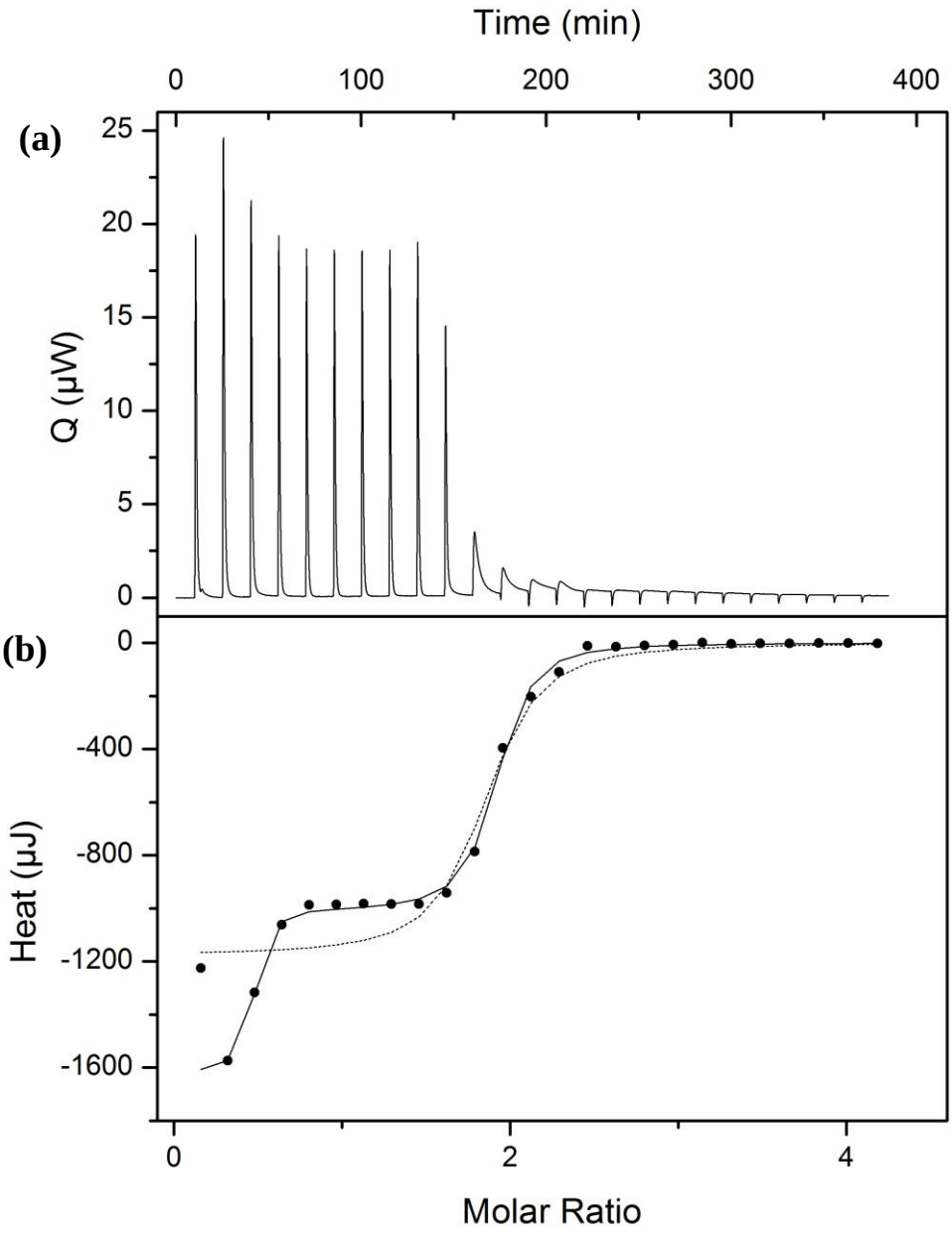

Figure 5.9. (a) Real-time ITC thermogram for exchange reaction between CdSe and AgOTf at 25 °C in toluene. (b) Integrated heat data with fitted model. Dotted line - single sites; solid line - multiple sites model.

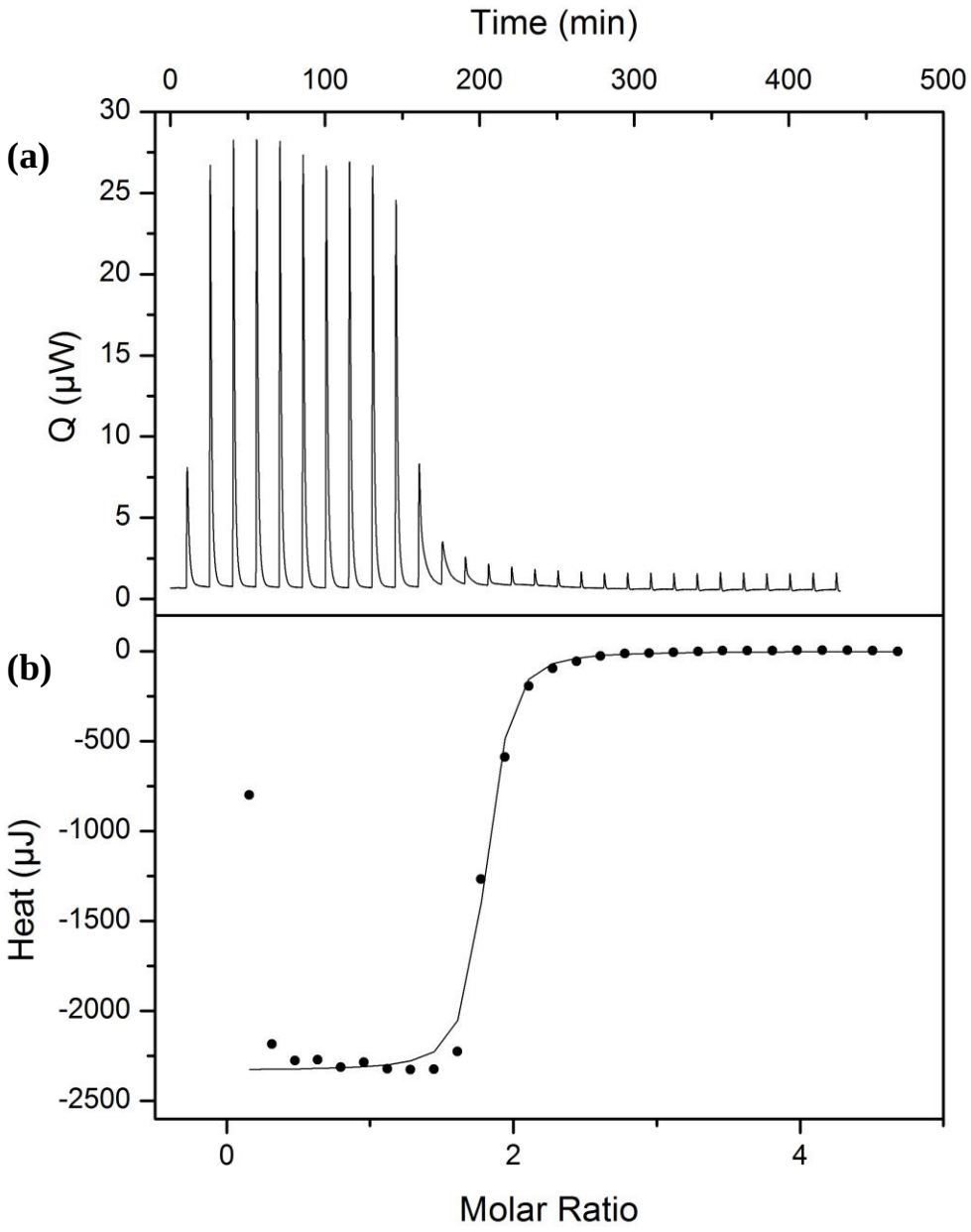

Figure 5.10. (a) Real-time ITC thermogram for exchange reaction between 3.5 nm CdSe and AgOTf at 25 °C in toluene. (b) Integrated heat data with fitted model

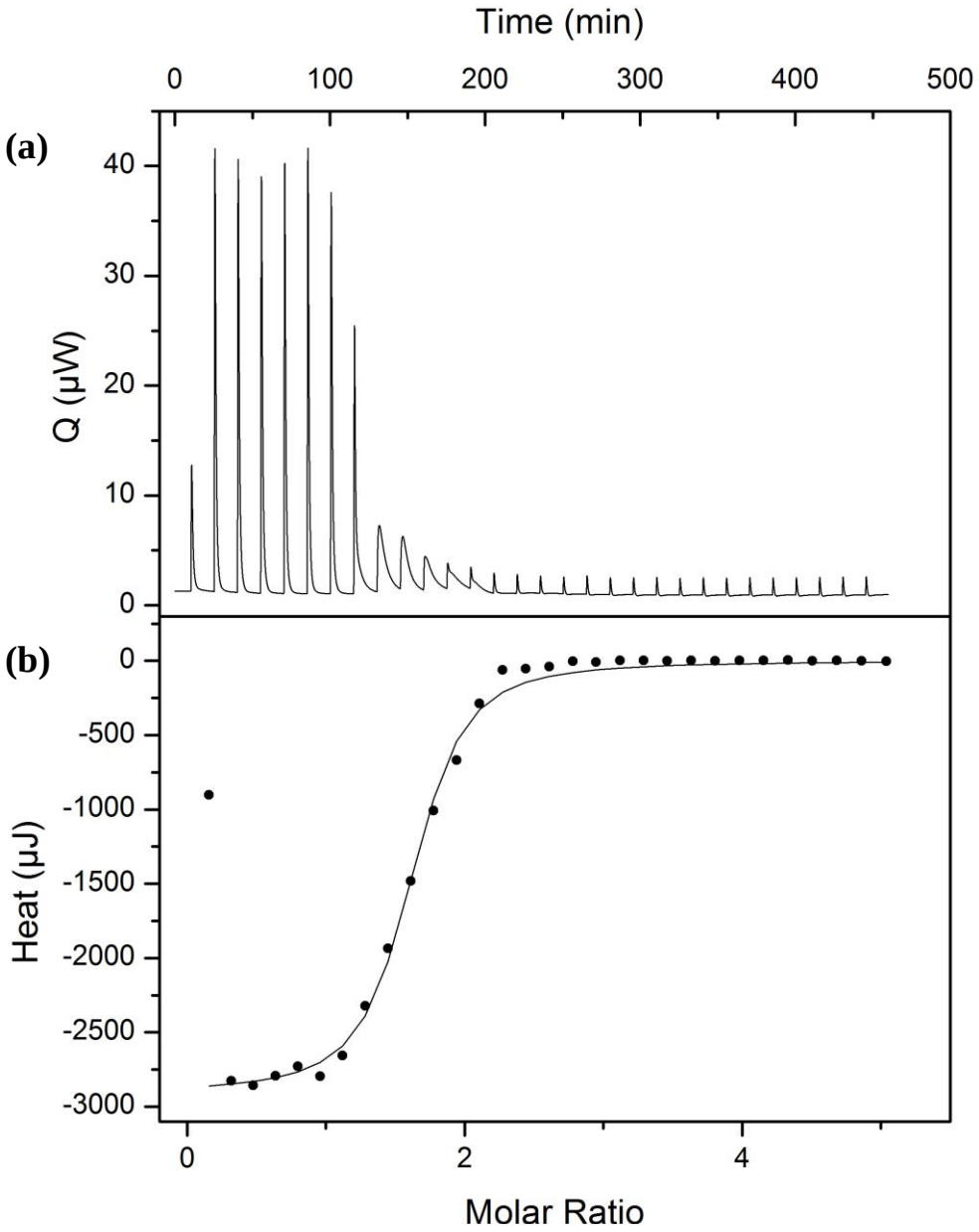

Figure 5.11. (a) Real-time ITC thermogram for exchange reaction between 6.2nm CdSe and AgOTf at 25 °C in toluene. (b) Integrated heat data with fitted model

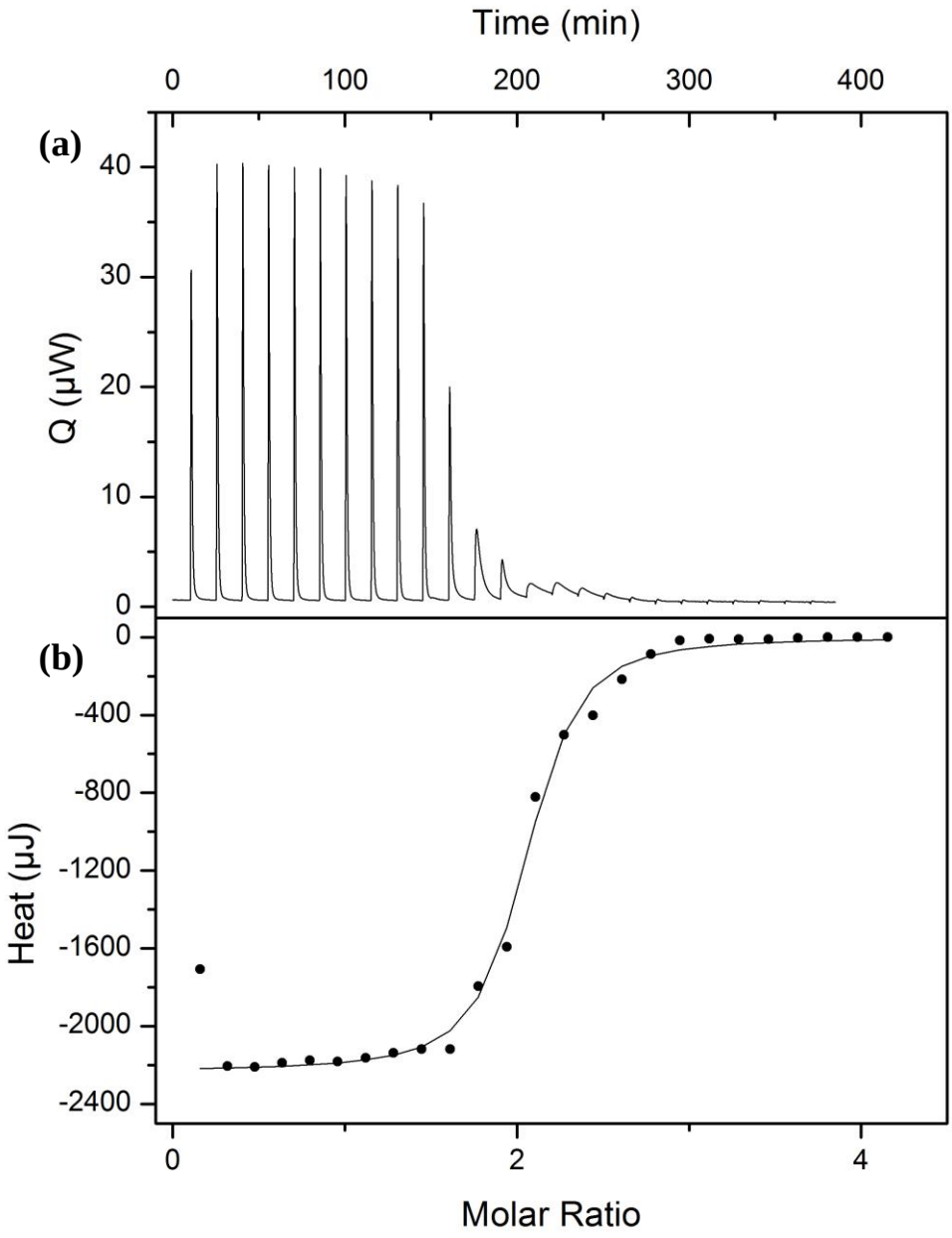

Figure 5.12. (a) Real-time ITC thermogram for exchange reaction between as synthesized 6.2nm CdSe and AgOTf at 25 °C in toluene. (b) Integrated heat data with fitted model

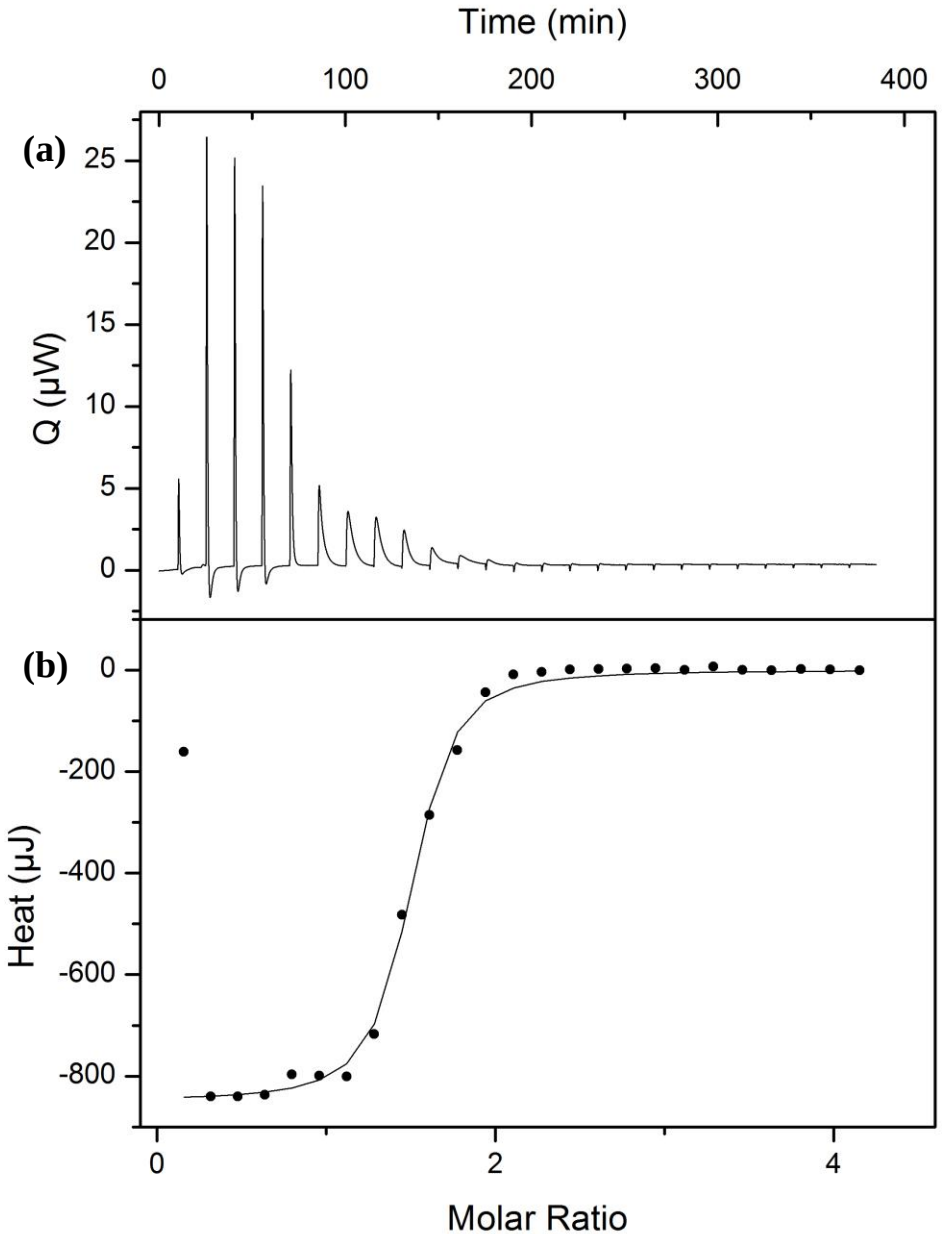

Figure 5.13. (a) Real-time ITC thermogram for exchange reaction between trioctylphosphine oxide capped 6.2nm CdSe and AgOTf at 25 °C in toluene. (b) Integrated heat data with fitted model

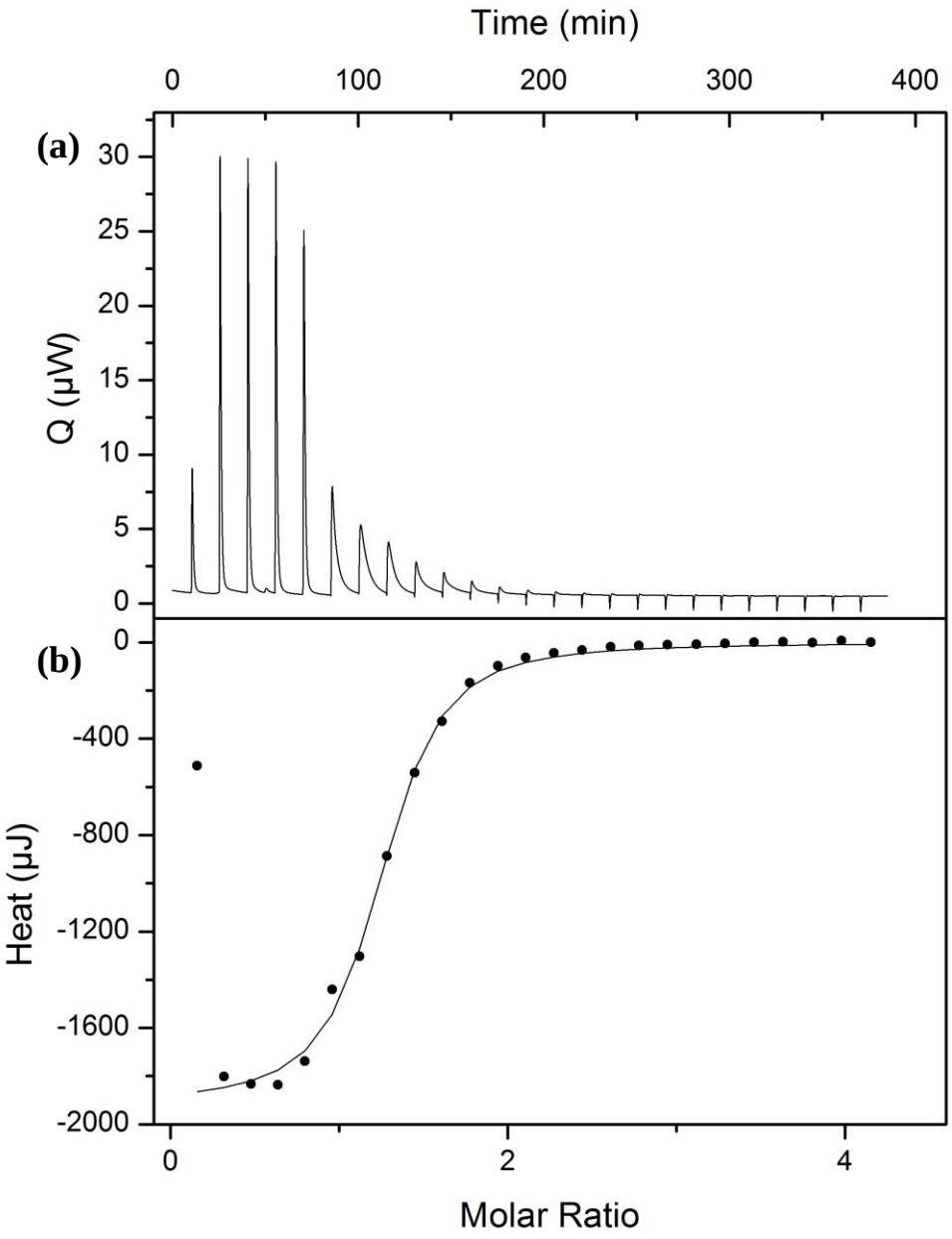

Figure 5.14. (a) Real-time ITC thermogram for exchange reaction between octylamine capped 6.2nm CdSe and AgOTf at 25 °C in toluene. (b) Integrated heat data with fitted model

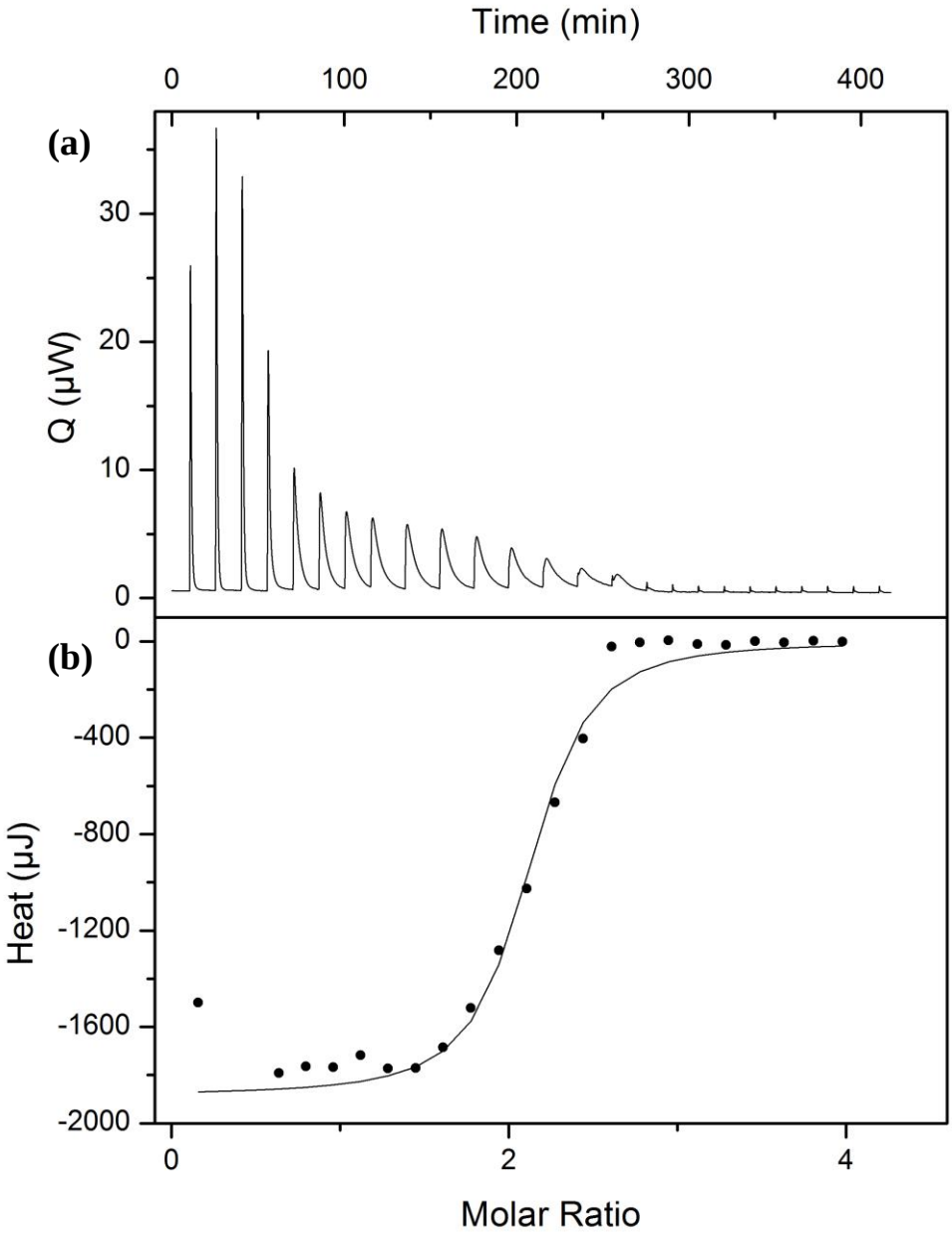

Figure 5.15. (a) Real-time ITC thermogram for exchange reaction between octanethiol capped 6.2nm CdSe and AgOTf at 25 °C in toluene. (b) Integrated heat data with fitted model.

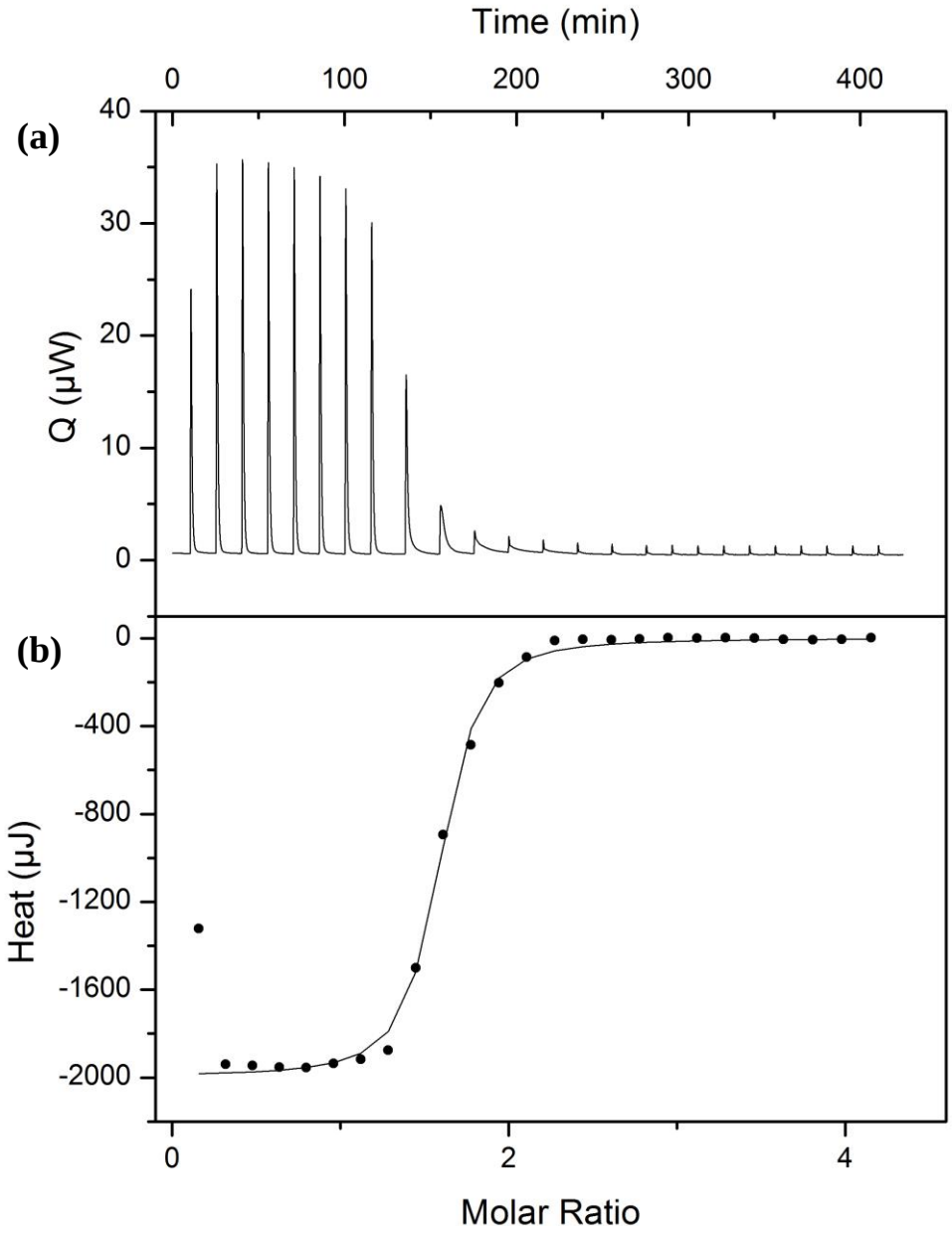

Figure 5.16. (a) Real-time ITC thermogram for exchange reaction between octanoic acid capped 6.2nm CdSe and AgOTf at 25 °C in toluene. (b) Integrated heat data with fitted model

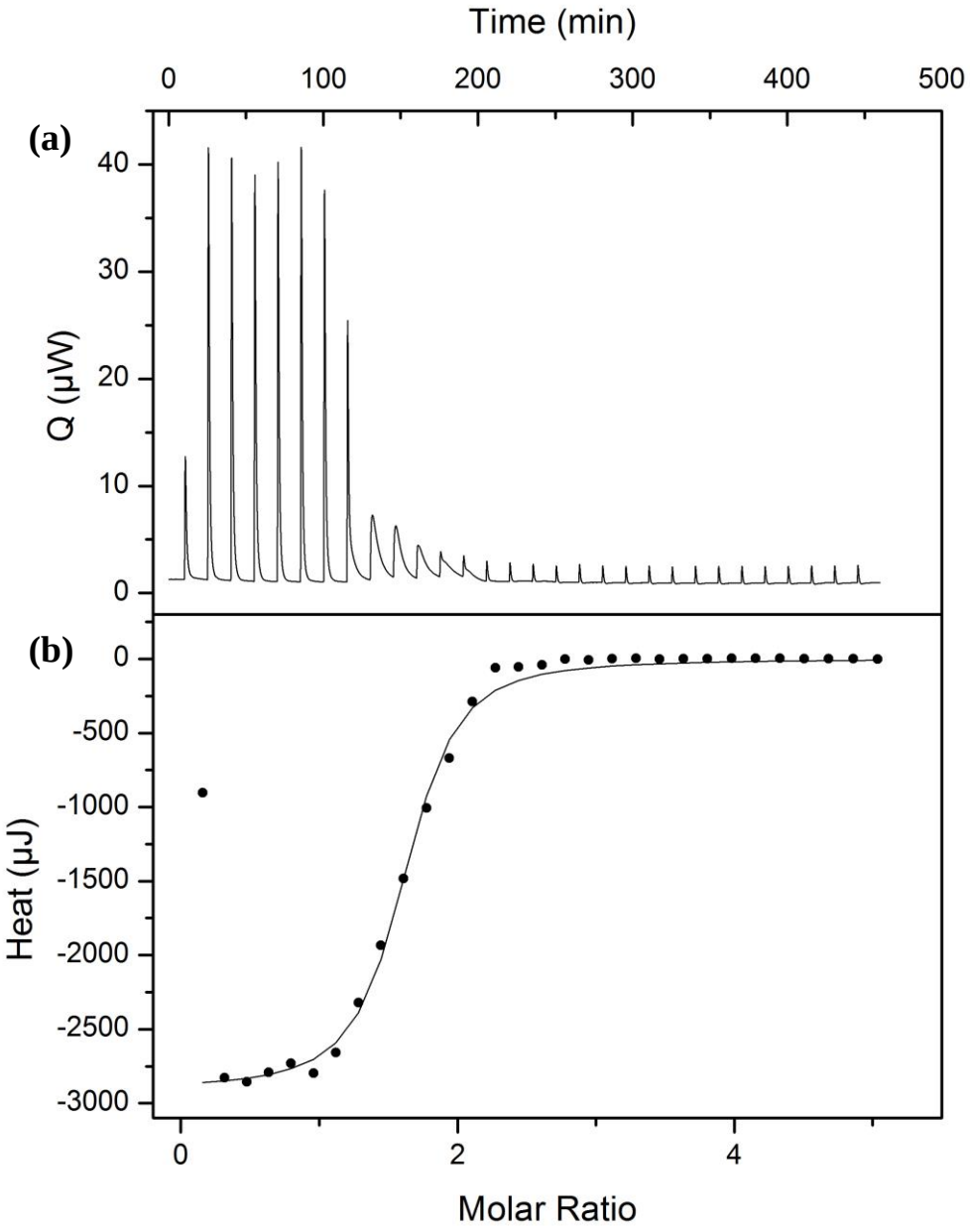

Figure 5.17. (a) Real-time ITC thermogram for exchange reaction between hexadecylamine capped 6.2nm CdSe and AgOTf at 25 °C in toluene. (b) Integrated heat data with fitted model

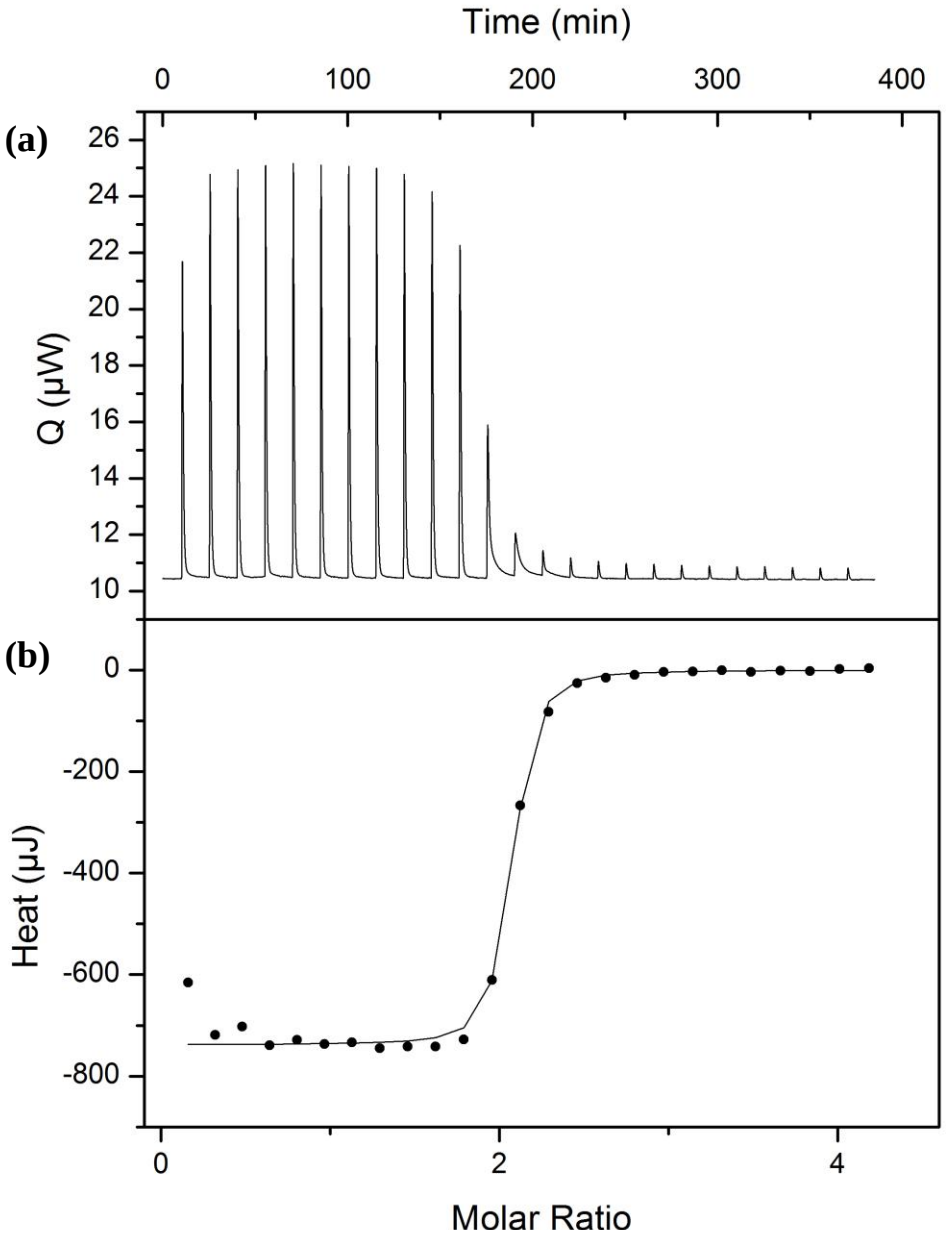

Figure 5.18. (a) Real-time ITC thermogram for exchange reaction between 2.2 nm CdSe and $AgNO_3$ at 15 °C in acetonitrile. (b) Integrated heat data with fitted model

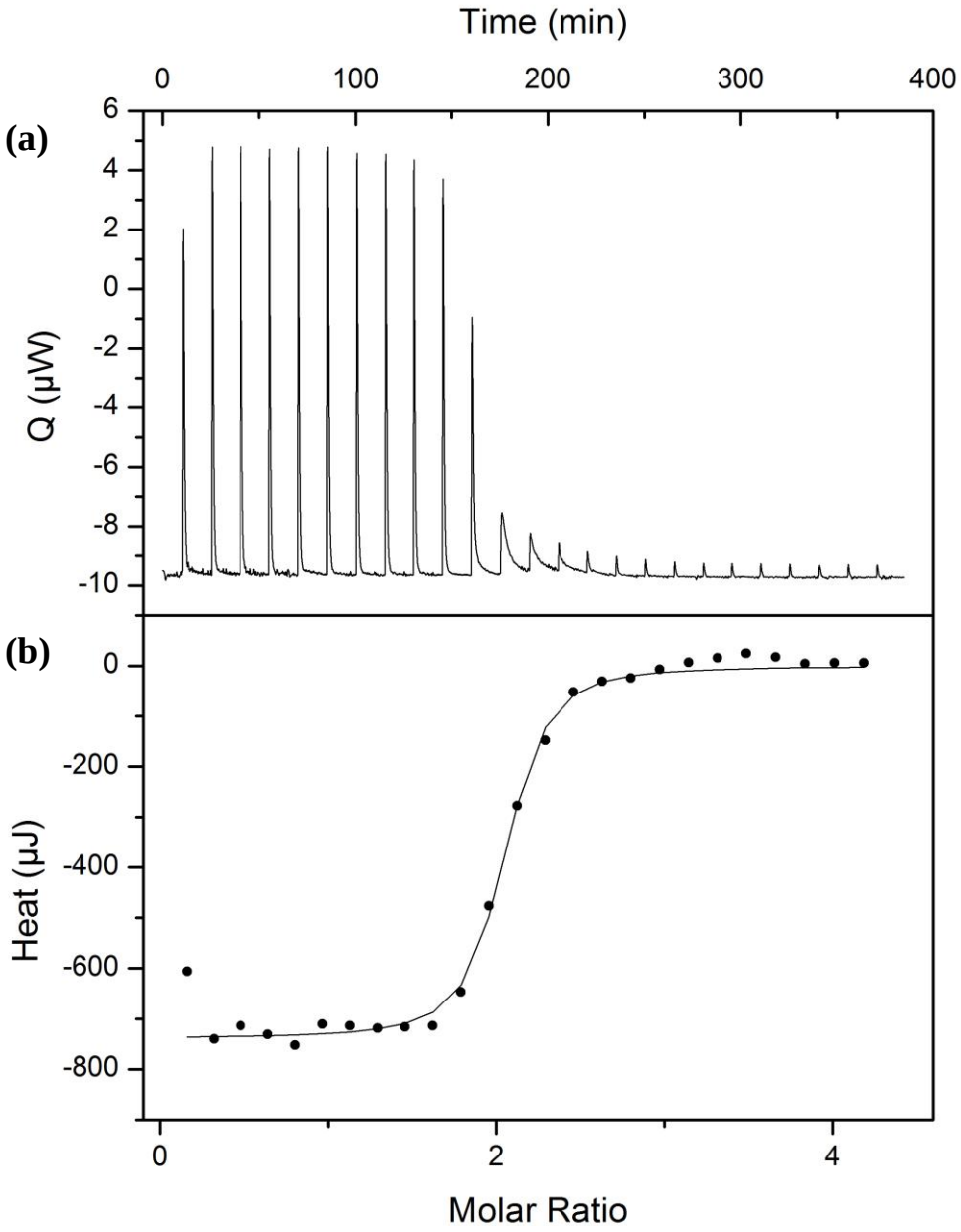

Figure 5.19. (a) Real-time ITC thermogram for exchange reaction between 2.2 nm CdSe and $AgNO_3$ at 35 °C in acetonitrile. (b) Integrated heat data with fitted model

5.6 References.

1. Rivest, J. B.; Jain, P. K., *Chem. Soc. Rev.* **2013,** *42* (1), 89-96.
2. Beberwyck, B. J.; Surendranath, Y.; Alivisatos, A. P., *J. Phys. Chem. C* **2013,** *117* (39), 19759-19770.
3. Wiseman, T.; Williston, S.; Brandts, J. F.; Lin, L.-N., *Anal. Biochem.* **1989,** *179* (1), 131-137.
4. Moschetta, E. G.; Gans, K. M.; Rioux, R. M., *J. Catal.* **2013,** *302*, 1-9.
5. Son, D. H.; Hughes, S. M.; Yin, Y.; Paul Alivisatos, A., *Science* **2004,** *306* (5698), 1009-1012.
6. Pearson, R. G., *J. Am. Chem. Soc.* **1963,** *85* (22), 3533-3539.
7. Diaz-Torres, R.; Alvarez, S., *Dalton Transactions* **2011,** *40* (40), 10742-10750.
8. Liu, L.; Guo, Q.-X., *Chem. Rev.* **2001,** *101* (3), 673-696.
9. Searle, M. S.; Williams, D. H., *J. Am. Chem. Soc.* **1992,** *114* (27), 10690-10697.
10. Ranganathan, R.; Bakhshi, N. N.; Mathews, J. F., *The Canadian Journal of Chemical Engineering* **1977,** *55* (5), 544-551.
11. Pan, A.; Biswas, T.; Rakshit, A. K.; Moulik, S. P., *The Journal of Physical Chemistry B* **2015,** *119* (52), 15876-15884.
12. Boles, M. A.; Ling, D.; Hyeon, T.; Talapin, D. V., *Nat Mater* **2016,** *15* (2), 141-153.
13. Sperling, R. A.; Parak, W. J., Philosophical Transactions of the Royal Society A: Mathematical, Physical and Engineering Sciences **2010,** 368 (1915), 1333-1383.

14. von Holt, B.; Kudera, S.; Weiss, A.; Schrader, T. E.; Manna, L.; Parak, W. J.; Braun, M., *J. Mater. Chem.* **2008,** *18* (23), 2728-2732.

15. Sahu, A.; Kang, M. S.; Kompch, A.; Notthoff, C.; Wills, A. W.; Deng, D.; Winterer, M.; Frisbie, C. D.; Norris, D. J., *Nano Lett.* **2012,** *12* (5), 2587-2594.

16. Anderson, N. C.; Hendricks, M. P.; Choi, J. J.; Owen, J. S., *J. Am. Chem. Soc.* **2013,** *135* (49), 18536-18548.

17. Moon, G. D.; Ko, S.; Xia, Y.; Jeong, U., *ACS Nano* **2010,** *4* (4), 2307-2319.

18. Nasar, A.; Shamsuddin, M., *Journal of the Less Common Metals* **1990,** *158* (1), 131-135.

19. Nasar, A.; Shamsuddin, M., *Metallurgical and Materials Transactions B* **1997,** *28* (3), 519-522.

20. Kolthoff, I. M.; Coetzee, J. F., *J. Am. Chem. Soc.* **1957,** *79* (8), 1852-1858.

21. Morris-Cohen, A. J.; Donakowski, M. D.; Knowles, K. E.; Weiss, E. A., *J. Phys. Chem. C* **2010,** *114* (2), 897-906.

22. Davidowski, S. K.; Lisowski, C. E.; Yarger, J. L., *Magn. Reson. Chem.* **2016,** *54* (3), 234-238.

23. Chan, E. M.; Marcus, M. A.; Fakra, S.; ElNaggar, M.; Mathies, R. A.; Alivisatos, A. P., *The Journal of Physical Chemistry A* **2007,** *111* (49), 12210-12215.

24. Freire, E.; Mayorga, O. L.; Straume, M., *Anal. Chem.* **1990,** *62* (18), 950A-959A.

25. Freyer, M. W.; Lewis, E. A., Isothermal Titration Calorimetry: Experimental Design, Data Analysis, and Probing Macromolecule/Ligand Binding and Kinetic Interactions. In *Methods in Cell Biology*, Academic Press: 2008; Vol. Volume 84, pp 79-113.

26. Burnouf, D.; Ennifar, E.; Guedich, S.; Puffer, B.; Hoffmann, G.; Bec, G.; Disdier, F.; Baltzinger, M.; Dumas, P., *J. Am. Chem. Soc.* **2012,** *134* (1), 559-565.

27. Protière, M.; Nerambourg, N.; Renard, O.; Reiss, P., *Nanoscale Research Letters* **2011,** *6* (1), 1-14.

28. Jasieniak, J.; Smith, L.; Embden, J. v.; Mulvaney, P.; Califano, M., *J. Phys. Chem. C* **2009,** *113* (45), 19468-19474.

Appendix
NMR Spectra

^{1}H and ^{13}C NMR Spectra

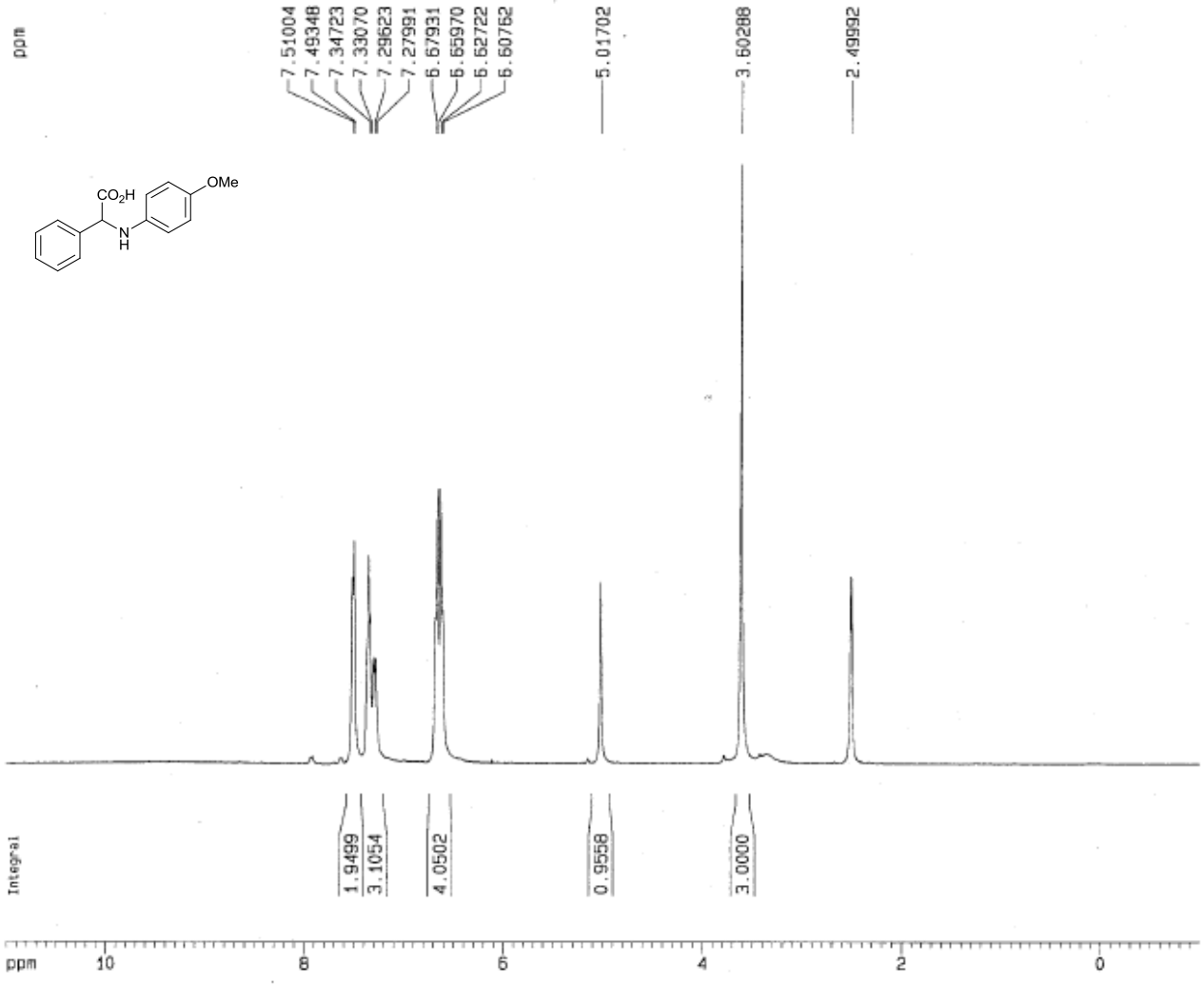


```
Current Data Parameters
NAME                  p-H
EXPNO                   1
PROCNO                  1

F2 - Acquisition Parameters
Date_            20121017
Time                11.04
INSTRUM             spect
PROBHD     5 mm BBI 1H-
PULPROG             zg30
TD                 65536
SOLVENT             DMSO
NS                    16
DS                     2
SWH              8278.146 Hz
FIDRES           0.126314 Hz
AQ               3.9584243 sec
RG                   181
DW                60.400 usec
DE                 6.00 usec
TE                300.0 K
D1             1.00000000 sec

------------ CHANNEL f1 ---------
NUC1                  1H
P1                 6.45 usec
PL1                0.00 dB
SFO1          400.1324710 MHz

F2 - Processing parameters
SI                 32768
SF            400.1300025 MHz
WDW                   no
SSB                    0
LB                 0.00 Hz
GB                     0
PC                  1.00

1D NMR plot parameters
CX                20.00 cm
F1P               11.000 ppm
F1                4401.43 Hz
F2P               -1.000 ppm
F2                -400.13 Hz
PPMCM             0.60000 ppm/cm
HZCM            240.07800 Hz/cm
```

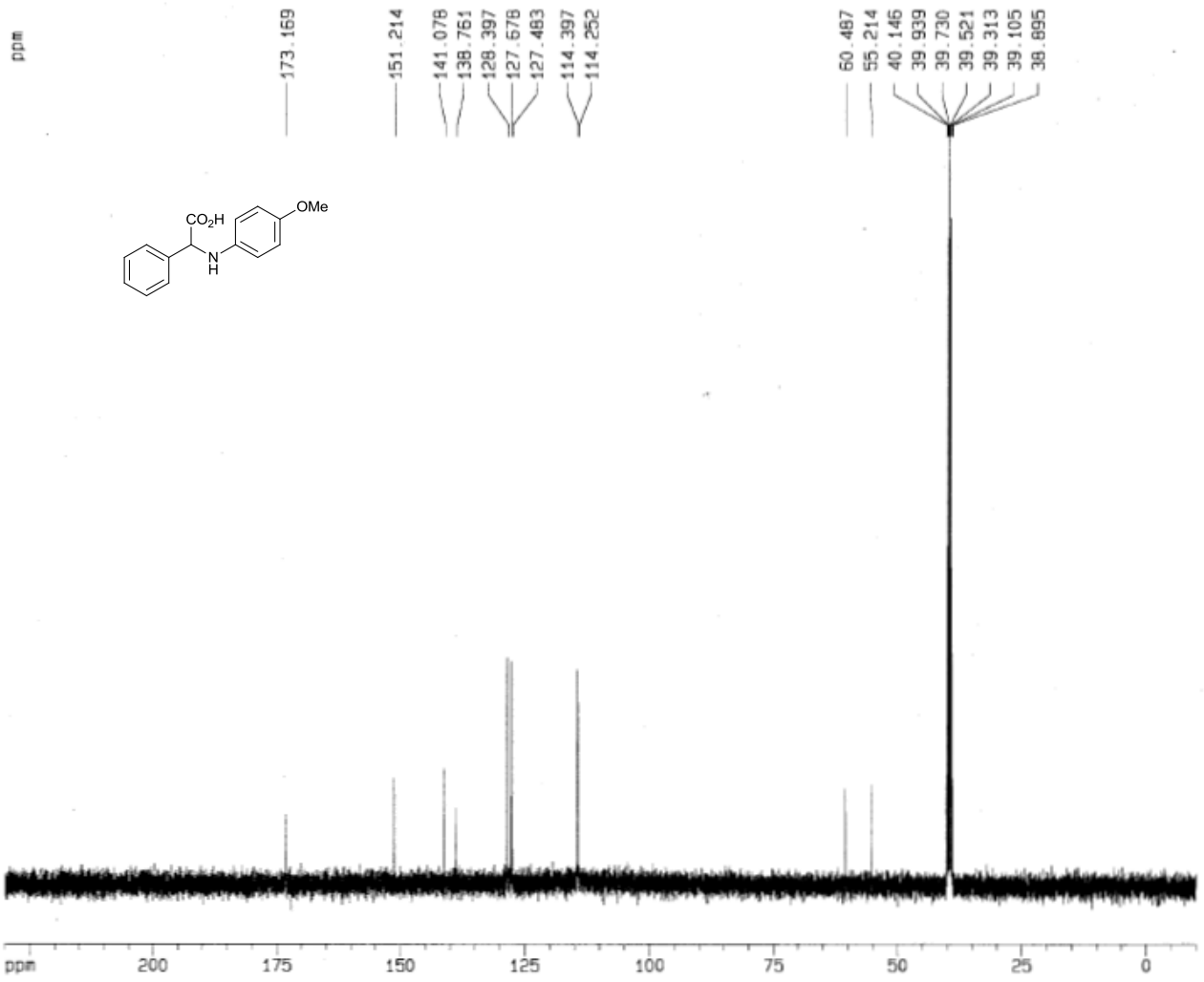

Current Data Parameters

NAME	p_H
EXPNO	2
PROCNO	1

F2 - Acquisition Parameters

Date_	20121017
Time	17.09
INSTRUM	spect
PROBHD	5 mm BBI 1H-
PULPROG	zgpg30
TD	65536
SOLVENT	CDCl3
NS	1024
DS	4
SWH	25125.629 Hz
FIDRES	0.383387 Hz
AQ	1.3042164 sec
RG	11585.2
DW	19.900 usec
DE	6.00 usec
TE	300.0 K
D1	2.00000000 sec
d11	0.03000000 sec
d12	0.00002000 sec

========== CHANNEL f1 ==========

NUC1	13C
P1	15.35 usec
PL1	-6.00 dB
SFO1	100.6237959 MHz

========== CHANNEL f2 ==========

CPDPRG2	waltz16
NUC2	1H
PCPD2	114.00 usec
PL2	0.00 dB
PL12	24.00 dB
PL13	24.00 dB
SFO2	400.1316005 MHz

F2 - Processing parameters

SI	32768
SF	100.6128152 MHz
WDW	no
SSB	0
LB	0.00 Hz
GB	0
PC	1.40

1D NMR plot parameters

CX	20.00 cm
F1P	230.000 ppm
F1	23140.95 Hz
F2P	-10.000 ppm
F2	-1006.13 Hz
PPMCM	12.00000 ppm/cm
HZCM	1207.35376 Hz/cm

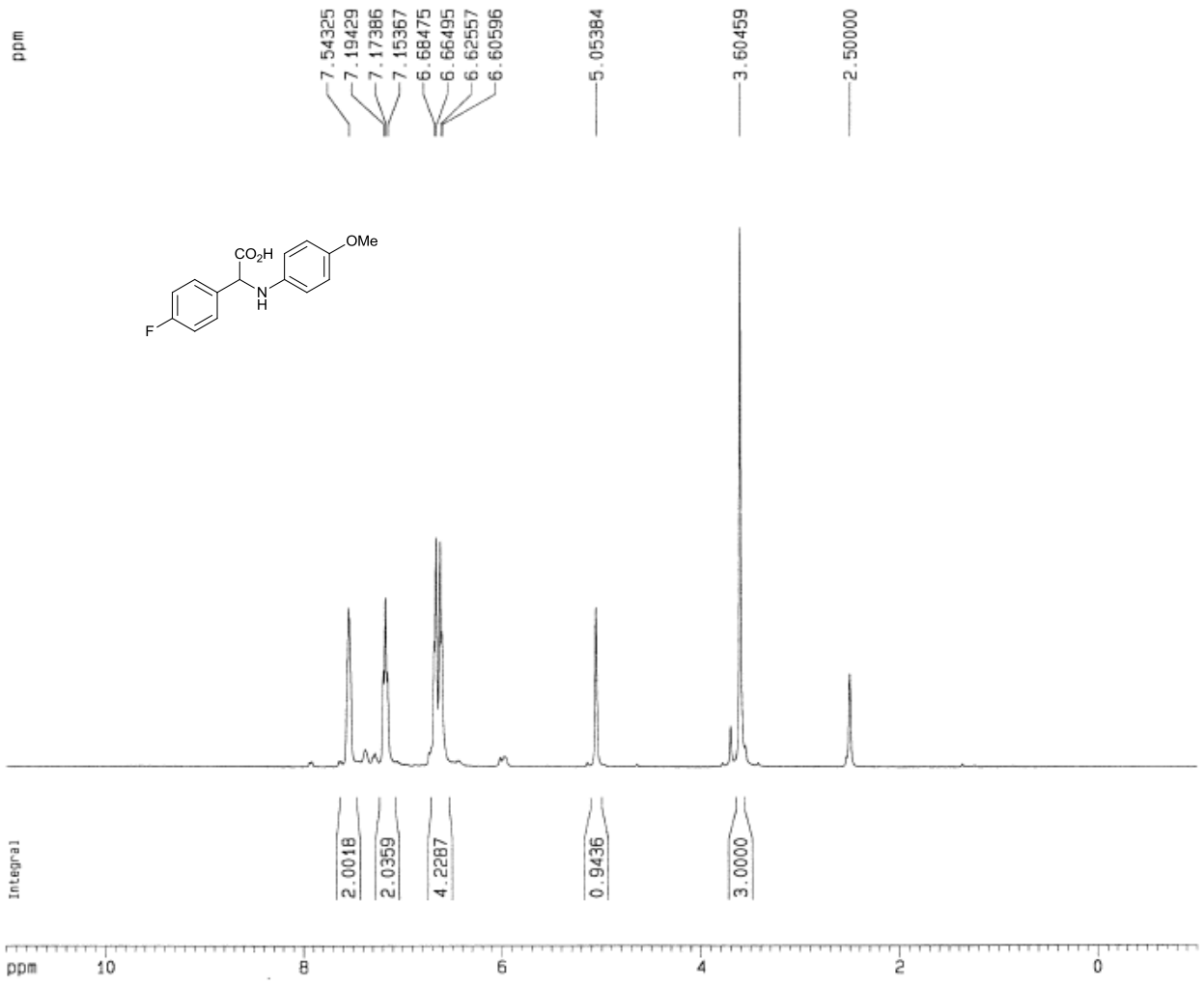


```
Current Data Parameters
NAME                  p_F
EXPNO                   7
PROCNO                  1

F2 - Acquisition Parameters
Date_           20121104
Time               11.37
INSTRUM             spect
PROBHD     5 mm BBI 1H-
PULPROG             zg30
TD                 65536
SOLVENT             DMSO
NS                    32
DS                     2
SWH             8278.146 Hz
FIDRES          0.126314 Hz
AQ              3.9584243 sec
RG                 203.2
DW                60.400 usec
DE                 6.00 usec
TE                300.0 K
D1             1.00000000 sec

============ CHANNEL f1 ========
NUC1                   1H
P1                   6.45 usec
PL1                  0.00 dB
SFO1         400.1324710 MHz

F2 - Processing parameters
SI                  32768
SF           400.1300024 MHz
WDW                    no
SSB                     0
LB                   0.00 Hz
GB                      0
PC                   1.00

1D NMR plot parameters
CX                  20.00 cm
F1P                11.000 ppm
F1                 4401.43 Hz
F2P                -1.000 ppm
F2                 -400.13 Hz
PPMCM             0.60000 ppm/cm
HZCM            240.07800 Hz/cm
```

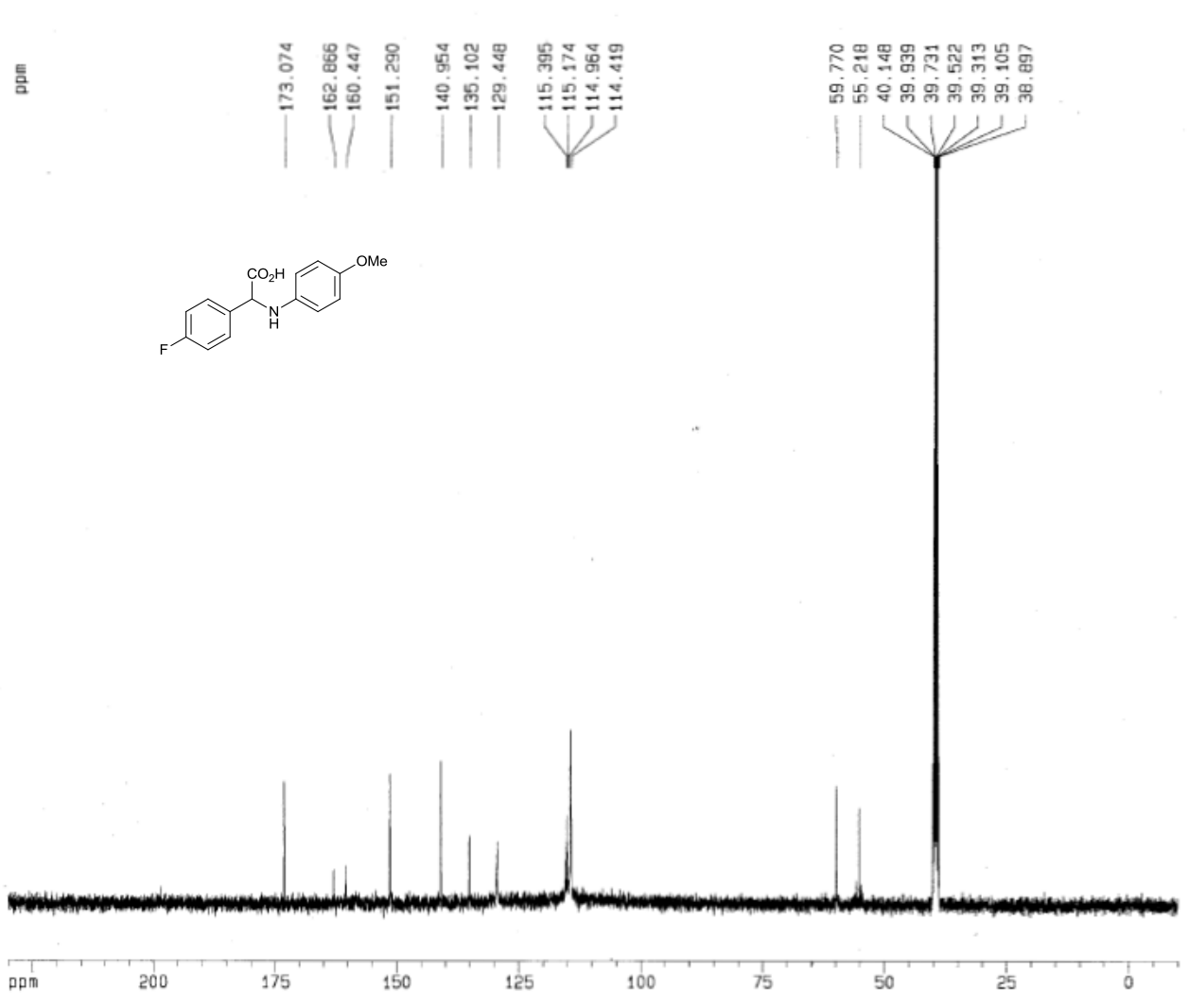


```
Current Data Parameters
NAME                  p_F
EXPNO                   8
PROCNO                  1

F2 - Acquisition Parameters
Date_              20121104
Time                  12.36
INSTRUM               spect
PROBHD     5 mm BBI 1H-
PULPROG             zgpg30
TD                   65536
SOLVENT               DMSO
NS                    1024
DS                       4
SWH              25125.629 Hz
FIDRES               0.383387 Hz
AQ                1.3042164 sec
RG                   16384
DW                  19.900 usec
DE                   6.00 usec
TE                  300.0 K
D1                2.00000000 sec
d11               0.03000000 sec
d12               0.00002000 sec

============ CHANNEL f1 ============
NUC1                    13C
P1                   16.35 usec
PL1                  -6.00 dB
SF01            100.6237959 MHz

============ CHANNEL f2 ============
CPDPRG2              waltz16
NUC2                    1H
PCPD2               114.00 usec
PL2                   0.00 dB
PL12                 24.00 dB
PL13                 24.00 dB
SF02            400.1316005 MHz

F2 - Processing parameters
SI                      32768
SF              100.6128129 MHz
WDW                        EM
SSB                         0
LB                   1.00 Hz
GB                          0
PC                   1.40

1D NMR plot parameters
CX                   20.00 cm
F1P                 230.000 ppm
F1                23140.95 Hz
F2P                -10.000 ppm
F2                 -1006.13 Hz
PPMCM             12.00000 ppm/cm
HZCM              1207.35376 Hz/cm
```

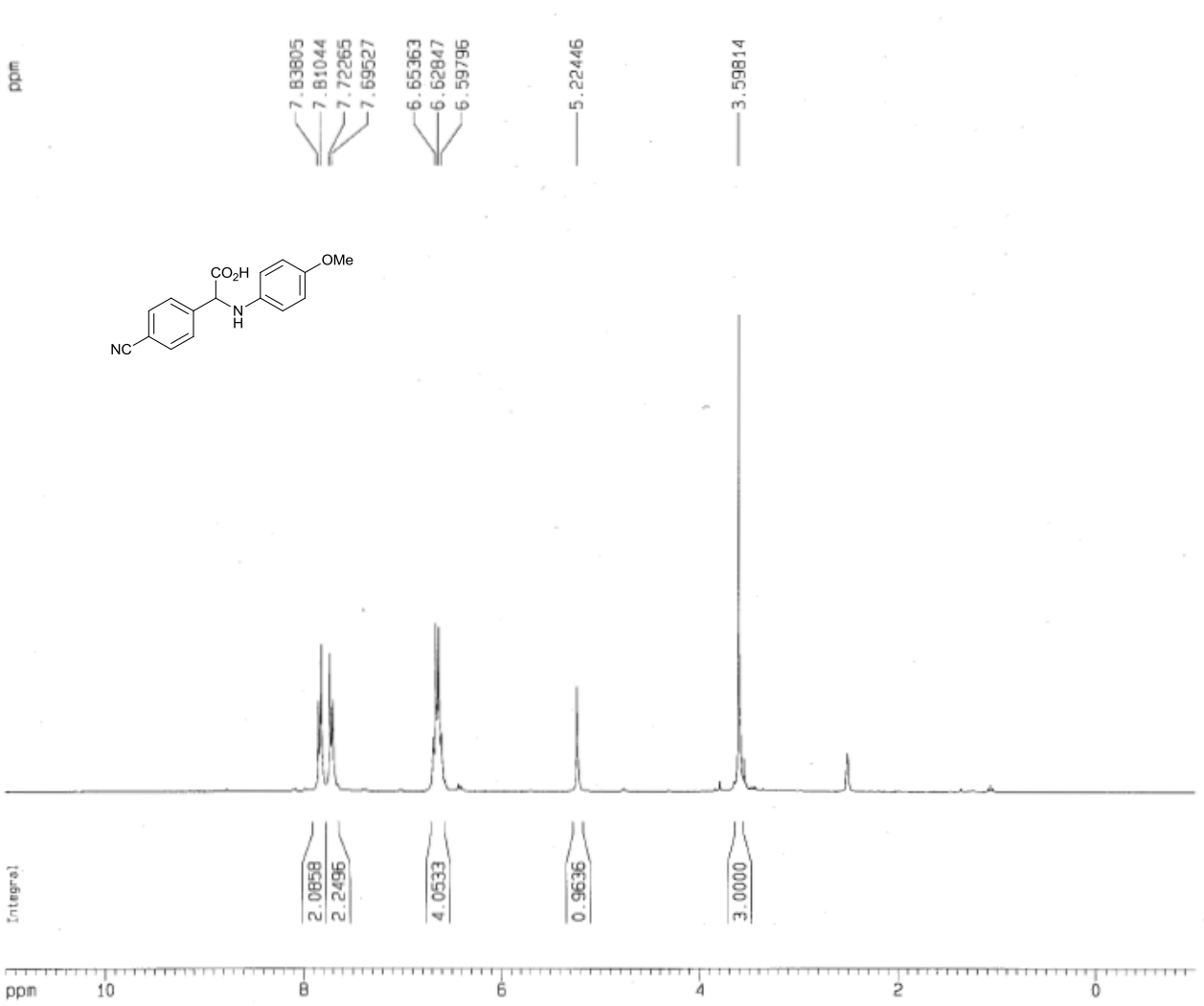


```
Current Data Parameters
NAME                  AAS_12
EXPNO                     40
PROCNO                     1

F2 - Acquisition Parameters
Date_               20121121
Time                   10.13
INSTRUM                spect
PROBHD     5 mm QNP 1H/1
PULPROG                zg30
TD                    65536
SOLVENT                DMSO
NS                        16
DS                         2
SWH                6172.839 Hz
FIDRES             0.094190 Hz
AQ                 5.3084660 sec
RG                     161.3
DW                    81.000 usec
DE                     6.00 usec
TE                    300.0 K
D1                1.00000000 sec

============ CHANNEL f1 =========
NUC1                       1H
P1                      12.10 usec
PL1                      0.00 dB
SFO1             299.8718518 MHz

F2 - Processing parameters
SI                        32768
SF               299.8700046 MHz
WDW                          no
SSB                           0
LB                       0.00 Hz
GB                            0
PC                         1.00

1D NMR plot parameters
CX                       20.00 cm
F1P                      11.000 ppm
F1                     3298.57 Hz
F2P                     -1.000 ppm
F2                    -299.87 Hz
PPMCM                 0.60000 ppm/cm
HZCM                179.92200 Hz/cm
```

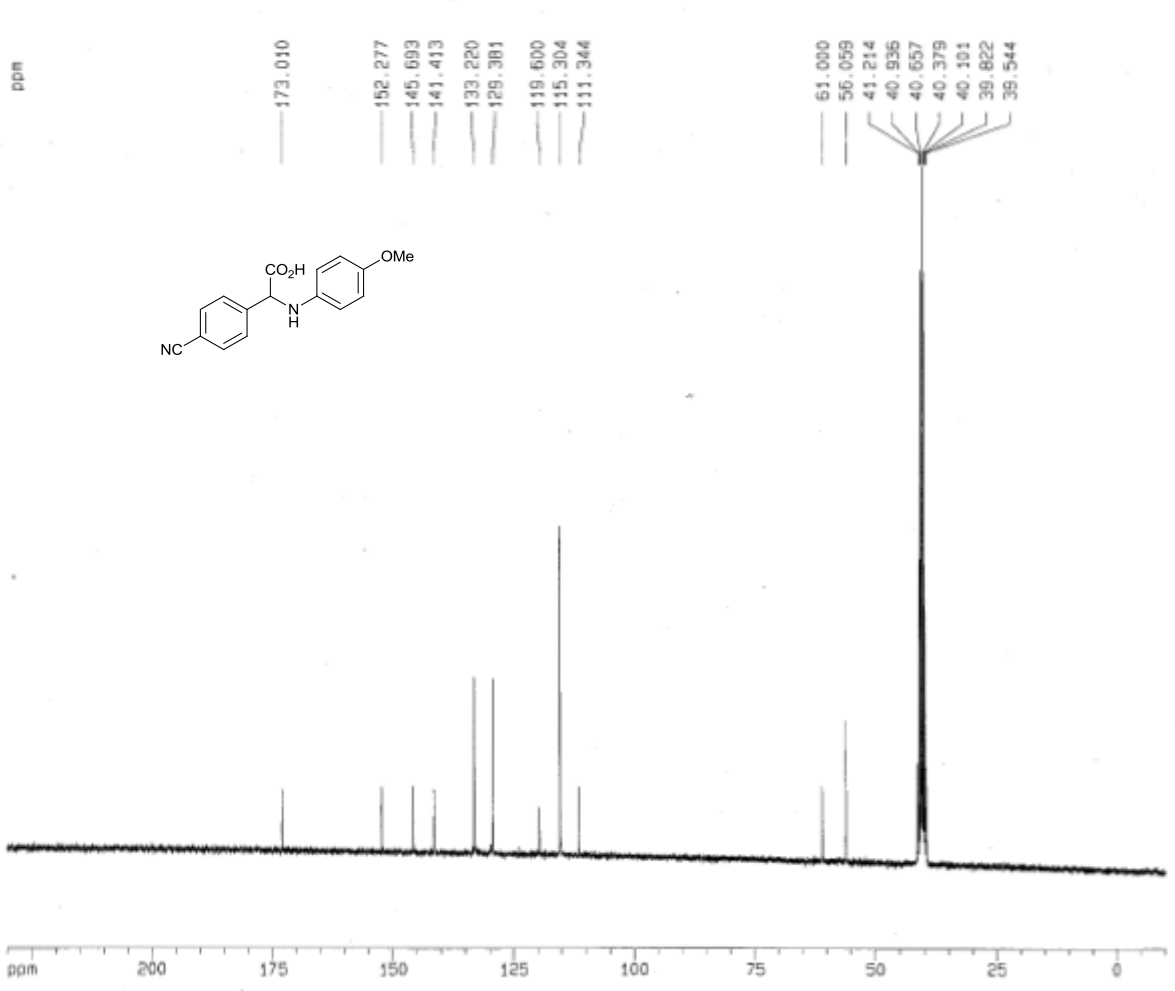


```
Current Data Parameters
NAME                  AAS_12
EXPNO                     39
PROCNO                     1

F2 - Acquisition Parameters
Date_              20121121
Time                   10.19
INSTRUM                spect
PROBHD     5 mm QNP 1H/1
PULPROG                zgpg30
TD                      65536
SOLVENT                 DMSO
NS                        770
DS                          4
SWH                18796.992 Hz
FIDRES                0.286815 Hz
AQ                    1.7433076 sec
RG                       1024
DW                     26.600 usec
DE                      6.00 usec
TE                     300.0 K
D1                  2.00000000 sec
D11                 0.03000000 sec
D12                 0.00002000 sec

======== CHANNEL f1 ========
NUC1                      13C
P1                       5.25 usec
PL1                     -6.00 dB
SFO1               75.4108357 MHz

======== CHANNEL f2 ========
CPDPRG2                waltz16
NUC2                       1H
PCPD2                  115.00 usec
PL2                      0.00 dB
PL12                    19.70 dB
PL13                    19.70 dB
SFO2              299.8711995 MHz

F2 - Processing parameters
SI                        32768
SF                 75.4023410 MHz
WDW                       EM
SSB                        0
LB                      1.00 Hz
GB                         0
PC                      1.40

1D NMR plot parameters
CX                     20.00 cm
F1P                   230.000 ppm
F1                  17342.54 Hz
F2P                   -10.000 ppm
F2                   -754.02 Hz
PPMCM                 12.00000 ppm/cm
HZCM                  504.82819 Hz/cm
```

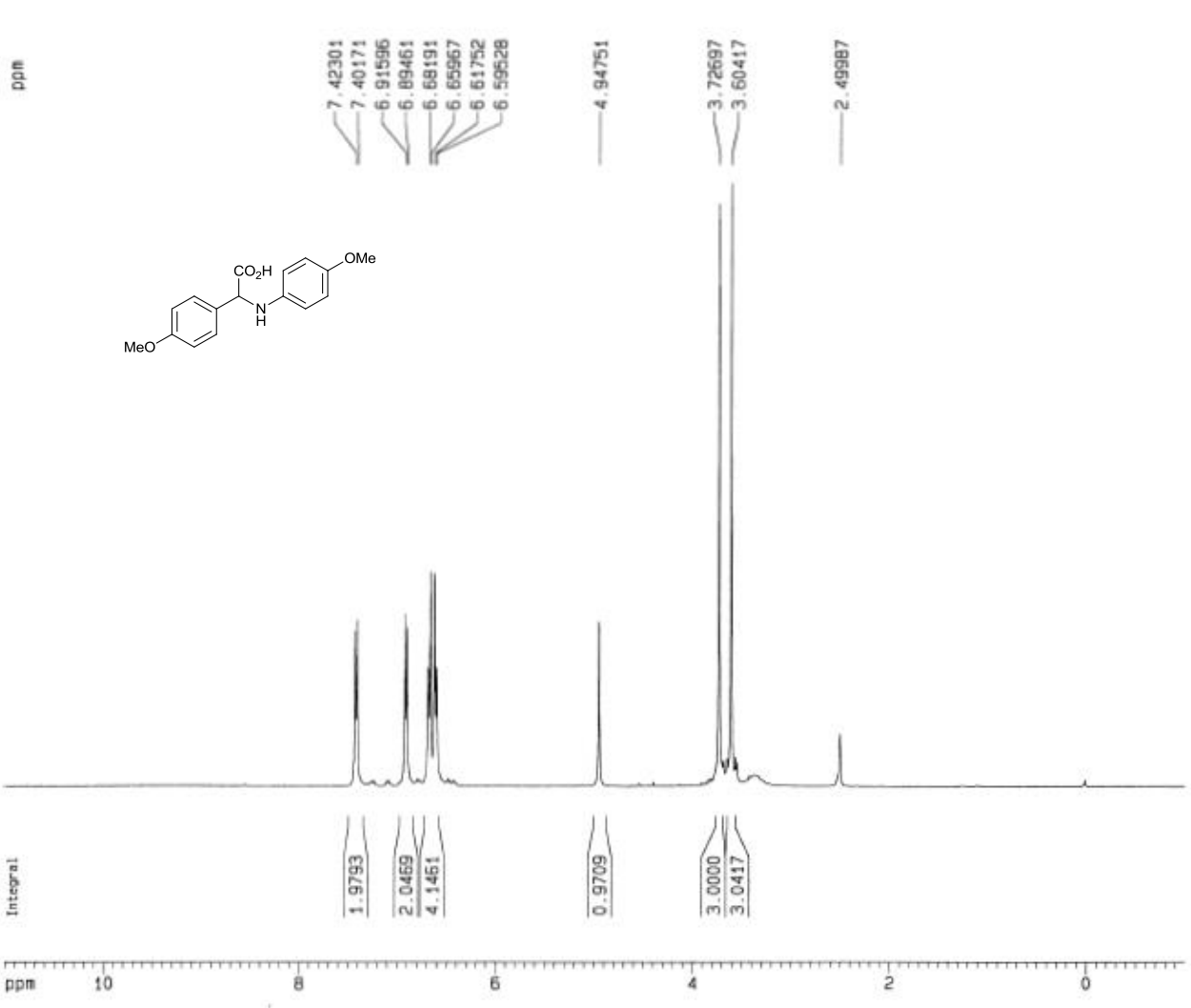

Current Data Parameters
NAME p_OMe
EXPNO 2
PROCNO 1

F2 - Acquisition Parameters
Date_ 20121023
Time 10.27
INSTRUM spect
PROBHD 5 mm BBI 1H-
PULPROG zg30
TD 65536
SOLVENT DMSO
NS 16
DS 2
SWH 8278.146 Hz
FIDRES 0.126314 Hz
AQ 3.9584243 sec
RG 143.7
DW 60.400 usec
DE 6.00 usec
TE 300.0 K
D1 1.00000000 sec

========== CHANNEL f1 ========
NUC1 1H
P1 6.45 usec
PL1 0.00 dB
SFO1 400.1324710 MHz

F2 - Processing parameters
SI 32768
SF 400.1300024 MHz
WDW no
SSB 0
LB 0.00 Hz
GB 0
PC 1.00

1D NMR plot parameters
CX 20.00 cm
F1P 11.000 ppm
F1 4401.43 Hz
F2P -1.000 ppm
F2 -400.13 Hz
PPMCM 0.60000 ppm/cm
HZCM 240.07800 Hz/cm

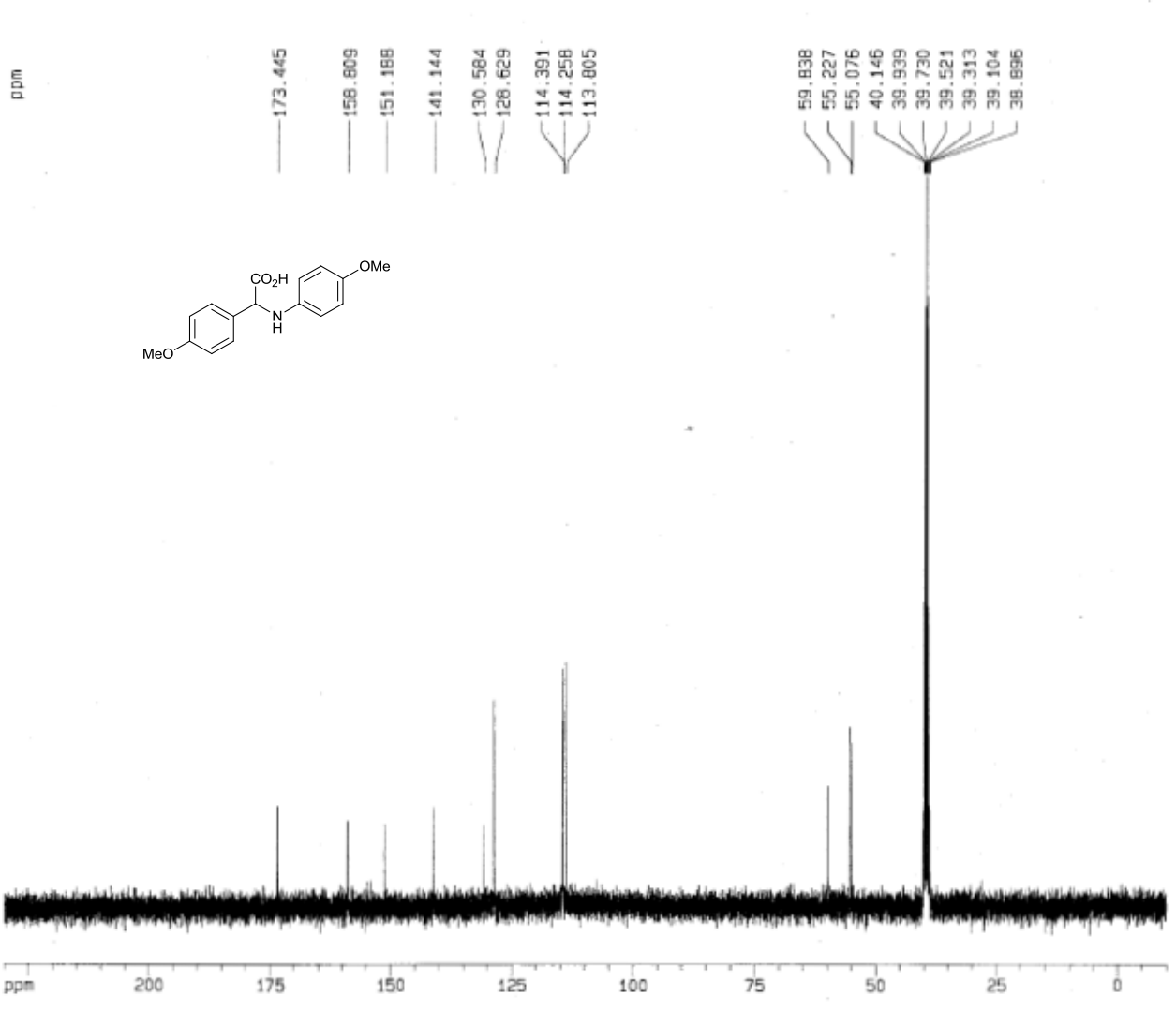


```
Current Data Parameters
NAME                  p_OMe
EXPNO                     4
PROCNO                    1

F2 - Acquisition Parameters
Date_              20121023
Time                  16.57
INSTRUM               spect
PROBHD     5 mm BBI 1H-
PULPROG              zgpg30
TD                    65536
SOLVENT                DMSO
NS                     1024
DS                        4
SWH               25125.629 Hz
FIDRES            0.383387 Hz
AQ                1.3042164 sec
RG                    16384
DW                   19.900 usec
DE                    6.00 usec
TE                   300.0 K
D1                2.00000000 sec
d11               0.03000000 sec
d12               0.00002000 sec

========== CHANNEL f1 ==========
NUC1                    13C
P1                    16.35 usec
PL1                   -6.00 dB
SFO1           100.6237988 MHz

========== CHANNEL f2 ==========
CPDPRG2              waltz16
NUC2                    1H
PCPD2                114.00 usec
PL2                   0.00 dB
PL12                 24.00 dB
PL13                 24.00 dB
SFO2           400.1316005 MHz

F2 - Processing parameters
SI                     32768
SF             100.6128145 MHz
WDW                       no
SSB                        0
LB                      0.00 Hz
GB                         0
PC                      1.40

1D NMR plot parameters
CX                     20.00 cm
F1P                   230.000 ppm
F1                  23140.95 Hz
F2P                   -10.000 ppm
F2                   -1006.13 Hz
PPMCM                12.00000 ppm/cm
HZCM              1207.35376 Hz/cm
```

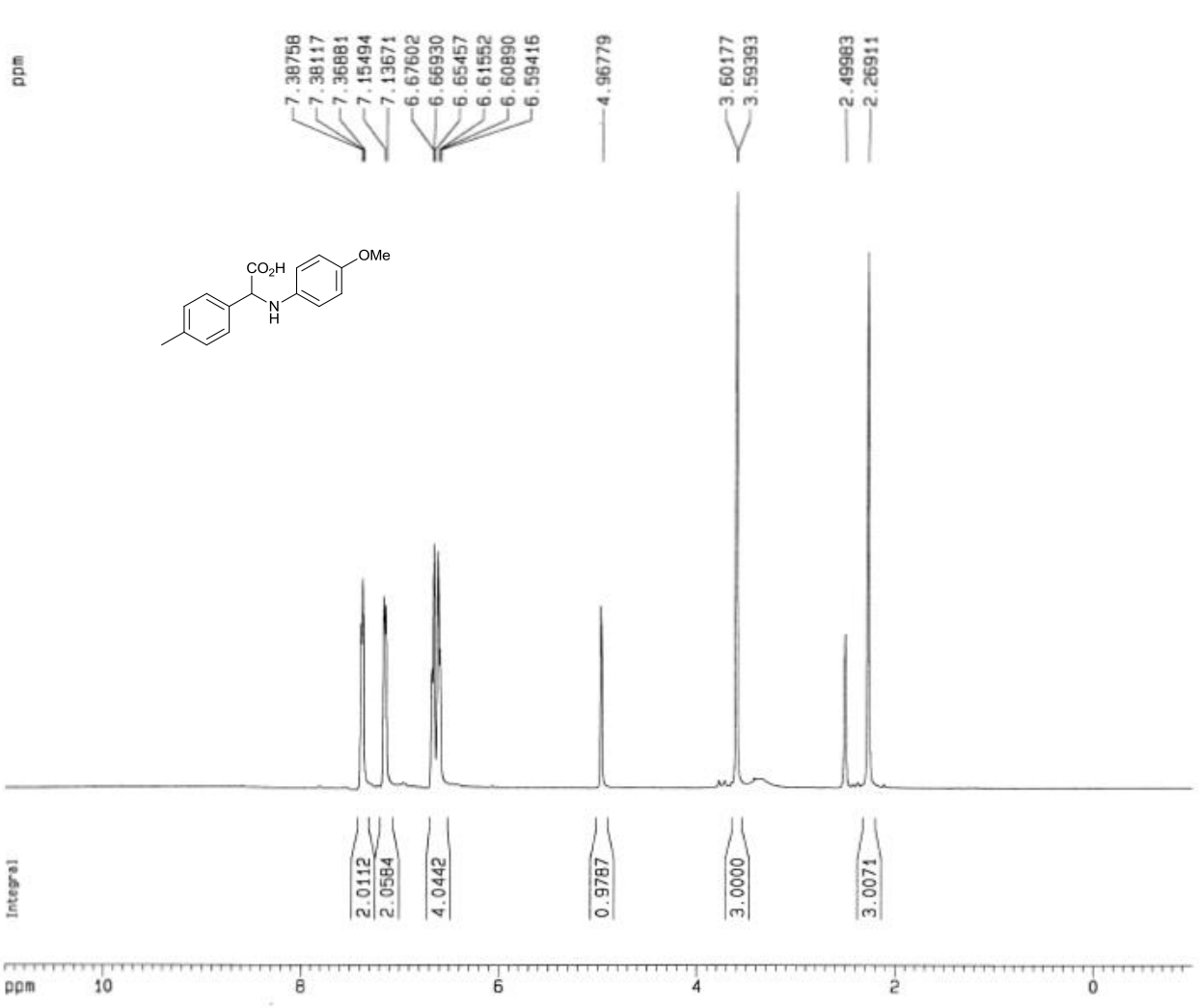


```
Current Data Parameters
NAME                  p_Me
EXPNO                    5
PROCNO                   1

F2 - Acquisition Parameters
Date_              20121025
Time                  9.57
INSTRUM              spect
PROBHD     5 mm BBI 1H-
PULPROG               zg30
TD                   65536
SOLVENT               DMSO
NS                      64
DS                       2
SWH                8278.146 Hz
FIDRES             0.126314 Hz
AQ                 3.9584243 sec
RG                     181
DW                  60.400 usec
DE                   6.00 usec
TE                  300.0 K
D1                1.00000000 sec

============ CHANNEL f1 ========
NUC1                     1H
P1                    6.45 usec
PL1                   0.00 dB
SFO1             400.1324710 MHz

F2 - Processing parameters
SI                       32768
SF                400.1300029 MHz
WDW                      no
SSB                      0
LB                    0.00 Hz
GB                       0
PC                    1.00

1D NMR plot parameters
CX                   20.00 cm
F1P                 11.000 ppm
F1                 4401.43 Hz
F2P                 -1.000 ppm
F2                 -400.13 Hz
PPMCM               0.60000 ppm/cm
HZCM              240.07800 Hz/cm
```

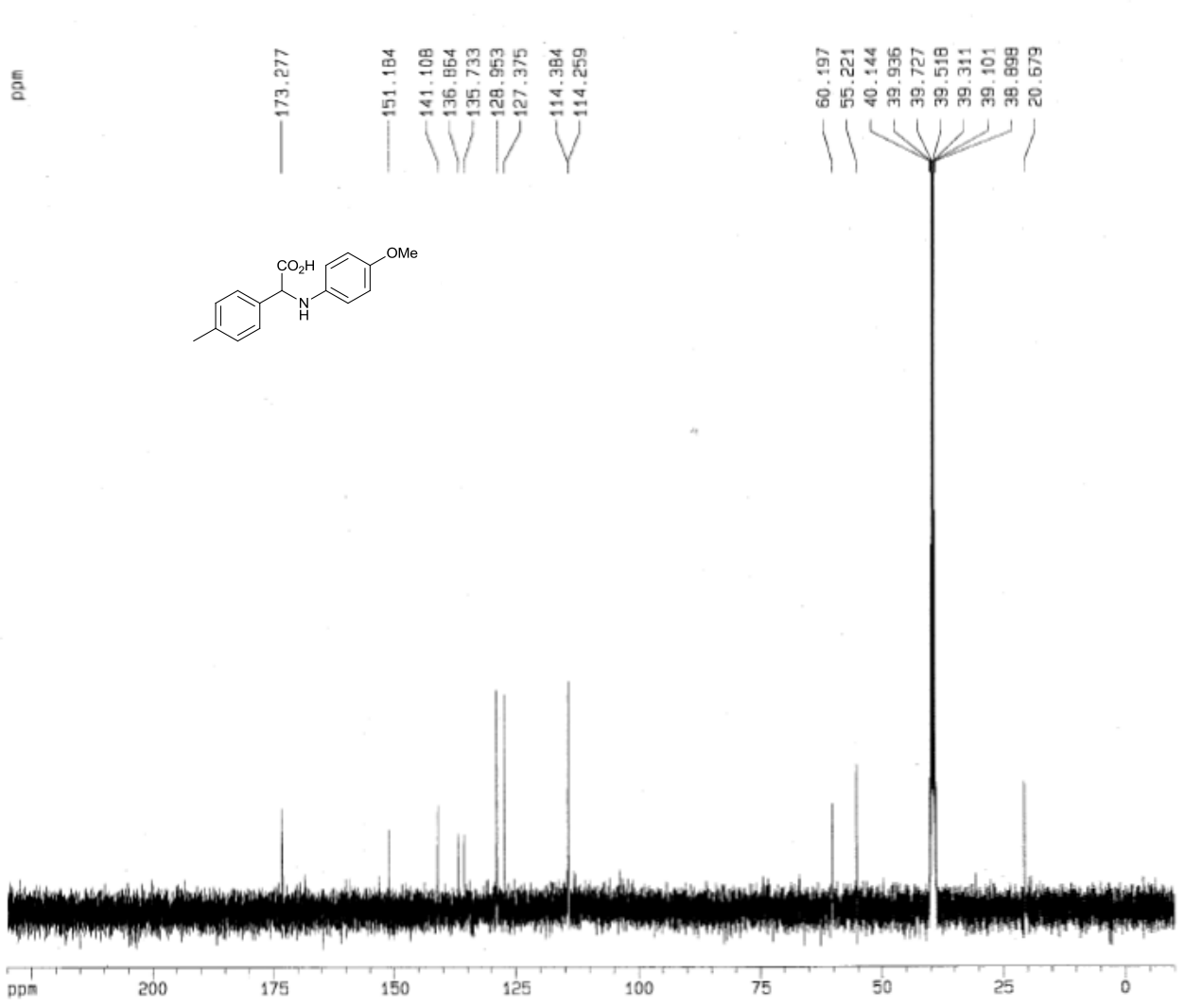


```
Current Data Parameters
NAME                   Mp
EXPNO                   2
PROCNO                  1

F2 - Acquisition Parameters
Date_            20121024
Time                17.54
INSTRUM             spect
PROBHD     5 mm BBI 1H-
PULPROG          zgpg30
TD                  65536
SOLVENT              DMSO
NS                   1024
DS                      4
SWH           25125.629 Hz
FIDRES         0.383387 Hz
AQ             1.3042164 sec
RG                  16384
DW                19.900 usec
DE                 6.00 usec
TE                300.0 K
D1            2.00000000 sec
d11           0.03000000 sec
d12           0.00002000 sec

========== CHANNEL f1 ==========
NUC1                13C
P1                16.35 usec
PL1               -6.00 dB
SFO1         100.6237959 MHz

========== CHANNEL f2 ==========
CPDPRG2          waltz16
NUC2                1H
PCPD2             114.00 usec
PL2                0.00 dB
PL12              24.00 dB
PL13              24.00 dB
SFO2         400.1316005 MHz

F2 - Processing parameters
SI                  32768
SF           100.6128152 MHz
WDW                    no
SSB                     0
LB                 0.00 Hz
GB                      0
PC                   1.40

1D NMR plot parameters
CX                 20.00 cm
F1P               230.000 ppm
F1              23140.95 Hz
F2P               -10.000 ppm
F2              -1006.13 Hz
PPMCM          12.00000 ppm/cm
HZCM         1207.35376 Hz/cm
```

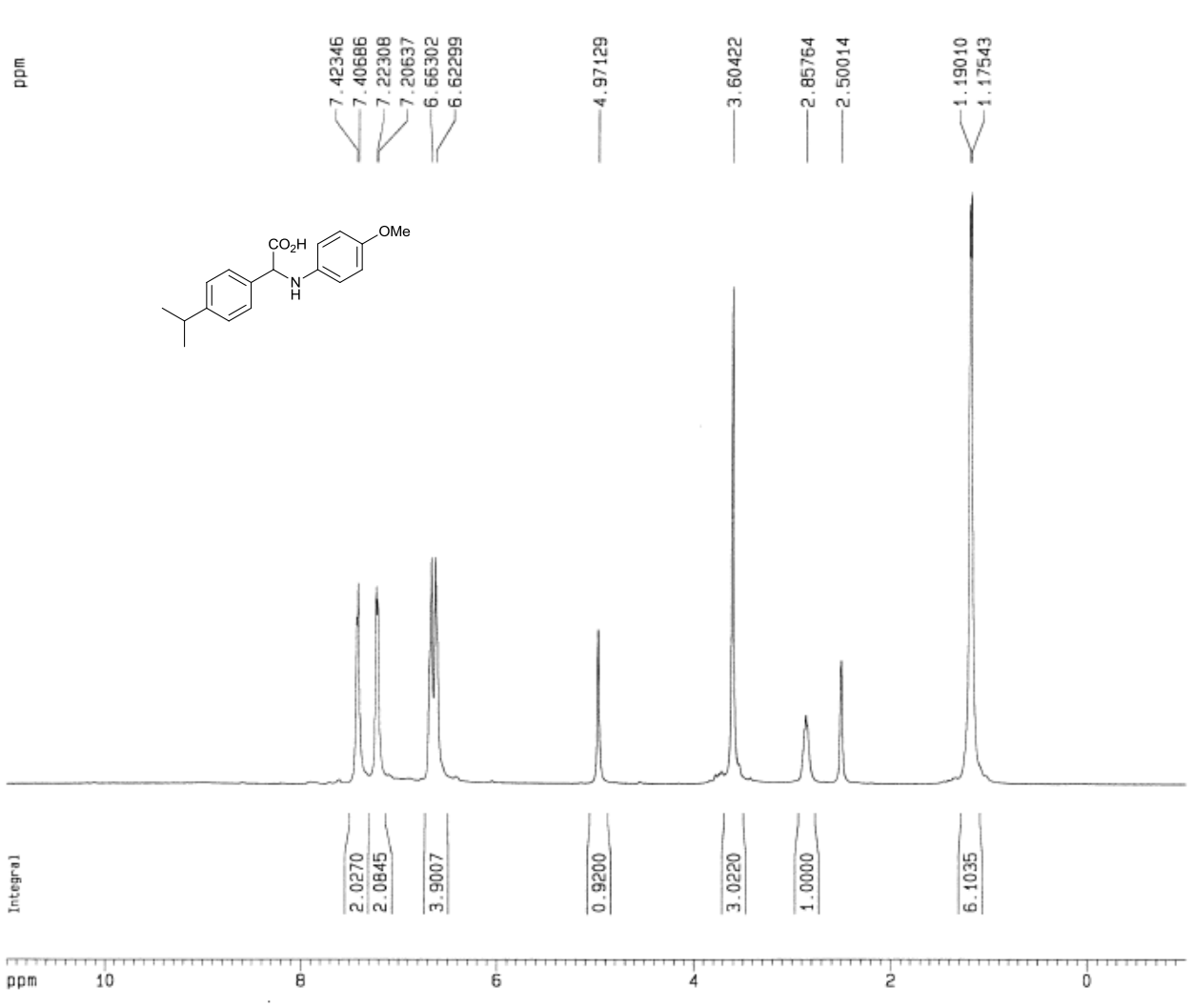


```
Current Data Parameters
NAME                  4_iso
EXPNO                     1
PROCNO                    1

F2 - Acquisition Parameters
Date_              20121031
Time                  12.03
INSTRUM               spect
PROBHD     5 mm BBI 1H-
PULPROG                zg30
TD                    65536
SOLVENT                DMSO
NS                       32
DS                        2
SWH                8278.146 Hz
FIDRES            0.126314 Hz
AQ                3.9584243 sec
RG                     80.6
DW                   60.400 usec
DE                    6.00 usec
TE                   300.0 K
D1                1.00000000 sec

============ CHANNEL f1 ========
NUC1                      1H
P1                     6.45 usec
PL1                    0.00 dB
SFO1            400.1324710 MHz

F2 - Processing parameters
SI                     32768
SF              400.1300019 MHz
WDW                       no
SSB                        0
LB                     0.00 Hz
GB                         0
PC                      1.00

1D NMR plot parameters
CX                    20.00 cm
F1P                  11.000 ppm
F1                  4401.43 Hz
F2P                  -1.000 ppm
F2                  -400.13 Hz
PPMCM                0.60000 ppm/cm
HZCM               240.07800 Hz/cm
```

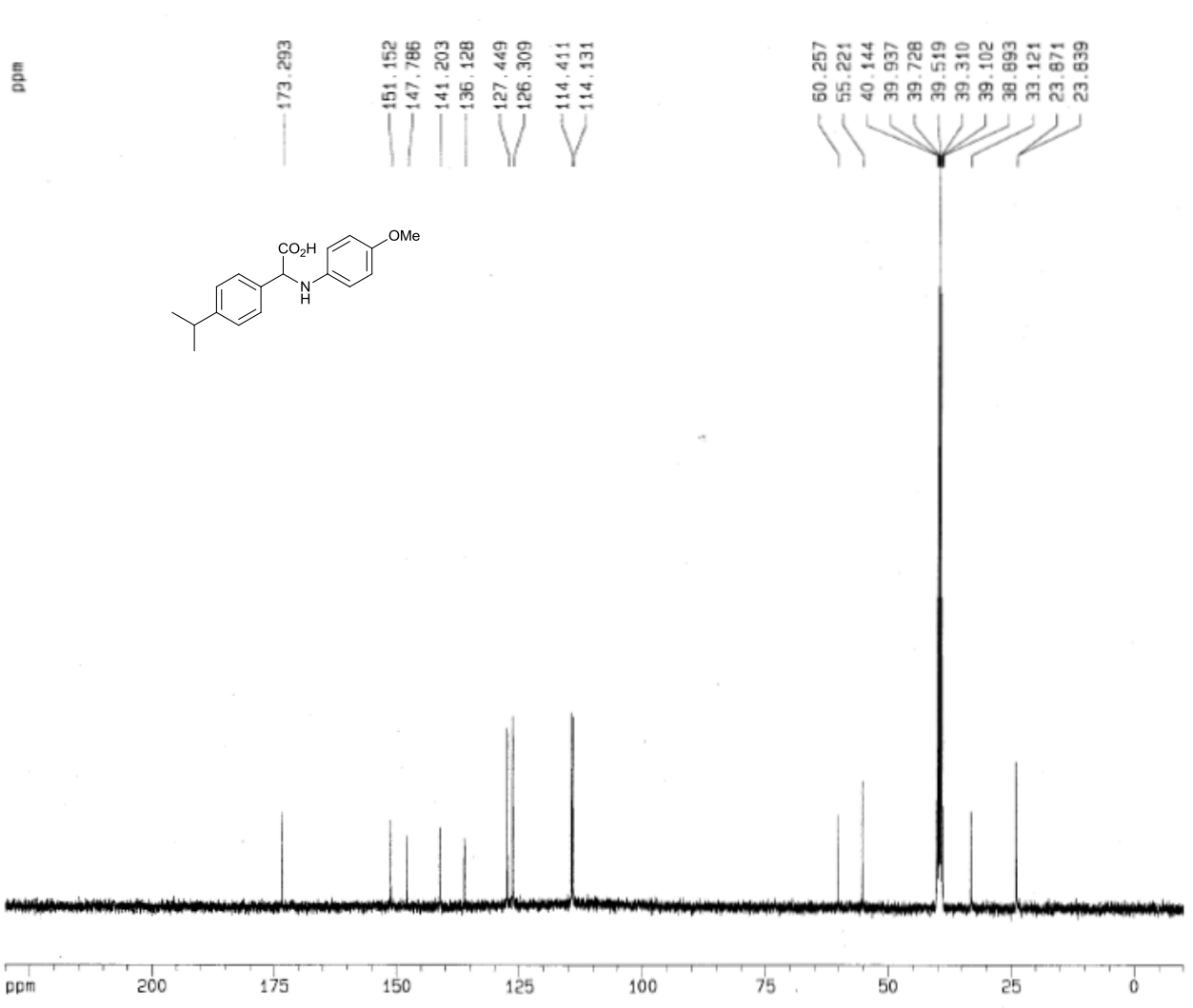


```
Current Data Parameters
NAME                  4_)so
EXPNO                     2
PROCNO                    1

F2 - Acquisition Parameters
Date_              20121031
Time                  13.05
INSTRUM               spect
PROBHD     5 mm BBI 1H-
PULPROG               zgpg30
TD                     65536
SOLVENT                DMSO
NS                      1024
DS                         4
SWH                25125.629 Hz
FIDRES             0.383387 Hz
AQ                 1.3042164 sec
RG                     16384
DW                    19.900 usec
DE                     6.00 usec
TE                    300.0 K
D1                 2.00000000 sec
d11                0.03000000 sec
d12                0.00002000 sec

============ CHANNEL f1 ============
NUC1                     13C
P1                     15.35 usec
PL1                    -6.00 dB
SFO1             100.6237959 MHz

============ CHANNEL f2 ============
CPDPRG2               waltz16
NUC2                     1H
PCPD2                 114.00 usec
PL2                    0.00 dB
PL12                  24.00 dB
PL13                  24.00 dB
SFO2             400.1316005 MHz

F2 - Processing parameters
SI                       32768
SF               100.6128152 MHz
WDW                        EM
SSB                         0
LB                     1.00 Hz
GB                          0
PC                     1.40

1D NMR plot parameters
CX                    20.00 cm
F1P                  230.000 ppm
F1                  23140.95 Hz
F2P                  -10.000 ppm
F2                  -1006.13 Hz
PPMCM                12.00000 ppm/cm
HZCM              1207.35376 Hz/cm
```

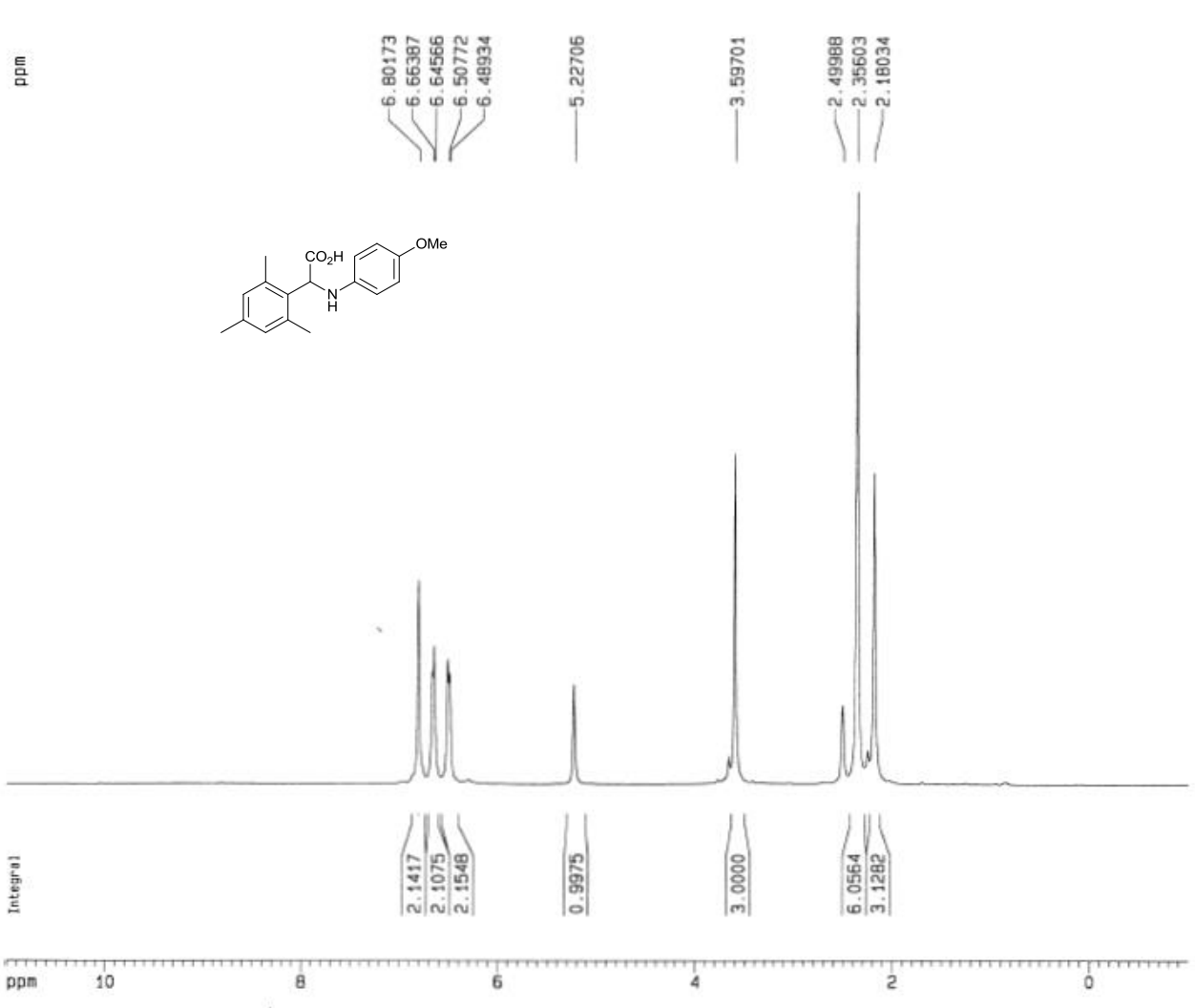


```
Current Data Parameters
NAME                  mes
EXPNO                   1
PROCNO                  1

F2 - Acquisition Parameters
Date_              20121025
Time                 11.46
INSTRUM              spect
PROBHD     5 mm BBI 1H-
PULPROG              zg30
TD                  65536
SOLVENT              DMSO
NS                     32
DS                      2
SWH              8278.146 Hz
FIDRES           0.126314 Hz
AQ               3.9584243 sec
RG                   71.8
DW                 60.400 usec
DE                  6.00 usec
TE                 300.0 K
D1              1.00000000 sec

============ CHANNEL f1 ========
NUC1                   1H
P1                   6.45 usec
PL1                  0.00 dB
SFO1           400.1324710 MHz

F2 - Processing parameters
SI                  32768
SF             400.1300024 MHz
WDW                    no
SSB                     0
LB                   0.00 Hz
GB                      0
PC                   1.00

1D NMR plot parameters
CX                  20.00 cm
F1P                 11.000 ppm
F1                4401.43 Hz
F2P                -1.000 ppm
F2                -400.13 Hz
PPMCM              0.60000 ppm/cm
HZCM             240.07800 Hz/cm
```

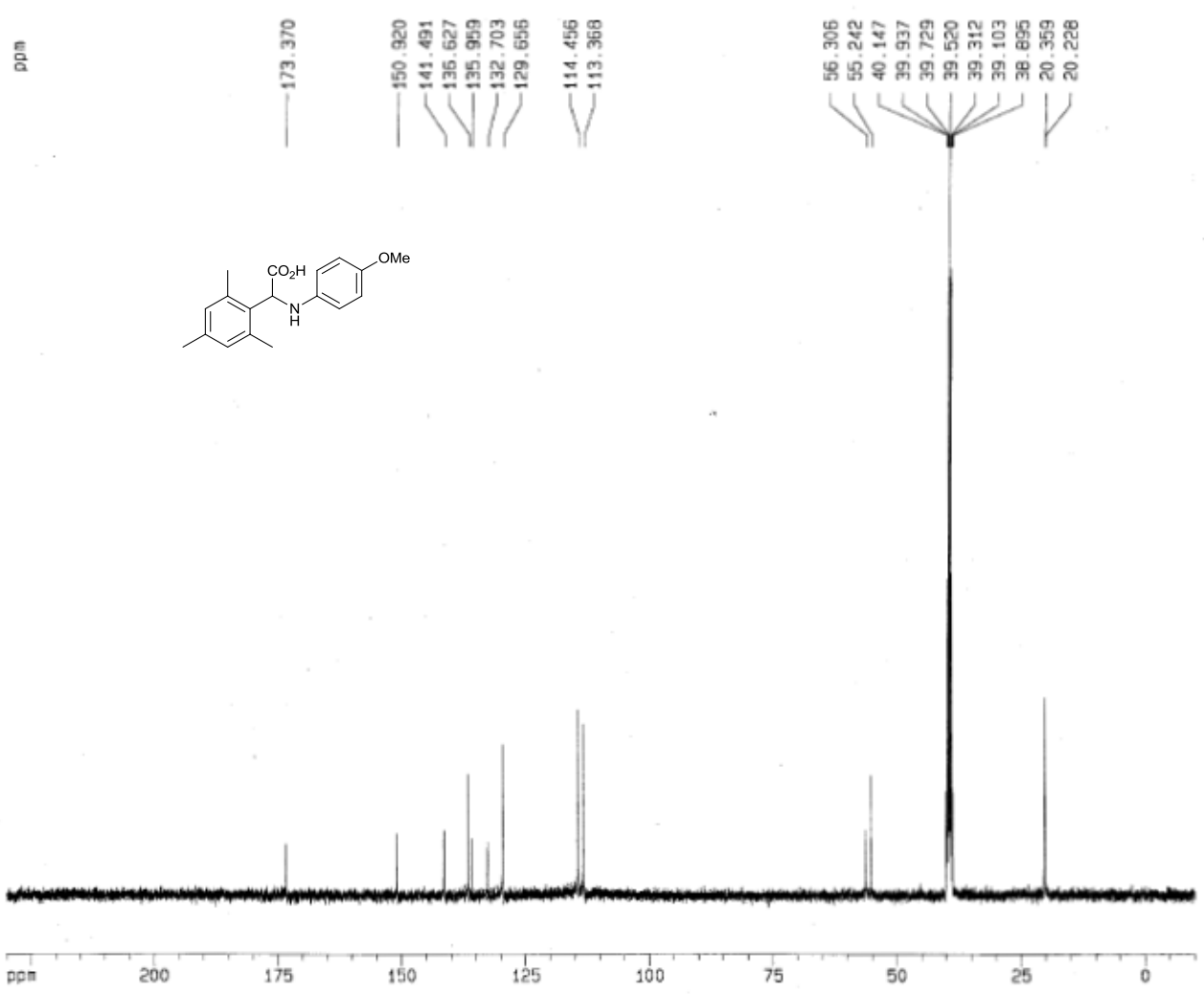


```
Current Data Parameters
NAME                  nes
EXPNO                   2
PROCNO                  1

F2 - Acquisition Parameters
Date_           20121025
Time               12.49
INSTRUM            spect
PROBHD     5 mm BBI 1H-
PULPROG          zgpg30
TD                65536
SOLVENT            DMSO
NS                 1024
DS                    4
SWH            25125.629 Hz
FIDRES         0.383397 Hz
AQ             1.3042164 sec
RG                16384
DW                19.900 usec
DE                 6.00 usec
TE                300.0 K
D1             2.00000000 sec
D11            0.03000000 sec
D12            0.00002000 sec

============ CHANNEL f1 ============
NUC1                13C
P1                15.35 usec
PL1               -6.00 dB
SFO1         100.6237959 MHz

============ CHANNEL f2 ============
CPDPRG2         waltz16
NUC2                1H
PCPD2             114.00 usec
PL2                0.00 dB
PL12              24.00 dB
PL13              24.00 dB
SFO2         400.1316005 MHz

F2 - Processing parameters
SI                 32768
SF           100.6128145 MHz
WDW                  EM
SSB                   0
LB                 1.00 Hz
GB                    0
PC                 1.40

1D NMR plot parameters
CX                20.00 cm
F1P              230.000 ppm
F1             23140.95 Hz
F2P              -10.000 ppm
F2             -1006.13 Hz
PPMCM             12.00000 ppm/cm
HZCM           1207.35376 Hz/cm
```

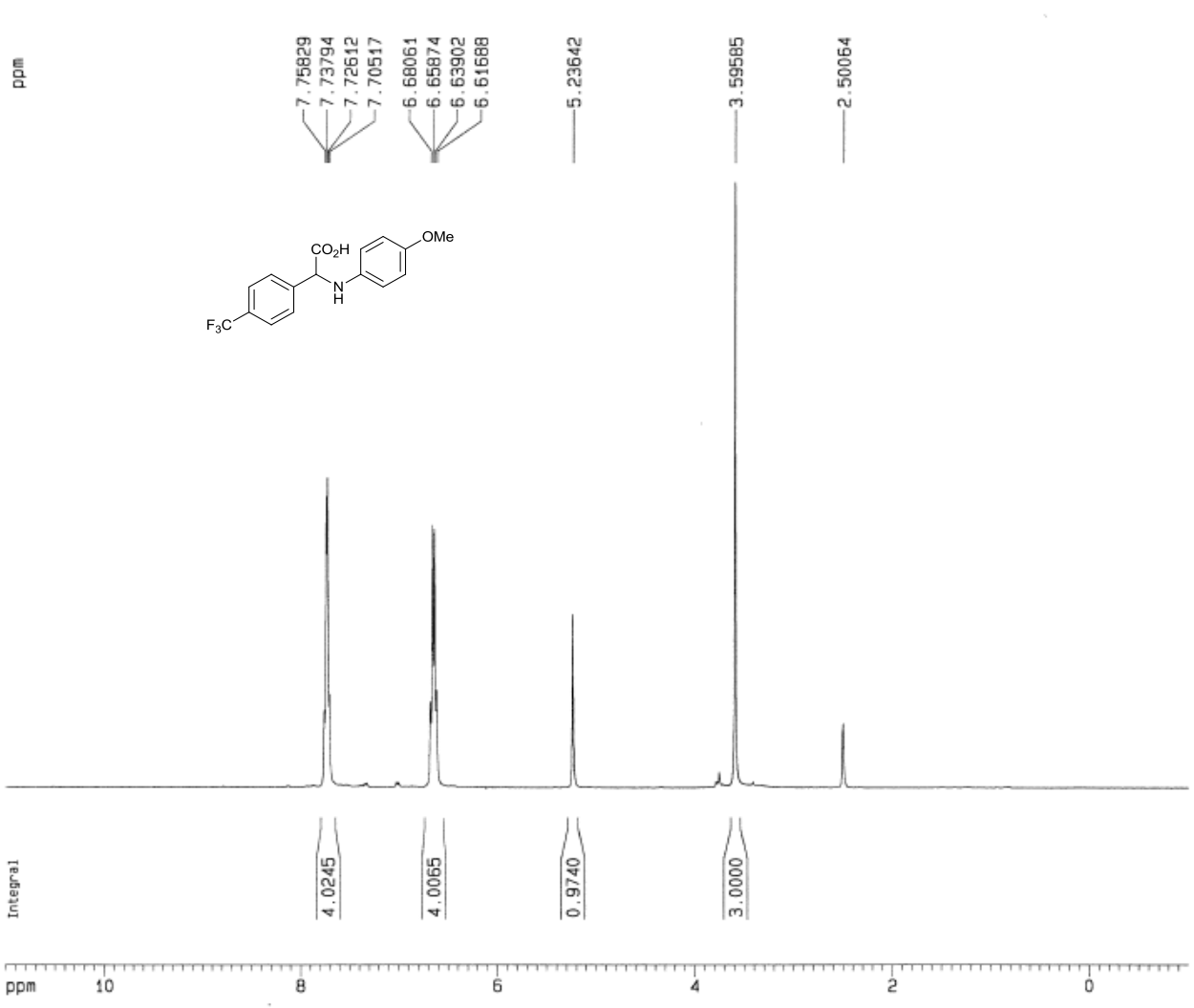


```
Current Data Parameters
NAME                  p_CF3
EXPNO                     2
PROCNO                    1

F2 - Acquisition Parameters
Date_              20121017
Time                  13.23
INSTRUM               spect
PROBHD     5 mm BBI 1H-
PULPROG                zg30
TD                    65536
SOLVENT                DMSO
NS                       16
DS                        2
SWH                8278.146 Hz
FIDRES            0.126314 Hz
AQ                3.9584243 sec
RG                    143.7
DW                   60.400 usec
DE                    6.00 usec
TE                   300.0 K
D1                1.00000000 sec

------------ CHANNEL f1 ---------
NUC1                     1H
P1                    6.45 usec
PL1                   0.00 dB
SFO1             400.1324710 MHz

F2 - Processing parameters
SI                       32768
SF                400.1300026 MHz
WDW                         no
SSB                          0
LB                    0.00 Hz
GB                           0
PC                    1.00

1D NMR plot parameters
CX                   20.00 cm
F1P                 11.000 ppm
F1                 4401.43 Hz
F2P                 -1.000 ppm
F2                 -400.13 Hz
PPMCM              0.60000 ppm/cm
HZCM             240.07800 Hz/cm
```

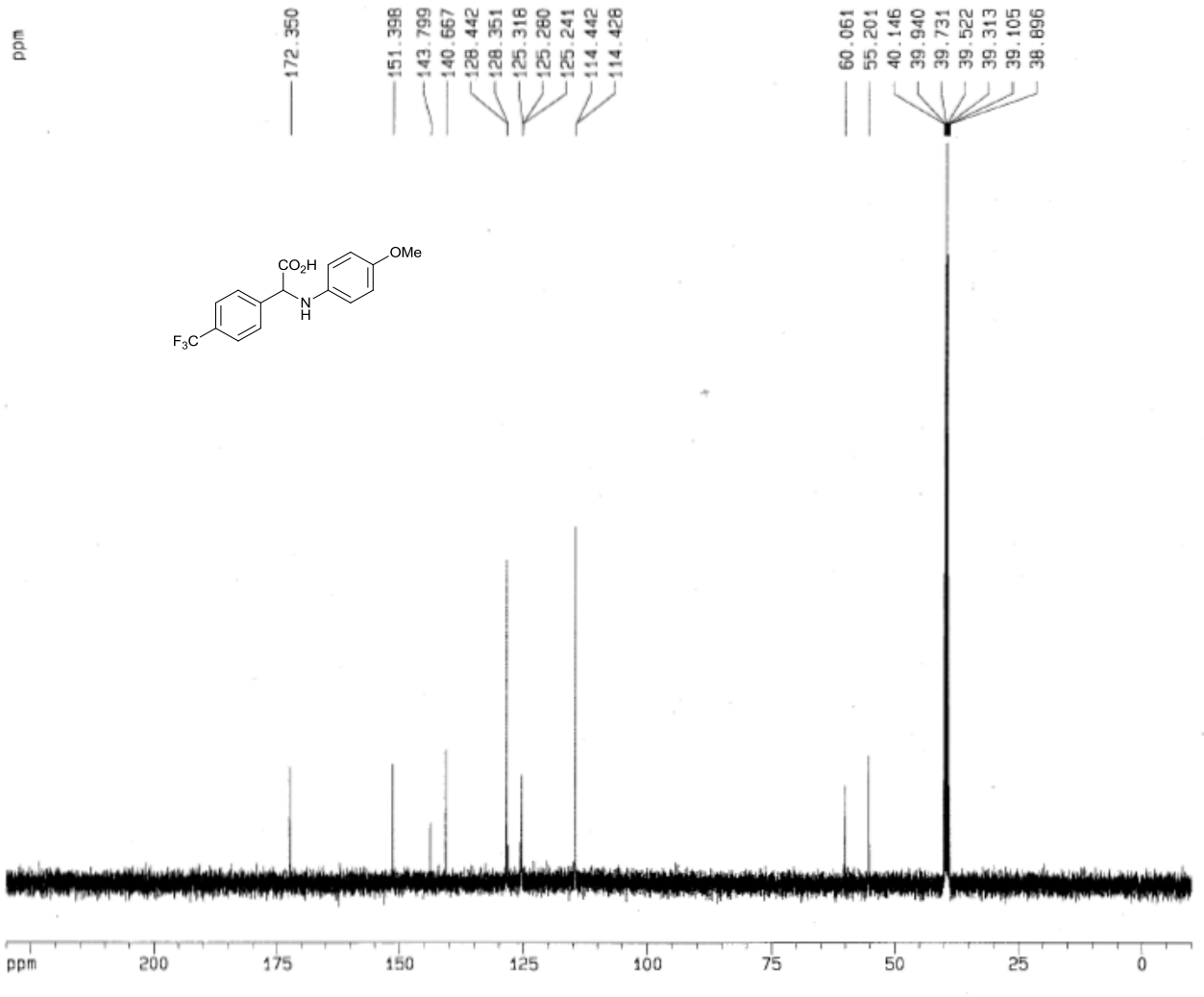


```
Current Data Parameters
NAME                  p_CF3
EXPNO                     1
PROCNO                    1

F2 - Acquisition Parameters
Date_              20121017
Time                 16.08
INSTRUM              spect
PROBHD     5 mm BBI 1H-
PULPROG              zgpg30
TD                    65536
SOLVENT                DMSO
NS                     1024
DS                        4
SWH              25125.629 Hz
FIDRES               0.383387 Hz
AQ                1.3042164 sec
RG                    16384
DW                   19.900 usec
DE                    6.00 usec
TE                   300.0 K
D1                2.00000000 sec
d11               0.03000000 sec
d12               0.00002000 sec

========== CHANNEL f1 ==========
NUC1                     13C
P1                     15.35 usec
PL1                    -6.00 dB
SFO1            100.6237959 MHz

========== CHANNEL f2 ==========
CPDPRG2              waltz16
NUC2                     1H
PCPD2                 114.00 usec
PL2                    0.00 dB
PL12                  24.00 dB
PL13                  24.00 dB
SFO2            400.1316005 MHz

F2 - Processing parameters
SI                       32768
SF              100.6128129 MHz
WDW                         no
SSB                          0
LB                        0.00 Hz
GB                           0
PC                        1.40

1D NMR plot parameters
CX                       20.00 cm
F1P                     230.000 ppm
F1                    23140.95 Hz
F2P                    -10.000 ppm
F2                    -1006.13 Hz
PPMCM                 12.00000 ppm/cm
HZCM                1207.35376 Hz/cm
```

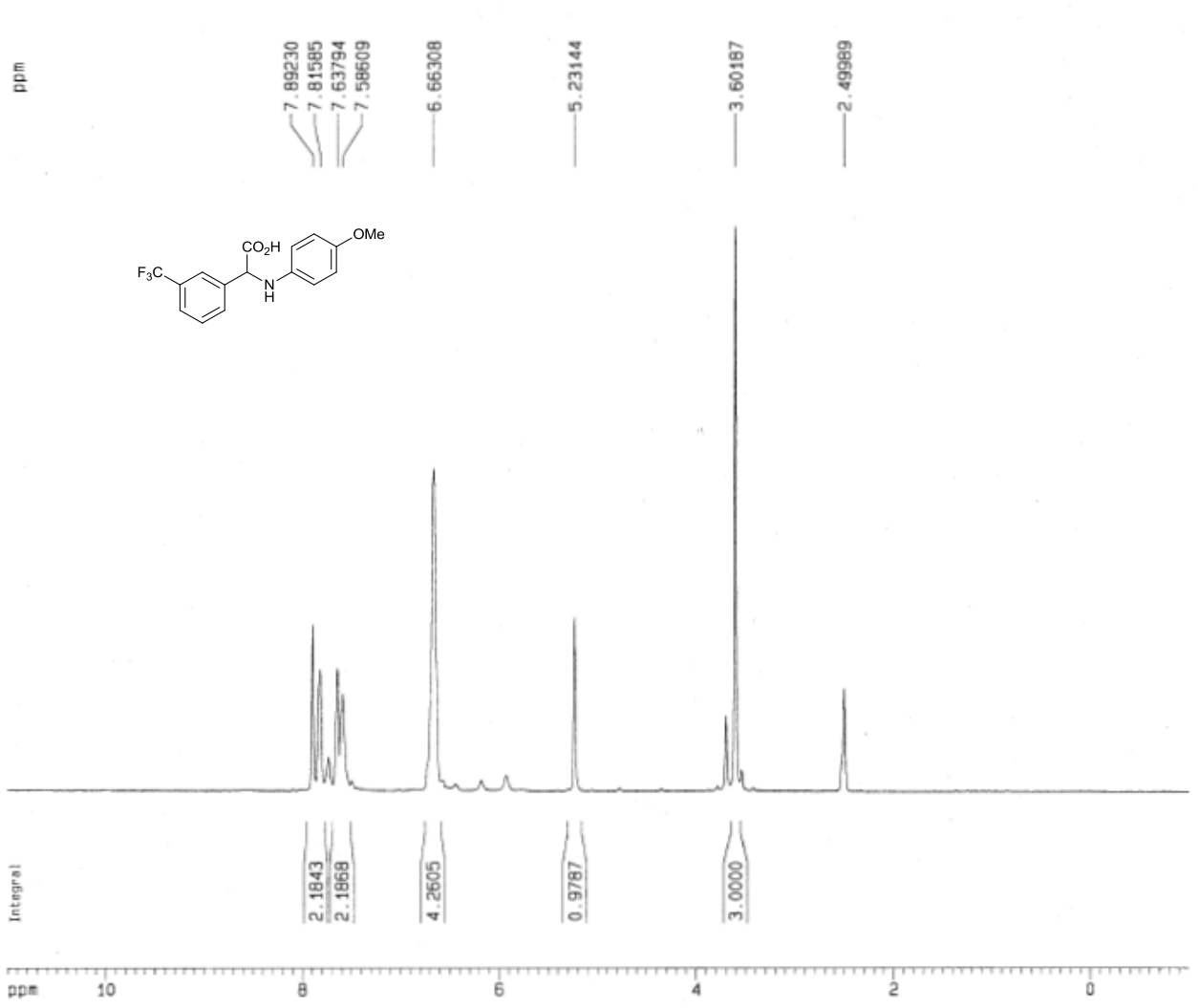


```
Current Data Parameters
NAME                  m_CF3
EXPNO                     6
PROCNO                    1

F2 - Acquisition Parameters
Date_              20121105
Time                 14.54
INSTRUM              spect
PROBHD     5 mm BBI 1H-
PULPROG              zg30
TD                  65536
SOLVENT              DMSO
NS                      32
DS                       2
SWH               8278.146 Hz
FIDRES            0.126314 Hz
AQ                3.9584243 sec
RG                   322.5
DW                  60.400 usec
DE                   6.00 usec
TE                  300.0 K
D1                1.00000000 sec

============ CHANNEL f1 ========
NUC1                    1H
P1                   6.45 usec
PL1                  0.00 dB
SFO1           400.1324710 MHz

F2 - Processing parameters
SI                   32768
SF             400.1300031 MHz
WDW                     no
SSB                      0
LB                    0.00 Hz
GB                       0
PC                    1.00

1D NMR plot parameters
CX                   20.00 cm
F1P                 11.000 ppm
F1                 4401.43 Hz
F2P                 -1.000 ppm
F2                 -400.13 Hz
PPMCM              0.60000 ppm/cm
HZCM             240.07800 Hz/cm
```

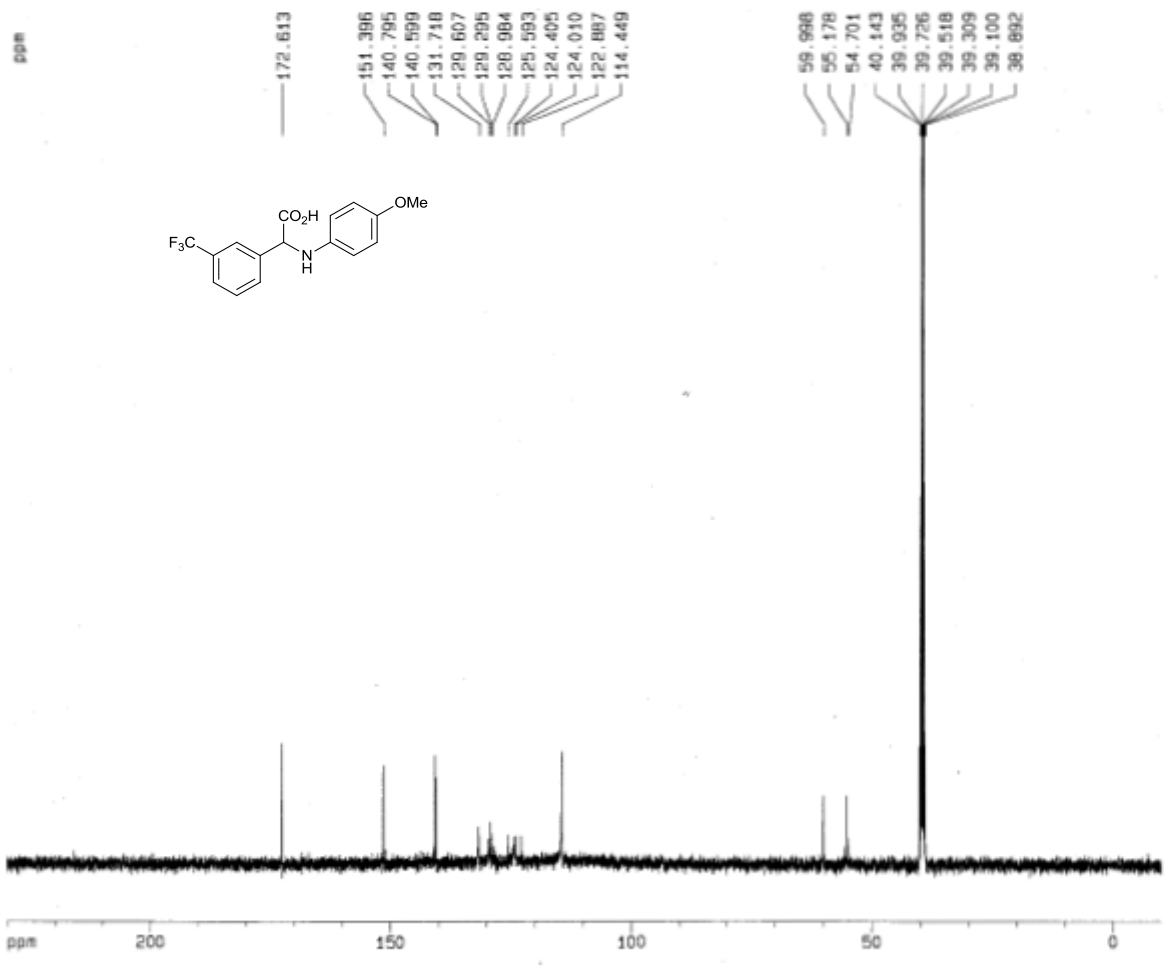


```
Current Data Parameters
NAME                  a_CF3
EXPNO                     7
PROCNO                    1

F2 - Acquisition Parameters
Date_              20121105
Time                  16.55
INSTRUM                spect
PROBHD     5 mm BBI 1H-
PULPROG              zgpg30
TD                    65536
SOLVENT                DMSO
NS                     1024
DS                        4
SWH                25125.629 Hz
FIDRES             0.383387 Hz
AQ                 1.3042164 sec
RG                     13004
DW                  19.900 usec
DE                   6.00 usec
TE                  300.0 K
D1                 2.00000000 sec
d11                0.03000000 sec
d12                0.00002000 sec

========== CHANNEL f1 ==========
NUC1                      13C
P1                      16.35 usec
PL1                     -6.00 dB
SFO1              100.6237959 MHz

========== CHANNEL f2 ==========
CPDPRG2                waltz16
NUC2                       1H
PCPD2                  114.00 usec
PL2                     0.00 dB
PL12                   24.00 dB
PL13                   24.00 dB
SFO2              400.1316005 MHz

F2 - Processing parameters
SI                        32768
SF                100.6128137 MHz
WDW                          EM
SSB                           0
LB                      1.00 Hz
GB                            0
PC                      1.40

1D NMR plot parameters
CX                     20.00 cm
F1P                   230.000 ppm
F1                  23140.95 Hz
F2P                   -10.000 ppm
F2                  -1006.13 Hz
PPMCM                12.00000 ppm/cm
HZCM               1207.35376 Hz/cm
```

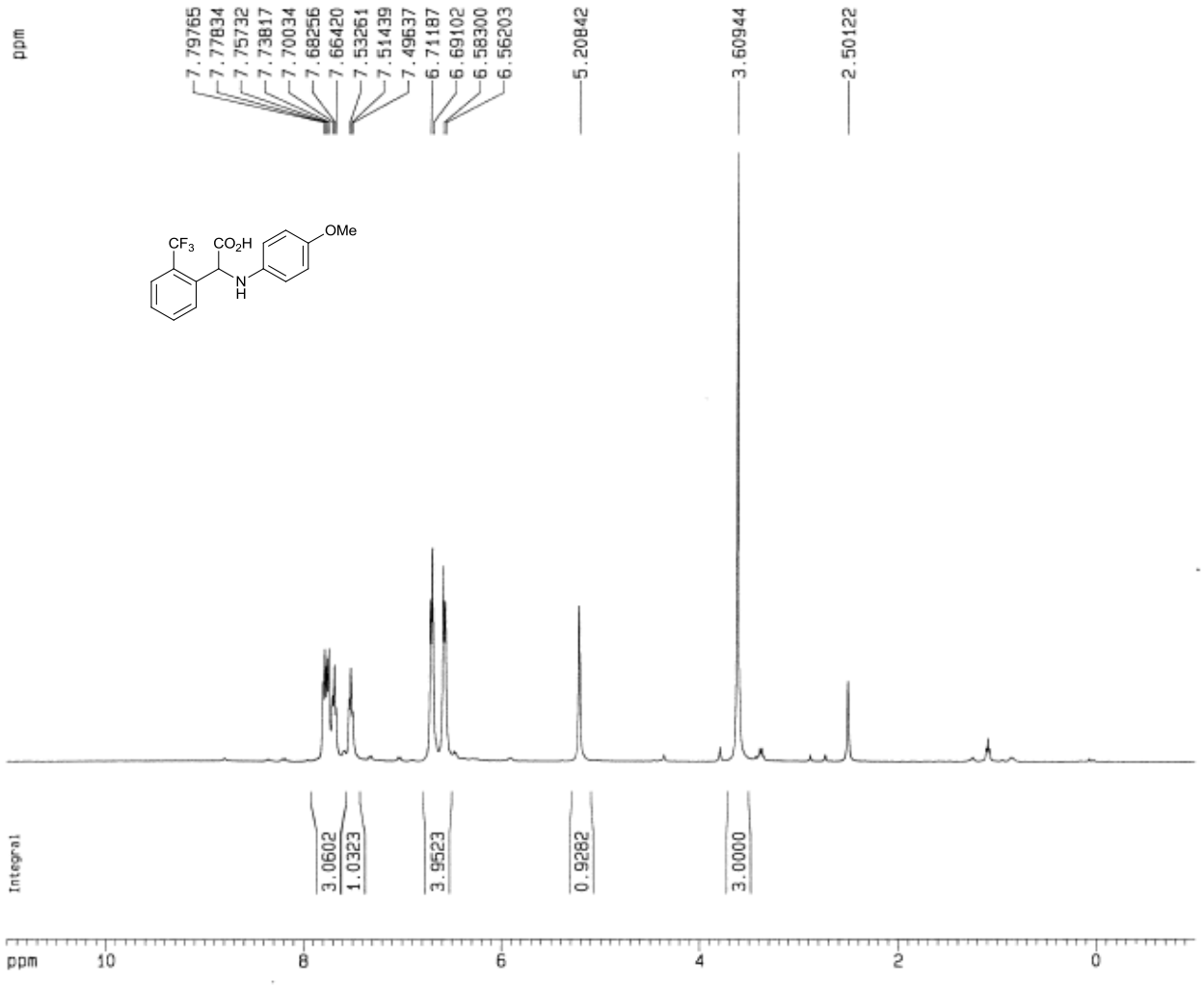


```
Current Data Parameters
NAME                  2_CF3
EXPNO                     4
PROCNO                    1

F2 - Acquisition Parameters
Date_              20121018
Time                  10.43
INSTRUM               spect
PROBHD     5 mm BBI 1H-
PULPROG                zg30
TD                    65536
SOLVENT                DMSO
NS                       16
DS                        2
SWH                8278.146 Hz
FIDRES            0.126314 Hz
AQ                3.9584243 sec
RG                      128
DW                   60.400 usec
DE                    6.00 usec
TE                   300.0 K
D1                1.00000000 sec

========== CHANNEL f1 =========
NUC1                      1H
P1                     6.45 usec
PL1                    0.00 dB
SFO1             400.1324710 MHz

F2 - Processing parameters
SI                       32768
SF                400.1300021 MHz
WDW                         no
SSB                          0
LB                     0.00 Hz
GB                           0
PC                     1.00

1D NMR plot parameters
CX                    20.00 cm
F1P                  11.000 ppm
F1                  4401.43 Hz
F2P                  -1.000 ppm
F2                  -400.13 Hz
PPMCM                0.60000 ppm/cm
HZCM               240.07800 Hz/cm
```

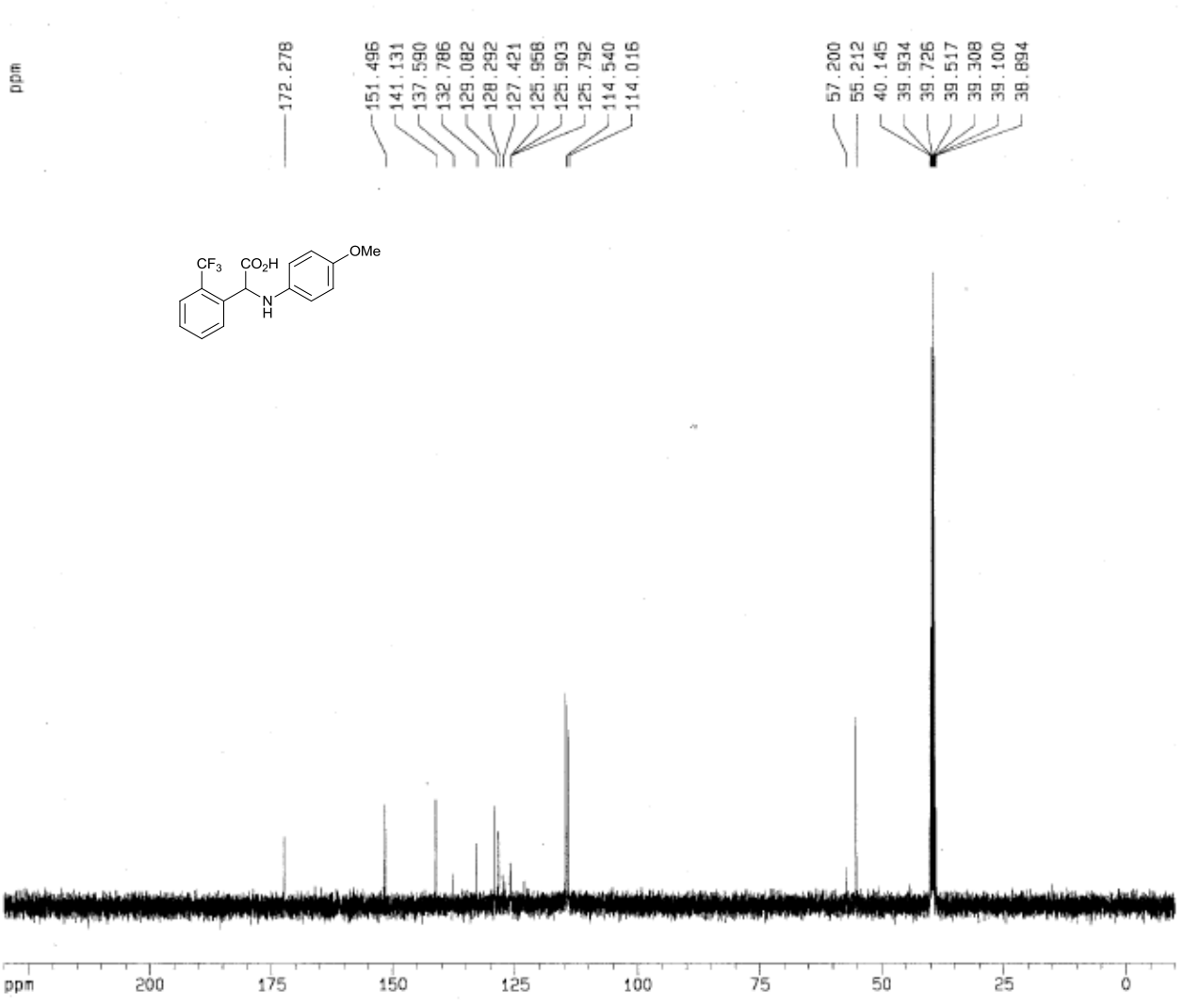


```
Current Data Parameters
NAME                  2_CF3
EXPNO                     3
PROCNO                    1

F2 - Acquisition Parameters
Date_              20121018
Time                  14.55
INSTRUM               spect
PROBHD     5 mm BBI 1H-
PULPROG               zgpg30
TD                     65536
SOLVENT                DMSO
NS                      954
DS                        4
SWH               25125.629 Hz
FIDRES            0.383387 Hz
AQ                1.3042164 sec
RG                    16384
DW                   19.900 usec
DE                    6.00 usec
TE                   300.0 K
D1                2.00000000 sec
d11               0.03000000 sec
d12               0.00002000 sec

========== CHANNEL f1 ==========
NUC1                     13C
P1                     16.35 usec
PL1                    -6.00 dB
SFO1           100.6237959 MHz

========== CHANNEL f2 ==========
CPDPRG2               waltz16
NUC2                      1H
PCPD2                 114.00 usec
PL2                    0.00 dB
PL12                  24.00 dB
PL13                  24.00 dB
SFO2           400.1316005 MHz

F2 - Processing parameters
SI                     32768
SF             100.6128137 MHz
WDW                       no
SSB                        0
LB                      0.00 Hz
GB                         0
PC                      1.40

1D NMR plot parameters
CX                     20.00 cm
F1P                   230.000 ppm
F1                  23140.95 Hz
F2P                   -10.000 ppm
F2                  -1006.13 Hz
PPMCM                 12.00000 ppm/cm
HZCM                1207.35376 Hz/cm
```

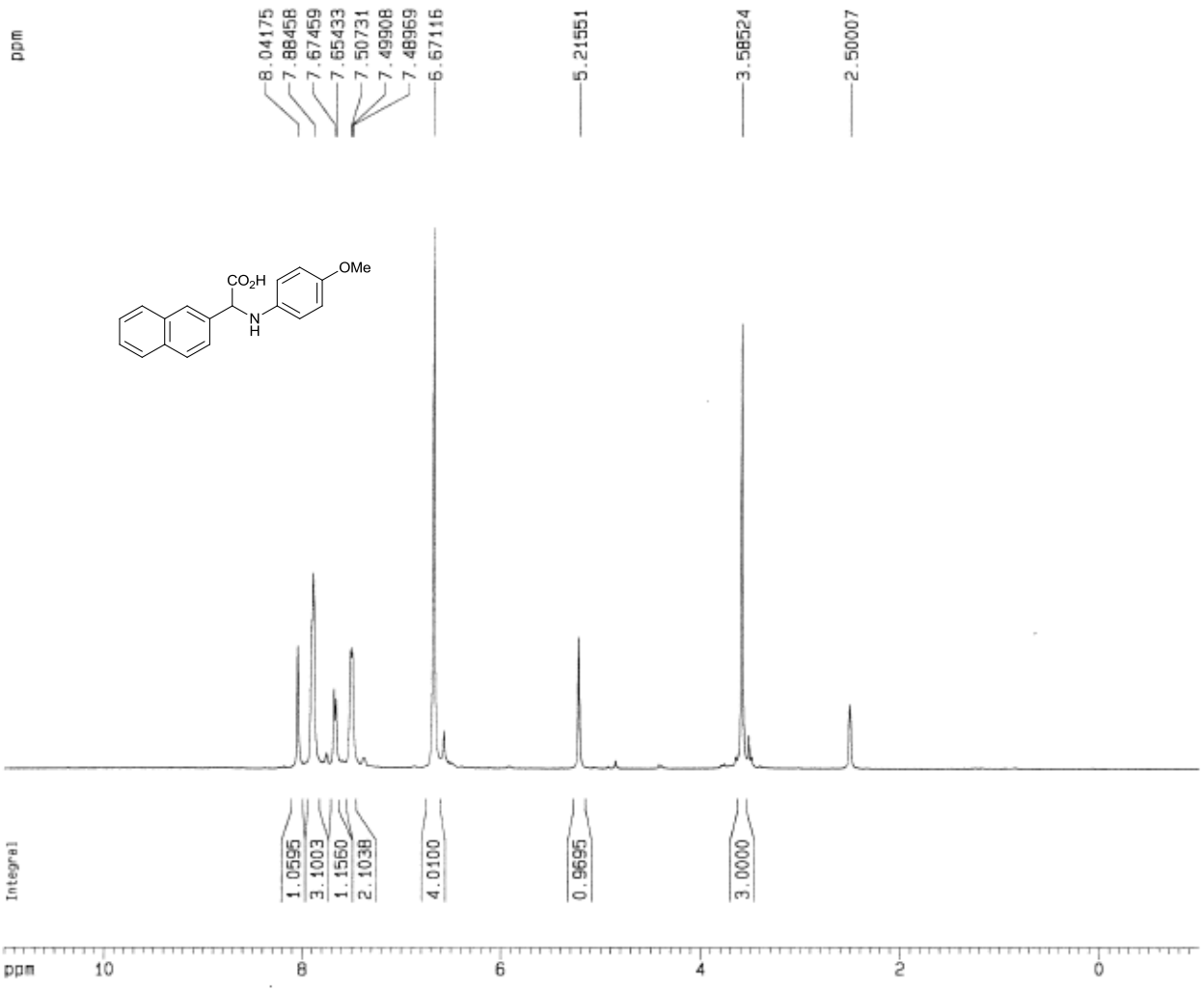


```
Current Data Parameters
NAME                  2_Nap
EXPNO                     1
PROCNO                    1

F2 - Acquisition Parameters
Date_              20121106
Time                  9.50
INSTRUM               spect
PROBHD     5 mm BBI 1H-
PULPROG                zg30
TD                    65536
SOLVENT                DMSO
NS                       16
DS                        2
SWH                8278.146 Hz
FIDRES            0.126314 Hz
AQ                3.9584243 sec
RG                    228.1
DW                   60.400 usec
DE                    6.00 usec
TE                   300.0 K
D1                1.00000000 sec

============ CHANNEL f1 =========
NUC1                      1H
P1                     6.45 usec
PL1                    0.00 dB
SFO1            400.1324710 MHz

F2 - Processing parameters
SI                     32768
SF              400.1300029 MHz
WDW                       no
SSB                        0
LB                     0.00 Hz
GB                         0
PC                     1.00

1D NMR plot parameters
CX                    20.00 cm
F1P                  11.000 ppm
F1                  4401.43 Hz
F2P                  -1.000 ppm
F2                  -400.13 Hz
PPMCM                0.60000 ppm/cm
HZCM               240.07800 Hz/cm
```

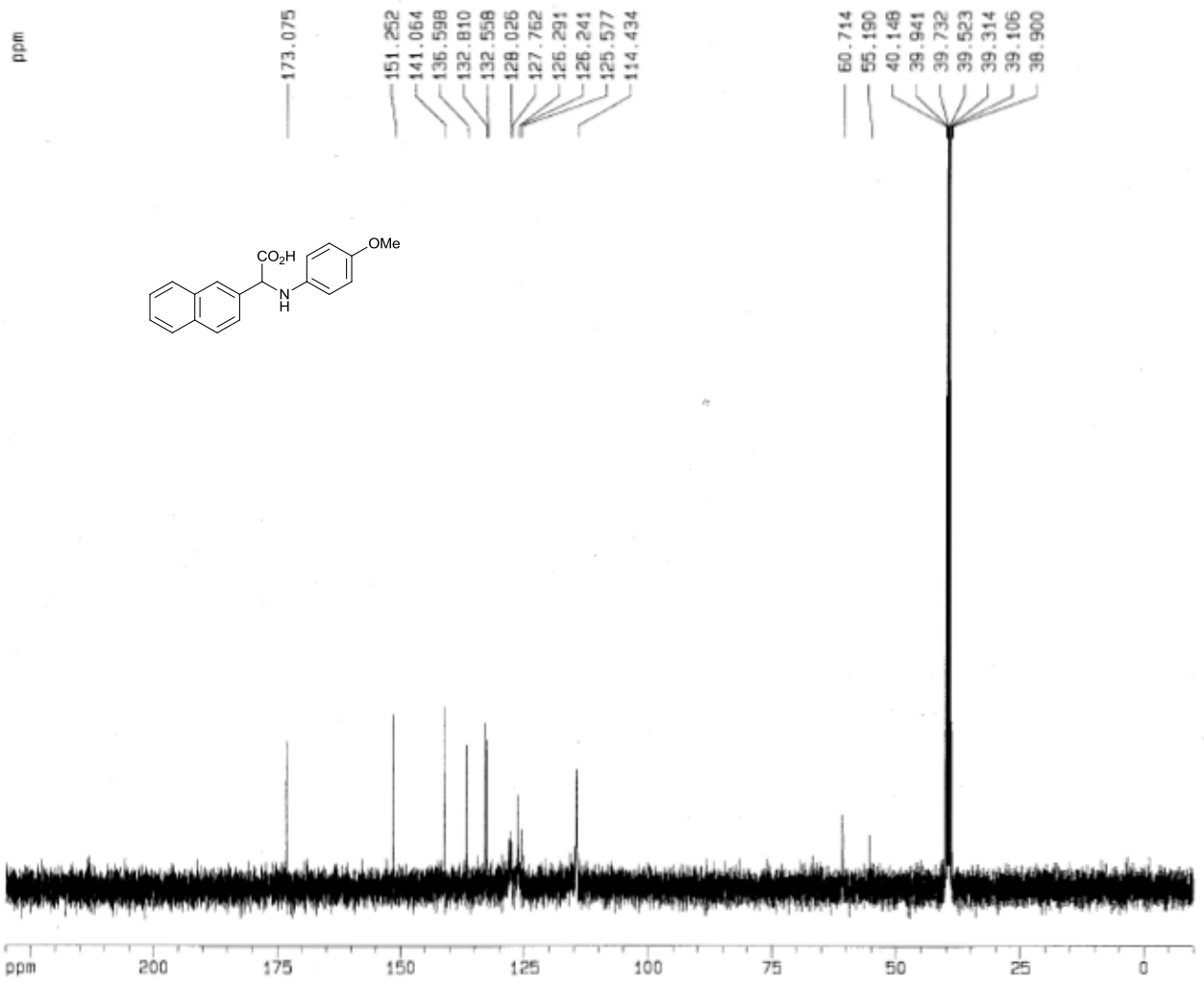


```
Current Data Parameters
NAME                  2_Nap
EXPNO                     2
PROCNO                    1

F2 - Acquisition Parameters
Date_              20121106
Time                  13.06
INSTRUM               spect
PROBHD     5 mm BBI 1H-
PULPROG               zgpg30
TD                     65536
SOLVENT                DMSO
NS                      1024
DS                         4
SWH               25125.629 Hz
FIDRES            0.383387 Hz
AQ                1.3042164 sec
RG                     16384
DW                   19.900 usec
DE                    6.00 usec
TE                   300.0 K
D1                2.00000000 sec
D11               0.03000000 sec
D12               0.00002000 sec

========== CHANNEL f1 ==========
NUC1                     13C
P1                     16.35 usec
PL1                    -6.00 dB
SFO1           100.6237959 MHz

========== CHANNEL f2 ==========
CPDPRG2               waltz16
NUC2                       1H
PCPD2                 114.00 usec
PL2                    0.00 dB
PL12                  24.00 dB
PL13                  24.00 dB
SFO2           400.1316005 MHz

F2 - Processing parameters
SI                       32768
SF             100.6128145 MHz
WDW                         no
SSB                          0
LB                        0.00 Hz
GB                           0
PC                        1.40

1D NMR plot parameters
CX                       20.00 cm
F1P                     230.000 ppm
F1                    23140.95 Hz
F2P                    -10.000 ppm
F2                    -1006.13 Hz
PPMCM                 12.00000 ppm/cm
HZCM                1207.35376 Hz/cm
```

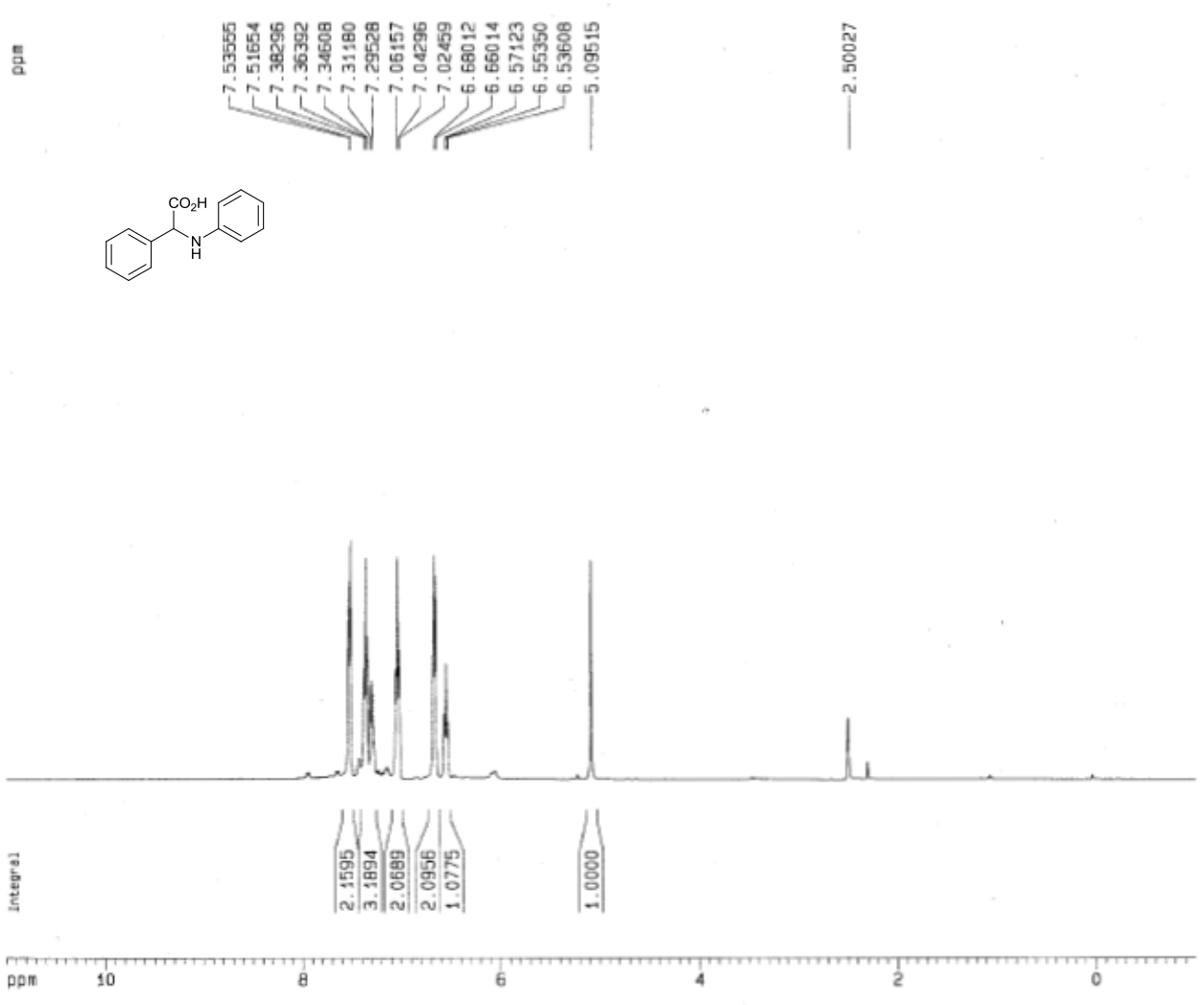


```
Current Data Parameters
NAME                  aas_02_01
EXPNO                         3
PROCNO                        1

F2 - Acquisition Parameters
Date_                  20130104
Time                      16.56
INSTRUM                   spect
PROBHD     5 mm BBI 1H-
PULPROG                   zg30
TD                       65536
SOLVENT                   DMSO
NS                           16
DS                            2
SWH                 8278.146 Hz
FIDRES              0.126314 Hz
AQ                  3.9584243 sec
RG                       203.2
DW                    60.400 usec
DE                     6.00 usec
TE                     300.0 K
D1                 1.00000000 sec

========== CHANNEL f1 ========
NUC1                      1H
P1                     6.45 usec
PL1                    0.00 dB
SFO1             400.1324710 MHz

F2 - Processing parameters
SI                       32768
SF                400.1300021 MHz
WDW                         no
SSB                          0
LB                     0.00 Hz
GB                           0
PC                        1.00

1D NMR plot parameters
CX                    20.00 cm
F1P                   11.000 ppm
F1                   4401.43 Hz
F2P                  -1.000 ppm
F2                   -400.13 Hz
PPMCM                0.60000 ppm/cm
HZCM               240.07800 Hz/cm
```

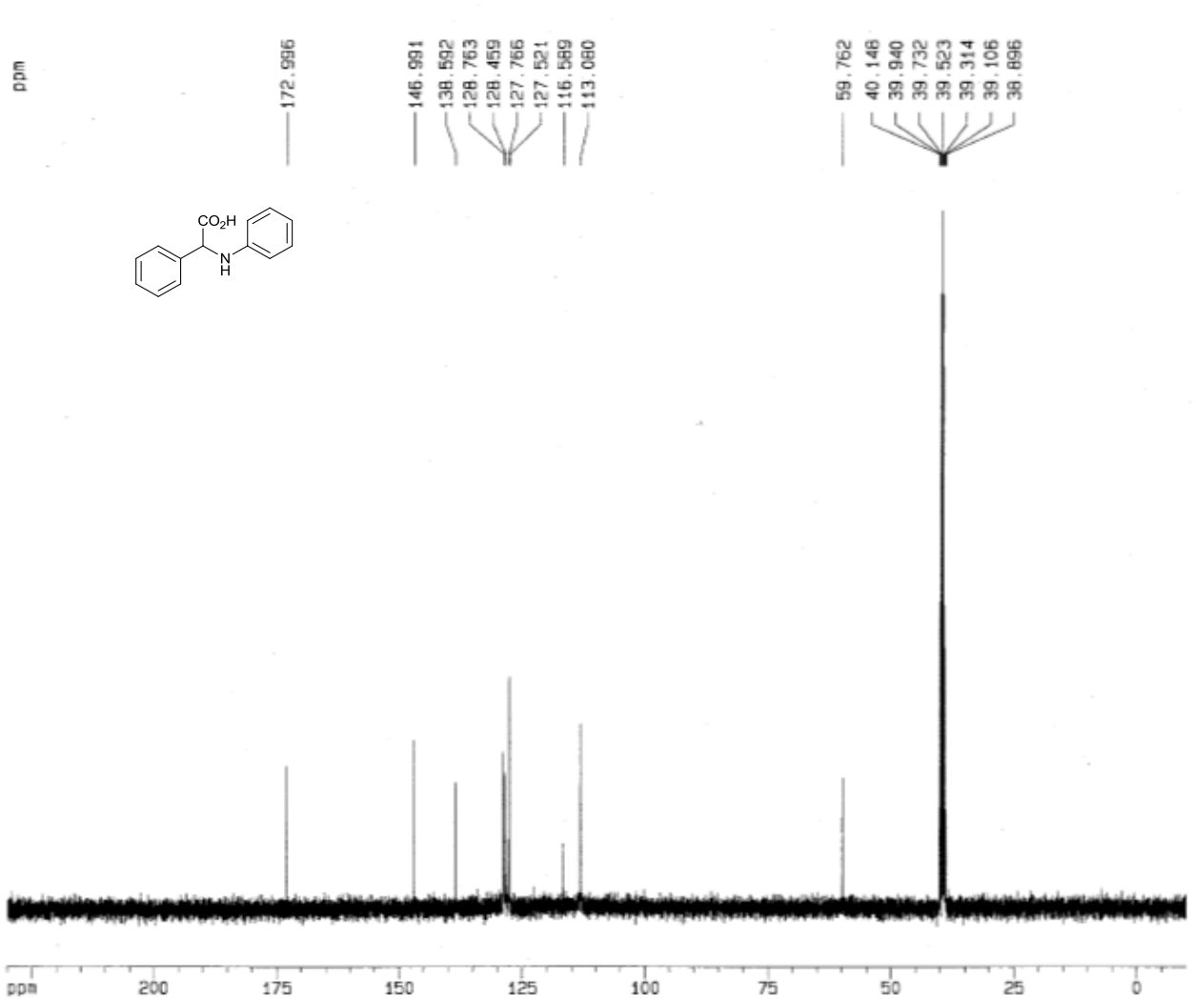


```
Current Data Parameters
NAME                  aes_02_01
EXPNO                         4
PROCNO                        1

F2 - Acquisition Parameters
Date_               20130104
Time                     17.06
INSTRUM                  spect
PROBHD     5 mm BBI 1H-
PULPROG                 zgpg30
TD                       65536
SOLVENT                   CDCl3
NS                         1024
DS                            4
SWH                  25125.529 Hz
FIDRES               0.383387 Hz
AQ                   1.3042164 sec
RG                       16384
DW                      19.900 usec
DE                       6.00 usec
TE                      300.0 K
D1                   2.00000000 sec
d11                  0.03000000 sec
d12                  0.00002000 sec

============ CHANNEL f1 ============
NUC1                      13C
P1                      16.35 usec
PL1                     -6.00 dB
SFO1                100.6237958 MHz

------------ CHANNEL f2 ------------
CPDPRG2                 waltz16
NUC2                        1H
PCPD2                   114.00 usec
PL2                       0.00 dB
PL12                     24.00 dB
PL13                     24.00 dB
SFO2                400.1315005 MHz

F2 - Processing parameters
SI                        32768
SF                  100.6128145 MHz
WDW                          no
SSB                           0
LB                       0.00 Hz
GB                            0
PC                        1.40

1D NMR plot parameters
CX                       20.00 cm
F1P                     230.000 ppm
F1                    23140.95 Hz
F2P                     -10.000 ppm
F2                    -1006.13 Hz
PPMCM                 12.00000 ppm/cm
HZCM                1207.35376 Hz/cm
```

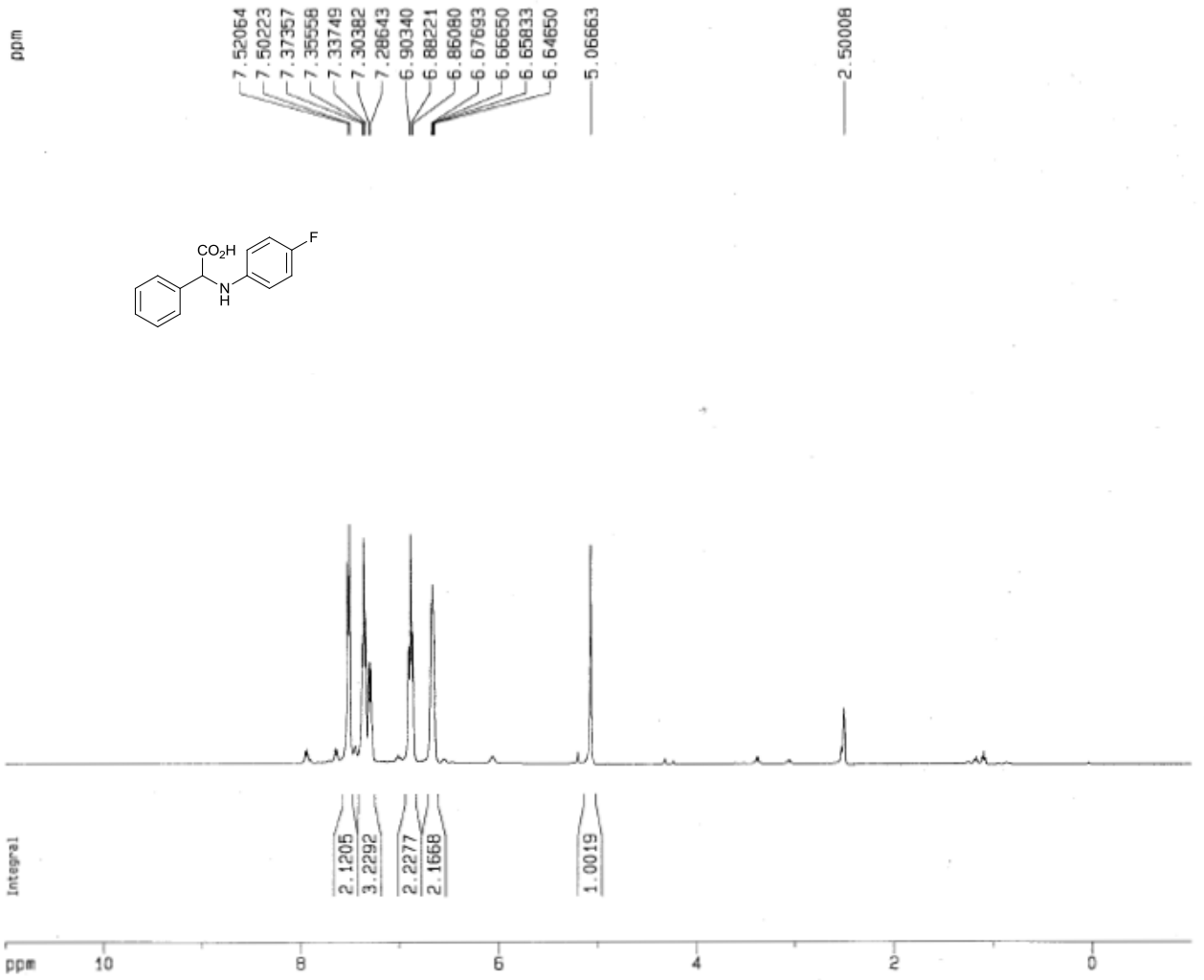


```
Current Data Parameters
NAME        p_fanil_acid
EXPNO                  1
PROCNO                 1

F2 - Acquisition Parameters
Date_           20130101
Time               11.13
INSTRUM            spect
PROBHD     5 mm BBI 1H-
PULPROG             zg30
TD                 65536
SOLVENT             DMSO
NS                    16
DS                     2
SWH             8278.146 Hz
FIDRES          0.126314 Hz
AQ              3.9584243 sec
RG                  45.3
DW                 60.400 usec
DE                  6.00 usec
TE                 300.0 K
D1             1.00000000 sec

============ CHANNEL f1 ========
NUC1                   1H
P1                  6.45 usec
PL1                 0.00 dB
SFO1         400.1324710 MHz

F2 - Processing parameters
SI                  32768
SF           400.1300029 MHz
WDW                    no
SSB                     0
LB                   0.00 Hz
GB                      0
PC                   1.00

1D NMR plot parameters
CX                  20.00 cm
F1P                11.000 ppm
F1                4401.43 Hz
F2P                -1.000 ppm
F2                -400.13 Hz
PPMCM             0.60000 ppm/cm
HZCM            240.07800 Hz/cm
```

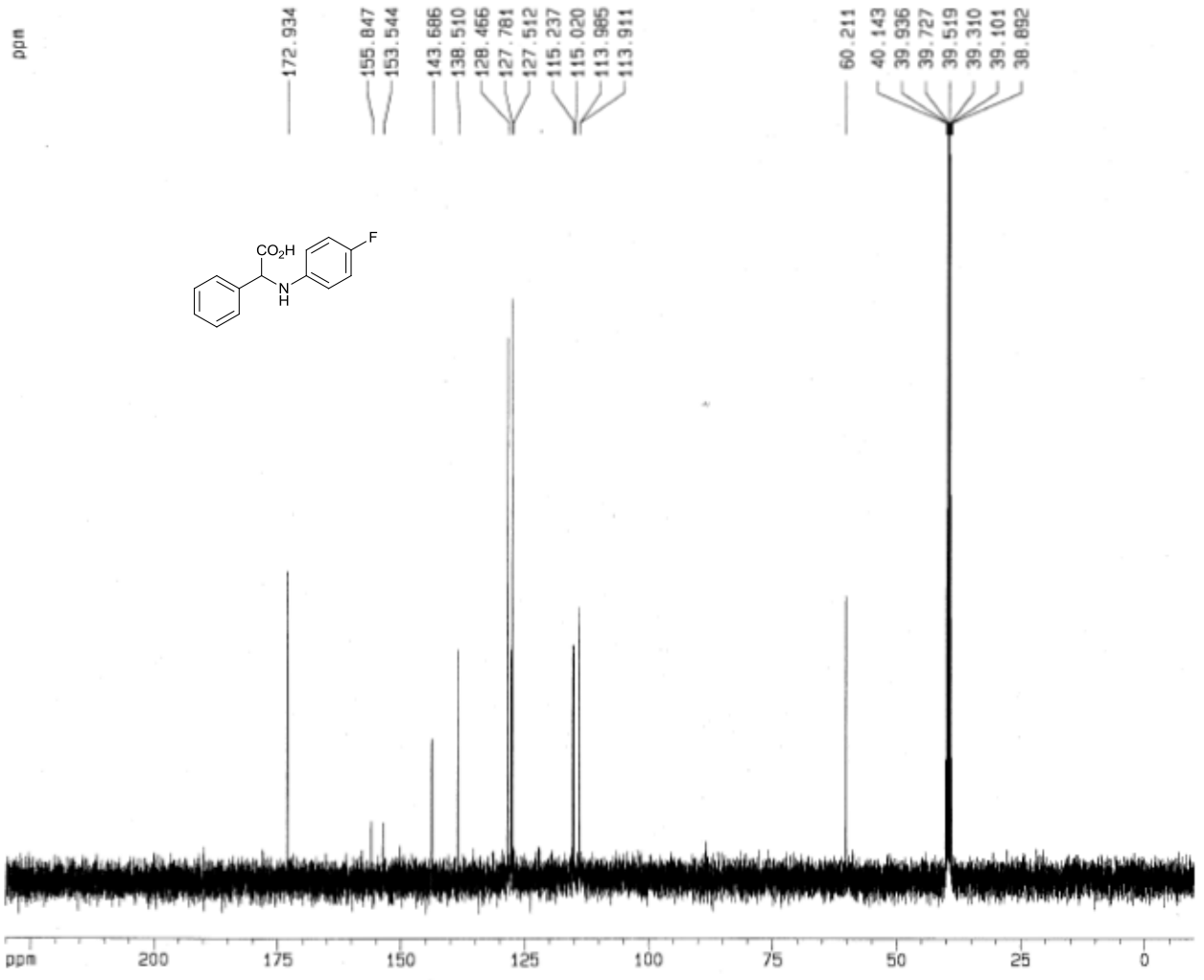


```
Current Data Parameters
NAME        p_fenil_acid
EXPNO                  2
PROCNO                 1

F2 - Acquisition Parameters
Date_           20130101
Time               11.53
INSTRUM            spect
PROBHD     5 mm BBI 1H-
PULPROG          zgpg30
TD                65536
SOLVENT            DMSO
NS                   606
DS                     4
SWH            25125.629 Hz
FIDRES         0.383387 Hz
AQ             1.3042164 sec
RG                 16384
DW                19.900 usec
DE                 6.00 usec
TE                300.0 K
D1             2.00000000 sec
d11            0.03000000 sec
d12            0.00002000 sec

========== CHANNEL f1 ==========
NUC1                13C
P1                16.35 usec
PL1               -6.00 dB
SFO1         100.6237959 MHz

========== CHANNEL f2 ==========
CPDPRG2         waltz16
NUC2                1H
PCPD2             114.00 usec
PL2                0.00 dB
PL12              24.00 dB
PL13              24.00 dB
SFO2         400.1316005 MHz

F2 - Processing parameters
SI                 32768
SF           100.6128137 MHz
WDW                   no
SSB                    0
LB                 0.00 Hz
GB                     0
PC                 1.40

1D NMR plot parameters
CX                20.00 cm
F1P              230.000 ppm
F1             23140.95 Hz
F2P              -10.000 ppm
F2             -1006.13 Hz
PPMCM          12.00000 ppm/cm
HZCM         1207.35376 Hz/cm
```

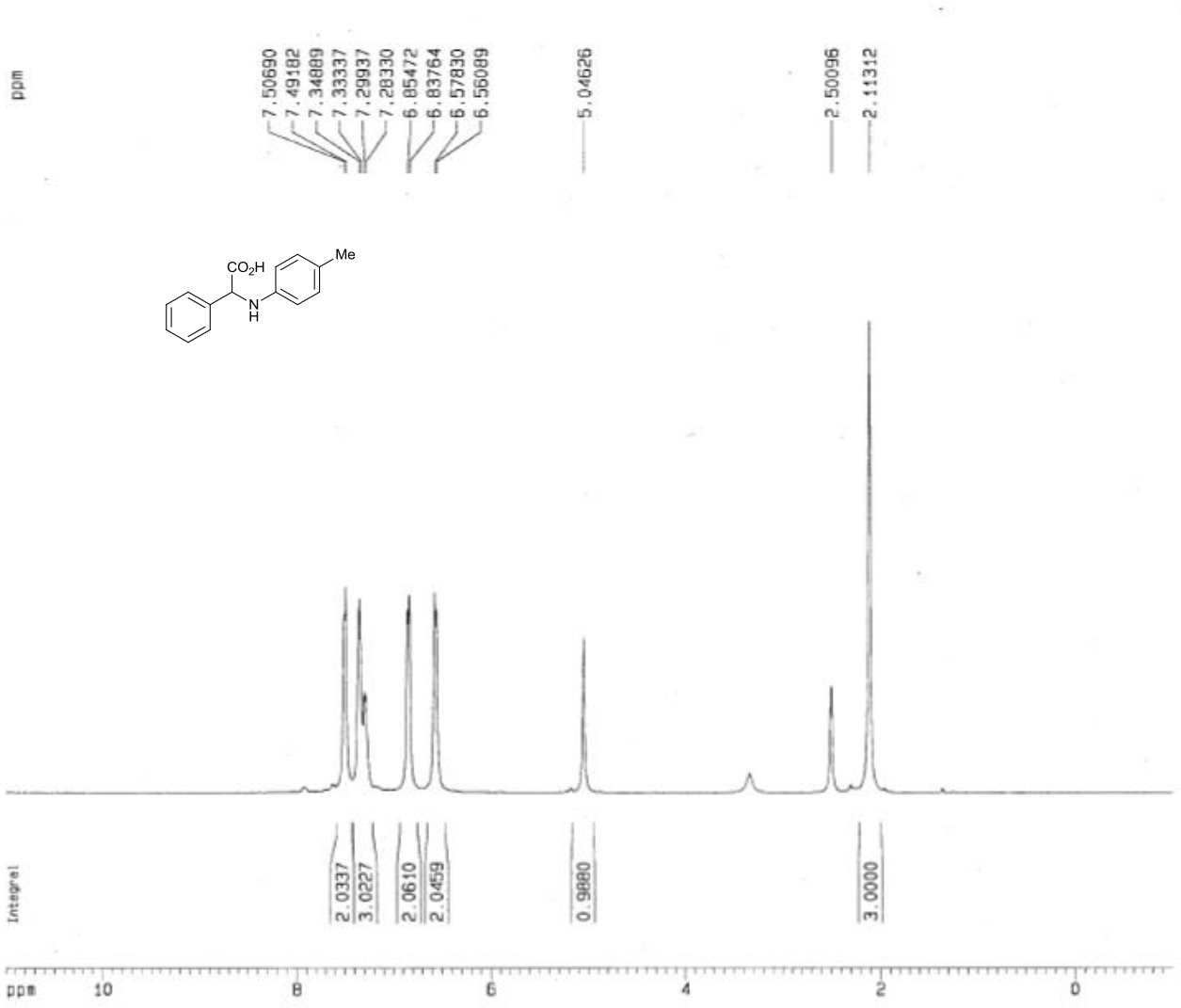


```
Current Data Parameters
NAME                AAS_02_03
EXPNO                       2
PROCNO                      1

F2 - Acquisition Parameters
Date_              20130108
Time                  14.01
INSTRUM                spect
PROBHD     5 mm BBI 1H-
PULPROG                zg30
TD                    65536
SOLVENT                DMSO
NS                        16
DS                         2
SWH               8278.146 Hz
FIDRES            0.126314 Hz
AQ                3.9584243 sec
RG                      114
DW                 60.400 usec
DE                  6.00 usec
TE                 300.0 K
D1                1.00000000 sec

============ CHANNEL f1 =========
NUC1                       1H
P1                       6.45 usec
PL1                      0.00 dB
SFO1              400.1324710 MHz

F2 - Processing parameters
SI                        32768
SF                400.1300021 MHz
WDW                         no
SSB                          0
LB                        0.00 Hz
GB                           0
PC                        1.00

1D NMR plot parameters
CX                       20.00 cm
F1P                      11.000 ppm
F1                     4401.43 Hz
F2P                      -1.000 ppm
F2                     -400.13 Hz
PPMCM                 0.60000 ppm/cm
HZCM                240.07800 Hz/cm
```

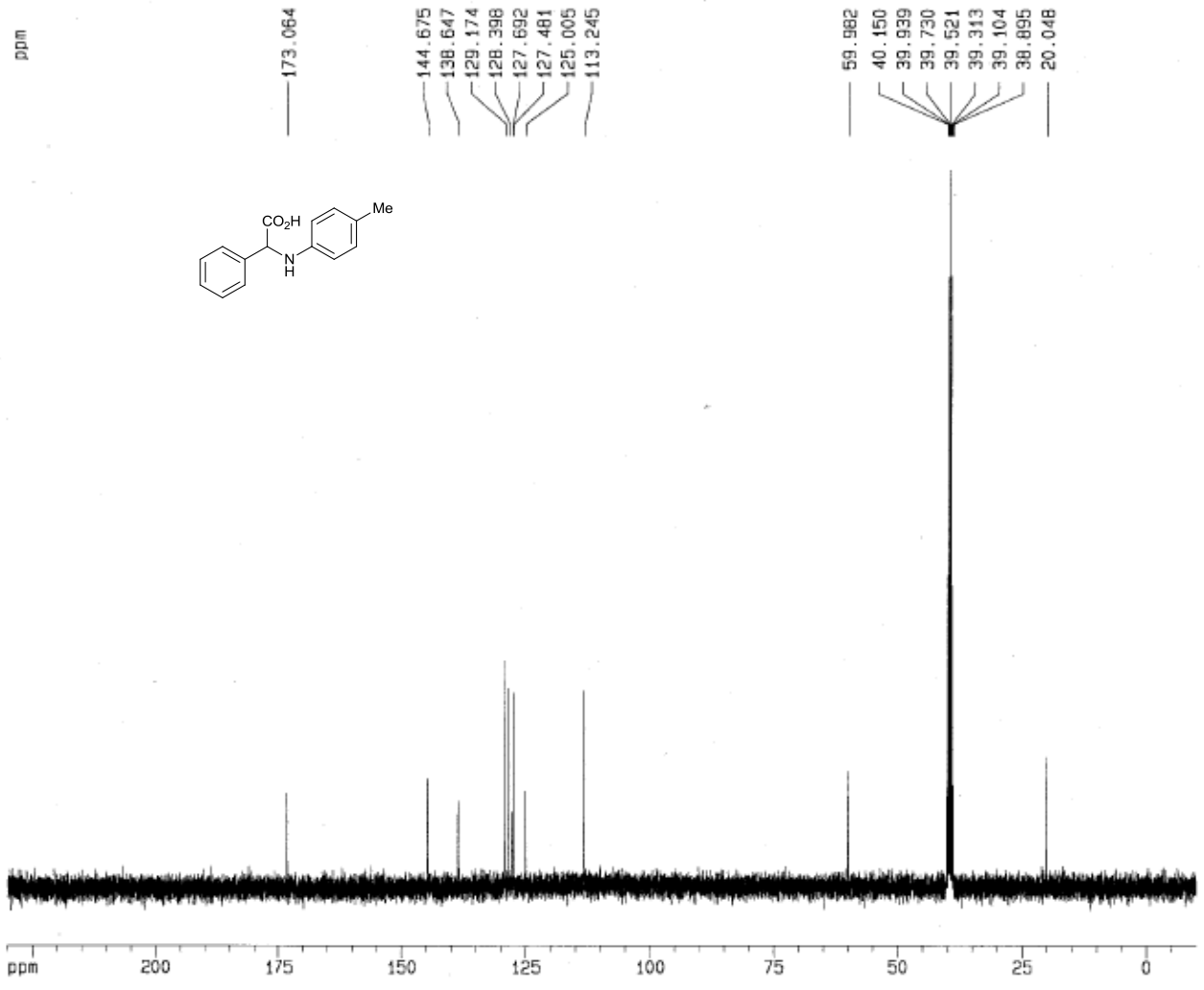


```
Current Data Parameters
NAME            AAS_02_03
EXPNO                   3
PROCNO                  1

F2 - Acquisition Parameters
Date_          20130108
Time               15.02
INSTRUM            spect
PROBHD     5 mm BBI 1H-
PULPROG          zgpg30
TD                65536
SOLVENT            DMSO
NS                 1024
DS                    4
SWH           25125.629 Hz
FIDRES        0.383387 Hz
AQ            1.3042164 sec
RG                16384
DW               19.900 usec
DE                6.00 usec
TE               300.0 K
D1            2.00000000 sec
d11           0.03000000 sec
d12           0.00002000 sec

========== CHANNEL f1 ==========
NUC1               13C
P1               16.35 usec
PL1              -6.00 dB
SFO1         100.6237959 MHz

========== CHANNEL f2 ==========
CPDPRG2          waltz16
NUC2               1H
PCPD2            114.00 usec
PL2               0.00 dB
PL12             24.00 dB
PL13             24.00 dB
SFO2         400.1316005 MHz

F2 - Processing parameters
SI                32768
SF           100.6128160 MHz
WDW                  no
SSB                   0
LB                 0.00 Hz
GB                    0
PC                 1.40

1D NMR plot parameters
CX                20.00 cm
F1P              230.000 ppm
F1            23140.95 Hz
F2P              -10.000 ppm
F2            -1006.13 Hz
PPMCM            12.00000 ppm/cm
HZCM          1207.35376 Hz/cm
```

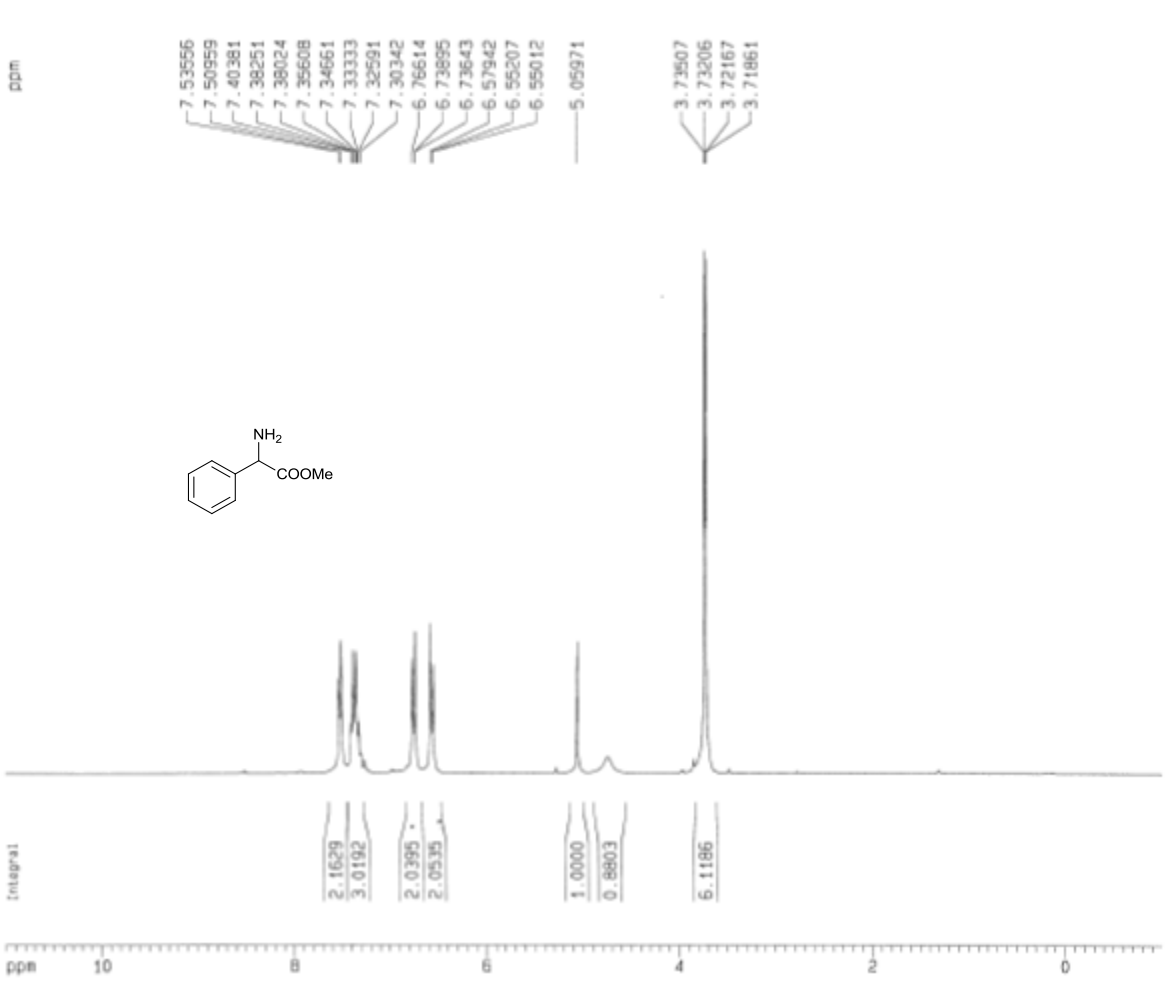


```
Current Data Parameters
NAME      AAS_01_01_25_2
EXPNO                  1
PROCNO                 1

F2 - Acquisition Parameters
Date_           20130204
Time               20.18
INSTRUM            spect
PROBHD     5 mm QNP 1H/1
PULPROG            zg30
TD                65536
SOLVENT           CDCl3
NS                    16
DS                     2
SWH            6172.839 Hz
FIDRES         0.094190 Hz
AQ             5.3084660 sec
RG                  80.6
DW                81.000 usec
DE                 6.00 usec
TE                300.0 K
D1             1.00000000 sec

========== CHANNEL f1 =========
NUC1                  1H
P1                 12.10 usec
PL1                 0.00 dB
SFO1          299.8718518 MHz

F2 - Processing parameters
SI                 32768
SF           299.8700093 MHz
WDW                   no
SSB                    0
LB                  0.00 Hz
GB                     0
PC                  1.00

1D NMR plot parameters
CX                 20.00 cm
F1P               11.000 ppm
F1                3298.57 Hz
F2P               -1.000 ppm
F2                -299.87 Hz
PPMCM             0.60000 ppm/cm
HZCM            179.92200 Hz/cm
```

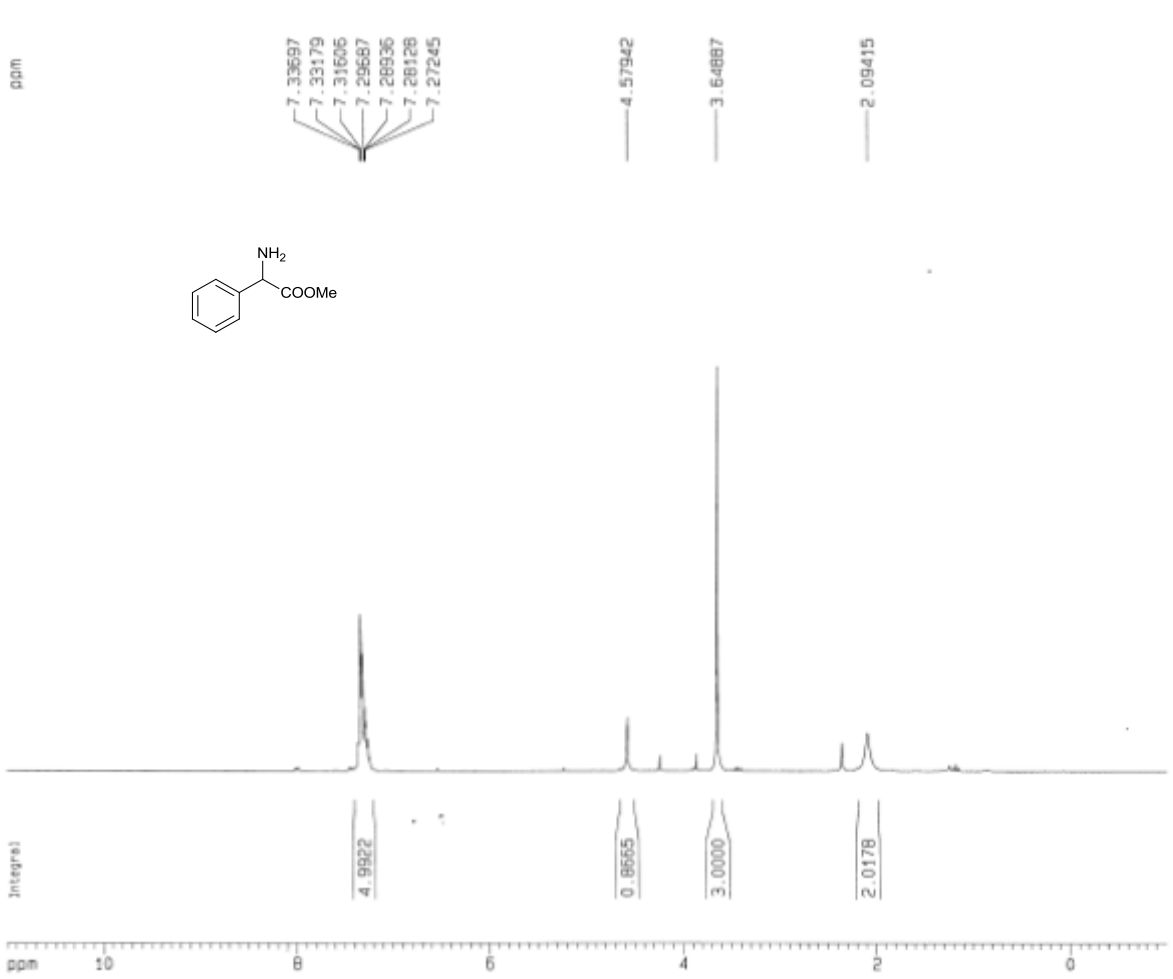

Current Data Parameters
NAME AAS_01_01_25_3
EXPNO 2
PROCNO 1

F2 - Acquisition Parameters
Date_ 20130205
Time 16.21
INSTRUM spect
PROBHD 5 mm QNP 1H/1
PULPROG zg30
TD 65536
SOLVENT CDCl3
NS 16
DS 2
SWH 6172.839 Hz
FIDRES 0.094190 Hz
AQ 5.3084660 sec
RG 64
DW 81.000 usec
DE 6.00 usec
TE 300.0 K
D1 1.00000000 sec

========== CHANNEL f1 ==========
NUC1 1H
P1 12.10 usec
PL1 0.00 dB
SFO1 299.8718518 MHz

F2 - Processing parameters
SI 32768
SF 299.8700082 MHz
WDW no
SSB 0
LB 0.00 Hz
GB 0
PC 1.00

1D NMR plot parameters
CX 20.00 cm
F1P 11.000 ppm
F1 3298.57 Hz
F2P -1.000 ppm
F2 -299.87 Hz
PPMCM 0.60000 ppm/cm
HZCM 179.92200 Hz/cm

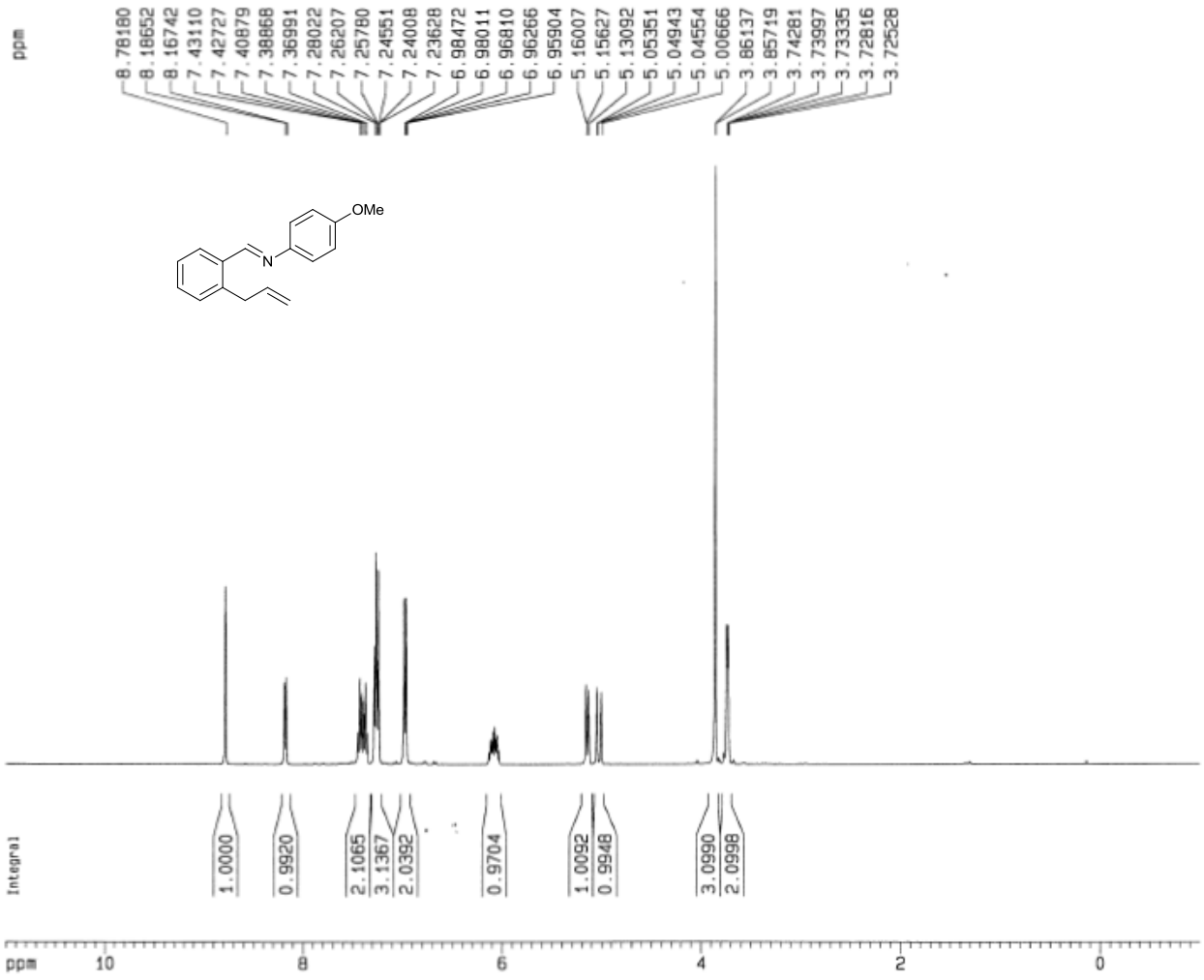


```
Current Data Parameters
NAME                  im
EXPNO                  4
PROCNO                 1

F2 - Acquisition Parameters
Date_           20130312
Time               10.29
INSTRUM            spect
PROBHD     5 mm BBI 1H-
PULPROG             zg30
TD                 65536
SOLVENT            CDCl3
NS                    16
DS                     2
SWH              8278.146 Hz
FIDRES           0.126314 Hz
AQ               3.9584243 sec
RG                  35.9
DW                 60.400 usec
DE                  6.00 usec
TE                300.0 K
D1             1.00000000 sec

============ CHANNEL f1 =========
NUC1                   1H
P1                  6.45 usec
PL1                 0.00 dB
SFO1          400.1324710 MHz

F2 - Processing parameters
SI                 32768
SF            400.1300000 MHz
WDW                   no
SSB                    0
LB                  0.00 Hz
GB                     0
PC                  1.00

1D NMR plot parameters
CX                 20.00 cm
F1P                11.000 ppm
F1               4401.43 Hz
F2P                -1.000 ppm
F2               -400.13 Hz
PPMCM              0.60000 ppm/cm
HZCM             240.07800 Hz/cm
```

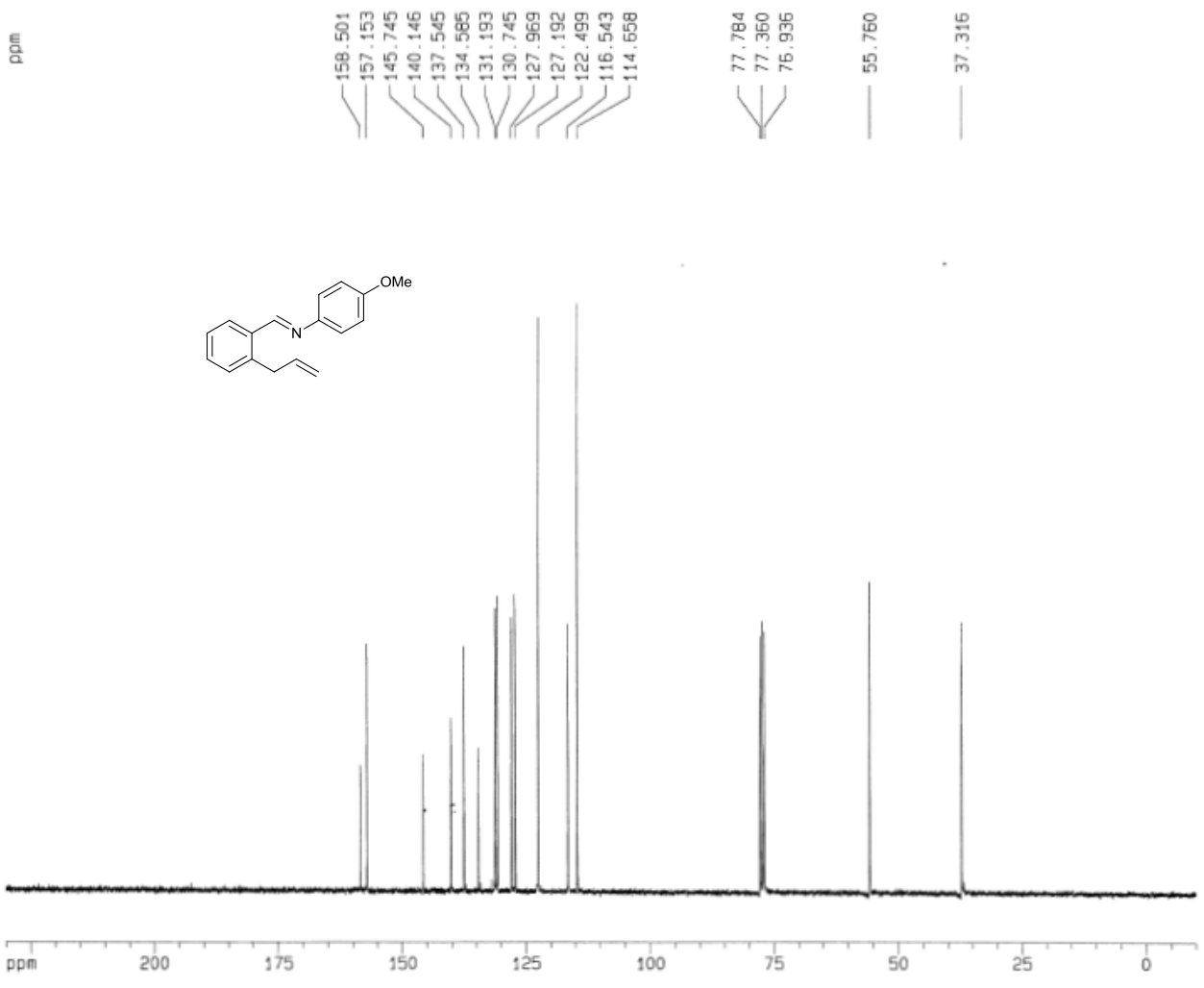


```
Current Data Parameters
NAME      2-allylbenzpnp
EXPNO                  5
PROCNO                 1

F2 - Acquisition Parameters
Date_           20130306
Time               14.38
INSTRUM            spect
PROBHD    5 mm QNP 1H/1
PULPROG          zgpg30
TD                65536
SOLVENT            CDCl3
NS                   421
DS                     4
SWH          18796.992 Hz
FIDRES        0.286819 Hz
AQ            1.7433076 sec
RG                812.7
DW               26.600 usec
DE                6.00 usec
TE               300.0 K
D1           2.00000000 sec
D11          0.03000000 sec
D12          0.00002000 sec

============ CHANNEL f1 ============
NUC1                13C
P1                 5.25 usec
PL1               -6.00 dB
SFO1         75.4106357 MHz

============ CHANNEL f2 ============
CPDPRG2         waltz16
NUC2                1H
PCPD2             115.00 usec
PL2                0.00 dB
PL12              19.70 dB
PL13              19.70 dB
SFO2         299.8711995 MHz

F2 - Processing parameters
SI                 32768
SF           75.4023549 MHz
WDW                   EM
SSB                    0
LB                  1.00 Hz
GB                     0
PC                  1.40

1D NMR plot parameters
CX                 20.00 cm
F1P               230.000 ppm
F1              17342.54 Hz
F2P               -10.000 ppm
F2               -754.02 Hz
PPMCM             12.00000 ppm/cm
HZCM            904.82825 Hz/cm
```

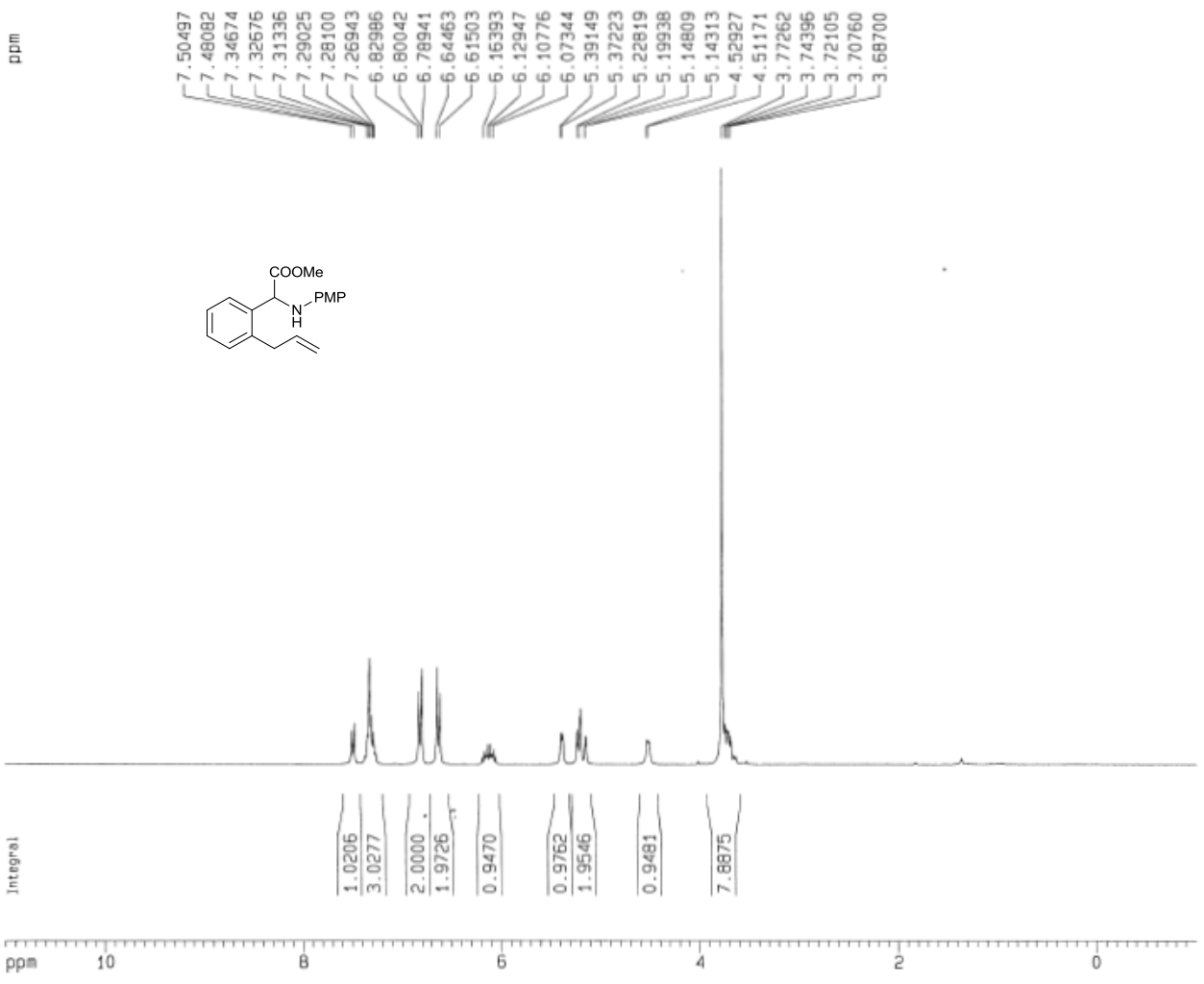


```
Current Data Parameters
NAME            AAS_15_Me
EXPNO                   1
PROCNO                  7

F2 - Acquisition Parameters
Date_            20130313
Time                15.41
INSTRUM             spect
PROBHD    5 mm QNP 1H/1
PULPROG              zg30
TD                  65536
SOLVENT             CDCl3
NS                     16
DS                      2
SWH              6172.839 Hz
FIDRES           0.094190 Hz
AQ               5.3084660 sec
RG                   50.8
DW                 81.000 usec
DE                  6.00 usec
TE                 300.0 K
D1              1.00000000 sec

============ CHANNEL f1 =========
NUC1                   1H
P1                  12.10 usec
PL1                  0.00 dB
SFO1          299.8718518 MHz

F2 - Processing parameters
SI                  32768
SF            299.8700000 MHz
WDW                    no
SSB                     0
LB                   0.00 Hz
GB                      0
PC                   1.00

1D NMR plot parameters
CX                  20.00 cm
F1P                11.000 ppm
F1                3298.57 Hz
F2P                -1.000 ppm
F2                -299.87 Hz
PPMCM             0.60000 ppm/cm
HZCM            179.92200 Hz/cm
```

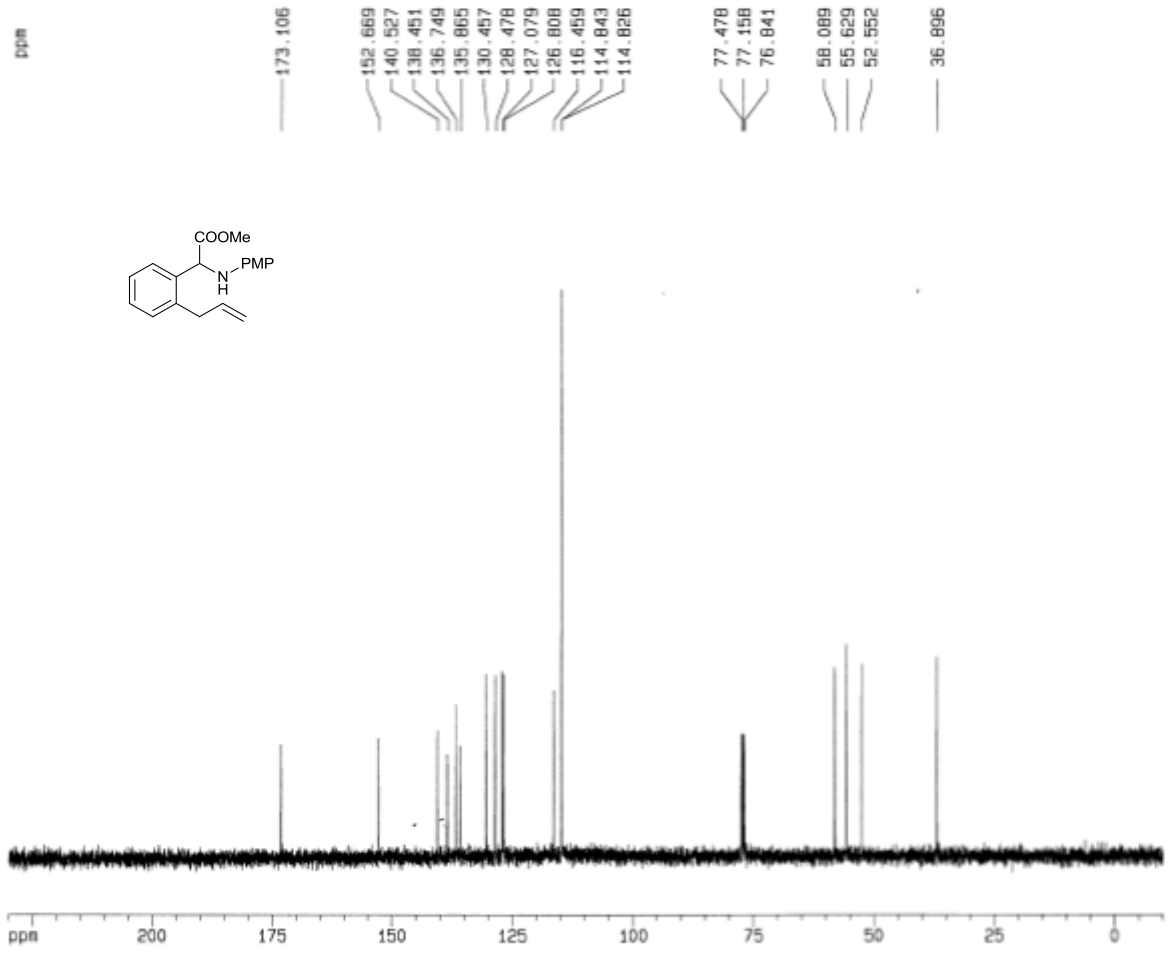


```
Current Data Parameters
NAME            aas_15_Me
EXPNO                    3
PROCNO                   1

F2 - Acquisition Parameters
Date_          20130313
Time               16.35
INSTRUM            spect
PROBHD     5 mm BBI 1H-
PULPROG          zgpg30
TD                65536
SOLVENT             CDCl3
NS                     80
DS                      4
SWH            25125.629 Hz
FIDRES         0.383387 Hz
AQ             1.3042164 sec
RG                   8192
DW                19.900 usec
DE                 6.00 usec
TE                300.0 K
D1             2.00000000 sec
d11            0.03000000 sec
d12            0.00002000 sec

============ CHANNEL f1 ============
NUC1                  13C
P1                  16.35 usec
PL1                 -6.00 dB
SFO1          100.6237959 MHz

============ CHANNEL f2 ============
CPDPRG2          waltz16
NUC2                  1H
PCPD2              114.00 usec
PL2                 0.00 dB
PL12               24.00 dB
PL13               24.00 dB
SFO2          400.1316005 MHz

F2 - Processing parameters
SI                    32768
SF            100.6127731 MHz
WDW                      EM
SSB                       0
LB                     1.00 Hz
GB                        0
PC                     1.40

1D NMR plot parameters
CX                    20.00 cm
F1P                  230.000 ppm
F1                 23140.94 Hz
F2P                  -10.000 ppm
F2                 -1006.13 Hz
PPMCM                12.00000 ppm/cm
HZCM               1207.35327 Hz/cm
```

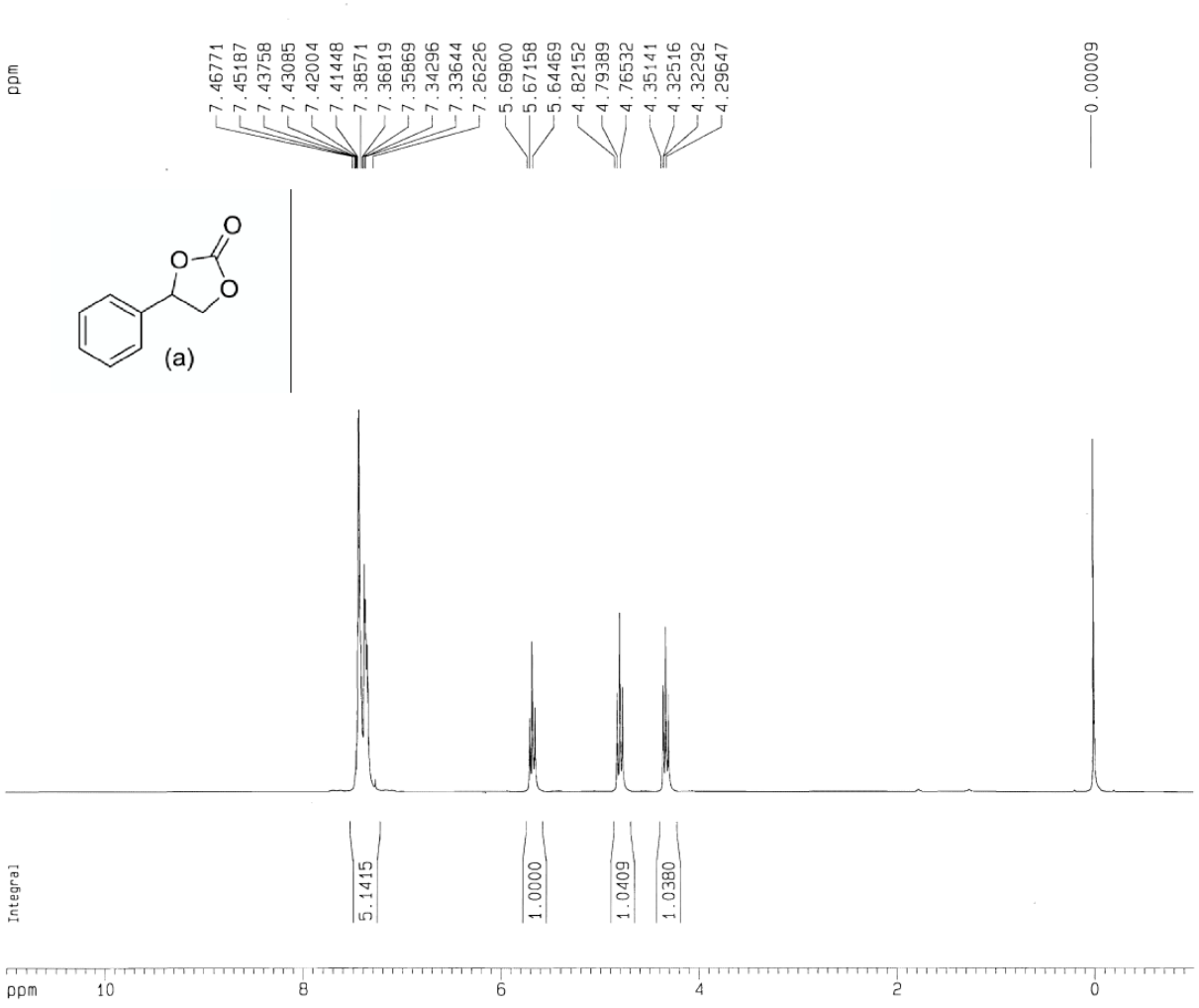


```
Current Data Parameters
NAME          styrenecarb
EXPNO                   7
PROCNO                  1

F2 - Acquisition Parameters
Date_            20151207
Time                17.45
INSTRUM             spect
PROBHD     5 mm QNP 1H/1
PULPROG             zg30
TD                 65536
SOLVENT            CDCl3
NS                    16
DS                     2
SWH             6172.839 Hz
FIDRES          0.094190 Hz
AQ              5.3084660 sec
RG                  80.6
DW                81.000 usec
DE                 6.00 usec
TE                300.0 K
D1             1.00000000 sec

============ CHANNEL f1 ========
NUC1                   1H
P1                  12.10 usec
PL1                  0.00 dB
SFO1          299.8718518 MHz

F2 - Processing parameters
SI                 32768
SF           299.8700089 MHz
WDW                   no
SSB                    0
LB                  0.00 Hz
GB                     0
PC                  1.00

1D NMR plot parameters
CX                 20.00 cm
F1P               11.000 ppm
F1              3298.57 Hz
F2P               -1.000 ppm
F2              -299.87 Hz
PPMCM           0.60000 ppm/cm
HZCM          179.92200 Hz/cm
```

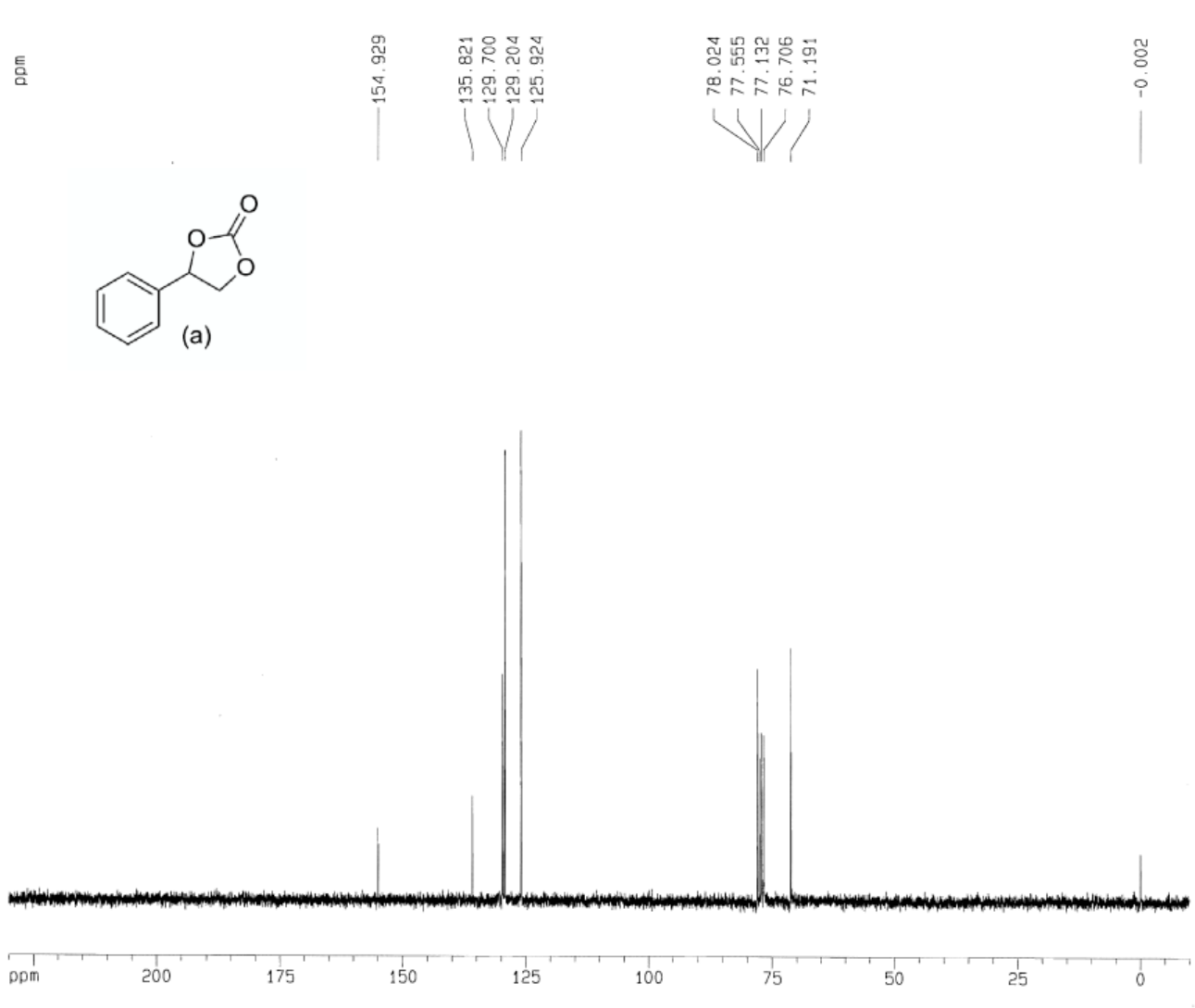


```
Current Data Parameters
NAME          styrenecarb
EXPNO                   8
PROCNO                  1

F2 - Acquisition Parameters
Date_              20151207
Time                  17.49
INSTRUM               spect
PROBHD    5 mm QNP 1H/1
PULPROG             zgpg30
TD                   65536
SOLVENT              CDCl3
NS                      28
DS                       4
SWH               18796.992 Hz
FIDRES            0.286819 Hz
AQ                1.7433076 sec
RG                    4096
DW                  26.600 usec
DE                   6.00 usec
TE                  300.0 K
D1                2.00000000 sec
D11               0.03000000 sec
D12               0.00002000 sec

============ CHANNEL f1 =========
NUC1                   13C
P1                    5.25 usec
PL1                  -6.00 dB
SFO1             75.4106357 MHz

============ CHANNEL f2 =========
CPDPRG2             waltz16
NUC2                   1H
PCPD2                115.00 usec
PL2                   0.00 dB
PL12                 19.70 dB
PL13                 19.70 dB
SFO2            299.8711995 MHz

F2 - Processing parameters
SI                    32768
SF               75.4023753 MHz
WDW                      EM
SSB                       0
LB                     1.00 Hz
GB                        0
PC                     1.40

1D NMR plot parameters
CX                    20.00 cm
F1P                  230.000 ppm
F1                 17342.54 Hz
F2P                  -10.000 ppm
F2                 -754.02 Hz
PPMCM             12.00000 ppm/cm
HZCM             904.82849 Hz/cm
```

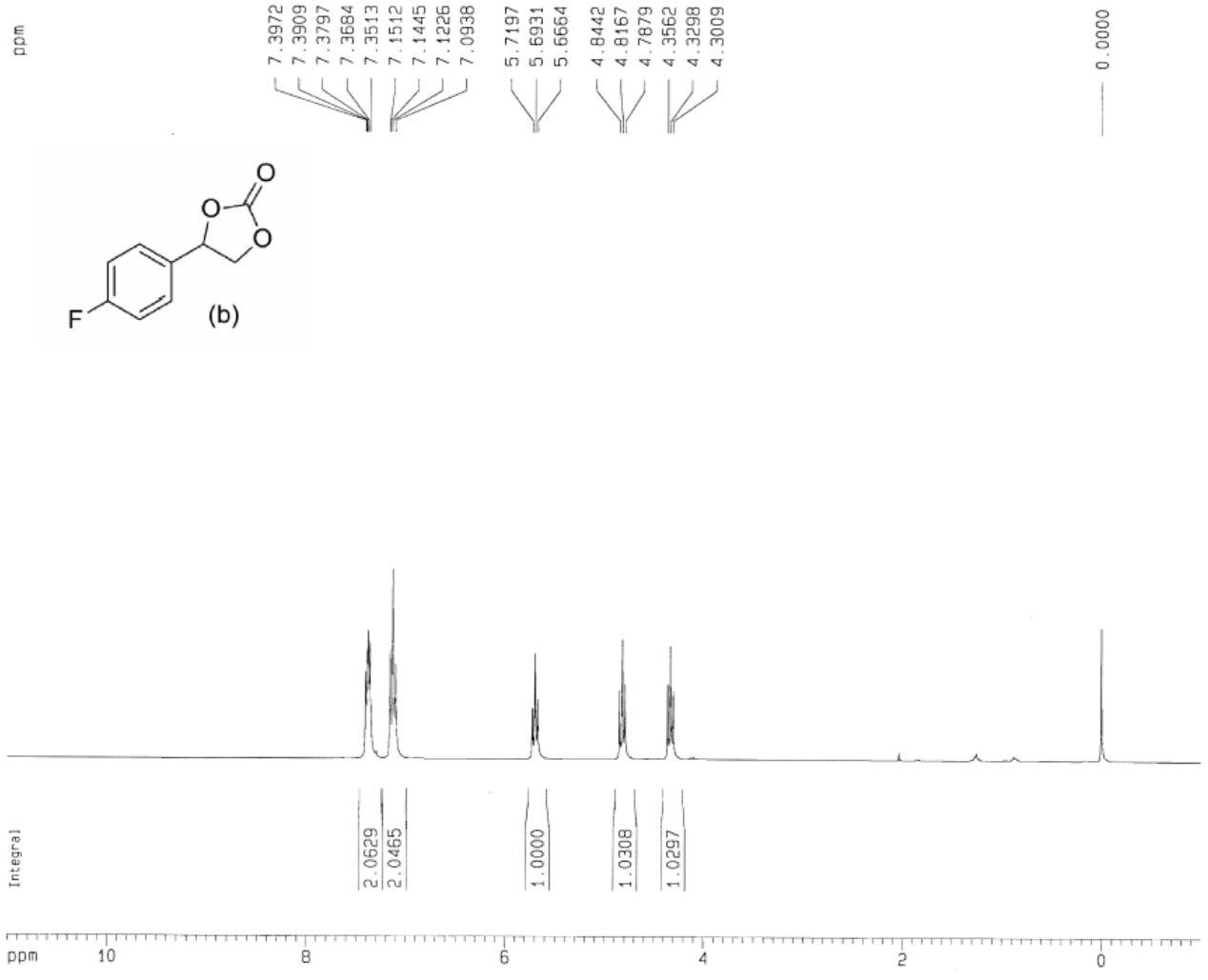


```
Current Data Parameters
NAME                 4_Fstycarb
EXPNO                         1
PROCNO                        1

F2 - Acquisition Parameters
Date_                  20151207
Time                      10.07
INSTRUM                   spect
PROBHD     5 mm QNP 1H/1
PULPROG                   zg30
TD                       65536
SOLVENT                  CDCl3
NS                          16
DS                           2
SWH                 6172.839 Hz
FIDRES              0.094190 Hz
AQ                  5.3084660 sec
RG                        80.6
DW                   81.000 usec
DE                    6.00 usec
TE                    300.0 K
D1                 1.00000000 sec

============ CHANNEL f1 =========
NUC1                         1H
P1                    12.10 usec
PL1                    0.00 dB
SFO1              299.8718518 MHz

F2 - Processing parameters
SI                       32768
SF                299.8700006 MHz
WDW                         no
SSB                          0
LB                    0.00 Hz
GB                           0
PC                        1.00

1D NMR plot parameters
CX                   20.00 cm
F1P                 11.000 ppm
F1                  3298.57 Hz
F2P                 -1.000 ppm
F2                  -299.87 Hz
PPMCM               0.60000 ppm/cm
HZCM              179.92200 Hz/cm
```

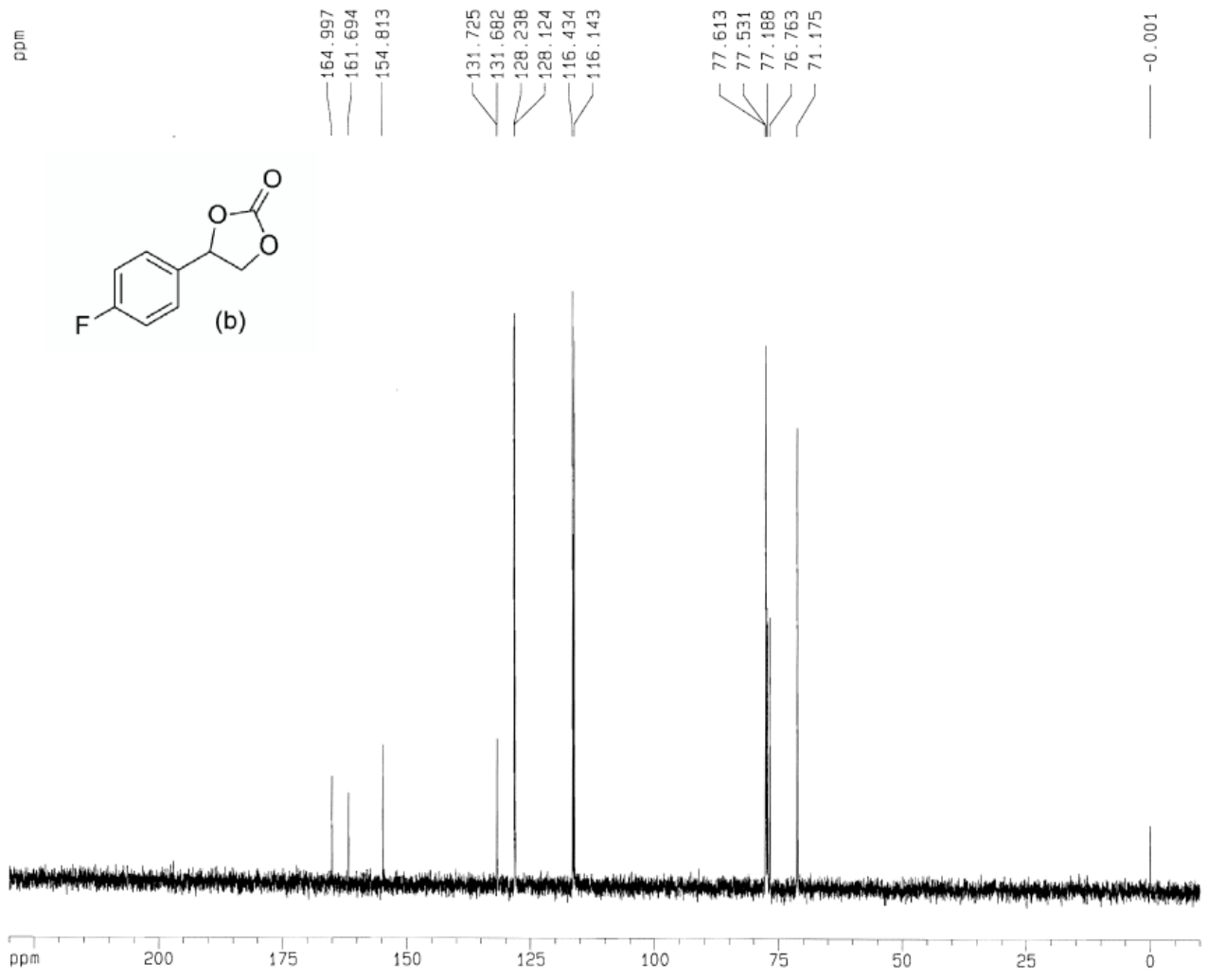


```
Current Data Parameters
NAME          4_Fstycarb
EXPNO                  2
PROCNO                 1

F2 - Acquisition Parameters
Date_           20151207
Time               10.09
INSTRUM            spect
PROBHD    5 mm QNP 1H/1
PULPROG          zgpg30
TD                65536
SOLVENT           CDCl3
NS                   42
DS                    4
SWH           18796.992 Hz
FIDRES        0.286819 Hz
AQ            1.7433076 sec
RG                 2048
DW               26.600 usec
DE                6.00 usec
TE               300.0 K
D1            2.00000000 sec
D11           0.03000000 sec
D12           0.00002000 sec

============ CHANNEL f1 ============
NUC1                13C
P1                5.25 usec
PL1              -6.00 dB
SFO1         75.4106357 MHz

============ CHANNEL f2 ============
CPDPRG2         waltz16
NUC2                1H
PCPD2           115.00 usec
PL2               0.00 dB
PL12             19.70 dB
PL13             19.70 dB
SFO2        299.8711995 MHz

F2 - Processing parameters
SI                 32768
SF           75.4023713 MHz
WDW                   EM
SSB                   0
LB                 1.00 Hz
GB                    0
PC                 1.40

1D NMR plot parameters
CX                20.00 cm
F1P              230.000 ppm
F1             17342.54 Hz
F2P              -10.000 ppm
F2              -754.02 Hz
PPMCM          12.00000 ppm/cm
HZCM          904.82849 Hz/cm
```

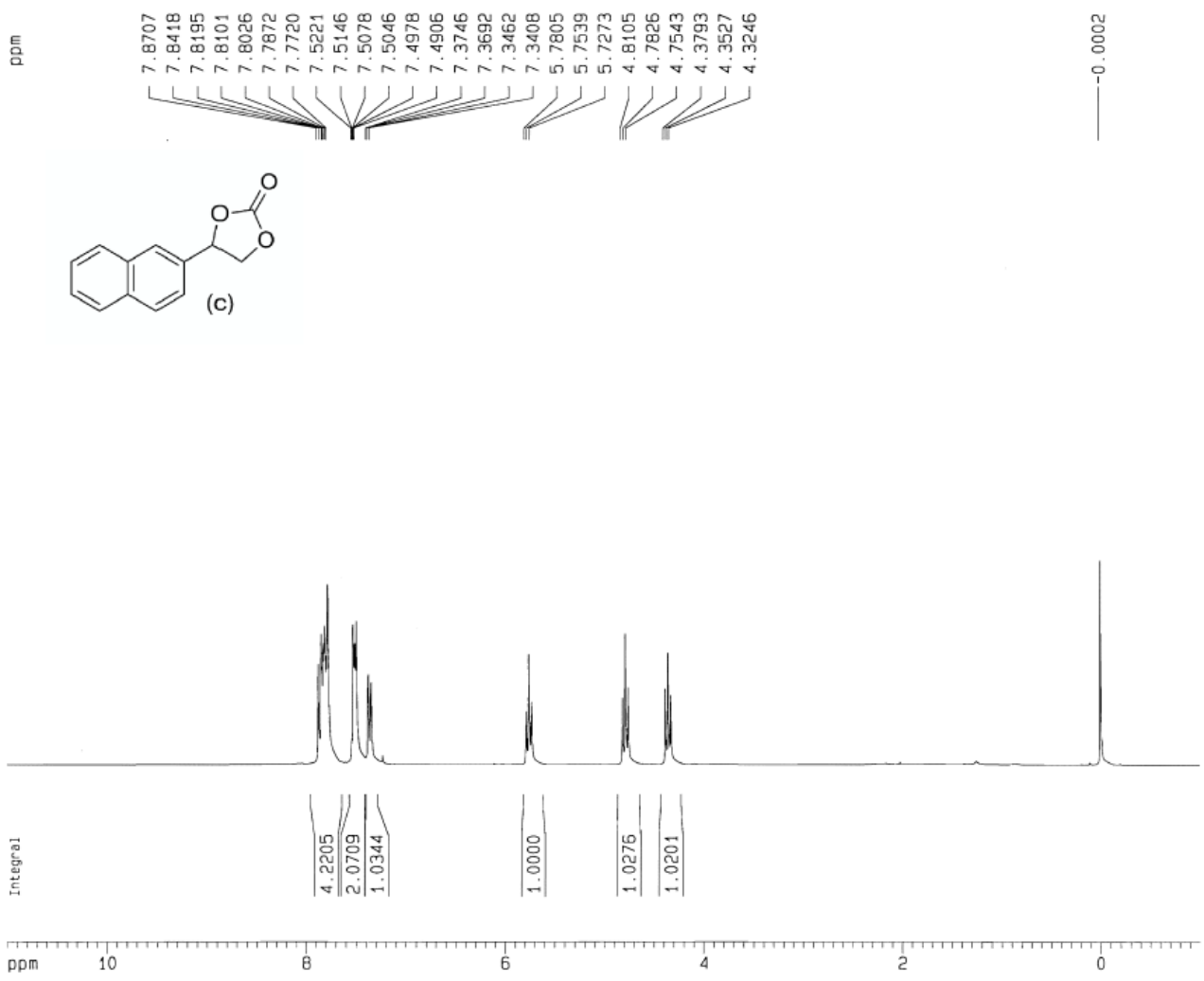


```
Current Data Parameters
NAME            nap_carb
EXPNO                  2
PROCNO                 1

F2 - Acquisition Parameters
Date_           20151128
Time               14.32
INSTRUM            spect
PROBHD    5 mm QNP 1H/1
PULPROG             zg30
TD                 65536
SOLVENT            CDCl3
NS                    16
DS                     2
SWH           6172.839 Hz
FIDRES        0.094190 Hz
AQ            5.3084660 sec
RG                  80.6
DW               81.000 usec
DE                6.00 usec
TE               300.0 K
D1            1.00000000 sec

========== CHANNEL f1 ========
NUC1                   1H
P1                 12.10 usec
PL1                 0.00 dB
SFO1         299.8718518 MHz

F2 - Processing parameters
SI                 32768
SF           299.8700196 MHz
WDW                   no
SSB                    0
LB                  0.00 Hz
GB                     0
PC                  1.00

1D NMR plot parameters
CX                 20.00 cm
F1P               11.000 ppm
F1                3298.57 Hz
F2P                -1.000 ppm
F2                -299.87 Hz
PPMCM             0.60000 ppm/cm
HZCM            179.92201 Hz/cm
```

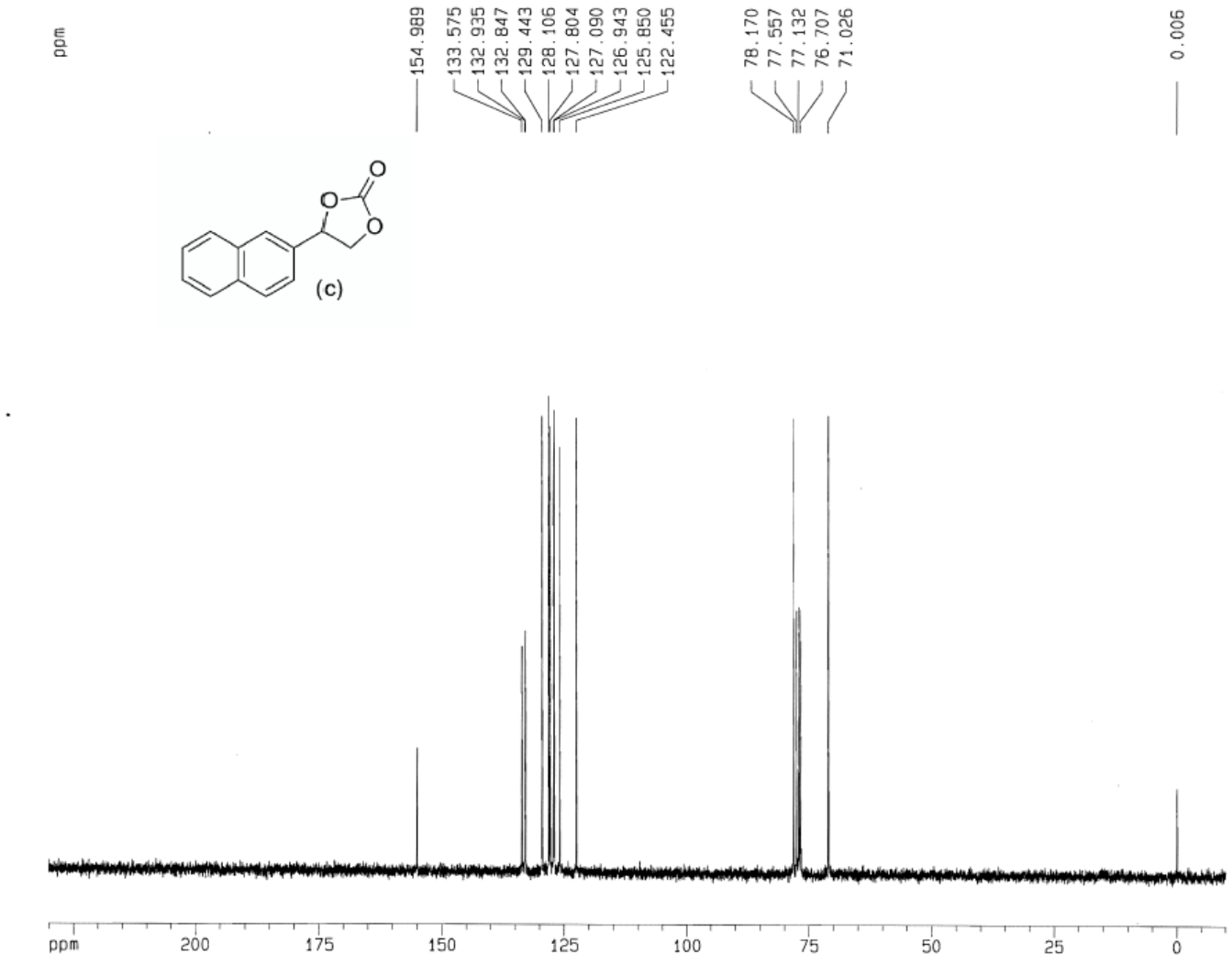


```
Current Data Parameters
NAME                  nap_carb
EXPNO                        3
PROCNO                       1

F2 - Acquisition Parameters
Date_              20151128
Time                    14.45
INSTRUM                 spect
PROBHD     5 mm QNP 1H/1
PULPROG                 zgpg30
TD                       65536
SOLVENT                  CDCl3
NS                         165
DS                           4
SWH                18796.992 Hz
FIDRES              0.286819 Hz
AQ                  1.7433076 sec
RG                     3649.1
DW                    26.600 usec
DE                     6.00 usec
TE                    300.0 K
D1                 2.00000000 sec
D11                0.03000000 sec
D12                0.00002000 sec

========== CHANNEL f1 ==========
NUC1                      13C
P1                       5.25 usec
PL1                     -6.00 dB
SFO1               75.4106357 MHz

========== CHANNEL f2 ==========
CPDPRG2                waltz16
NUC2                       1H
PCPD2                  115.00 usec
PL2                      0.00 dB
PL12                    19.70 dB
PL13                    19.70 dB
SFO2              299.8711995 MHz

F2 - Processing parameters
SI                       32768
SF                 75.4023794 MHz
WDW                         EM
SSB                          0
LB                        1.00 Hz
GB                           0
PC                        1.40

1D NMR plot parameters
CX                       20.00 cm
F1P                     230.000 ppm
F1                    17342.55 Hz
F2P                    -10.000 ppm
F2                     -754.02 Hz
PPMCM                 12.00000 ppm/cm
HZCM                 904.82861 Hz/cm
```

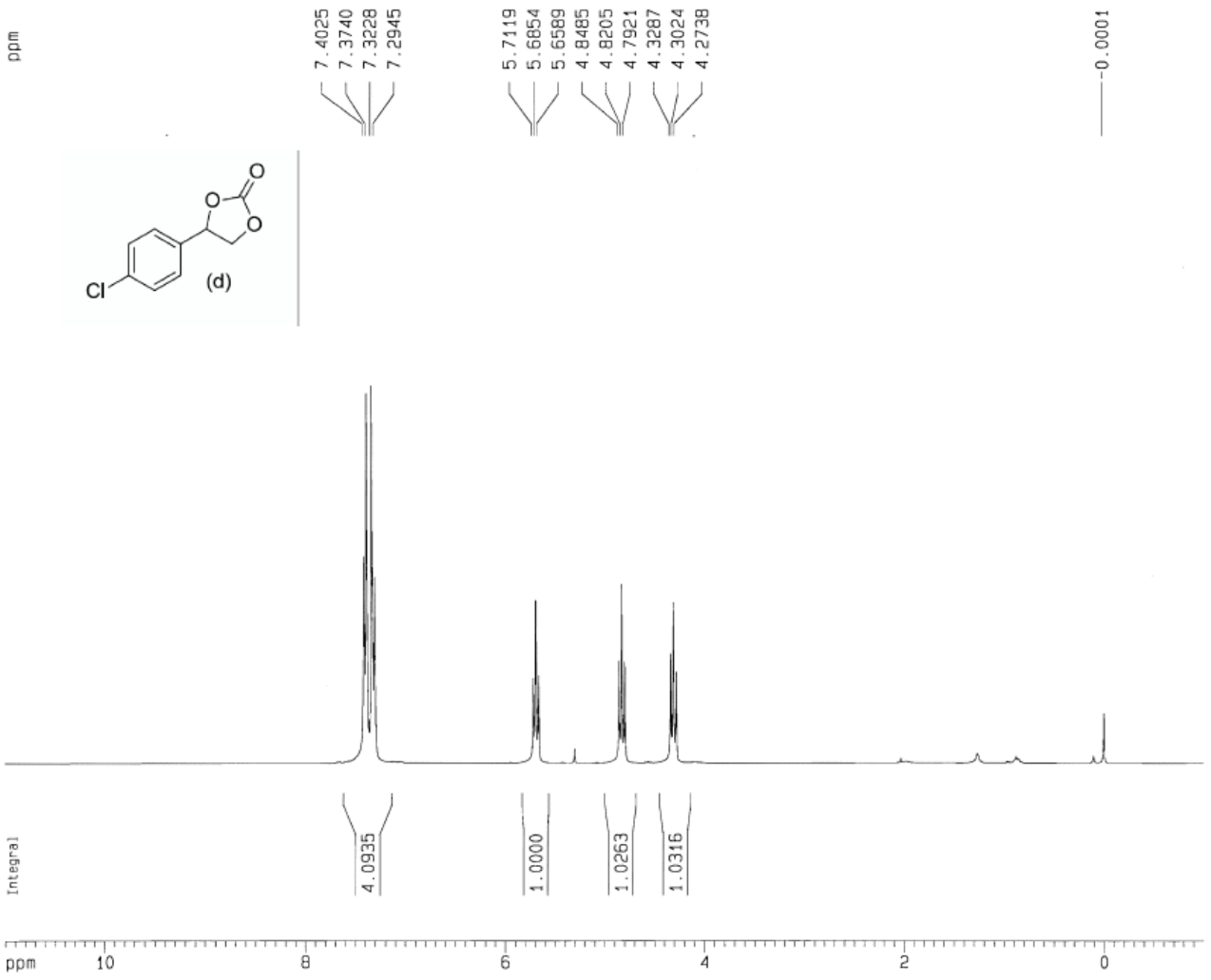


```
Current Data Parameters
NAME       4_Cl_stycarbo
EXPNO                  1
PROCNO                 1

F2 - Acquisition Parameters
Date_           20151111
Time               15.21
INSTRUM            spect
PROBHD    5 mm QNP 1H/1
PULPROG             zg30
TD                 65536
SOLVENT            CDCl3
NS                    16
DS                     2
SWH             6172.839 Hz
FIDRES          0.094190 Hz
AQ              5.3084660 sec
RG                    57
DW                81.000 usec
DE                 6.00 usec
TE                300.0 K
D1           1.00000000 sec

========== CHANNEL f1 =========
NUC1                  1H
P1                 12.10 usec
PL1                 0.00 dB
SFO1          299.8718518 MHz

F2 - Processing parameters
SI                 32768
SF           299.8699974 MHz
WDW                   EM
SSB                    0
LB                  0.30 Hz
GB                     0
PC                  1.00

1D NMR plot parameters
CX                 20.00 cm
F1P                11.000 ppm
F1               3298.57 Hz
F2P                -1.000 ppm
F2               -299.87 Hz
PPMCM           0.60000 ppm/cm
HZCM          179.92200 Hz/cm
```

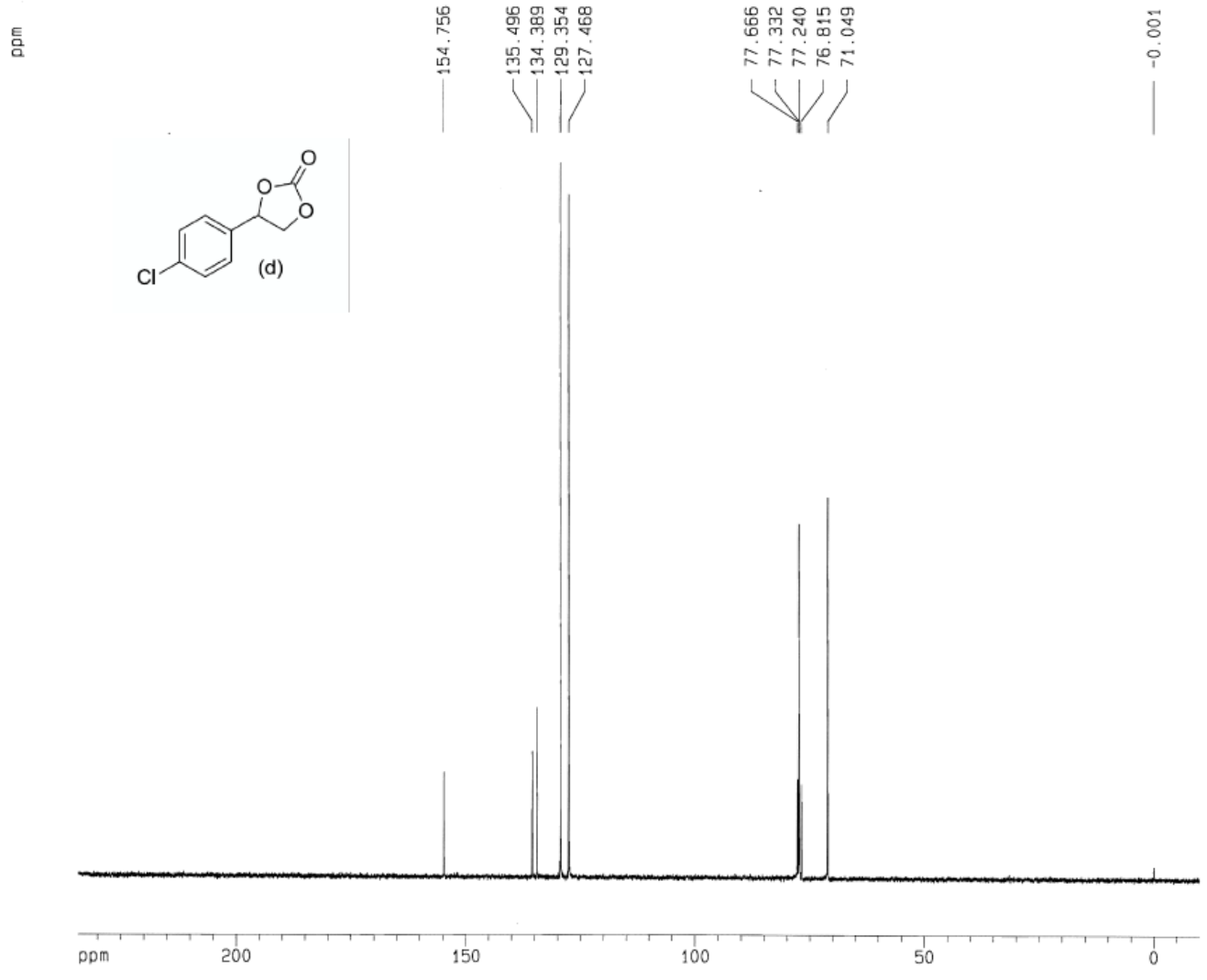


```
Current Data Parameters
NAME       4_Cl_stycarbo
EXPNO                  2
PROCNO                 1

F2 - Acquisition Parameters
Date_           20151111
Time               15.31
INSTRUM            spect
PROBHD     5 mm QNP 1H/1
PULPROG          zgpg30
TD                65536
SOLVENT           CDCl3
NS                  102
DS                    4
SWH           18796.992 Hz
FIDRES        0.286819 Hz
AQ            1.7433076 sec
RG                 4096
DW               26.600 usec
DE                6.00 usec
TE               300.0 K
D1            2.00000000 sec
D11           0.03000000 sec
D12           0.00002000 sec

====== CHANNEL f1 ========
NUC1                13C
P1                 5.25 usec
PL1               -6.00 dB
SFO1          75.4106357 MHz

====== CHANNEL f2 ========
CPDPRG2         waltz16
NUC2                1H
PCPD2            115.00 usec
PL2                0.00 dB
PL12              19.70 dB
PL13              19.70 dB
SFO2         299.8711995 MHz

F2 - Processing parameters
SI                 32768
SF            75.4023753 MHz
WDW                   EM
SSB                    0
LB                  1.00 Hz
GB                     0
PC                  1.40

1D NMR plot parameters
CX                 20.00 cm
F1P               250.000 ppm
F1                18850.59 Hz
F2P               -10.000 ppm
F2                -754.02 Hz
PPMCM             13.00000 ppm/cm
HZCM             980.23083 Hz/cm
```

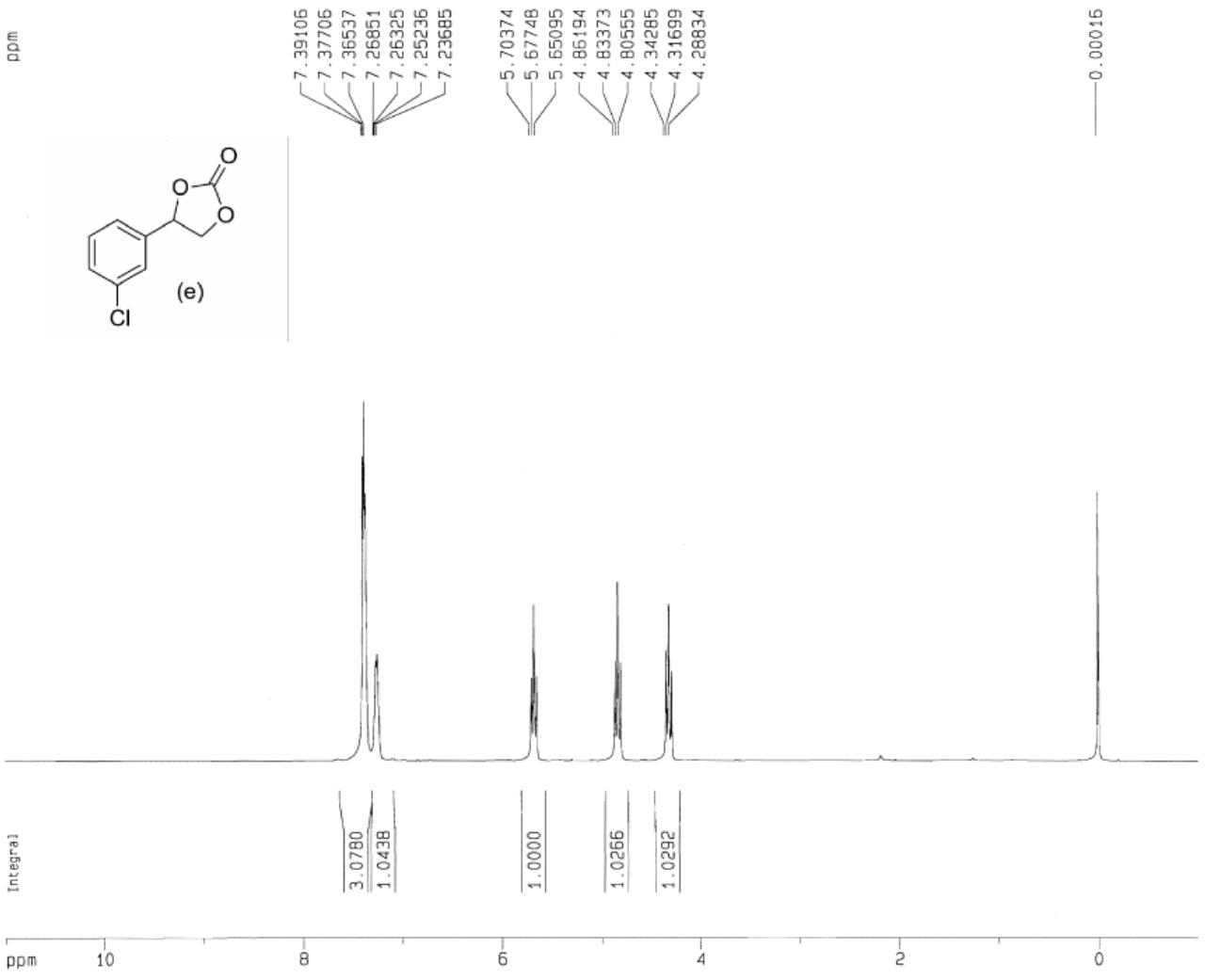


```
Current Data Parameters
NAME          3_Cl_sty_DC
EXPNO                   1
PROCNO                  1

F2 - Acquisition Parameters
Date_           20151116
Time               17.27
INSTRUM            spect
PROBHD     5 mm QNP 1H/1
PULPROG            zg30
TD                65536
SOLVENT           CDCl3
NS                   16
DS                    2
SWH           6172.839 Hz
FIDRES        0.094190 Hz
AQ            5.3084660 sec
RG                 80.6
DW               81.000 usec
DE                6.00 usec
TE               300.0 K
D1           1.00000000 sec

========== CHANNEL f1 ========
NUC1                  1H
P1                12.10 usec
PL1                0.00 dB
SFO1         299.8718518 MHz

F2 - Processing parameters
SI                32768
SF           299.8700029 MHz
WDW                  EM
SSB                   0
LB                 0.30 Hz
GB                    0
PC                 1.00

1D NMR plot parameters
CX                20.00 cm
F1P               11.000 ppm
F1              3298.57 Hz
F2P               -1.000 ppm
F2              -299.87 Hz
PPMCM          0.60000 ppm/cm
HZCM         179.92200 Hz/cm
```

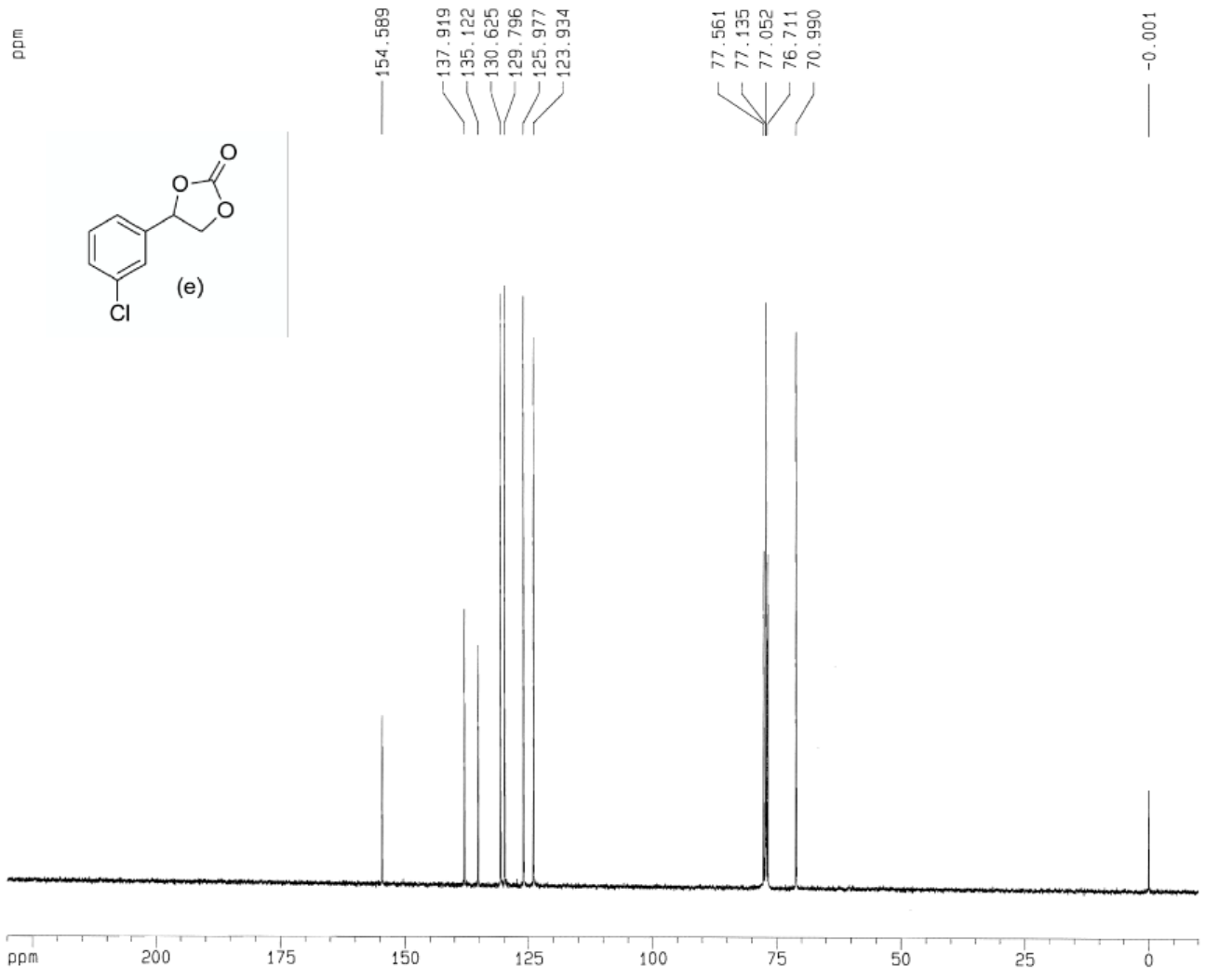


```
Current Data Parameters
NAME          3_Cl_sty_OC
EXPNO                   2
PROCNO                  1

F2 - Acquisition Parameters
Date_          20151116
Time              18.32
INSTRUM           spect
PROBHD    5 mm QNP 1H/1
PULPROG          zgpg30
TD                65536
SOLVENT           CDCl3
NS                 1024
DS                    4
SWH           18796.992 Hz
FIDRES        0.286819 Hz
AQ            1.7433076 sec
RG                 2048
DW               26.600 usec
DE                6.00 usec
TE               300.0 K
D1            2.00000000 sec
D11           0.03000000 sec
D12           0.00002000 sec

========== CHANNEL f1 ==========
NUC1               13C
P1                5.25 usec
PL1              -6.00 dB
SFO1         75.4106357 MHz

========== CHANNEL f2 ==========
CPDPRG2         waltz16
NUC2                1H
PCPD2           115.00 usec
PL2               0.00 dB
PL12             19.70 dB
PL13             19.70 dB
SFO2        299.8711995 MHz

F2 - Processing parameters
SI                32768
SF           75.4023748 MHz
WDW                  EM
SSB                   0
LB                 1.00 Hz
GB                    0
PC                 1.40

1D NMR plot parameters
CX                20.00 cm
F1P              230.000 ppm
F1             17342.54 Hz
F2P              -10.000 ppm
F2             -754.02 Hz
PPMCM          12.00000 ppm/cm
HZCM          904.82849 Hz/cm
```

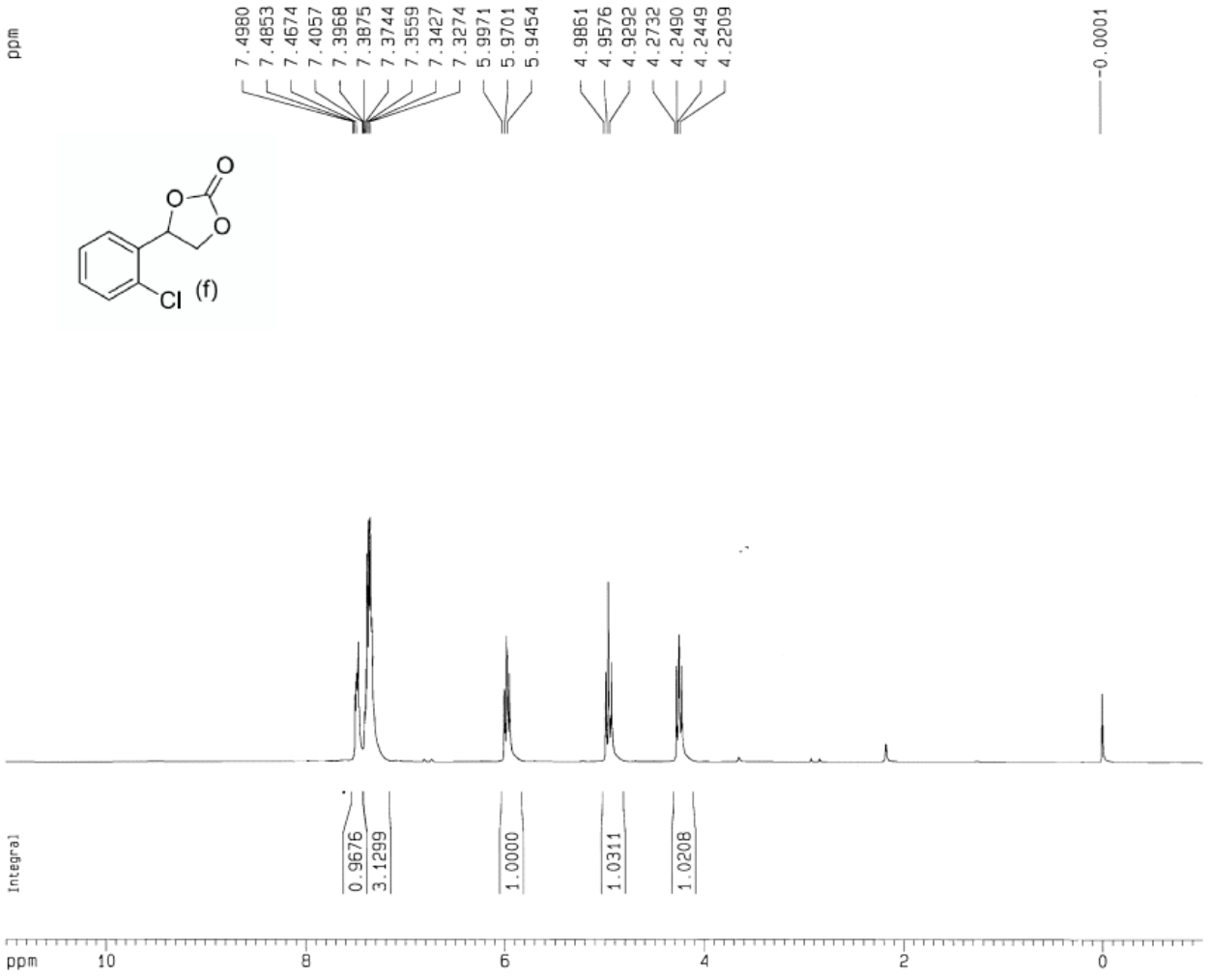


```
Current Data Parameters
NAME        2_Cl_Sty_carb
EXPNO                   1
PROCNO                  1

F2 - Acquisition Parameters
Date_            20151128
Time                13.21
INSTRUM             spect
PROBHD     5 mm QNP 1H/1
PULPROG             zg30
TD                 65536
SOLVENT            CDCl3
NS                    16
DS                     2
SWH             6172.839 Hz
FIDRES          0.094190 Hz
AQ              5.3084660 sec
RG                  35.9
DW                81.000 usec
DE                 6.00 usec
TE                300.0 K
D1             1.00000000 sec

============ CHANNEL f1 =========
NUC1                   1H
P1                  12.10 usec
PL1                  0.00 dB
SFO1         299.8718518 MHz

F2 - Processing parameters
SI                 32768
SF          299.8699872 MHz
WDW                   EM
SSB                    0
LB                  0.30 Hz
GB                     0
PC                  1.00

1D NMR plot parameters
CX                 20.00 cm
F1P                11.000 ppm
F1               3298.57 Hz
F2P                -1.000 ppm
F2               -299.87 Hz
PPMCM            0.60000 ppm/cm
HZCM           179.92200 Hz/cm
```

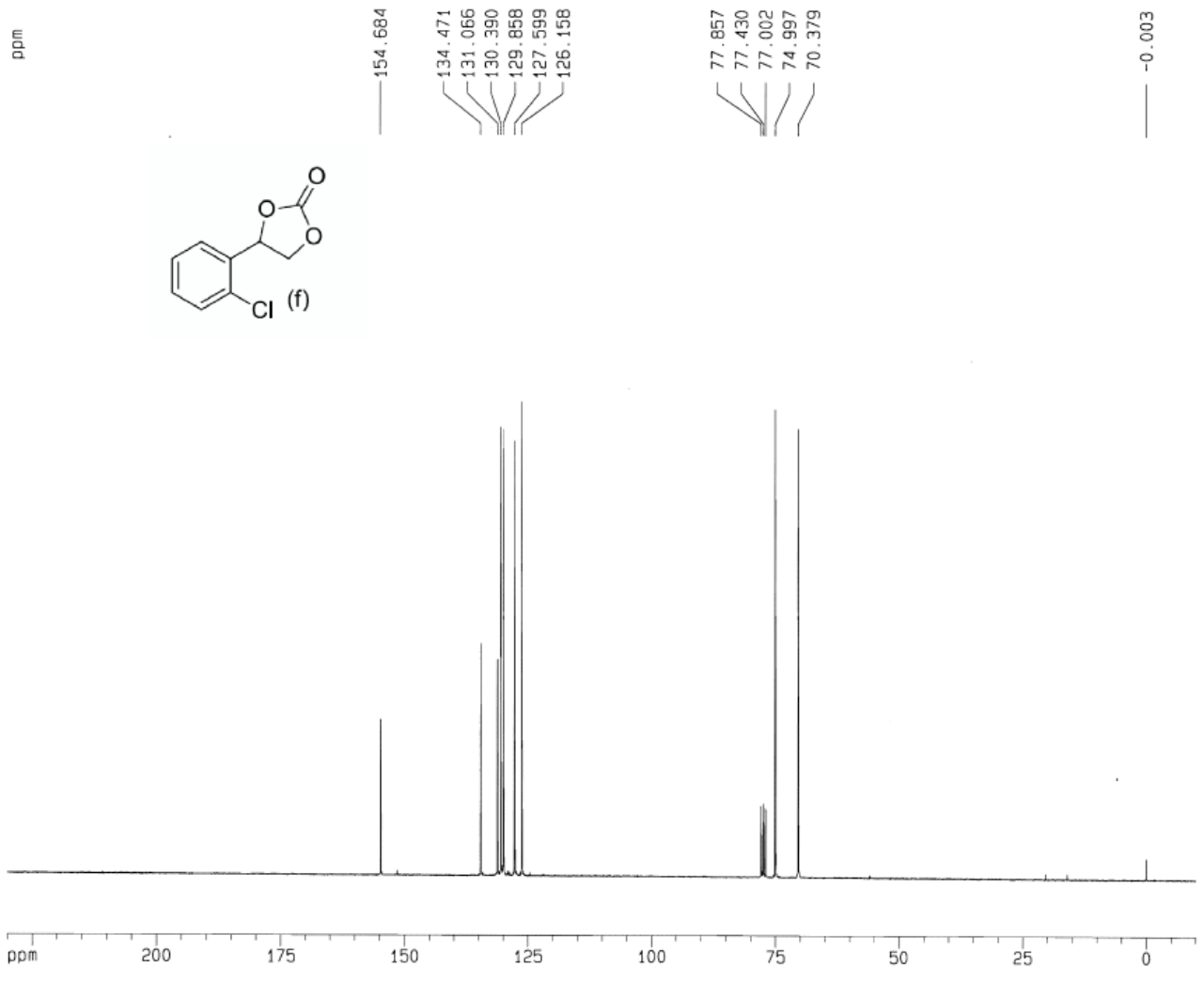


```
Current Data Parameters
NAME        2_Cl_Sty_carb
EXPNO                   2
PROCNO                  1

F2 - Acquisition Parameters
Date_            20151128
Time                14.27
INSTRUM             spect
PROBHD     5 mm QNP 1H/1
PULPROG          zgpg30
TD                 65536
SOLVENT            CDCl3
NS                   961
DS                     4
SWH           18796.992 Hz
FIDRES         0.286819 Hz
AQ             1.7433076 sec
RG                  1024
DW                26.600 usec
DE                 6.00 usec
TE                300.0 K
D1             2.00000000 sec
D11            0.03000000 sec
D12            0.00002000 sec

============ CHANNEL f1 ==========
NUC1                13C
P1                 5.25 usec
PL1               -6.00 dB
SF01          75.4106357 MHz

============ CHANNEL f2 ==========
CPDPRG2         waltz16
NUC2                1H
PCPD2             115.00 usec
PL2                0.00 dB
PL12              19.70 dB
PL13              19.70 dB
SF02         299.8711995 MHz

F2 - Processing parameters
SI                 32768
SF            75.4023731 MHz
WDW                   EM
SSB                    0
LB                  1.00 Hz
GB                     0
PC                  1.40

1D NMR plot parameters
CX                20.00 cm
F1P              230.000 ppm
F1              17342.54 Hz
F2P              -10.000 ppm
F2              -754.02 Hz
PPMCM           12.00000 ppm/cm
HZCM           904.82849 Hz/cm
```

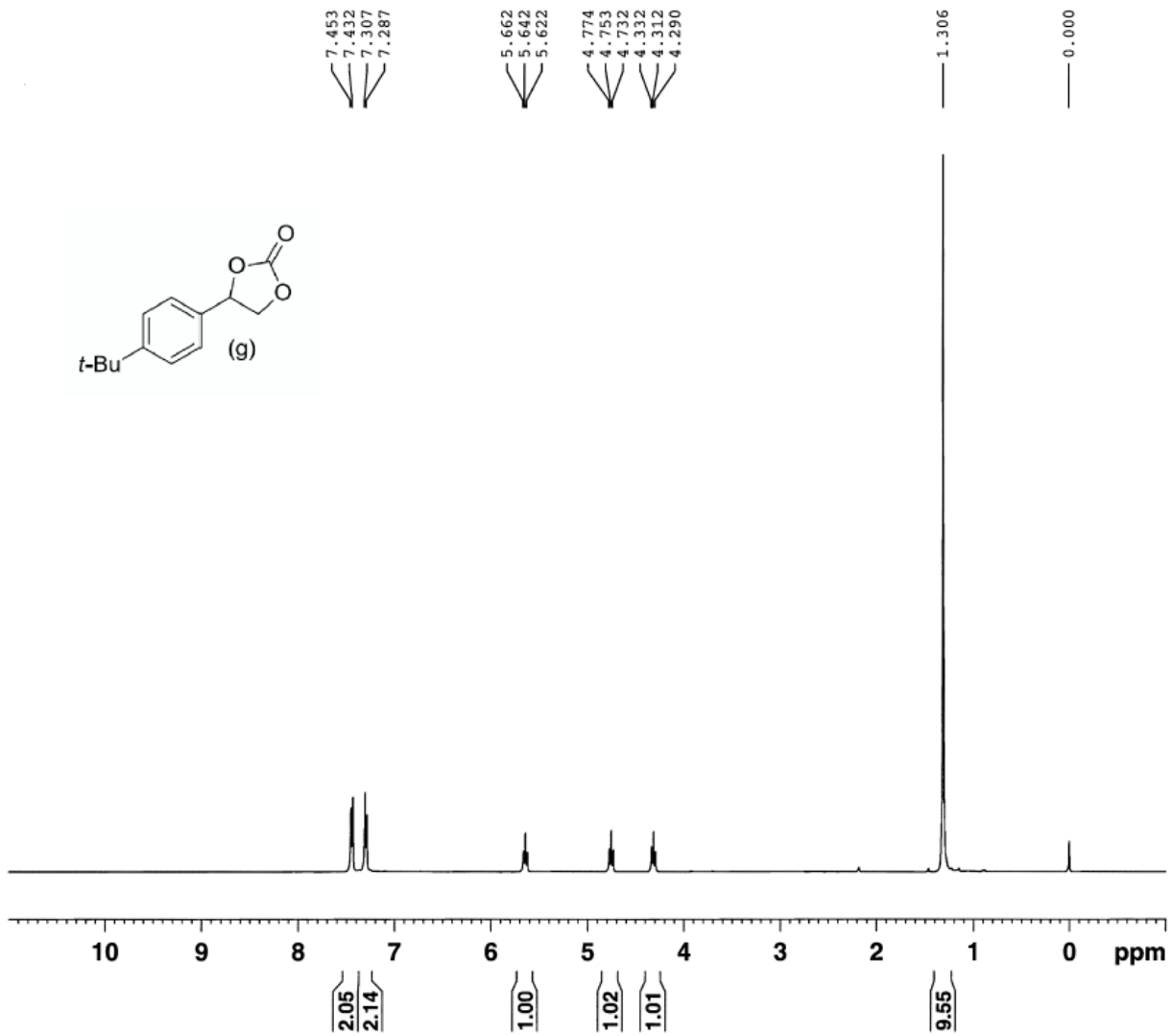


```
Current Data Parameters
NAME       4_tBusty_carb
EXPNO                  3
PROCNO                 1

F2 - Acquisition Parameters
Date_           20151128
Time               14.25
INSTRUM            spect
PROBHD   5 mm Multinucl
PULPROG             zg30
TD                 54634
SOLVENT            CDCl3
NS                    16
DS                     2
SWH             8278.146 Hz
FIDRES          0.151520 Hz
AQ              3.2999437 sec
RG                  90.5
DW                60.400 usec
DE                 6.00 usec
TE                294.6 K
D1             1.00000000 sec
TD0                    1

======== CHANNEL f1 ========
NUC1                  1H
P1                 7.50 usec
PL1                1.00 dB
SFO1         400.1324710 MHz

F2 - Processing parameters
SI                 65536
SF           400.1300144 MHz
WDW                   no
SSB                    0
LB                 0.00 Hz
GB                     0
PC                 1.00
```

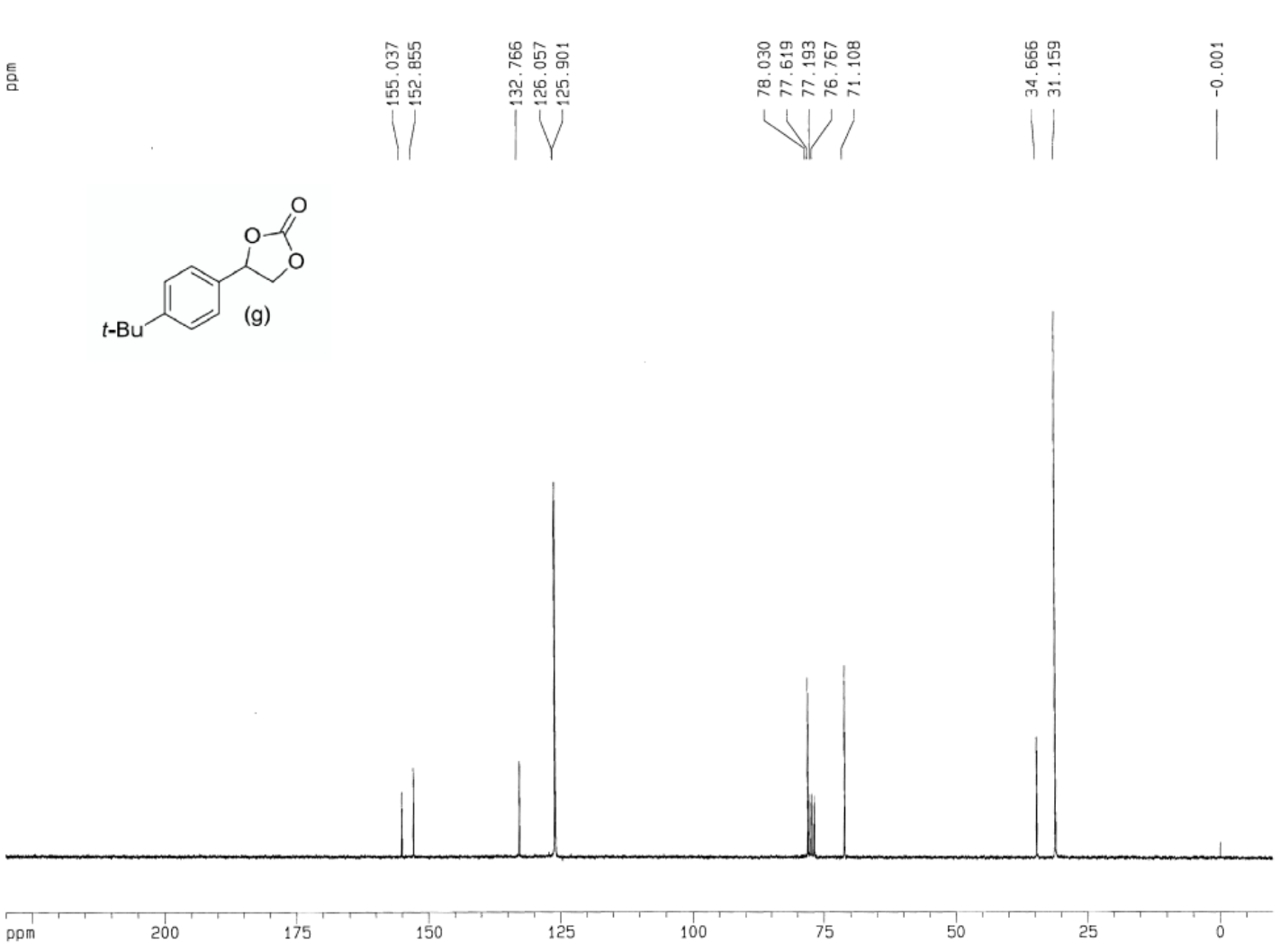

Current Data P
NAME 4_tb
EXPNO
PROCNO

F2 - Acquisiti
Date_
Time
INSTRUM
PROBHD 5 mm
PULPROG
TD
SOLVENT
NS
DS
SWH
FIORES
AQ
RG
DW
DE
TE
D1 2
D11 0
D12 0

========== C
NUC1
P1
PL1
SF01 7

========== C
CPDPRG2
NUC2
PCPD2
PL2
PL12
PL13
SF02 29

F2 - Processin
SI
SF 7
WDW
SSB
LB
GB
PC

1D NMR plot pa
CX
F1P
F1
F2P
F2
PPMCM
HZCM

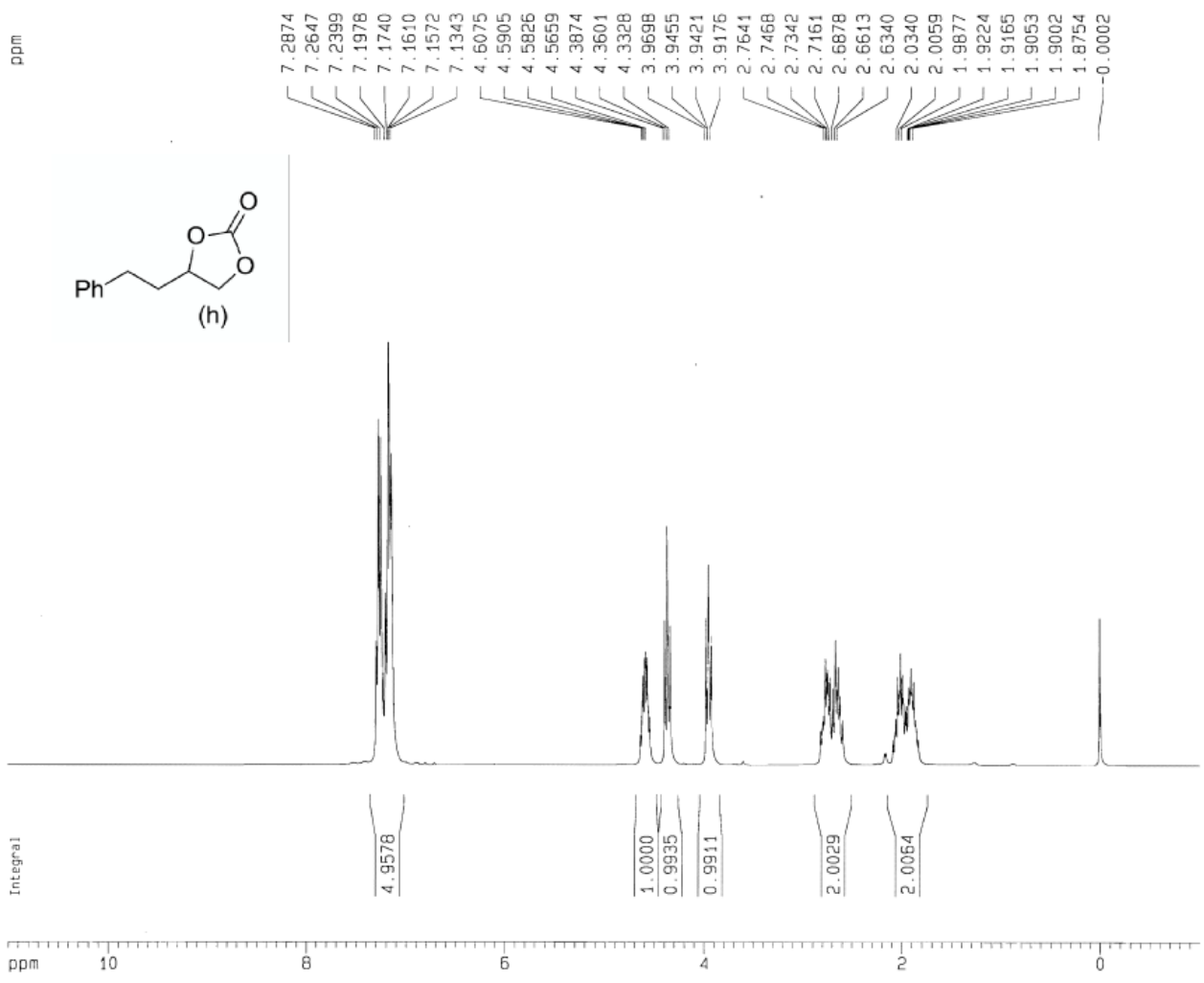


```
Current Data Parameters
NAME        4_Ph_But_Carb
EXPNO                   1
PROCNO                  1

F2 - Acquisition Parameters
Date_            20151130
Time                14.09
INSTRUM             spect
PROBHD     5 mm QNP 1H/1
PULPROG             zg30
TD                 65536
SOLVENT            CDCl3
NS                    16
DS                     2
SWH             6172.839 Hz
FIDRES          0.094190 Hz
AQ              5.3084660 sec
RG                  25.4
DW                81.000 usec
DE                 6.00 usec
TE                300.0 K
D1             1.00000000 sec

========== CHANNEL f1 =========
NUC1                   1H
P1                  12.10 usec
PL1                  0.00 dB
SFO1         299.8718518 MHz

F2 - Processing parameters
SI                  32768
SF          299.8700225 MHz
WDW                    EM
SSB                     0
LB                   0.30 Hz
GB                      0
PC                   1.00

1D NMR plot parameters
CX                  20.00 cm
F1P                 11.000 ppm
F1                3298.57 Hz
F2P                -1.000 ppm
F2                -299.87 Hz
PPMCM             0.60000 ppm/cm
HZCM            179.92201 Hz/cm
```

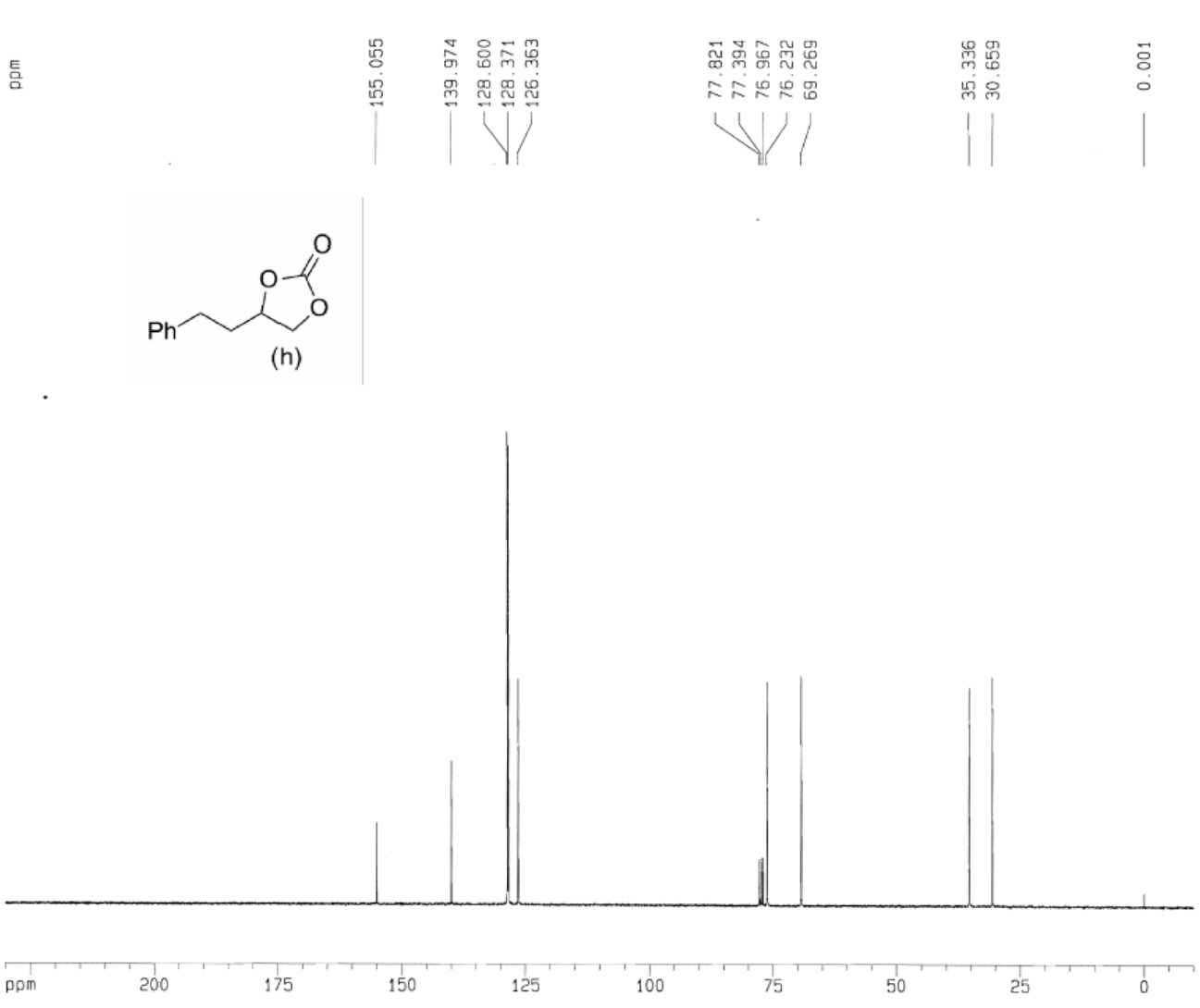


```
Current Data Parameters
NAME        4_Ph_But_Carb
EXPNO                   2
PROCNO                  1

F2 - Acquisition Parameters
Date_            20151130
Time                14.16
INSTRUM             spect
PROBHD    5 mm QNP 1H/1
PULPROG           zgpg30
TD                 65536
SOLVENT            CDCl3
NS                    81
DS                     4
SWH           18796.992 Hz
FIDRES        0.286819 Hz
AQ            1.7433076 sec
RG                  1024
DW                26.600 usec
DE                 6.00 usec
TE                300.0 K
D1           2.00000000 sec
D11          0.03000000 sec
D12          0.00002000 sec

========== CHANNEL f1 ========
NUC1                13C
P1                 5.25 usec
PL1               -6.00 dB
SFO1         75.4106357 MHz

========== CHANNEL f2 ========
CPDPRG2         waltz16
NUC2                1H
PCPD2             115.00 usec
PL2                0.00 dB
PL12              19.70 dB
PL13              19.70 dB
SFO2        299.8711995 MHz

F2 - Processing parameters
SI                 32768
SF           75.4023822 MHz
WDW                   EM
SSB                    0
LB                 1.00 Hz
GB                     0
PC                  1.40

1D NMR plot parameters
CX                20.00 cm
F1P              230.000 ppm
F1             17342.55 Hz
F2P              -10.000 ppm
F2              -754.02 Hz
PPMCM          12.00000 ppm/cm
HZCM          904.82861 Hz/cm
```

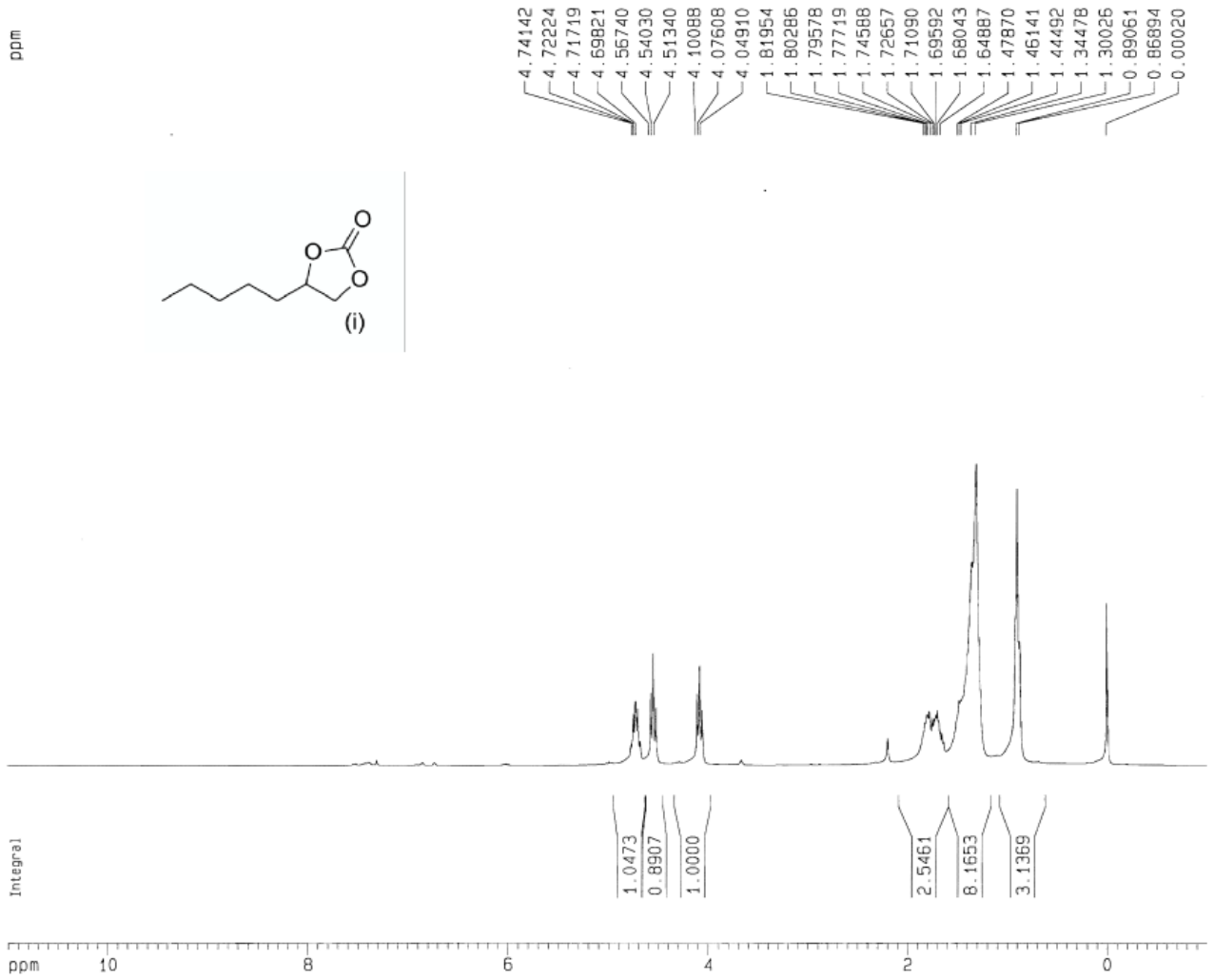

Current Data Parameters
NAME octene_carb
EXPNO 1
PROCNO 1

F2 - Acquisition Parameters
Date_ 20151130
Time 13.54
INSTRUM spect
PROBHD 5 mm DNP 1H/1
PULPROG zg30
TD 65536
SOLVENT CDCl3
NS 16
DS 2
SWH 6172.839 Hz
FIDRES 0.094190 Hz
AQ 5.3084660 sec
RG 50.8
DW 81.000 usec
DE 6.00 usec
TE 300.0 K
D1 1.00000000 sec

========== CHANNEL f1 ========
NUC1 1H
P1 12.10 usec
PL1 0.00 dB
SFO1 299.8718518 MHz

F2 - Processing parameters
SI 32768
SF 299.8699963 MHz
WDW EM
SSB 0
LB 0.30 Hz
GB 0
PC 1.00

1D NMR plot parameters
CX 20.00 cm
F1P 11.000 ppm
F1 3298.57 Hz
F2P -1.000 ppm
F2 -299.87 Hz
PPMCM 0.60000 ppm/cm
HZCM 179.92200 Hz/cm

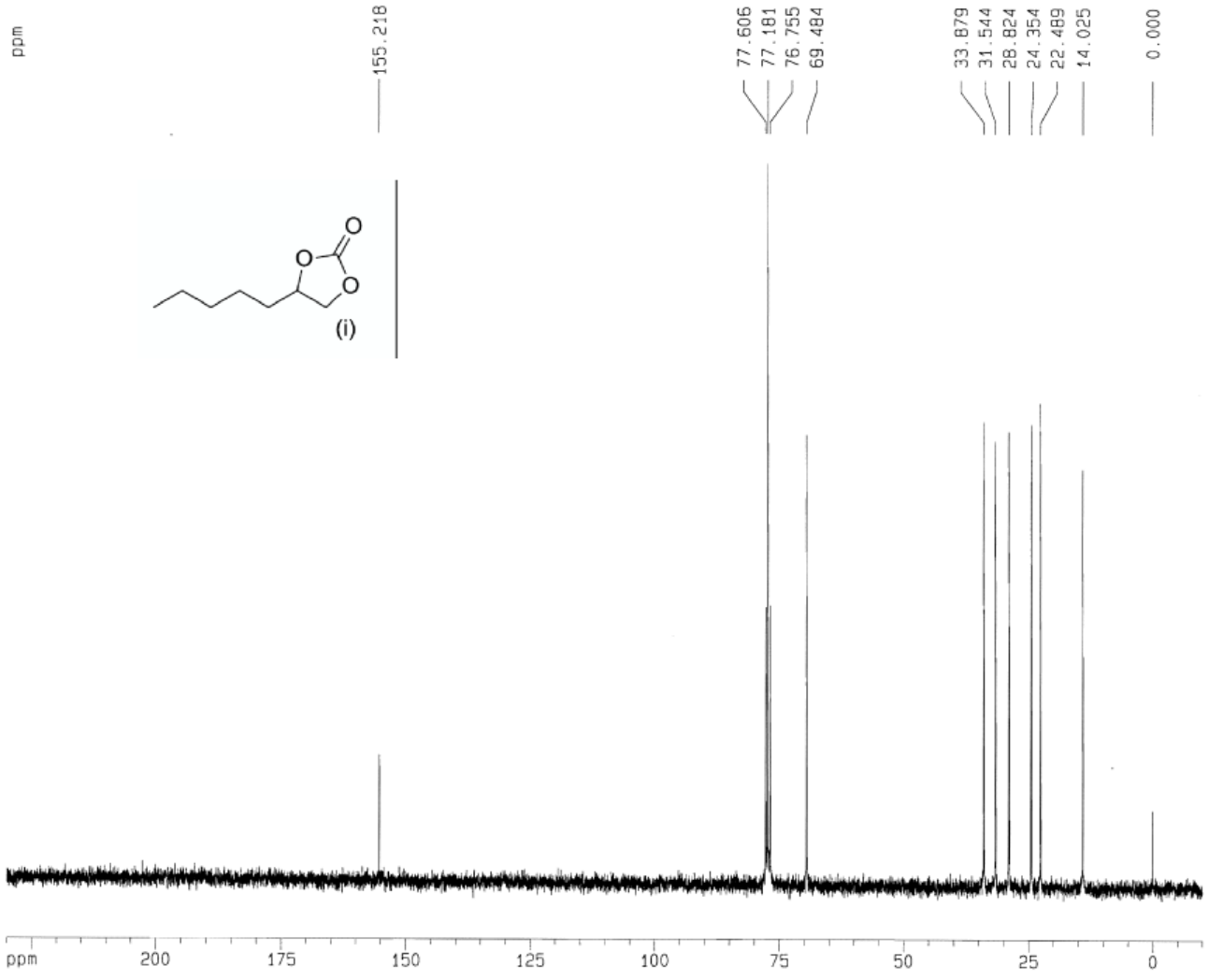


```
Current Data Parameters
NAME          octene_carb
EXPNO                   2
PROCNO                  1

F2 - Acquisition Parameters
Date_          20151130
Time             14.03
INSTRUM          spect
PROBHD    5 mm QNP 1H/1
PULPROG         zgpg30
TD               65536
SOLVENT          CDCl3
NS                 108
DS                   4
SWH          18796.992 Hz
FIDRES       0.286819 Hz
AQ           1.7433076 sec
RG                4096
DW              26.600 usec
DE               6.00 usec
TE              300.0 K
D1           2.00000000 sec
D11          0.03000000 sec
D12          0.00002000 sec

============ CHANNEL f1 =========
NUC1               13C
P1                5.25 usec
PL1              -6.00 dB
SFO1         75.4106357 MHz

============ CHANNEL f2 =========
CPDPRG2         waltz16
NUC2               1H
PCPD2          115.00 usec
PL2              0.00 dB
PL12            19.70 dB
PL13            19.70 dB
SFO2        299.8711995 MHz

F2 - Processing parameters
SI                32768
SF           75.4023690 MHz
WDW                EM
SSB                0
LB              1.00 Hz
GB                 0
PC              1.40

1D NMR plot parameters
CX              20.00 cm
F1P            230.000 ppm
F1            17342.54 Hz
F2P            -10.000 ppm
F2             -754.02 Hz
PPMCM          12.00000 ppm/cm
HZCM          904.82837 Hz/cm
```

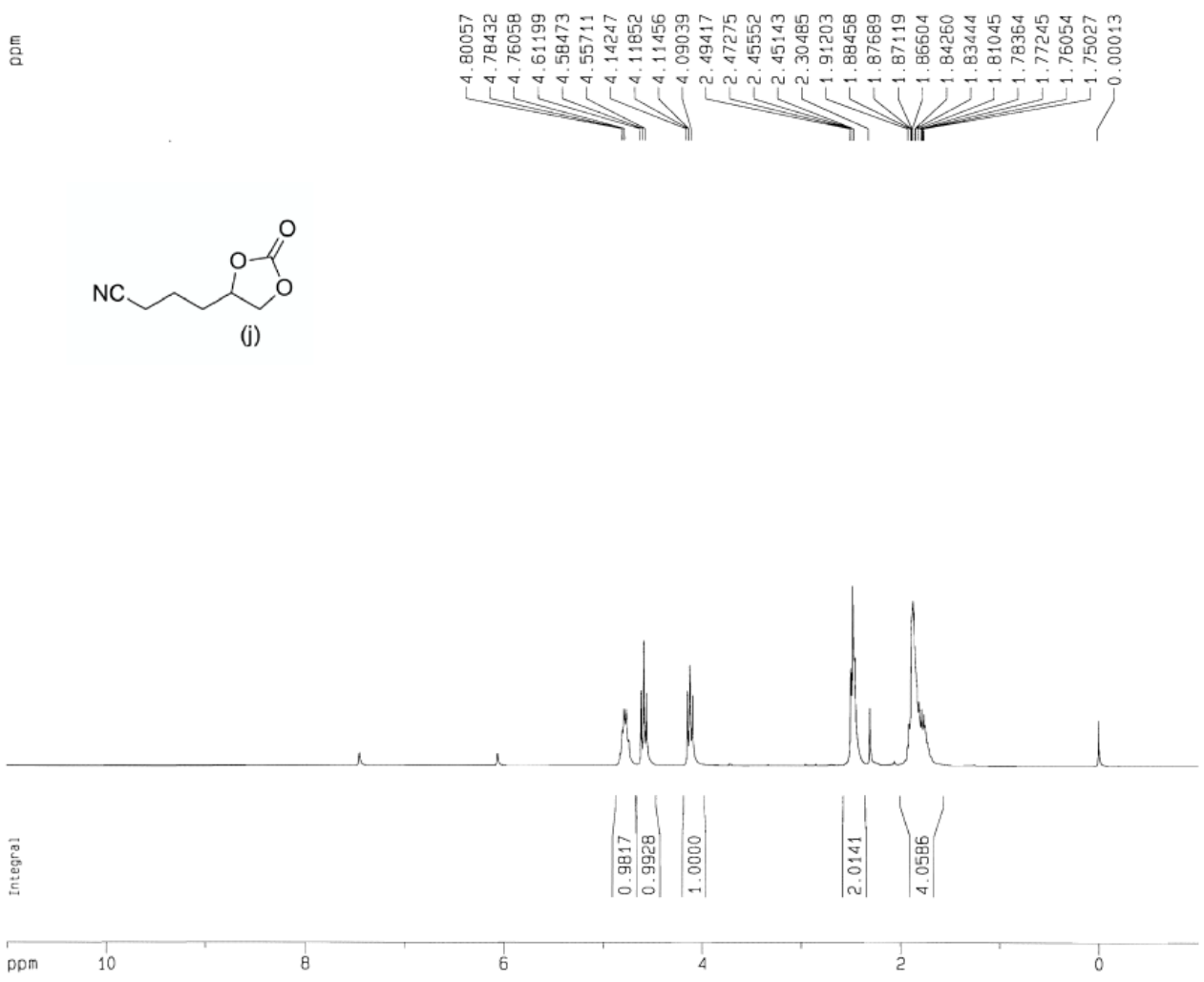


```
Current Data Parameters
NAME       6_CN_hex_carb
EXPNO                  8
PROCNO                 1

F2 - Acquisition Parameters
Date_           20151207
Time                9.56
INSTRUM            spect
PROBHD     5 mm QNP 1H/1
PULPROG             zg30
TD                 65536
SOLVENT            CDCl3
NS                    16
DS                     2
SWH             6172.839 Hz
FIDRES          0.094190 Hz
AQ              5.3084660 sec
RG                  25.4
DW                81.000 usec
DE                 6.00 usec
TE                300.0 K
D1             1.00000000 sec

============ CHANNEL f1 ========
NUC1                   1H
P1                  12.10 usec
PL1                  0.00 dB
SFO1          299.8718518 MHz

F2 - Processing parameters
SI                 32768
SF           299.8699575 MHz
WDW                   no
SSB                    0
LB                  0.00 Hz
GB                     0
PC                  1.00

1D NMR plot parameters
CX                 20.00 cm
F1P                11.000 ppm
F1               3298.57 Hz
F2P                -1.000 ppm
F2               -299.87 Hz
PPMCM            0.60000 ppm/cm
HZCM           179.92198 Hz/cm
```

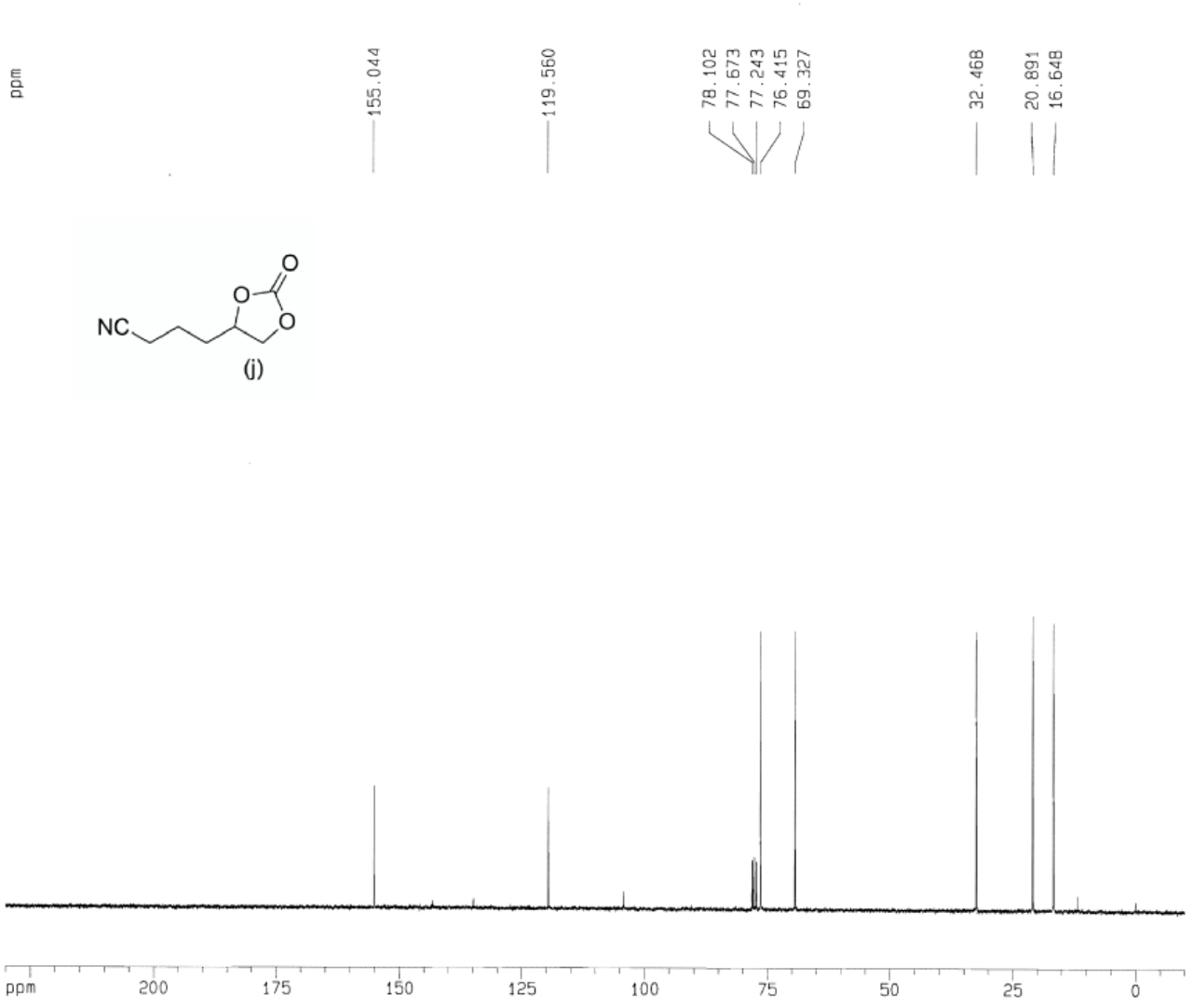


```
Current Data Parameters
NAME        6_CN_hex_carb
EXPNO                   9
PROCNO                  1

F2 - Acquisition Parameters
Date_            20151207
Time                10.00
INSTRUM             spect
PROBHD     5 mm QNP 1H/1
PULPROG          zgpg30
TD                 65536
SOLVENT            CDCl3
NS                    30
DS                     4
SWH           18796.992 Hz
FIDRES        0.286819 Hz
AQ            1.7433076 sec
RG                  1024
DW                26.600 usec
DE                 6.00 usec
TE                300.0 K
D1           2.00000000 sec
D11          0.03000000 sec
D12          0.00002000 sec

============ CHANNEL f1 ==========
NUC1                13C
P1                 5.25 usec
PL1               -6.00 dB
SFO1         75.4106357 MHz

============ CHANNEL f2 ==========
CPDPRG2         waltz16
NUC2                1H
PCPD2             115.00 usec
PL2                0.00 dB
PL12              19.70 dB
PL13              19.70 dB
SFO2        299.8711995 MHz

F2 - Processing parameters
SI                 32768
SF           75.4023667 MHz
WDW                   EM
SSB                    0
LB                  1.00 Hz
GB                     0
PC                  1.40

1D NMR plot parameters
CX                 20.00 cm
F1P               230.000 ppm
F1              17342.54 Hz
F2P               -10.000 ppm
F2               -754.02 Hz
PPMCM          12.00000 ppm/cm
HZCM          904.82837 Hz/cm
```

Vita
Ajay A Sathe

Ajay Sathe was born in 1988 and raised in Mumbai, India. He obtained his B.Tech degree in Pharmaceutical Science and Technology at the Institute of Chemical Technology, Mumbai, India. During his undergraduate studies he investigated the effect of ultrasound on the hydrolysis of diazonium salts under the direction of Prof. S. D. Samant and Prof. K. G. Akamanchi. Ajay then joined Penn State to pursue his doctoral studies in the labs of Prof. Alexander Radosevich and Prof. Robert Rioux. During his graduate career he worked on utilization of carbon dioxide in organic synthesis, flow chemistry and thermodynamic measurements of cation exchange reactions in semiconductor nanocrystals. Upon graduation Ajay will join Intel Corp. as a process engineer in the etching division at Hillsboro, OR.